Development of bio-inspired hydrogels for tissue regeneration

RASHMI JAIN

A thesis submitted for the partial fulfillment of
the degree of Doctor of Philosophy

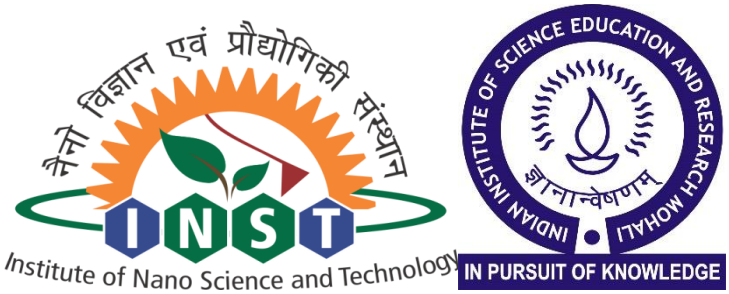

Institute of Nano Science and Technology
Habitat Centre, Sector-64, Phase-10, Mohali, Punjab 160062, India
Indian Institute of Science Education and Research Mohali
Knowledge city, Sector 81, SAS Nagar, Manauli PO, Mohali 140306, Punjab, India.

March2020

Dedicated to my beloved family and respected teachers

Declaration

The work presented in this thesis has been carried out by me under the guidance of Dr.Sangita Roy at the Institute of Nano Science and Technology Mohali. This work has not been submitted in part or in full for a degree, a diploma, or a fellowship to any other university or institute. Whenever contributions of others are involved, every effort is made to indicate this clearly, with due acknowledgement of collaborative research and discussions. This thesis is a bonafide record of original work done by me and all sources listed within have been detailed in the bibliography.

RASHMI JAIN

In my capacity as the supervisor of the candidate's thesis work, I certify that the above statements by the candidate are true to the best of my knowledge.

Dr. SANGITA ROY

Acknowledgements

This thesis represents not only the culmination of a scientific endeavor for me professionally, but also a journey of personal development and a discovery of identity for which I am profoundly indebted to so many people. I offer my gratitude to all those who contributed to the success of the work presented in this thesis and made this journey successful with everlasting memories.

First of all, it's my great pleasure to express my deep sense of gratitude to my supervisor Dr. Sangita Roy, for giving me the amazing opportunity to pursue research in the wonderful world of hydrogels and believing in my research abilities. She gave me complete scientific freedom for working in the research areas of my choice. Her constant guidance, support and motivation have been immensely helpful in the completion of this journey. Her assurance and encouragement during the hard times when research plans did not work are gratefully acknowledged.

I would like to thank the Institute of Nano Science and Technology for providing institutional infrastructure, research facilities, and resources to accomplish my research work. I also want to thank IISER Mohali for the infrastructure facility.

I wish to express my gratitude to Professor Hirendra Nath Ghosh, Director, INST for his continuous support in every aspect. My sincere thanks to Professor Ashok Kumar Ganguli, founding Director, INST Mohali, for his constant support and guidance. My special words of thanks go to late Shri P.K. Datta, former Dean students INST Mohali, for always being so kind, helpful, and motivating. I am highly thankful to Dr. **Prakash P. Neelakandan**an, Dr. **Debabrata Patra,** the members of my doctoral advisory committee for their valuable suggestions and guidance which helped in my doctoral studies. I would extend my gratitude towards Dr. Deepa Ghosh, Dr. Sharmishtha Sinha, and Dr. Tapasi Sen for useful discussions during my research work. I would like to thank Dr. Dibyendu Das for his timely guidance. I am also grateful to all faculty members and staff of INST Mohali for their direct and indirect support.

I also take this opportunity to express my love and gratitude to all my teachers for their kind love and leading me to the right path. Without their guidance, blessing, and support I would not have been here. I would like to extend my gratitude towards Dr. Amita Joshi, my M. Pharma supervisor for instigating the desire of research in me.

I would like to acknowledge *Vaibhav Bajpai (TEM operator) is for his* timely technical support.

I take this opportunity to extend my profound thanks to my group members, Harsimran Kaur, Pooja Sharma, Vijay Kumar Pal, Sourav Sen, and Archita Sharma for their generous co-operation and assistance in research. I personally want to extend my thanks to my batch mates and friends Swati Tanwar, Rajinder Kumar, Dimple Sharma, Anup Srivastava, Ritu Rai, Naimat Kalim Bari, Soumen Ash, Ankur Sharma, Ashmeet Singh, Munish Shorie, Renu Rani, Pulkit, Atul Dev, and Harmanjit Kaur, who were always there to help whenever I needed and never let me down during these Ph.D. days. Your encouragement and company out of the institute is greatly acknowledged.

Most importantly none of this would have been possible without the support of my family. I deeply express my love and gratitude to my lovable father Mr Rakesh Kumar Jain and mother Mrs Meena Jain for their faith and belief in me and my capabilities. I want to thank my younger brother Mr Ankit Jain for his unconditional love and support.

Abraham Lincoln once said "In the end, it’s not the years in your life that count. It's the life in your years". It's hard to list all the people who have directly or indirectly contributed to making this journey successful, I thank them all.

This acknowledgement will be incomplete without thanking God, the supreme power for giving me a healthy body and mind, and a beautiful place to live.

RASHMI JAIN

Table of Contents

Abstract

Mimicking the functional cues of native extracellular matrix (ECM) is elementary to understand and control the processes that regulate cell physiology and cell fate. Extensive groundwork on the structural and biological complexity of ECM has revealed the critical paramaters for the design of synthetic ECM that can control cellular behavior. These parameters include tuning of biophysical properties (stiffness, elasticity), biochemical properties (bioactive peptide epitopes), and nano-architecture (nanofibrillar structure, porosity) of the designer scaffold. Recent advances in the construction of ECM mimetic materials have directed the efforts towards tissue specific scaffold design and are primarily based on exploration of bioactive peptides. The concept of molecular self-assembly coupled with rich peptide chemistry holds great potential to fabricate diverse functional materials. Inspired by the design of mother nature, we have developed a series of bioactive functional scaffolds, using minimalist design approach to fabricate the synthetic mimics of ECM, which can have potential implications in tissue engineering. To this direction, we initially explored the short functional motifs i.e. IKVAV and YIGSR, of basement membrane protein of natural ECM, i.e. Laminin, which has critical role in cell adhesion, migration and proliferation. Our study emphasizes on the role of differential environmental conditions i.e. solvent switch in tailoring the self-assembling properties of these designed peptides. We tuned the physiochemical and structural properties of these novel peptide based scaffolds to effectively modulate the differential interactions with different cell types. Apart from individual peptides, we explored the self-assembling properties of IKVAV and YIGSR peptides in combination. Interestingly, these short laminin peptides were highly biocompatible and able to mimic biological properties of native protein, including proliferation, adhesion, neurite extension, neuronal marker expression and cell cycle regulation, indicating their role in controlling neuronal cell behavior. The next step was intended to achieve the complex multi-functional hierarchical composition and structure by simply mixing the two functional peptides derived from collagen and laminin proteins. Gelation was induced in short collagen mimetic peptide by the addition of laminin mimetic peptides, thus creating multifunctional scaffolds for regulating the growth of both fibroblast as well as neuronal cells. Our studies revealed that maintenance of hydrophilic-lipophilic balance (HLB) within the molecule is crucial for designing an ideal hydrogelator. In order to achieve detailed understanding on rationale behind the gelator design, our attempt was directed to establish a sequence-structure relationship with respect to systematic variations in hydrophobic-hydrophilic balance within designer peptides. For the first time, differential role of aliphatic vs aromatic hydroxyl group has been established towards shape controlled synthesis of gold nanoparticles.

Furthermore, non-conventional approach for modulation of physical parameter of the self-assembly in a single molecular domain was explored, without changing chemistry of the gelator. Highly tuneable gels were created by the interaction of non-gelator peptides and specific proteins which represents the ‘out of equilibrium’ structures. The present work underpins the development of tunable functional materials, mainly inspired from biological origin, which could essentially create the ideal microenvironment to provide essential biochemical and biophysical cues to the relevant cell types. These biomimetic materials hold great potential to be developed as next-generation biomaterials for biomedical applications.

List of Figures

List of tables

Abbreviations

A	Adenine
ACN	Acetonitrile
AFM	Atomic force microscopy
BLI	Biolayer interferometry
BP	Bis(2-(methacryloyloxy)-ethyl) phosphate
BMP-2	Bone morphogenetic *protein-2*
C	Cytosine
Cbz	Carboxybenzyl
CD	Circular dichroism
CMP	Collagen mimetic peptides
CLSM	Confocal laser scanning microscopy
CSR	Controlled shear rate
CSS	Controlled shear stress
3 D	Three dimensional
DAPI	4′,6′-diamidino-2-phenylindole
DCM	Dichloromethane
DIC	Diisopropyl carbodiimide
DIPEA	N, N-Diisopropylethylamine
DMF	Dimethyl formamide
DMEM	Dulbecco's modified Eagle's medium
DMSO	Dimethyl sulfoxide
DNA	Deoxyribonucleic acid
ECM	Extracellular matrix
EGF	Epidermal growth factor
EDT	1,2- Ethanedithiol
FTIR	Fourier-transform infrared spectroscopy
FAK	Focal adhesion kinases
Fmoc	Fluorenylmethoxycarbonyl
FBS	Foetal bovine serum
G′	Storage modulus
G″	loss modulus
GAG's	Glycosaminoglycans
GdL	Glucono-δ-lactone
HBTU	O-(Benzotriazol-1-yl)-N,N,N′,N′- tetramethyluronium hexafluoro-phosphate
Hz	Hertz
hMSCs	Human mesenchymal stem/stromal cells
ITC	Isothermal titration calorimetry
kJ/ mole	Kilo joule per mole
LMWG	Low molecular weight gelator
LPPS	Liquid phase peptide synthesis
MALDI	Matrix--assisted laser desorption/ionization
MAPK	Mitogen-activated protein kinases
MHz	Megahertz
MGC	Minimum gelation concentration
MMP7	Matrix metalloproteinase 7
MS	Mass spectroscopy
MTT	3-(4,5-dimethylthiazol-2-yl)-2,5-diphenyl bromide
Nap	2- Napthoxy acetic acid

NMR	Nuclear Magnetic Resonance
PA	Peptide amphiphile
PBS	Phosphate buffer saline
PEG	Poly-ethylene glycol
PHEMA	Poly (2-hydroxyethyl methacrylate
PLA	Poly-lactic acid
PMA	Poly-methacrylate
Ppm	Parts per million
PI	Propidium iodide
PVA	Poly vinyl alcohol
Pyr	2- Pyrene butyric acid
SPPS	Solid Phase Peptide Synthesis
T	Thymine
TEM	Transmission electron microscopy
TFA	Trifluoroacetic acid
TGF-b1	Transforming growth factor beta 1
TLC	Thin layer chromatography
ThT	Thioflavin T
TMS	Tetramethylsilane $Si(CH_3)_4$
XRD	X-Ray Diffraction

Thesis outline

The research work carried during the fulfillment of this thesis includes following chapters:

Chapter 1: Introduction

This chapter will cover the overview of natural extracellular matrix (ECM), its composition, structure and functions which motivates the design of synthetic extracellular mimics. Fundamentals of hydrogel formation will be discussed, which would showcase the use of molecular self-assembly approach as a simple and elegant methodology for bottom-up nanofabrication of the soft materials. Furthermore, the role of the designer gels will be delineated towards developing ~~as~~ a synthetic scaffold. A brief discussion about β-amyloid assemblies to explain the mechanistic and structural aspects of short self-assembling peptides will also be included. This chapter will finally introduce the applicability of bioactive short peptide hydrogels for biomedical and tissue engineering applications.

Chapter 2. Methodology

This chapter describes the synthetic protocols and characterization techniques used for the work presented in this thesis. Standard peptide synthesis procedures of solid phase and liquid phase synthesis will be discussed in detail. Different gelation methods for the preparation of hydrogels like solvent triggered, heat-cool, pH switch, etc. will be discussed in this chapter. The fundamentals of various spectroscopic and microscopic techniques like FTIR, CD, Fluorescence, AFM, XRD, TEM, Fluorescence microsopy, Confocal laser scanning microscopy, Rheology, Biolayer interferometry, Flow cytometry, etc and their applicability in our work, will be discussed further in this section.

Chapter 3: Differential self-assembly of Laminin derived short peptides using solvent mediated approach

This chapter mainly focuses on the minimalist approach for the rational design and synthesis of short peptide sequences derived from the extracellular matrix (ECM) protein laminin (IKVAV and YIGSR). Further, the tuning of self-assembly pathways by the non-conventional solvent mediated approach is shown which leads to diverse nanostructures from a single gelator molecule. The effect of solvent nature on the self-assembling behavior of peptides was assessed by various microscopic, spectroscopic and rheological analysis. In order to, make these mixed solvent gels suitable for bio-applications, an effective solvent exchange method was also elucidated.

Chapter 4: Laminin conjugate hydrogels for controlling neuronal cell behavior

The biofunctional properties of laminin derived peptides were explored in this chapter. The mechanical, morphological and spectroscopic properties of co-assembled laminin peptides i.e Fmoc IKVAV and Fmoc YIGSR were investigated. The cell-substrate interactions were investigated by culturing neuronal cells like C6 and SHSY5Y cells with these hydrogel scaffolds. The cytocompatability and proliferation of both the cells were checked through MTT assay and Alamar blue assay. The cultured cells were visualized for their viability and healthy morphology using Live-dead staining. The regulation of normal cellular functions can be assessed by quantification of certain neuronal markers.

Chapter 5: Designing a bifunctional extracellular matrix mimic from co-assembled collagen and laminin derived short peptides

This chapter will include synthesis of Napthoxy acetic acid appended collagen and laminin mimetic peptides, which will be further mixed to attain a complex hierarchical structure to mimic native extracellular matrix. Their gelation method will be discussed and various characterization techniques to evaluate the gelation properties of co-assembling peptides. The mechanical stiffness measurements has been carried out by rheology, while microscopic analysis of nanostructures was investigated by AFM and TEM and the secondary structure investigation was completed ~~by~~ using CD, FTIR, and thioflavin T binding assays, which will be discussed in detail. Further, the results obtained for cell culture studies will be discussed which were assessed in terms of biocompatibility, proliferation, and migration through MTT and alamar blue assays. The future application of such scaffolds for 3D cell culture will be discussed which highlights its use as an injectable hydrogel for encapsulation and delivery of cells.

Chapter 6: Understanding the structure-function correlation of ultra short amyloid peptides towards synthesizing organic-inorganic hybrid materials

This chapter includes the design of library of dipeptides modified with aromatic groups having different hydrophobicities and different C-terminal amino acid residue. The evidences for effect of overall hydrophobicity of peptides on mechanical stiffness, morphology, and secondary structure were studied in detail. The fundamentals of structure-property relationship derived from various physiochemical characterization was further extended to structure-function correlation. This part of work demonstrates the differential role of aromatic and aliphatic hydroxyl groups in controlling the shape of the in-situ synthesized gold nanoparticles by

hydrogels. This chapter talks about design and development of organic-metal hybrids with controlled properties.

Chapter 7: Highly tuneable gels formed by the co-assembly of peptide and protein

Protein-peptide co-assembly is a rarely used approach to trigger gelation in a non-gelator short peptides. This chapter discusses about non-conventional approach of using several different proteins to access different non-equilibrium structures corresponding to diverse gels formed in a single gelator domain. Interestingly, fixed concentration of a short peptide (Cbz FL) was utilized to form diverse nanomaterials by simply varying the concentration of protein. To check the specificity of this interaction, several other non-gelator dipeptide analogues and different proteins of variable hydropathy index were explored for gelation. The nature of binding of protein and peptide were analysed using BLI and ITC. This chapter discusses about the novel approach of creating differential hydrogels at physiological conditions and can also be used as enzyme immobilization technique.

Chapter 8: Future work and conclusions

This chapter summarizes them key findings of work discussed in previous chapters. It also discusses the future prospects of biomaterials developed during this thesis in the field of stem cell differentiation and tissue engineering.

Chapter 1

Introduction

1.1 Motivation of Work

Tissue injury and organ failures are common and serious medical conditions which can be life threatening. Currently available treatment options include drug therapy, surgical repair, organ transplantations and artificial prostheses. However, the number of untreated patients was constantly growing due to limited supply of donated organs available for such procedures and end-stage failure of available donated organs. Another important issue associated with compatibility with allografts resulting in severe immune responses. Tissue engineering or regenerative medicine aims to restore the functions of the damaged tissues/organs using patient's own cells. To engineer a tissue construct, a biomaterial scaffold is needed to grow cells that is capable of recapitulating the extracellular matrix (ECM) microenvironment to promote tissue development. To meet up with this emerging medical need, a hug emphasis has been laid to develop functional nanomaterials. Combining principles of material science and *in vitro* cell culture can be an effective approach to develop substitutes for tissue repair and regeneration. However, the development of artificial cell scaffolds with high biocompatibility and tuneable structural and mechanical properties still remained a challenge in the field of tissue engineering. Moreover, the progress in biomaterials design is focused towards bioactive three dimensional scaffolds that can mimic native ECM. Developing peptide hydrogels with tailorable properties is one of the effective approaches to obtain appropriate synthetic ECM.

1.2 Tissue Engineering

Tissue engineering is defined as an interdisciplinary field that applies the principles of engineering and life sciences toward the development of biological substitutes that restore, maintain, or improve tissue function. [1-3] Tissue engineering aims to create organs from scratch in the laboratory, which can be transplanted into the patients. [4,5] To achieve this aim, three key components are involved; they are cells, scaffolds and growth regulating factors, often referred to as tissue engineering triad (figure 1.1). [6-9] Cells can be autologus or xenogenic which grows and multiply to develop a tissue. Another important component is scaffold that is generally composed of biomaterials forming three dimensional network structures and provides appropriate environment and structural support for cell attachment and tissue development, subsequently. [10-13] The biological signaling molecules such as growth factors plays important role in instructing cells to express desired phenotypes. Therefore, the physical structure, chemical composition and biological functionality are the essential attributes to biomaterials for

tissue engineering. [14-16] Hence, design and development of an appropriate scaffold offers a great scope as well as challenge for the progress of tissue engineering field.

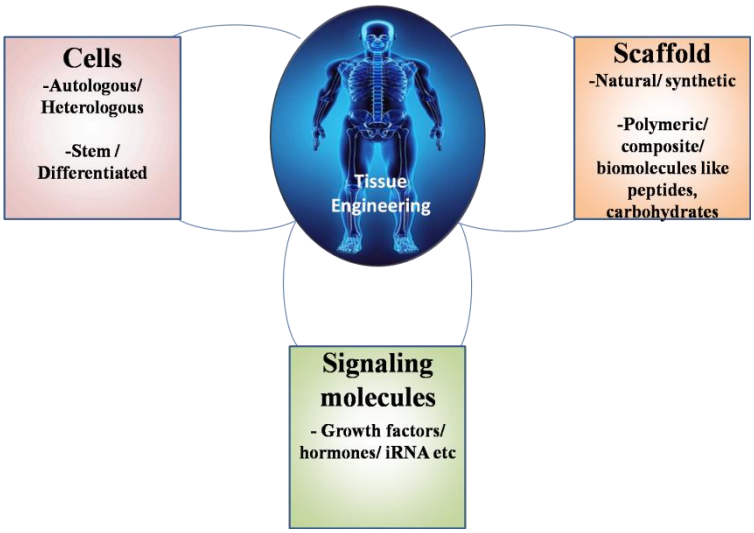

Figure 1.1 *Components of tissue engineering*

1.3 Extracellular matrix

In mammalian body, the cellular reactions are regulated by the highly complex microenvironment, called an extracellular matrix (ECM). [17, 18] ECM is a gel-like biological material that forms a physical network for encapsulation of cells. In the past, ECM was considered as an inert framework, filling intercellular spaces and provides physical support. However, recent investigations have clarified the role of ECM, which is much more complex than it was thought to be. [19-21] ECM acts as an active component for controlling cell behavior and fate, which is secreted and maintained by the cells. It is believed that the cellular organization is a reflection of matrix composition. [22, 23]

Broadly, the ECM is composed of three major classes of macromolecules i.e. fibrous proteins, glycosaminoglycans (GAG's), and proteoglycans. [24] Although the basic composition of all the tissues is same, different variants of macromolecules and their variable proportions, determine the differential physical properties of different tissues. The fundamental fibrous proteins include collagens, elastin, laminins, fibronectins, etc. [25, 26] These constituents have different vital roles which regulate the cell viability, migration, proliferation, differentiation and gene expression. [27, 29] Among these, Collagen is the most abundant component and constitutes about 30% of the total protein content of the body. It plays a major role in providing tensile strength to the tissues and organs and also regulates cell adhesion and migration. Collagens, along with elastin, impart

elasticity to the tissues. [30-32] The elasticity of the tissue is dependent on the concentration of elastin present within the tissue. The elastin helps tissues to regain their structure upon physical pressure or stretching and prevents permanent deformation of the tissue. Another important class of ECM protein is Fibronectins, which participate in cell adhesion and guides cell migration. These play a major role in cell-matrix and cell-cell interactions and also helpful in wound healing. A three amino acid oligopeptide, RGD (arginine-glycine-aspartate) was recognized as adhesion site in fibronectin proteins which binds to the cells through cell surface integrin receptors. [33-35] Laminins are another important class of ECM proteins, which is mainly found in the basement membrane and acts as glue for joining dissimilar types of tissues together. Laminin has a heterotrimeric structure consisting of three different polypeptide chains (α, β, and γ). [36, 37] They play an important role in cell adhesion by interacting through integrin, heparin, or dystroglycan receptors. [38] Different intracellular signaling pathways involving phosphatases, mitogen-activated protein kinases (MAPK), focal adhesion kinases (FAK), and cytoskeletal components are activated in cells by interacting laminin with integrin receptors. Laminin-integrin interactions also regulate cellular behavior such as viability, migration, adhesion, proliferation and differentiation. [39-42]

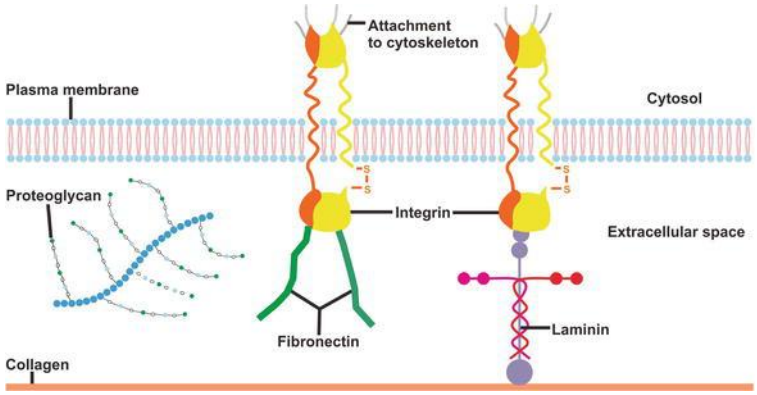

Figure 1.2 *Diagrammatic representations of extracellular matrix components (taken from ref 43)*

1.4 Design criteria's for an ECM mimic:

In natural ECM, the cells and the complex biomolecules coexists within a nanofibrous 3D-network. The mechanical properties of tissues are determined by the exclusive physical, topological and biochemical composition of ECM. [44, 45] To design an artificial ECM mimic, a matrix should be simple and biocompatible, possess structural architecture similar to native ECM and should be able to direct and control cell behavior. The appropriate porosity with high surface area is greatly desirable, which can provide suitable space for the growth of cells and

blood vessels. The mechanical integrity as well as biocompatibility is essential requisites for the design of scaffolds. The scaffold material should be biodegradable and the degradation rate should be similar to that with the rate of formation of new tissue. Ultimately, the scaffold should be able to interact with the cells through attachment, migration, growth, differentiation, but at the same time should avoid unfavorable tissue reaction like macrophage activation, inflammation, or apoptosis. Cell-matrix interaction can be induced by various physical and chemical cues. The physical cues can be incorporated in the form of mechanical properties and structural architecture, while chemical cues are incorporated into the matrix as cell adhesive peptides, growth factors, etc. [12, 17, 18]

1.5 Hydrogels as ECM substitutes:

In the past few decades, hydrogels have gained inevitable attention to be developed as ECM analogue for tissue engineering applications. Traditionally, hydrogels are the versatile biomaterials having 3D cross-linked network structure. Their high water content, tissue like elasticity and nanofibrous architecture make them ideal candidates for native ECM mimics. [46-49] Moreover, mild and cyto-compatible methods of formation ease of modification with chemical functionalities, tunable mechanical properties and degradability offers close similarities to the properties of natural ECM. Based on mode of interaction between the building blocks, hydrogels can be broadly classified into two types: physical gels and chemical gels. [50] In physical gels, the reversible non-covalent interactions such as hydrogen bonding, hydrophobic interactions, π-π stacking, van der Waals interactions, and/or electrostatic interactions between different segments of building blocks are involved to hold the network together. The transition from sol-to-gel, in physical gels, is triggered in response to change in environmental conditions such as pH, ionic strength, temperature, solvent, etc. While the chemical gels, on the other hand involves irreversible covalent interactions between the segments of monomeric building blocks. In addition to this, hydrogels can be classified in various ways, depending upon their source, type of composition, network electrical charges or stimuli responsiveness, as shown in figure 1.3. [51]

Similar to natural ECM, the hydrogel physical properties are dependent upon the nature and composition of the materials used. Hydrogels can be synthesized from either natural or synthetic materials. [50-52] Naturally derived polymers may include ECM components like collagen, fibrin, hyaluronic acid, matrigel, dextran, etc. [53-57] However, poor reproducibility due to batch-to-batch variation, risk of contamination, difficulty in purification, poor control over biochemical

and mechanical properties are some of the major issues associated with natural biomaterials. On the other hand, synthetically derived polymers like poly-ethylene glycol (PEG), polyvinyl alcohol (PVA), polymethacrylate (PMA), poly-lactic acid (PLA), etc have fixed composition, adjustable physiochemical properties and reproducibility. [58-60] However, lack of cell recognition signals is the major drawback for synthetic polymers, which limits their use in biomedical applications. Moreover, their bioinert nature and ability to integrate with biochemical cues, makes them suitable platforms to control cell behavior and mimic complex natural ECM system.

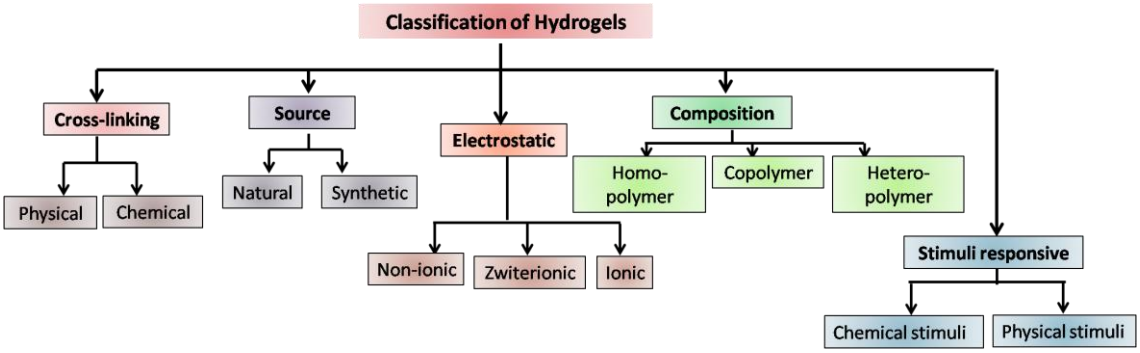

Figure 1.3 *Hydrogels classification on the basis of different parameters (adapted from ref 51)*

1.5.1 Applications of Hydrogels

Hydrogels are highly advantageous materials because of their multiple desirable properties. Hydrogels have potential applications in the field of domestics, pharmaceuticals, biomedicine and industries. Their excellent adsorbing, retention, and releasing properties expand the scope of utilities in day-to-day life. Their flexible structure, high water content, and biocompatibility, makes it suitable to use for biomedical purposes. Some of the major uses of hydrogels are listed below:

1) Domestic Use: Hydrogel materials have plenty of usages in everyday life. Diapers are one the breakthrough in common man's life. The super-absorbent properties of diapers owing to the high water retention capacities of hydrogel materials keep the diaper dry, even after absorbing considerable amount of liquid. [61] Cosmetics are an important part of modern daily life. Usually, the cosmetic products like 'beauty masks' claims to hydrate skin, anti-aging effects and restores its elasticity and are made with engineered collagen Other products like sunscreens and mascara also use Pecogels. Furthermore, some commercially available products act as complex-drug delivery systems such as Hydro Gel Face Masks by Fruit and Passion Boutiques

Inc. performs the moisturizing action of polymeric gels along with release of active biomolecules like vitamin C or B3. Smart hydrogels made up of pH sensitive materials are a huge advancement in the field of cosmetics. Such hydrogels are used for the delivery of cosmetic drugs like niacinamide, arbutin, adenosine, etc, which have skin whitening or wrinkle treatment properties. [61]

Perfume delivery is another important application of hydrogels which showed a rise in the nineties in the form of delivery technologies for volatile species. The aim to develop devices for delivery of volatile compounds was to control the slow dispensing of fragrances to the surroundings that can last long. Such hydrogel based approaches involve the swelling properties of hydrogels, which triggers the release of perfume smell. This technology had replaced the classic salt-based (sodium dodecylbenzene sulphonate) tablets with novel, fancier house care solutions. [61]

2) Pharmaceuticals:

Controlled drug delivery is one of the major concerns for effective therapy, which needs administration of therapeutic substances at the site of action at controlled rates for specific periods that can overcome the limitations of traditional drug delivery systems of frequent drug formulation intake and high dosage due to non-specific site delivery. The excellent properties of hydrogels make them potential choice for drug delivery applications of both hydrophobic as well as hydrophilic drugs. The release of loaded drugs is dependent on the permeability of the matrix. In addition to this, hydrogels also store and prevent the drugs from hostile environments and release them with the desired kinetics profile. With the generation of novel smart biomaterials, stimuli-responsive drug delivery systems were developed, in which drug release can be activated by the local changes such as pH, temperature, or presence of specific enzymes or by some remote stimuli. [51, 62, 63]

Figure 1.4 *Applications of hydrogel in different fields (individual images adapted from Wikipedia)*

3) Biomedical Applications:

Tissue engineering: Hydrogels are widely used materials for tissue engineering as it is capable of providing three dimensional microenvironments for cells to adhere, proliferate and migrate. Furthermore, the bioactive motifs incorporated within the matrix dictate the biological activities and functions of the cells. The ideal scaffold design and selection of material for any particular application depend on different variables including physical properties, biological properties and mass transport properties and the surrounding environment where the scaffold is to be placed. The materials used for scaffold design in tissue engineering can be derived from materials of synthetic or natural origin. A very huge list of tissues for which the hydrogel application is augmented is available in the literature including blood vessels, muscle, kidney, skin, cardiac, adipose, retina etc. However, we describe the state of art and versatility of hydrogel based tissue engineering in few areas such as bone, cartilage, intervertebral disc and neural tissues. [64]

Bone regeneration: Calcium phosphate based ceramics and their derivatives are the most exploited molecules in bone tissue engineering. Hydroxyapatite containing hydrogels also been reported for excellent bone remodeling. [65] Bone regeneration and neo-bone formation using hMSCs have been reported in a hyaluronic acid based hydrogel with BMP-2 as a carrier vehicle. BMP-2 is a prolific morphogenic factor that promotes adhesion properties of hyaluronic acid. Moreover, these polymeric gels grafted with the peptide motif RGDSK and showed excellent osteoblast adhesion. [66]

Cartilage repair: Damaged cartilage in joints causes swelling, pain and impaired mobility. If some tissue-like articular cartilage is damaged, they lose its regeneration capacity due to avascularity and low proliferation rates of the remaining chondrocytes. [67] [68] Polysaccharides such as chitosan, dextran and hyaluronic acid are often used for the preparation of hydrogels for cartilage engineering because the cartilage ECM contains an abundant amount of polysaccharides. [69-72] A photo polymerized composite hydrogel of gelatin and methacrylamide for encapsulating growth factors (e.g. TGF-b1) and cells. [73] Another approach includes the modification of polymeric scaffolds with signal molecules such as RGD (integrin based), matrix metalloproteinase 7 (MMP7) to encapsulate hMSCs for cartilage repair and regeneration. [74]

Neural tissue regeneration: Limited endogenous repair capacity of neural cells demands more attention and exogenous assistance to restore the functions of neural tissues. [75] Brain being the softest tissue requires mechanical properties of the scaffold similar to endogenous tissue. It was evidenced from the reports that alginate, agarose, chitosan, methylcellulose and dextrin blended gels with lower values of modulus have the ability to interact with neural cells. [76] Self-assembling peptide gels are elegant materials for neural tissue engineering. [77] $RADA_{16}$ and short laminin derived motif IKVAV were successfully used to demonstrate the regeneration of rat brain injury model. [78, 79]

Intervertebral disc regeneration: With age, the regeneration capacity of the intervertebral disc is severely compromised, which pushes the requirement of developing scaffold materials for the treatment of disc degeneration. Hydrogels can be used as a supplement /reinforcement or replacement material for nucleus pulposus tissue or as a shock absorbent material placed in the core of IVD. [80] Many hydrogels including poly-N-acetylglucosamine were investigated *in vitro* as well as *in vivo*, which have mechanical properties similar to those of nucleus pulposus. The peptide derived hydrogels such as KLD-12, crosslinked collagen derived biomaterials and other synthetic and composite biomaterials including PVA/PVP, poly (N-isopropyl acrylamide) and

tween/NVP/cellulose were also evaluated as replacement prostheses for nucleus pulposus. [83-85]

Wound Healing: Wound healing is a potential application of highly biocompatible and bioactive materials to treat damaged skin tissues. Chronic, non-healing, wounds are very painful and become a burden on the patients and often result-in impaired mobility, tissue amputation or sometimes even death. The ideal wound management involves 3 main steps: (1) protection of wounds from external agents (bacterial infections, mechanical stress), (2) accelerates wound closure with proper moisture maintenance between wound and dressing and (3) minimize/ avoid scar formation and can be removed easily without further trauma to the wound. Naturally-derived hyaluronic acid, gelatin, collagen, fibrin, etc are promising materials because of their presence in ECM of human skin. Moreover, other naturally derived materials, which are used for the preparation of wound healing systems include cellulose, copolymers of alginate-chitosan, chitosan-gelatin-honey, or biphasic gelatin-silk. [86]

Contact lenses: Contact lenses are the pioneering application of hydrogels. The oxygen permeability of biomaterial is one of the prime factors to be considered for designing a contact lens, which would prevent hypoxic stress of the cornea. Moreover, hydrogels can fulfill most of the requirements of contact lens design and depending upon their elasticity; can be classified as 'Hard' or 'Soft'. Hard contact lenses are majorly based on polymers of dihydroxy methcrylates, methacryclic acid, or acrylamides which are long lasting but poorly accepted by the users. However, soft lenses are made up of hydrogels and particularly silicone hydrogels are more suitable for prolonged wear times and are safer against infections than conventional hydrogels. [51, 61]

4) Industrial applications:

Biosensors: A biosensor refers to a physical and chemical sensor in combination, which can detect and report any change in the biophysical properties of the system. Now-a-days, biosensors are becoming popular as a practical tool to cover wide range of applications in the areas of home-based diagnostics, environmental monitoring and point-of-care testing. All biosensors have a biological recognition part, in common, like enzymes, antibodies, living cells or micro-organism, which has specificity towards one analyte and has least interference with the other species. [87-89]

Pollutant Removal: Dye and heavy metals are the common pollutants found in industrial wastewater, which has become a serious threat to public health and ecosystem. Removal of heavy metals from wastewater resources has gained huge practical and scientific interest.

Hydrogels with carboxyl, nitrogen, sulphonic, phosphonic groups are generally used as absorbents for removal of heavy metals and toxic compounds or recovery of dyes from effluents. Polyelectrolytes have binding affinities towards oppositely charged metal ions and such hydrogels have a significant role in removal of heavy metals. The removal of dyes and metal ions, using chitosan, alginate, starch and cellulose derivatives was based on chelating or ion exchange mechanisms, owing to their amino and hydroxyl functional groups. Furthermore, the polymeric materials were modified using different approaches like carbodiimide chemistry, glycine substitution, nanoparticle formation, etc, to improve their adsorption capacity and mechanical resistance. [90-92]

1.6 Self Assembly: Strategy to develop ECM mimic

"Beyond molecular chemistry based on the covalent bond there lies the field of supramolecular chemistry, whose goal is to gain control over the intermolecular bond"- *Jean-Marie Lehn*.

The term supramolecular chemistry was first used by Jean-Marie Lehn to describe the well organized supermolecules formed from self-association of several molecular components. Later, in 1987, Pedersen, Cram and Lehn won the Nobel Prize for their pioneering work with crown ethers and Cryptands, which opened up new routes toward the development of molecular assemblies that are held by weak forces, e.g., hydrogen bonding and van der Waals interactions. [93, 94] This multifarious subject is concerned with the formation of physical polymers that are bound together by specific intermolecular interactions rather than covalent interactions. [95, 96] The science of building supramolecular structures is completely out of the realm of molecular chemistry, which solely depends on making and breaking of covalent bonds. [96] Although the pioneering work of Jean-Marie Lehn was based on inclusion compounds and cryptand cages, but soon the field of supramolecular chemistry extended beyond the scope of host-guest interactions and covered all the organized systems originated through reversible non-covalent forces including gels, films, liquid crystals, nanostructures, polymers, etc. [98] Broadly speaking, supramolecular chemistry is the study of interactions between the molecules, rather than, within a molecule or in other words, it is a science of building complex structures from molecules instead of atoms.

Molecular self-assembly is a ubiquitous phenomenon in chemistry, material science and biology. In general, self-assembly can be explained as a combination of 'assembly' that means 'to put together' and the 'self' that implies 'without outside help or on its own'. [99] In 1990's, the concept of self-assembly at nanoscale was pioneered by Professor George Whitesides,

which was further developed to create functional bulk materials. [100-102] Later in 2016, the Noble Prize was to Professor Fraser Stoddart for his excellent work in development of template directed protocols for the synthesis of mechanically interlocked systems such as rotaxanes and catenanes, using the molecular recognition and self-assembly processes. [103] Basically, self-assembly is a driving force for the spontaneous organization of individual components to form ordered patterns, at all scales. Although, wide range diversity in the systems formed by self-assembly can be observed, but originally, they all rely on the reversible supramolecular interactions. [104] The building blocks in supramolecular architectures are held together by non-covalent forces like hydrogen bonding, π-π stacking, hydrophobic interactions, electrostatic interactions, metal-ligand interactions, dipole-dipole interactions. [105-108] The forces are individually weak, but the sum of multiple forces results in the formation of highly stable and defined assemblies at nanometer scale, which otherwise is sustainable only when long and medium range forces work in agreement. [109]

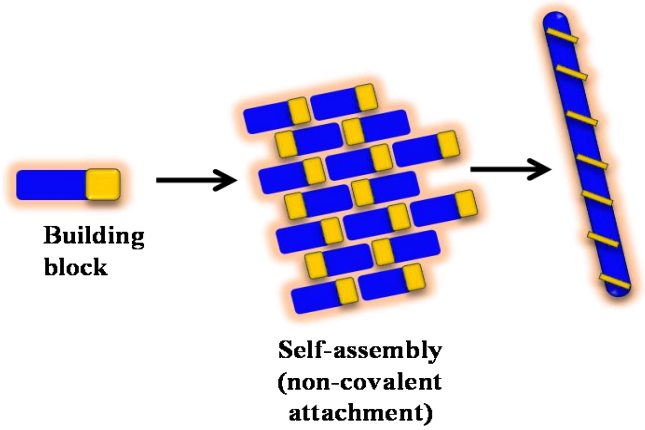

Figure 1.5 *Representative diagram of molecular self-assembly driven through non-covalent interactions and forming fiber as a higher ordered self-assembled structure.*

1.6.1 Types of Supramolecular interactions:

As mentioned above, the interactions involved in molecular self-assembly are weak non-covalent interactions. The bond energies of non-covalent interactions are known to be in the range of 5-80kJ/mol, which implies that they are weak in comparison to covalent bonds, having bond energies of ~100-400kJ/mol and thus necessitate the establishment of several links between building blocks to support self-assembly. [107-110] Majorly, these interactions are:

- H-bonding interactions: It is an association between a hydrogen atom and an electronegative atom (like N, O, or F). These bonds are highly directional and can be intermolecular (between two different molecules) or intramolecular (within the molecule). The functional groups that provide hydrogen atom for the bond is called as *hydrogen-bond donor* and the groups which provide electronegative atom is termed as *hydrogen-bond acceptor*. Generally, the strength of H-bond is mainly dependent on the nature of donor/acceptor, electro-negativity of the acceptor and also the surrounding media. The bond energy of H-bond ranges between 10-65kJ/mol. The combination of several H-bonds provides strength to the assembly and also helps in their spatial arrangement that enhances its specificity. [108]
- Aromatic Stacking (π-π Stacking): It is referred to an attractive interaction between π-electrons of aromatic rings when oriented face-to-face or face-to-edge. These are the dispersive interactions, which arise due to high polarizability of the aromatic rings and contribute to the stacking effects. The binding energies of π-π interaction range between 0-50kJ/mol. These interactions are being responsible for stability of molecules by forming a bond within a molecule. [110]
- Hydrophobic Effects: The hydrophobic effects are prominent when non-polar molecules are added in aqueous environments. To minimize the exposure to aqueous/polar solvents, the non-polar molecules tend to aggregate. However, hydrophobic effect is a function of entropy and therefore, their bond energy is difficult to assess. [108]
- Electrostatic Interactions: These interactions are involved between the ions or molecules of opposite charges. Columbic interactions can be attractive or repulsive. Ionic self-assembly is one the most common non-covalent interactions in biological systems and contributes to entropically unfavoured assemblies. It has been used as direct and reliable method for the stable organization of different building blocks (e.g., polyelectrolytes, charged surfactants, peptides, and lipids). These are long range nonselective forces having highest energies amongst all non covalent interactions of ~250kJ/mol. [104]

The reversible nature of non-covalent bonds makes supramolecular assemblies, a dynamic system. [108] As a result of their reversibility, the supramolecular systems are capable of undergoing dynamic rearrangements in response to environmental variations. The responsive nature of self-assembly process is highly advantageous because it helps to tune the properties of the resultant assembled material, according to the application. [111] The adaptability can be

rendered by simple modifications in the self-assembling monomer units, which alters the pattern of their interaction. The information for self-assembling systems is encoded in the molecular design of the building blocks synthesized via covalent interactions, which in turn, dictates the complementarity, cooperativity and multiplicity (number of bonding sites) of the system. Molecular self-assembly occurs in both natural as well synthetic systems. [112,113]

1.6.2 Self-assembly in nature:

Self-assembly is a fundamental process in nature, which encompasses a myriad of complex biological and physical instances. [114-117] The self-assembly is of prime importance to living systems which is dependent on 4 essential components, namely, proteins nucleic acids, carbohydrates and lipids. [108] These are the basic building blocks of life and give functionality to the cells. Biological systems in nature demonstrate the best utilization of supramolecular chemistry in fabricating functional materials, most economically and efficiently. [118] Nature creates highly complex biofunctional structures at nanoscale, with high precision and specificity, using molecular self-assembly approach. [119] Biology is replete with examples of highly complex functional systems formed by self-assembly, which are the source of inspiration for increasing interest towards synthetic self-assembling systems for biomedical and biotechnological applications. Some of the examples include bilayered lipid membranes, DNA double helices, protein tertiary structures, virus structure, enzymes. [120] DNA is a polymerized nucleotide, in which two antiparallel strands of DNA are stabilized through π-π interactions and H-bonding between cyclic purines (A, G) and pyrimidines (T, C) bases. [121, 122]

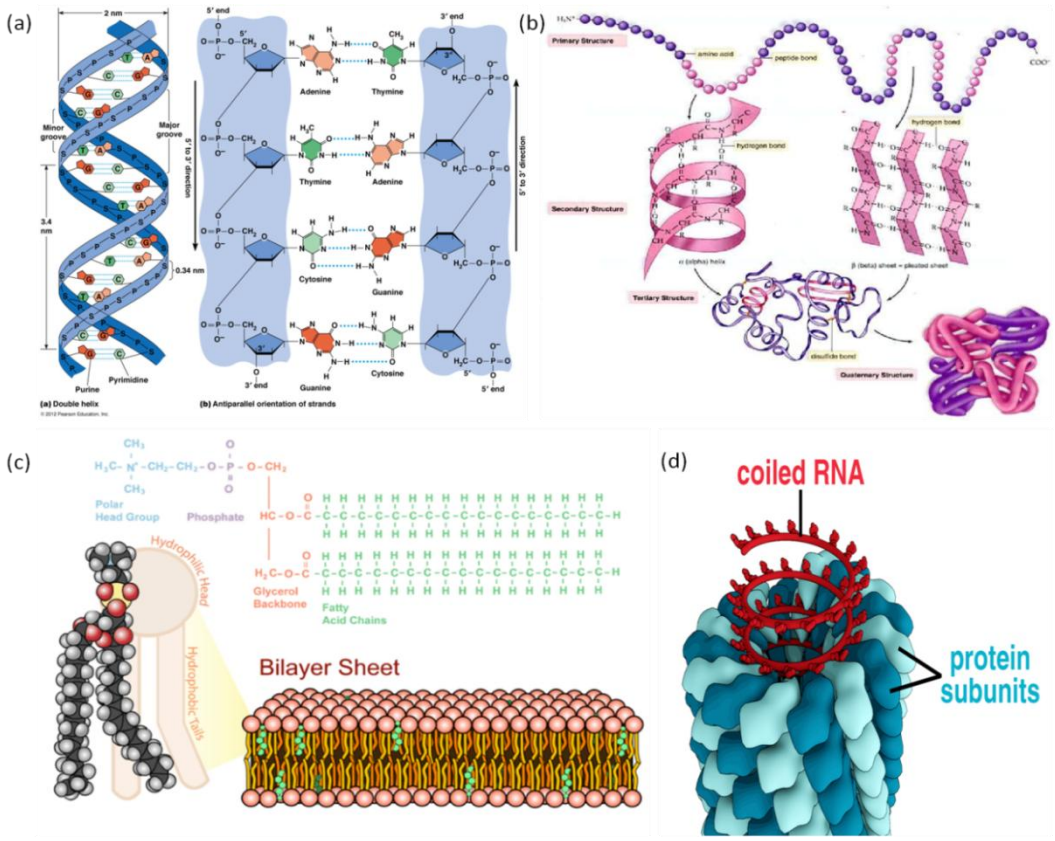

Figure 1.6 *Examples of self-assembly in nature showing (a) DNA double helix along with the interactions involved in itself-assembly, (b) protein folding with different hierarchical levels of self-assembly, (c) organization of amphiphilic phospholipids in cell membrane and (d) assembled structure of tobacco mosaic virus.(individual images taken from ref. 123-126)*

Protein folding is another self-assembly driven process, which controls the major activities of cells. The primary structure of peptide sequence is synthesized by linear strands of covalently liked amino acids, which further interacts through non-covalent interactions to form secondary (α-helices or β-sheet), tertiary and quaternary structures. Mostly, these tertiary structures are the functional units of proteins that act as catalytic sites or binding sites. These complex structures formed, serve as scaffolds for biological systems, transporting agents, biocatalyst, hormones, receptors, etc, besides their structural roles. Collagen is the most abundant protein in mammalian body, which is composed of three polypeptide chains, exclusively assembled in a triple helical manner. Similarly, actin protein, is the major constituent of cytoskeleton, forms cross-linked bundles or networks of microfilaments, having semisolid gel like properties and plays major role in regulating cellular motility. These examples illustrate that emergence of supramolecular chemistry is inspired by natural self-assembly and such fundamentals can be

applied for the development of novel self-assembling materials providing better control over their properties. [126-128]

1.7 Peptides

"Tiny protein building blocks called peptides will launch the age of designed materials within the next decade"- Shuguang Zhang

Since evolution, proteins are known to perform various biological functions with highly complex and specialized structures. Proteins are the natural condensation polymers of amino acids. Proteins are the products of dehydration reaction between the carboxyl group (-COOH) of one amino acid and amine group ($-NH_2$) of another amino acid, resulting in the formation of amide bonds. The short oligomeric sequences of amino acids are termed as 'peptides'. Although all amino acids have same basic structure, but each possesses different structures, physicochemical properties and biological functions, owing to the variable R group at the central carbon (Cα) position. Accordingly, these 20 naturally occurring amino acids can be divided into different categories such as polar, non-polar, charged (positively or negatively), aliphatic, aromatic, etc. [129,130] These differential functionalities make it possible to create a huge library of proteins and peptides having different biological functions, simply by varying the combination and length of amino acid sequences. These variable groups in the side chains participate in the supramolecular interactions such as aromatic amino acid residues form π-π stacking, charged residues interact through electrostatic

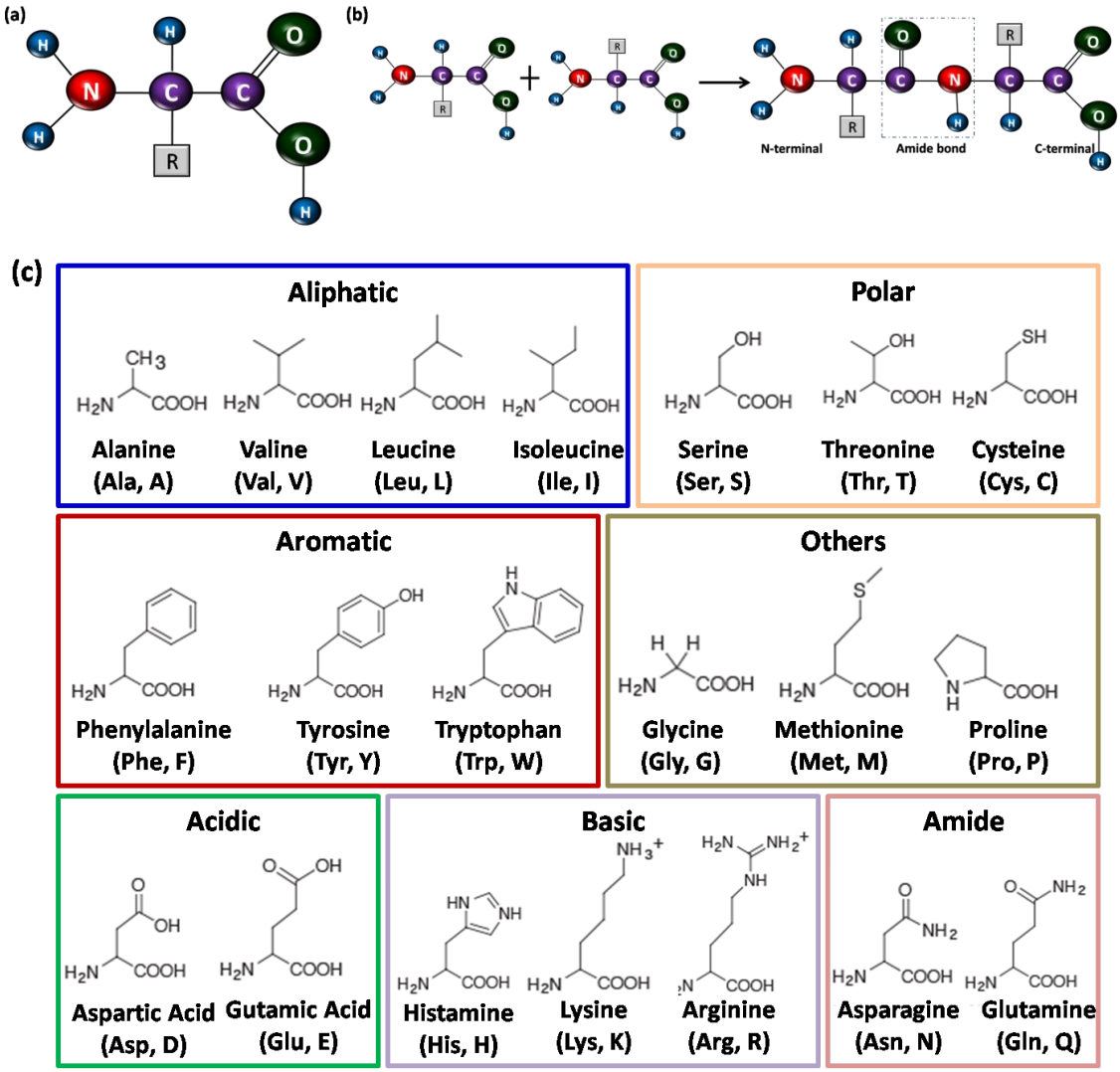

Figure 1.7 *(a) Basic structure of amino acid, (b) illustration of amide bond formation between two amino acids, and (c) structures and classification of 20 naturally occurring amino acids. (adapted from ref 130)*

interactions, polar amino acids enhance H-bonding interactions to form secondary peptide structures. Out of 20 amino acids present in the biological systems, 19 are containing stereocenter (α-carbon), to which four different groups are attached including amine, carboxylic acid and variable side chain. The chirality of amino acids (except glycine) provides additional complexity to the peptides to create diverse structures. [129] The advantageous attributes such as easy bottom-up synthesis, diversity and stability of peptide chemistry providing sites for desired modifications and ability to form highly organized structures, make peptides attractive class of

building blocks for designing functional materials with highly ordered self-assembled structures. [130-132]

1.8 Peptide Self-assembly:

In 1990's, the pioneering work of Ghadiri and co-workers demonstrated the formation of peptide nanotubes, which attracted great interest in exploring peptides as building blocks for design of nanomaterials. [133, 134] At the same time, S. Zhang was able to identify the spontaneous assembly 16-residue peptide into fibrous structures, which resulted into macroscopic membrane like structure. [135, 136] These pioneering studies demonstrated for the first time the scope of mimicking natural systems for designing nanomaterials. [130] Since then, diverse families of nanostructures have been explored using self-assembly of peptides. These nanostructures include nanotubes, nanorods, nanotapes, nanofibers, nanoribbons, coiled-coil/rod-coil nanostructures, nanoparticles, vesicles/ spherical structures, sheets, etc. [131]

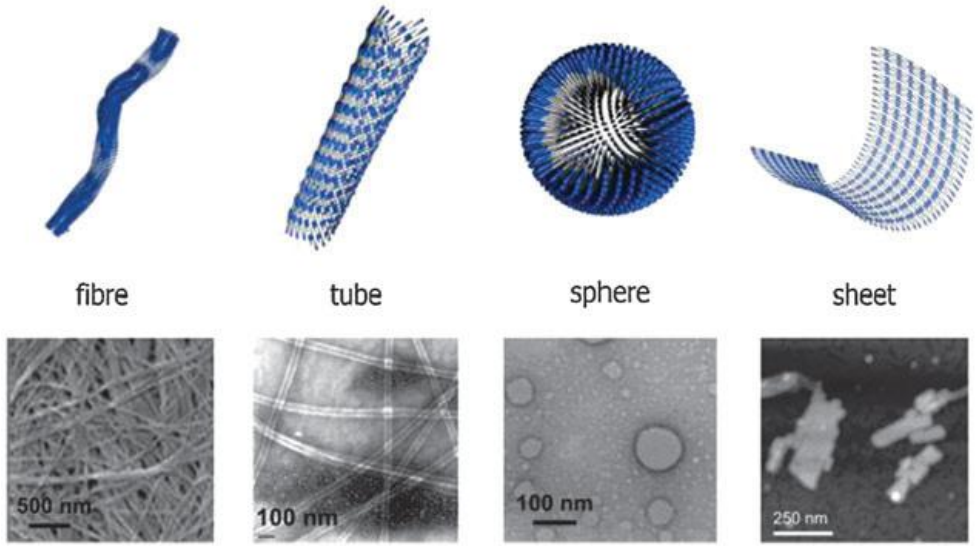

Figure 1.8 Different types of nanostructure formed via peptide self-assembly. (reprinted with permission from ref 132)

1.8.1 Classification of Peptide self-assemblies

The nature and sequence of amino acids in the primary structure of peptides govern their next level organization i.e. the secondary structure of peptides. These secondary structures can be of different types including β-sheets, β-hairpin, β-turns, α-helix, coiled coils. Based on the secondary structures formed, the self-assembling peptides can be majorly classified into following types:

1.8.1a Alpha helix Peptides (α-helix):

The α-helix is one of the main structural domains occurring in natural proteins. [137] In α-helix conformation, the molecules are spirally arranged and the right handed-helix are stabilized by intramolecular hydrogen bonds in the backbone between carbonyl group and amide hydrogen of fourth amino acid residue further along the chain (i, i+4). [138] Each turn of α-helix is composed of 3.6 amino acid residues. The α-helix backbone H-bonds are slightly weaker than those found in β-sheets, owing to their high exposure to surrounding water molecules and easy interaction with them. This is the reason, why α-helix motifs are located in the hydrophobic environments, in a cell and are unstable upon isolation. The intrinsic thermodynamic instability of α-helix in aqueous environment is due to its ability to form H-bonds with the water molecules, making it difficult for a single α-helix molecule to exist, as a stable self-assembling biomaterial. [139] However, the stability of α-helix provides a challenge to the researchers, because the stability of such peptides is also important for their active conformation and is essential for its target binding efficiency. Furthermore, it was identified that the intertwined structures of two or more α-helices formed very stable structures, which were termed as coiled coil structures. The design of typical coiled coil structure is based on the heptad (abcdefg) repeats of polar and hydrophobic amino acid residues. A heterodimer of two α-helices formed by coiled-coil interactions assembles into long (more than 10μm) and thick fibers (diameter of ~40-80nm). [140, 141]

Many natural materials such as α-keratin, myosin, collagen, etc are found to be rich in helical structural arrangement. Likewise, several synthetic helical polypeptides have been discovered as self-assembling systems to create diverse functionalities and among all *de novo* design principles, the coiled coil structure based α-helices were extensively explored. [142, 143] In this context, Woolfson and his group had carried out pioneering work to understand the alpha-helices and coiled-coil protein design. [144] The design based on the "sticky-end" strategy was most common, which provides dangling ends to nucleate and facilitates further growth of the α-helical peptides in a uniaxial direction. Using this approach, Woolfson and co-workers reported the design of 28-residue peptides showing coiled coil structures and explored their self-assembling properties. [145, 146] In contrast to this, Hartgerink's group demonstrated the self-assembled coiled coil nanofibrillar structures without sticky ends, using a 21 residue peptide. [147] The literature suggested that the coiled coil systems have been also explored as temperature and pH sensitive carriers to control the delivery of encapsulated molecules. [148] The available reports suggested that such sticky-ended long peptide self-assemblies have been also explored

to develop collagen mimetic peptides that can form hydrogels and other biomaterials. [149] Recently, caged structures from coiled-coil peptide modules were developed from Woolfsen's laboratory, which could potentially application as delivery vehicles for bioactive molecules. [150] So far, only long peptide sequences have been explored for designing self-assembled helical nanostructures to develop a range of functional materials. However, recent investigations revealed that ultra-short peptide sequences are also capable of assembling into diverse nanostructures through similar helical conformations that can have promising pharmaceutical and biotechnological implications.

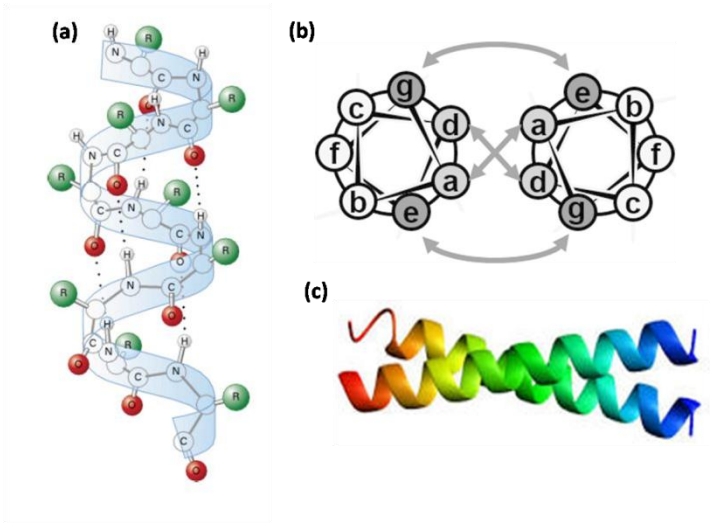

Figure 1.9 *Representative images of (a) α-helix arrangement of peptide through H-bonding, (b) helical wheel of a parallel coiled-coil showing heptad repeat residues and hydrophobic interactions between a and d as indicated by arrows and electrostatic interactions between e and g, (c) classic example of coiled coil α-helix structure.(taken from ref 148 and 151)*

Beta-sheet peptides (β-sheet):

β-sheets are widely occurring and most well studied protein/peptide self-assembling systems. Unlike α-helices, the H-bonding is formed between the residues in space rather than in the same peptide sequence i.e. the intermolecular H-bonding is formed. These interactions bring different regions of a sequence or different peptide chains close to form β-sheet structures. [152] Each peptide sequence is termed as β-strands. β-sheets are composed of laterally joined β- strands, by at least two or three backbone hydrogen bonds, which generally forms a twisted, pleated sheet. The pleated appearance of β-strands emerges due to tetrahedral bonding pattern at the C^{α} atom which reduces the distance between C^{α} i and C^{α}

i + 2 to be ~6 Å , rather than the 7.6 Å that is the expected distance between two fully extended trans peptides. Depending upon the alignment of the strands, these β-sheets can be classified into two types: parallel and anti-parallel. When all the β-strands are aligned in the same direction, for example, N- to C- terminal, they form parallel β-sheets and when the strands are arranged in opposite direction, then form antiparallel β-sheets. Additionally, electrostatic interactions between the alternating charged residues on the two strands further stabilizes the β-sheet structures. [153, 154]

Zhang et al. first demonstrated the self-assembly of synthetic peptides into fibrous nanostructures. They developed a class of oligopeptides with alternating hydrophobic and hydrophilic amino acid residue, which forms β-sheet rich nanofibers in aqueous solution. The designed peptide sequence Ac-AEAEAKAKAEAEAKAK (AEAK16) consists of complementary ionic residues, which have a strong tendency to interact with each other giving rise to β-sheets. [155, 156] The self-assembly is also stabilized by the hydrophobic effect of aqueous environment, which promotes the burying of hydrophobic residues between the hydrophobic surface of two peptide strands. [157] This class of peptides was later referred to as "Peptide Lego" by Zhang that involves the complementary interactions in the design. These β-sheets further stack together to form peptide fibers. [158, 159] The substitution of E with D and K with R, resulted into RADA-16 peptides, which may have two or more repeating units. The peptide based hydrogels were highly biocompatible and well supported the mammalian cell attachment, proliferation, migration and differentiation. [160] Both, AEAK16 and RADA16 peptides assumed to have antiparallel β-sheet arrangement, owing to repulsive electrostatic interactions in parallel arrangement. Among different RADA peptides, RADA16-I (with 4 repeating units) is commercially available as 'Puramatrix', an artificial substitute of natural ECM. [161, 162]

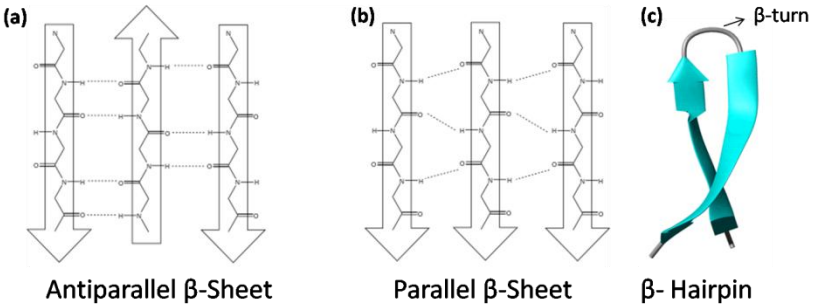

Figure 1.10 *Representative diagram of β-sheet arrangement showing (a) anti-parallel configuration, (b) parallel configuration and (c) β-hairpin structure with β-turn. (taken from ref 163)*

Beta- hairpin peptides:

β-hairpins represent another class of secondary structures of peptides, which are formed two when anti-parallel strands are linked by a short peptide sequence of 2-4 amino acids. The connecting loop between two strands is called as β-turns. The structure looks like hairpin and composed of β-strands that is why they are named as β-hairpins. [164] The length of these turns or loops can be variable and plays an important role in determining the 3D structures of protein or some specific function. Pochan and Schneider have extensively studied the self-assembly of β-hairpin forming peptides. In 2002, they first developed the MAX1 peptide (H_2N-VKVKVKVK^{D}PPTKVKVKVKV-$CONH_2$) with repeating units of valine (V) and lysine (K) residues along with intermittent tetrapeptide (-V^{D}PPT-), adopted to form type II-turns, where ^{D}P is the D isomer of proline. This peptide has the tendency to form random coils, when dissolved in water, but folded into β-hairpin structure in the presence of salts of Dulbecco's modified Eagle's medium (DMEM), a cell culture medium. The addition of salts or increased pH reduces the electrostatic repulsion between lysine residues and enhances intermolecular hydrogen bonds between the two peptide arms. [165, 166] Since then, several variants of MAX1 have been reported, which demonstrates the effects of hydrophobic and hydrophilic residue substitution on their self-assembly. [167,168] One such example includes MAX8, which is formed by the replacement of one lysine residue with glutamate that showed faster self-assembly at lower pH than MAX1 peptides, due to reduced repulsive positive charges. Both MAX1 and MAX8 peptides showed the propensity to form hydrogels in the presence of cell culture media and have potential applications in the field of biomedicine. [168]

Peptide amphiphiles:

Peptide amphiphiles (PA) represents class molecules designed with balanced hydrophobic and hydrophilic character and have self-assembling properties. Typically, a peptide amphiphile contains a distinct hydrophobic and hydrophilic region, similar to lipids or surfactants structure. A hydrophobic region may be composed of non-polar, aromatic amino acids or alkyl, acyl, lipidic tails, while hydrophilic region is composed of polar amino acids. [169, 170] The self-assembled structures formed from Pas include micelles, nanofibers, nanotubes, nanorods, and bilayers, which are stabilized by different non-covalent interactions such as hydrophobic, π-π

stacking, electrostatic or hydrogen bonding interactions. PAs assembles similar to lipid molecules, aligning hydrophobic tails inwards, which minimizes the exposure towards water. The self-assembly occurs only when the concentration of peptides increases above critical aggregation concentration. [171, 172]

In 1995, Tirrell et al. first proposed the design of PA which self-assembled into monolayer structures. These monolayers act as models for the investigation of membranes containing functional proteins. [173] Since then, wide variety of PA's has been explored to access diverse nanostructures for biomedical applications. [174] Stupp and Hartgerink proposed the design of PA, which consists of three different segments: a hydrophobic tail, a β-sheet forming peptide and hydrophilic peptide moiety which increases the solubility of whole molecule in water. [175, 176] These PA organizes in the form of cylindrical micelles by the participation of hydrogen bonds between β-sheet peptide region and hydrophobic interactions between hydrophobic alkyl tails. The free peptide ends are exposed at the surface of nanofibers in high density, which can be easily bio-functionalized. In the similar context, Stupp et al. reported an excellent example of lipidated PA composed of 5 different regions. A 16-carbon alkyl chain at N-terminal acts as a hydrophobic part, the second segment is composed of four cysteine residues that provide oxidative polymerization site via disulphide bonds. [176, 177] It is further attached to flexible linker of three glycine residues, followed by a phosphorylated serine that aids calcium binding or biomineralization. At last, a cell-targeting RGD motif is attached at the C-terminal end. This is a classical example for designing a PA intending for specific applications.

Although the structure of peptide amphiphiles resembles the surfactants, but their self-assembly mechanism greatly varies, due to the involvement of H-bonding. In general, the solubility of these peptide amphiphiles depends upon the number of hydrophobic amino acid residues in the tail group, as on increasing the number of residues result in reduced solubility and lesser propensity to aggregate. [178] However, the hydrophilic lipophilic balance can be adjusted by varying the number of polar amino acid residues in the head group leading to different nanostructures. [171] In a similar line, a study reported by Koutsopoulos' group showed the formation of nanovesicles using positively charged PA while, clusters of nanovesicles observed with negatively charged PA, which are arranged in necklace-like pattern, upon drying. The reason for rearrangement of nanostructures was that initially the vesicles are loosely bound in clustered form while, quick drying caused disassembly of clusters, and arrangement of nanovesicles in the form of necklace, on the negatively charged surface of mica. [179] Similarly, Zhang's group reported another series of PA composed of 1-2 residues of lysine or histidine

attached to A_6, V_6, or L_6 sequences, which showed the presence of nanotubes and nanovesicles, dependent on the pI (isoelectric pH). These nanostructures further self assemble to form membranous sheet like structures. [180] In the similar line, Hamley and coworkers explored the self-assembly of A_6R for antimicrobial activity and A_6RGD as a scaffold with cell adhesion motif. In last two decades, a plethora of such PA and their self-assembling properties have been reported, intended for different applications. [181, 182]

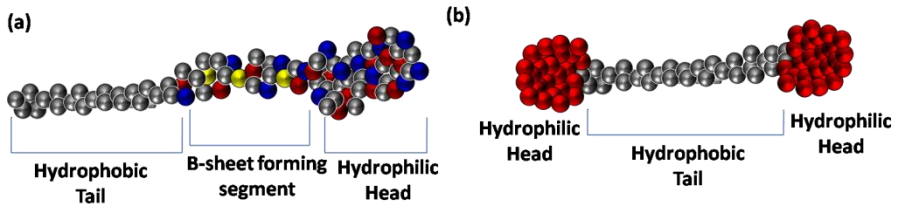

Figure 1.11 *Representative diagram depicting the structure of (a) peptide amphiphile and (b) peptide bolaamphiphile with hydrophilic and hydrophobic segments. (adapted from ref 176,183)*

Bola-amphiphiles

Bola-amphiphiles comprises another class of peptides in which a hydrophobic tail is attached to two hydrophilic tails. Peptide based bola-amphiphiles are less explored than other amphiphiles. In 1996, Shimizu et al. reported the fabrication of nanotubular assemblies using oligopeptide bola-amphiphiles and further used them for encapsulating vesicles. [184] The self-assembly was facilitated by two oligo-glycine head groups. Later, in 2000, Matsui followed a similar strategy and demonstrated the pH driven self-assembly of bis (N-α-amidoglycylglycine)-1.7-heptane bola-amphiphile into helical ribbons. [185] Recently, Das and co-workers illustrated the solvent polarity dependent morphogenesis of peptide bola-amphiphile. The design incorporates the PDI (perylene-diimide) as hydrophobic group and diphenylalanine sequence attached to two imide positions of PDI supporting π-stacking. These PA molecules assemble into wide range of morphologies such as nanofibers, nanorings, nanocups and hollow spheres, in the presence of different solvents. [186, 187]

Short aromatic Peptides:

In recent years, short aromatic peptides have attained great interest and developed as a broad class of self-assembling peptides. The reason for special interest in such peptide based nano-assemblies is their short length, relatively easy and cheap synthesis, high biocompatibility and

accessibility to diverse nanostructures. As the name suggests, the aromatic π-π interactions are the major driving force for the self-assembly of aromatic peptides and in turn, affects the gelation properties of the peptides. [188, 189] These peptides are usually composed of aromatic amino acids like phenylalanine (F), tyrosine (Y), tryptophan (W) or aromatic protecting groups such as fluorenylmethoxycarbonyl (Fmoc), naphthyl, pyrene, etc. [190] Reches and Gazit, firstly identified FF (diphenylalanine) as the shortest self-assembling peptide having propensity to form ordered structures such as nanotubes. These nanotubes extend upto micro-scale length and have remarkable mechanical strength. [191] Their high biocompatibility and good chemical and thermal stability demonstrate the potential to be developed as biosensors. After this, the gelation properties were studied using Fmoc-FF, which was recognized as the smallest structural unit of amyloid-like peptides. These gels were then investigated for biocompatibility for their exploration as cell culture scaffolds.

Since then, a lot of work has been done in the field of short aromatic peptides. Ulijn and co-workers extensively studied the self-assembly of short aromatic peptides including Fmoc FF. In the last decade, several aromatic short peptide analogues were created by simple alterations in the sequences. [189,190] Recently, Ulijn et al. proposed dynamic peptide libraries using combinatorial space for the discovery of self-assembling structures. Such study could be possible because of the small number of amino acids present in the short peptides, which otherwise would be difficult to explore with long chain peptides. [192] Xu et al. have also explored the potential of aromatic interactions in designing variety of supramolecular materials to a great extent. They showed the formation of different nanostructures from same peptides. [193, 194] Bing Xu's group demonstrated role of aromatic-aromatic interactions in the transition of α-helix to β-sheet conformation, upon mixing of two pentapeptides. It was the first report, which showed the biomimetic approach to generate peptide nanofibers with particular secondary structure through conformational restriction of peptide secondary structures by the involvement of aromatic-aromatic interactions. [195] The self-assembly process and mechanical properties of peptide hydrogels can be controlled by various factors such as pH, temperature, solvent, etc. The tunable properties of short aromatic peptide hydrogels are highly useful to tailor their properties in accordance with intended applications. [196]

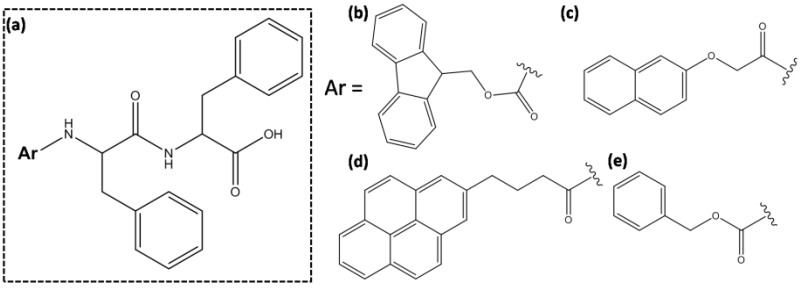

Figure 1.12: Classical example of shortest aromatic peptide (a) Diphenylalanine with aromatic moiety attached N-terminal end and few examples of commonly used aromatic moieties like (b) Fluorenylmethoxycarbonyl (Fmoc), (c) 2- Napthoxy acetic acid (Nap), (d) 2- Pyrene butyric acid (Pyr) and (e) Caboxybenzyl (Cbz). (adapted from ref 190)

Amyloid Peptides

Amyloid fibrils are the crucial example of natural protein self-assembly resulting into nano-fibrillar structures. The formation and accumulation of amyloid fibrils are indicative of various pathological conditions such as Alzheimer's disease, Parkinson's diseases, type II diabetes, and many others. [197,198] Amyloid fibrils are formed by polypeptides having 30-40 amino acid residues or longer and are characterized by β-sheet conformations. Aβ is the amyloid beta peptide, present as major component of the pathogenesis of Alzheimer's disease. [199-201] The Aβ typically varies in length ranging from 37-49 amino acid residues, among which sequence with 42 amino acid residues i.e. $A\beta_{42}$ is the most common isoform. The studies in the past decade have shown that short peptides such as tetra- to hexapeptides can form nano-fibrillar structures, which have biophysical and structural properties similar to that of amyloid fibrils. [202] These synthetic short peptides can be used as model system for studying the mechanism of biological self-assembly processes and generation of amyloid structures. Several functional peptide sequences inspired from various amyloidogenic peptides associated with pathological conditions, including FGAIL (from type II diabetes), KLVFF, KLVFFAE (from Alzheimer's disease), NFGSVQFV (Aortic medial amyloid), PPQGGYQQYN (Yeast prion protein), PHGGGWGQ (Creutzfeldt-Jakob disease) and many more have been explored. [203] To get the deeper insight into the mechanism of amyloid fibril formation, the minimum peptide fragments i.e. dipeptides were widely investigated. Although the exact mechanism of amyloid aggregation is unclear, the investigation of naturally formed amyloid plaques revealed that aromatic residues play a crucial role in the formation of amyloid fibrils. Diphenyalanine (FF) is identified as the

core motif of Alzheimer's β-amyloid peptide. [204] Therefore, FF is the basic sequence incorporated in the design of most of the self-assembling amyloid like-peptides.

1.9 Strategies to control self-assembly:

It has been known that subtle changes in the molecular structure of the gelator i.e. conventional route, alone are not sufficient for the formation of self-assembled structures. However, the choice of suitable gelation method is very crucial to trigger the nucleation and growth of self-assembled nanostructures, which is also termed as non-conventional route. Gel formation occurs when soluble state transformed into insoluble organized structures entrapping water in their nanofibrous network. Several ways have been adopted to induce self-assembly into gelator molecules. Some of the commonly used methods are as follows:

1. **Temperature triggered gelation:**

   Temperature tends to increase the solubility of the gelator in the solution, which otherwise was not easily soluble due to its hydrophobic nature. As the temperature is decreased, the solubility is reduced, promoting interactions between gelator molecules. The self-assembly is driven by the non-covalent interactions between the gelator molecules. Temperature-triggered gelation of Fmoc-based low molecular weight gelators (LMWG) was firstly reported by Vegners *et al.* in 1995. [205] The peptide (Fmoc-LD and analogues) was dissolved at high temperature (~100^0C) and cooled to below 60^0C, resulting into viscoelastic gel. Later, Das's group used temperature triggers to explore the hydrogelation property of cationic peptide amphiphiles with respect to their structural aspects as well as their gelation mechanism. [206, 207] The similar group further reported the class of antibacterial hydrogelators based on Fmoc-capped cationic amphiphiles, which showed gelation by heat-cool method. [208] Although, the heat-cool cycle process is common in literature to demonstrate the thermo-responsive behavior of gels, but it is less explored to induce gelation of peptide amphiphiles. However, use of temperature is more common in inducing gelation of polymeric materials such as gelatin. The temperature required gel formation and melting temperatures is also affected by the solvent environment.

2. **Solvent mediated gelation:**

   The hydrophobic component of LMWG imparts lower aqueous solubility to the gelators even at low concentrations, thus hinders their self-assembly. Solubilizing the hydrophobic peptide gelator in suitable solvent, followed by addition of poorly soluble

solvent can be an effective approach to overcome the solubility issues of hydrophobic peptides. The change in polarity of solvent promotes gelator-gelator interactions through various non covalent interactions to reduce exposure to the aqueous solvent and triggers self-assembly resulting in nanofibrillar structures. The solvent mediated approach has become one of the popular methods of gelation for short aromatic peptides due to the ease of preparation, since it involves little or no mixing of gelator in solvents, as reported in many cases in literature. In this direction, Mahler et al. first time demonstrated the solvent mediated approach to control the self-assembly of Fmoc-FF peptide. They dissolved Fmoc FF in water-miscible organic solvent and further diluted it with water, which leads to the formation of one-dimensional fibrillar structures transforming peptide solution to supramolecular gels. [208] Similar solvent triggered gelation approach was used by Adams group to demonstrate the role of solvent selection on the hydrogelation process and final gel phase properties. [209] The literature also suggests that solvent mediated approach results in quick gelation in comparison to other assembly methods.

3. **pH triggered gelation:**

Perhaps the pH triggered gelation is the most widely studied method of inducing self-assembly in LMWG. Mostly, the short aromatic peptides are covalently attached to hydrophobic groups at N-terminal, leaving the C-terminal free for deprotonation at higher pH, which results in highly soluble charged species. The solubility of these charged species decreases with the decrease in pH leading to self-assembly of the gelator. [210, 211] The pH triggered gelation is useful for the assembly of peptides containing charged amino acids. The solubility of charged peptides is dependent on the pH and imparts them inherent pH sensitivity. It has been reported by several groups that gelation occurs only when the pH of the solution is lowered than the pKa of the C-termini of these molecules. At the same time, it was also found that the pKa values of hydrophobically modified peptides are significantly higher than the corresponding unmodified dipeptides. [212, 213] To this direction, a report by Adams group demonstrated that the pKa values are related to the overall hydrophobicity of the gelator and most hydrophobic molecules exhibited the highest pKa values. [214] Therefore, changing the amino acid or an aromatic substituent can alter the hydrophobicity of the molecule and thus their pKa.

The literature suggests that most of the researchers used hydrochloric acid (HCl) as a trigger for the self-assembly of LMWG. In this context, Yang *et al*. first prepared the

library of naphthalene conjugated dipeptides and studied their gelation properties by initially dissolving them in NaOH (1N) and then adjusting the pH by adding HCl (1N) until a clear transparent gel was formed. The pH of the resulting gels was measured to be ~2. [215] Extensive studies were carried out by Ulijn *et al*. to understand the self-assembly mechanism of Fmoc FF in a pH triggered system. [212] They showed the dramatic pKa shifts of Fmoc FF which is reflected at the macroscopic as well as microscopic level. It has been found that Fmoc FF has the highest pKa value of ~9.9, which is the highest pKa value for any gelator and it can be dissolved above that pH only. However, Fmoc group is base labile and is unstable at high pH, but is stable at physiological pH. Therefore, gradually reducing the pH of Fmoc FF solution (by adding HCl) showed transformation from gel to viscous solution and further to precipitate, accompanied by conversion of flexible nanofibrillar structure to flat rigid ribbon like structures, at intermediate pH values.

The rate of pH change is critical because hydrogelation is a kinetically favored process. Generally, the slower pH change is likely to result in more ordered structures due to sufficient time provided for equilibration. Notably, Adams and coworkers demonstrated an alternative for adjusting pH that results into more reproducible hydrogels. They used of glucono-δ-lactone (GdL) instead of HCl, to adjust the pH of library of naphthalene-dipeptide based hydrogelators. [216] Another advantage of using this method is that it does not require shear force, which can often alter the gelation process and affects the final properties of the hydrogels.

Moreover, the pH switch can also be a convenient way to control the morphology of the self-assembled structures. A report by Kaler et al. elucidated the pH induced structural transitions of the self-assembling mixtures of amino acid lysine and anionic surfactants. The fibrillar structures are transformed into worm-like micelles when the acid concentration exceeds the equimolar value of lysine. [217] Similarly, Hassan's group showed the formation of long worm like assemblies, which are evolved from globular micellar structures. The reason for such transformation was the reduction of surface charge of micelles at higher pH. [218]

4. Salt/Metal ion induced gelation

The idea of using metal ions or salts to stabilize and functionalize proteins and peptides is evolved from nature. [219] Peptides have amino as well as carboxylic terminals which upon protonation or deprotonation interacts with oppositely charged metal ions or salts that provide structural stability and promotes self-assembly. These salts screen the

repulsive forces of charges and enhance cross-linking between less ordered structures to form highly ordered nanofibrillar networks. [220] In the series of β-hairpin peptides, Schneider *et al*. reported a 20 residue peptide having negatively charged non-natural amino acid which promotes metal binding affinity of the peptide. In the absence of Zn^{2+} ion, the protein remains in unfolded soluble state and subsequently self-assembles into a β-sheet rich fibrillar structure in a moderately rigid viscoelastic hydrogel. The 1:1 binding of Zn^{2+} and peptide was confirmed by various spectroscopic analyses. [221] The same group reports another peptide from a β-hairpin, MBHP, which showed affinity to a wide range of metal ions including Pb^{2+}, Pb^{2+}, Cd^{2+} and Hg^{2+}. [222]

A significant difference can be observed in the self-assembling properties of peptides in the presence of salts due to involvement of ionic bonding and alteration in ionic strength of the system. [223] The reports from P. K. Das's group showed the gelation of naphthalene based dipeptides in response to pH change from 11 to 4, but they showed gelation even at pH 11 in the presence of number of salts (Mg^{2+}, Ca^{2+}, Na^{+}, Li^{+}, K^{+} and NH^{4+}). It was assumed that gelation was proceeded by the formation of salt-bridges between carboxylate groups and metal ions that promotes cross-linking of micellar structures into a three dimensional network. [224-227] Similarly, Lauffenburger et al. showed the gelation of the biomimetic sequence (KFE12) at physiological pH as well as in the presence of salts. MAX1 peptide is another example showing the formation of differential secondary structures in the influence of salts. They tend to form random coil structures at physiological pH (7.4) but addition of salt to the solution leads to the formation of β-sheet rich self-assembled structures. [228]

The metal ions were not only used to induce gelation but it was also used to alter the mechanical and structural properties of self-assembled structures. The metals ions help in strengthening the cross-linking between the nano-fibers and thus can improve the mechanical properties of the hydrogels. [229] Xu *et al*. tailored the elasticity of the resulting supramolecular gels by up to five orders of magnitude by the addition of Ca^{2+} ions. The enhanced mechanical strength was the outcome of combined aromatic and electrostatic interactions. [230] A very recent report by our group showed the systematic study to highlight the importance of metal ions in controlling the supramolecular structures of ultra short peptides. In this study, histidine based dipeptide design was used to demonstrate the effect of metal binding on the mechanical properties and nano-architecture of the self-assembled systems, which can be often accompanied by gel-sol transition. [231] The studies showed that addition of salt can be a feasible method to tune

the mechanical properties of the soft nanomaterials for various biomedical and biotechnological applications.

5. Enzymatic gelation

In nature, the role of enzymes in self-assembly of biomolecules is the foundation of life and inspiration for designing synthetic self-assembling systems capable of forming hydrogels by the enzymatic action. [232,233] Enzymatic processes hold potential opportunities for performing molecular self-assembly in aqueous systems with high selectivity and specificity, which makes the system more biocompatible and suitable for biomedical applications. The enzymes can trigger the self-assembly process in two ways i.e. by bond making or by bond breaking. Both the ways convert precursor to hydrogelator, which is capable to undergo self-assembly under physiological conditions. [234] The Xu's and Ulijn's group presents plenty of examples of hydrogelators, which undergo enzyme-instructed formation of nanofibrous networks leading to subsequent hydrogelation. [235, 236] A dipeptide was enzymatically coupled to Fmoc-Phe by the catalytic action of protease (thermolysin) to develop Fmoc-tripeptide. [236] The π-πinteractions of Fluorenyl groups drive the self-assembly of Fmoc-tripeptide resulting in higher ordered self-assembled structures. This approach offers a facile route to create a library of supramolecular peptide hydrogels via thermodynamic control of nanofiber formation, which can be used as scaffolds for tissue engineering application. [237] Unlike thermolysin, there are some enzymes which break bond to convert precursor into a hydrogelator. Phosphatases are one of the commonly used enzymes, which breaks the P-O bond of phosphate and converts it to corresponding alcohol group. In this class, most of the gelators reported have an attached tyrosine phosphate residue, which is freely soluble in buffer solution. Xu *et al.* utilized the alkaline phosphatase to catalyze the dephosphorylation of Fmoc-tyrosine phosphate, which yield Fmoc-tyrosine molecule that can self assemble into insoluble nanostructures. [238] In contrast to this, another enzyme protein kinase phosphorylates the alcohol groups to convert them into soluble phosphate ligated peptide analogues. This enzyme switch phosphatase /kinase in combination can be used in the detection of enzyme inhibitors. [239] This enzyme pair was used to control the sol-gel-sol transformation of naphthalene conjugated pentapeptides. This sol-gel conversion approach is useful for both *in vitro* as well as *in vivo* applications.

The enzymatic hydrogelation can be useful in many other ways such as the cleaved phosphate group entrapped in the gel matrix can be used for biomineralization.

Leeuwenburgh and co-workers added the calcium ions to the hydrogel, which combines with phosphate groups to form calcium phosphate. This additional species significantly enhances the mechanical stiffness and thermal stability of the hydrogel. [240] The enzymatic hydrogelation of LMWG peptides allows the tailoring of the functional properties of the hydrogels in response to specific biological conditions. The small size of peptides allows designing of β-peptides, which offers superior bio-stability over α-peptide and their enzymatic hydrogelation can be triggered inside the cell. One of the examples of *in situ* hydrogelation was shown by Xu *et al.* where precursor was converted into a hydrogelator by the action of endogenous esterase, which formed nanofibrous network inside the cell. Such action was exploited as a mechanism to kill cancerous cells. [241] Similar enzymatic control was applied to achieve the antibacterial action from a precursor peptide designed with a cephem nucleus flanked between Nap-FF hydrogelator and a hydrophilic group. The addition of b-lactamase opens the b-lactam ring and released the hydrogelator to form hydrogel inside the bacterial cells. [242]

1.10 Aims and objectives:

The ultimate aim of this thesis is to fabricate a series of bioactive functional scaffolds, which can be developed as efficient synthetic mimics of natural extracellular matrix (ECM) and can have potential implications in tissue engineering. The research work was carried out with following specific objectives:

1) Design and synthesis of self-assembling short, bioactive peptide sequences especially based on laminin and collagen proteins of ECM.
2) Exploring molecular self-assembly behavior of designed peptides via different pathways accessed by different triggers such as solvents, pH, temperature and presence of proteins, etc.
3) Tuning the physical and biochemical properties of hydrogel scaffolds by developing multi-component systems through co-assembly or co-operative assembly
4) Characterization of physicochemical properties of the hydrogels using various spectroscopic, microscopic, and rheological analyses.
5) Assessment of biological properties of designed bioactive hydrogels by studying biocompatibility, viability, adhesion, proliferation, and migration to identify their potential as scaffolds for cell culture applications.

1.11 References

1) R. Langer, J. P. Vacanti, Tissue engineering, *Science*, 260 (1993,) 920–926.

2) R. Lanza, R. Langer and J. P. Vacanti, *Principles of tissue engineering*, Academic Press (2011).

3) Patrick CW, Mikos AG, McIntire LV, editors. *Frontiers in tissue engineering*. Oxford: Pergamon, (1998).

4) L. G. Griffith, G. Naughton, Tissue Engineering: Current Challenges and Expanding Opportunities, *Science*, 295 (2002) 1009-1016.

5) H. Fernandes, L. Moroni, C. van Blitterswijka, J. de Boer, Extracellular matrix and tissue engineering applications, *J. Mater. Chem.* 19 (2009) 5474–5484.

6) F. Rosso, A. Giordano, M. Barbarisi, A. Barbarisi, From cell-ECM interactions to tissue engineering. *J Cell Physiol* 199 (2004) 174–80.

7) G. Abatangelo, P. Brun, M. Radice, R. Cortivo, M. K. H. Auth MKH. Tissue engineering, In: Barbucci R, editor. *Integrated biomaterial science*, NewYork, Kluwer Academic (2001) 885–945.

8) J. L. Guo, Y. S. Kim, A. G. Mikos, Biomacromolecules for Tissue Engineering: Emerging Biomimetic Strategies, *Biomacromolecules*, 20 (2019) 2904−2912.

9) F. J. Brien, Biomaterials & scaffolds for tissue engineering. *Mater Today*, 14 (2011) 88-95.

10) B. P. Chan, K.W. Leong, Scaffolding in tissue engineering: general approaches and tissue-specific considerations. *Eur Spine J.* 17 (2008) 467-79.

11) J. A. Hubbell, Biomaterials in Tissue Engineering, Biotechnology, 13 (1995) 565-576.

12) M. P. Lutolf, J. A. Hubbell, Synthetic biomaterials as instructive extracellular microenvironments for morphogenesis in tissue engineering, *Nat. Biotech*. 23 (2005) 47-55.

13) E. S. Place, N. D. Evans, M. M. Stevens, Complexity in biomaterials for tissue engineering, nature materials, *Nat. Mater*. 8 (2009) 457-470.

14) A. Khademhosseini, R. Langer, A decade of progress in tissue engineering. Nat *Protoc* 11 (2016) 1775–1781.

15) B. Bakhshandeh, P. Zarrintaj, M. O. Oftadeh, F. Keramati, H. Fouladiha, S. Sohrabi-jahromi, Z. Ziraksaz, Tissue engineering; strategies, tissues, and biomaterials, *Biotech. Gen. Eng. Rev*. 33 (2017) 144-172.

16) K. Y. Lee, D. J. Mooney, Hydrogels for Tissue Engineering, *Chem. Rev.* 101 (2001), 1869-1880.

17) D. L. Kusindarta, H. Wihadmadyatami, The Role of Extracellular Matrix in Tissue Regeneration, *Tissue Regeneration*, Hussein Abdel hay El-Sayed Kaoud, IntechOpen, (2018).

18) B-S. Kima, I-K. Parkb, T. Hoshibac, H-L. Jiangd, Y-J. Choie, T. Akaikef, C-S. Cho, Design of artificial extracellular matrices for tissue engineering, *Prog. Polym. Sci*. 36 (2011) 238–268.

19) H. K. Kleinman, D. Philp, M. P. Hoffman, Role of the extracellular matrix in morphogenesis. *Curr Opin Biotechnol,* 14 (2003) 526-532.

20) D. W. L. Hukins, S. A. Weston, M. J. Humphries, A. J. Freemont, *Extracellular matrix. In Principles of Medical Biology,* Elsevier, 3 (1996) 181-232.

21) T. Kreis, R. Vale, Guidebook to the Extracellular Matrix, Anchor, and Adhesion Proteins, 2nd ed. A Sambrook & Tooze Publication at Oxford University Press: New York, (1999).

22) F. Gattazzo, A. Urciuolo, P. Bonald, Extracellular matrix: A dynamic microenvironment for stem cell niche, Biochim. Biophys. Acta - General Subjects, 1840 (2014) 2506-2519.

23) S.F. Badylak, The extracellular matrix as a biologic scaffold material. Biomaterials 28 (2007) 3587-3593.

24) B. Yue, Biology of the Extracellular Matrix: An Overview, J Glaucoma. (2014) S20–S23

25) P. D. Yurchenco, D. E. Birk, R. P. Mecham, Extracellular Matrix Assembly and Structure, 1st Edition, Academic Press, (1994).

26) A. D. TheocharisaSpyros, S. S. C. Gialeli, N. K. Karamanos, Extracellular matrix structure, *Adv. Drug Deliv. Rev*. 97 (2016) 4-27.

27) J. Halper, M. Kjaer, Basic Components of Connective Tissues and Extracellular Matrix: Elastin, Fibrillin, Fibulins, Fibrinogen, Fibronectin, Laminin, Tenascins and Thrombospondins, In: Halper J. (eds) Progress in Heritable Soft Connective Tissue Diseases. *Advances in Experimental Medicine and Biology*, 802 (2014) Springer, Dordrecht.

28) G. Plopper, The extracellular matrix and cell adhesion. In Cells, B. Lewin, L. Cassimeris, V. R. Lingappa, G. Plopper, Eds. Jones and Bartlett Publishers: London, (2007) 645-702.

29) K. von der Mark, L. Sorokin, (ed.) Adhesive glycoproteins, Wiley-Liss, New York, 293-328 (2002).

30) J. Rossert, B. de Crombrugghe, P. B. John, G. R. Lawrence, A. R. Gideon, Type I Collagen: Structure, Synthesis, and Regulation, Principles of Bone Biology, Academic Press, San Diego, (2002).

31) M. D. Shoulders, R.T. Raines, Collagen structure and stability. *Annu Rev Biochem* 78 (2009) 929-958.

32) K. E. Kubow, R. Vukmirovic, L. Zhe, E. Klotzsch, M. L. Smith, D. Gourdon, S. Luna & V. Vogel, Mechanical forces regulate the interactions of fibronectin and collagen I in extracellular matrix. *Nat Commun* 6 (2015), 8026.

33) E. Ruoslahti, Fibronectin and its receptors. Ann. Rev. Biochem. 57 (1988) 375-413.

34) J. R. Potts, I. D Campbell, Fibronectin structure and assembly. *Curr. Op. Cell Biol*. 6, (1994) 648-655.

35) S. Früh, I. Schoen, J. Ries, V. Vogel, Molecular architecture of native fibronectin fibrils. *Nat Commun* 6 (2015) 7275.

36) E. Hohenester, P. D. Yurchenco, Laminins in basement membrane assembly, Cell Adhesion & Migration, 7 (2013) 56-63.

37) A. Faissner, J. Reinhard, The extracellular matrix compartment of neural stem and glial progenitor cells, *Glia*, 63 (2015) 1330-1349.

38) R. Nishiuchi, J. Takagi, M. Hayashi, H. Ido, Y. Yagi, N. Sanzen T. Tsuji M. Yamada, K. Sekiguchi, Ligand-binding specificities of laminin-binding integrins: a comprehensive survey of laminin-integrin interactions using recombinant alpha3beta1, alpha6beta1, alpha7beta1 and alpha6beta4 integrins. *Matrix Biol* 25 (2006) 189-197.

39) F.M., Watt, Role of integrins in regulating epidermal adhesion, growth and differentiation. *Embo J.* 21 (2002) 3919-3926.

40) V. Givant-Horwitz, B. Davidson, R. Reich, Laminin-induced signaling in tumor cells. *Cancer Lett* 223 (2005). 1-10.

41) M. Gonzales, K. Haan, S. E. Baker, M. Fitchmun, I. Todorov, S. Weitzman, J. C.R. Jones, A cell signal pathway involving laminin-5, alpha3beta1 integrin, and mitogen-activated protein kinase can regulate epithelial cell proliferation. *Mol Biol Cell* 10 (1999) 259-270.

42) E. Hintermann, V. Quaranta, Epithelial cell motility on laminin-5: regulation by matrix assembly, proteolysis, integrins and erbB receptors. *Matrix Biol* 23 (2004) 75-85.

43) D. L. Kusindarta, H. Wihadmadyatami, The Role of Extracellular Matrix in Tissue Regeneration, In: *Tissue Regeneration,* Ed. By H. A. hay El-Sayed Kaoud, IntechOpen (2018).

44) G. E. Wnek, G. L. Bowlin, *Encyclopedia of biomaterials and biomedical engineering*. Marcel Dekker, Inc.: New York, 1 (2004) 89-90.

45) B. M. Sicari, R. Londono, S. F. Badylak, Extracellular Matrix as a Bioscaffold for Tissue Engineering, C. V. Blitterswijk, P. Thomsen, A. Lindahl, J. Hubbell, D.F. Williams, R. Cancedda, J.D.d. Bruijn, J. Sohier (Eds.), *Tissue Engineering*, Academic Press, Burlington (2008), 121-143.

46) H. Geckil, F. Xu, X. Zhang, S-J Moon, U. Demirci, Engineering hydrogels as extracellular matrix mimics, *Nanomedicine* (Lond). 5(2010) 469–484.

47) M. W. Tibbitt, K. S. Anseth, Hydrogels as Extracellular Matrix Mimics for 3D Cell Culture, *Biotechnol Bioeng*. 103(2009) 655–663.

48) C. D. Spice, Hydrogel scaffolds for tissue engineering: the importance of polymer choice, *Polym. Chem*. 11 (2020) 184–219.

49) G.S. Hussey, J. L. Dziki, S.F. Badylak, Extracellular matrix-based materials for regenerative medicine. *Nat. Rev. Mater*. 3 (2018) 159–173.

50) E.M. Ahmed, Hydrogel: Preparation, characterization, and applications: A review. *J. Adv. Res.* 6 (2015) 105–121.

51) M. Bahram, N. Mohseni, M. Moghtader, An Introduction to Hydrogels and Some Recent Applications, In: *Emerging Concepts in Analysis and Applications of Hydrogels*, Ed. By S. B. Majee, IntechOpen, (2016).

52) J. F. Mano, G. A. Silva, H. S. Azevedo, P. B. Malafaya, R. A. Sousa, S. S. Silva, L.F. Boesel, J. M. Oliveira, T. C. Santos, A. P. Marques, N. M. Neves, R. L. Reis, Natural origin biodegradable systems in tissue engineering and regenerative medicine: present status and some moving trends. *J. R. Soc. Interface*, 4, (2007), 999-1030.

53) M. S. Hahn, B. A. Teply, M. M. Stevens, S. M. Zeitels, R. Langer, R., Collagen composite hydrogels for vocal fold lamina propria restoration. *Biomaterials*, 27 (2006) 1104-1109.

54) J.A. Burdick, G.D. Prestwich, Hyaluronic acid hydrogels for biomedical applications. *Adv Mater* 23 (2011) H41-56.

55) T.A. Ahmed, E.V. Dare, M. Hincke, Fibrin: a versatile scaffold for tissue engineering applications. *Tissue Eng Part B Rev* 14, 199-215 (2008).

56) C.S. Hughes, L. M. Postovit, G. A. Lajoie, Matrigel: a complex protein mixture required for optimal growth of cell culture. *Proteomics* 10, (2010) 1886-1890.

57) J.A. Cadee, M. J. van Luyn, L. A. Brouwer, J. A. Plantinga, P. B. van Wachem, C. J. de Groot, W. den Otter W. E. Hennink, In vivo biocompatibility of dextran-based hydrogels. *J Biomed Mater Res* 50 (2000) 397-404.

58) A.S. Sawhney, C. P. Pathak, J. A. Hubbell, Bioerodible Hydrogels Based on Photopolymerized Poly(Ethylene Glycol)-Co-Poly(Alpha-Hydroxy Acid) Diacrylate Macromers. *Macromolecules* 26 (1993) 581-587.

59) P. Martens, K. S. Anseth, Characterization of hydrogels formed from acrylate modified poly(vinyl alcohol) macromers. *Polymer* 41 (2000) 7715-7722.

60) T.V. Chirila, I. J. Constable, J. G. Crawford, S. Vijayasekaran, D. E. Thompson, Y-C. Chen, W. A. Fletcher, B. J. Griffin, Poly(2-hydroxyethyl methacrylate) sponges as implant materials: in vivo and in vitro evaluation of cellular invasion. *Biomaterials* 14 (1993) 26-38.

61) N. Chirani, L. Yahia, L. Gritsch, F. L. Motta, S. Chirani, S. Faré, History and Applications of Hydrogels, *J. Biomed. Sci*. 4 (2015), 13-23.

62) J. Chena, X. Zoua, Self-assemble peptide biomaterials and their biomedical applications, *Bioactive Materials* 4 (2019) 120–131.

63) H. Park, K. Park, Hydrogels in bioapplications, In: Hydrogels and Biodegradable Polymers for Bioapplications, Ed. R. M. Ottenbrite, S. J Huang, K. Park, *ACS Symposium Series*; ACS Washington, (1996).

64) J. A. Hunt, R. Chen, T. van Veen, N. Bryan, Hydrogels for tissue engineering and regenerative medicine, J. Mater. Chem. B, 2 (2014) 5319–5338.

65) S. Fu, P. Ni, B. Wang, B. Chu, L. Zheng, F. Luo, J. Luo and Z. Qian, Injectable and thermo-sensitive PEG-PCL-PEG copolymer/collagen/n-HA hydrogel composite for guided bone regeneration, *Biomaterials*, 33 (2012) 4801-4809.

66) G. Hulsart-Billstr¨om, Q. Hu, K. Bergman, K. B. Jonsson, J. °Aberg, R. Tang, S. Larsson and J. Hilborn, Calcium phosphates compounds in conjunction with hydrogel as carrier for BMP-2: A study on ectopic bone formation in rats, *Acta Biomater*. 7 (2011) 3042-3049.

67) I. M. Khan, S. J. Gilbert, S. K. V. C. Duance and C. W. Archer, Cartilage integration: evaluation of the reasons for failure of integration during cartilage repair. A review. *Eur. Cells Mater*. 16 (2008) 26-39.

68) J. E. Jeon, K. Schrobback, D. W. Hutmacher and T. J. Klein, Dynamic compression improves biosynthesis of human zonal chondrocytes from osteoarthritis patients, *Osteoarthritis Cartilage*, 20 (2012) 906–915.

69) C. A. van Blitterswijk, *Tissue Engineering*, Academic Press, 1st edn, 2008.

70) J. Berger, M. Reist, J. M. Mayer, O. Felt and R. Gurny, Structure and interactions in covalently and ionically crosslinked chitosan hydrogels for biomedical applications, *Eur. J. Pharm. Biopharm*. 57 (2004) 35.

71) R. Jin, C. Hiemstra, Z. Zhong and J. Feijen, Enzyme-mediated fast in situ formation of hydrogels from dextran-tyramine conjugate, *Biomaterials*, 28 (2007) 2791-2800.

72) M. Kim, B. Hong, J. Lee, S. E. Kim, S. S. Kang, Y. H. Kim and G. Tae, Composite system of PLCL scaffold and heparin-based hydrogel for regeneration of partial-thickness cartilage defects, *Biomacromolecules*, 13, (2012) 2287-2298.

73) X. Hu, L. Ma, C. Wang and C. Gao, Gelatin hydrogel prepared by photo-initiated polymerization and loaded with TGF-beta1 for cartilage tissue engineering, *Macromol. Biosci*. 9 (2009) 1194-1201.

74) I. L. Kim, R. L. Mauck and J. A. Burdick, Hydrogel design for cartilage tissue engineering: a case study with hyaluronic acid, *Biomaterials*, 32 (2011) 8771-8782.

75) X. Li, E. Katsanevakis, X. Liu, N. Zhang and X. Wen, Engineering neural stem cell fates with hydrogel design for central nervous system regeneration, Prog. *Polym. Sci.* 37 (2012) 1105-1129.

76) J. M. Zuidema, M. M. Pap, D. B. Jaroch, F. A. Morrison and R. J. Gilbert, Fabrication and characterization of tunable polysaccharide hydrogel blends for neural repair, *Acta Biomater*. 7 (2011) 1634-1643.

77) T. C. Lim, W. S. Toh, L. S. Wang, M. Kurisawa and M. Spector, The effect of injectable gelatin-hydroxyphenylpropionic acid hydrogel matrices on the proliferation, migration, differentiation and oxidative stress resistance of adult neural stem cells, *Biomaterials*, 33 (2012) 3446-3455.

78) T. Y. Cheng, M. H. Chen, W. H. Chang, M. Y. Huang and T. W. Wang, Neural stem cells encapsulated in a functionalized self-assembling peptide hydrogel for brain tissue engineering, *Biomaterials*, 34 (2013) 2005-2016.

79) E. Y. Egawa, K. Kato, M. Hiraoka, T. Nakaji-Hirabayashi and H. Iwata, Enhanced proliferation *of neural stem cells in a collagen hydrogel incorporating engineered epidermal growth factor, Biomaterials*, 32 (2011) 4737-4743.

80) D. Gorapalli, A. Seth, J. Vournakis, C. Whyne, M. Akens, A. Zhang, M. Demcheva, E. Qamirani and A. Yee, Evaluation of a novel poly N-acetyl glucosamine (pGlcNAc) hydrogel for treatment of the degenerating intervertebral disc, *Life Sci*. 91 (2012) 1328-135.

81) J. Sun, Q. Zheng, Y. Wu, Y. Liu, X. Guo and W. Wu, Culture of nucleus pulposus cells from intervertebral disc on self-assembling KLD-12 peptide hydrogel scaffold, *Mater. Sci. Eng. C*, 30 (2010) 975.

82) E. C. Collin, S. Grad, D. I. Zeugolis, C. S. Vinatier, J. R. Clouet, J. J. Guicheux, P. Weiss, M. Alini and A. S. Pandit, An injectable vehicle for nucleus pulposus cell-based therapy, *Biomaterials*, 32 (2011) 2862-2870.

83) A. Joshi, G. Fussell, J. Thomas, A. Hsuan, A. Lowman, A. Karduna, E. Vresilovic and M. Marcolongo, Functional compressive mechanics of a PVA/PVP nucleus pulposus replacement, *Biomaterials*, 27 (2006) 176-184.

84) A. C. Borges, C. Eyholzer, F. Duc, P. E. Bourban, P. Tingaut, T. Zimmermann, D. P. Pioletti and J. A. E. M°anson, Nanofibrillated cellulose composite hydrogel for the replacement of the nucleus pulposus, *Acta Biomater*. 7 (2011) 3412-3421.

85) J. D. Thomas, G. Fussell, S. Sarkar, A. M. Lowman and M. Marcolongo, Synthesis and recovery characteristics of branched and grafted PNIPAAm-PEG hydrogels for the development of an injectable load-bearing nucleus pulposus replacement, *Acta Biomater*. 6 (2010) 1319-1328.

86) S. Saghazadeh, C. Rinoldi, M. Schot, S. S. Kashaf. F. Sharifi, E. Jalilian, K. Nuutila, G. Giatsidis, P. Mostafalu, H. Derakhshandeh, K. Yue, W. Swieszkowski, A. Memic, A. Tamayol, A. Khademhosseini, Drug Delivery Systems and Materials for Wound Healing Applications, *Adv Drug Deliv Rev.* 127 (2018) 138–166.

87) M.C. Koetting, J.T. Peters, S.D. Steichen, N.A. Peppas, Stimulus-responsive Hydrogels: Theory, Modern Advances, and Applications, *Mater. Sci. Eng. R*. 93 (2015) 1-49.

88) G. G. Adams, Y. Cui, J.H. Mitchell, M.J. Taylor, Rheological and Diffusion Properties of a Dextran-con A Polymer in the Presence of Insulin and Magnesium, *Rheol. Acta*. 45(2006) 611-620.

89) D. Buenger, F. Topuz, J. Groll, Hydrogels in Sensing Applications, *Prog. Polym. Sci*. 37(2012) 1678-1719.

90) E. Ramírez, S.G. Burillo, C.B. Díaz, G. Roa, B. Bilyeu, Use of pH-sensitive Polymer Hydrogels in Lead Removal from Aqueous Solution, *J. Hazard. Mater*. 192 (2011) 432-439.

91) E. S. Dragan, Design and Applications of Interpenetrating Polymer Network Hydrogels, *Chem. Eng. J.* 243 (2014) 572-590.

92) A. Ramesh, H. Hasegawa, W. Sugimoto, T. Maki, K. Ueda, Adsorption of Gold (III), Platinum (IV) and Palladium (II) onto Glycine Modified Crosslinked Chitosan Resin, Bioresource Technol. 99 (2008) 3801-3809.

93) P. J. Cragg, Supramolecular Chemistry: From Biological Inspiration to Biomedical Applications, Springer, (2010).

94) J.-M. Lehn, Supramolecular Chemistry—Scope and Perspectives Molecules, Supermolecules, and Molecular Devices (Nobel Lecture), *Angew. Chem. Int. Ed*. 27 (1988) 89-112.

95) J.-M. Lehn, Toward self-organization and complex matter, *Science*, 295 (2002) 2400-2403.

96) D. J. Prockop and A. Fertala, The Collagen Fibril: The Almost Crystalline Structure*J. Struct. Biol*., 122 (1998) 111-118.

97) S. Choi, N. Bowden and G. M. Whitesides, Macroscopic, Hierarchical, Two-Dimensional Self-Assembly, *Angew. Chem., Int. Ed.* 38 (1999) 3078-3081.

98) A. Klug, *Angew. Chem*., 95 (1983) 579.

99) G. Whitesides, J.P. Mathias, C. T. Seto, Molecular self-assembly and nanochemistry: a chemical strategy for the synthesis of nanostructures, *Science*, 254 (1991)1312−1319

100) A. C. Mendes, E. T. Baran, R. L. Reis, H. S. Azevedo, Self-assembly in nature: using the principles of nature to create complex nanobiomaterials, *WIREs Nanomed Nanobiotechnol*, 5 (2013) 582–612.

101) C. T. Seto,G. M. J. Whitesides, Molecular self-assembly through hydrogen bonding: supramolecular aggregates based on the cyanuric acid-melamine lattice, *Am. Chem. Soc*. 115 (1993) 905−916.

102) J. P. Mathias, E. E. Simanek, C. T. Seto, G. Whitesides, Self-Assembly Through Hydrogen Bonding: Preparation and Characterization of Three New Types of Supramolecular Aggregates Based on Parallel, Cyclic CA_3•M_3'Rosettes', *Angew. Chem., Int. Ed.* 32 (1993) 1766−1769.

103) D. A. Leigh, Genesis of the Nanomachines: The 2016 Nobel Prize in Chemistry, 55 (2016), 14506-14508.

104) T. F. A. De Greef, M. M. J. Smulders, M. Wolffs, A. P. H. J. Schenning, R. P. Sijbesma, E. W. Meijer, Supramolecular polymerization, *Chem. Rev.* 109 (2009) 5687-5754.

105) Y. S. Lee, Self-Assembly and Nanotechnology: A Force Balance Approach, Wiley, (2008).

106) V. Balzani, A. Credi, M. Venturi, The Bottom-Up Approach to Molecular-Level Devices and Machines, *Chem. Eur. J.* 2002, 8, 5524-5532.

107) G. Whitesides, J. Mathias, C. Seto, Science 1991, 254, 1312-1319.

108) J. W. Steed, J. L. Atwood, Supramolecular Chemistry, Wiley, (2009).

109) H. Xu, X. Zhang, J. Sun, S. Cui, Supramolecular chemistry: from molecular architectures to functional assemblies, *Encyclopedia of Life Support System*, (2010).

110) J. W. Steed, D. R. Turner, K. J. Wallace, *Core concepts in supramolecular chemistry and nanochemistry*, John Wiley, (2007).

111) F. J. M. Hoeben, P. Jonkheijm, E. W. Meijer, A. P. H. J. Schenning, About supramolecular assemblies of piconjugated systems. *Chem Rev*, 105 (2005)1491–1546.

112) K. Liu, Y. Kang, Z. Wang, X. Zhang, 25th anniversary article: reversible and adaptive functional supramolecular materials: "noncovalent interaction" matters, *Adv. Mater.* 25 (2013) 5530-5548.

113) J. D. Badjić, A. Nelson, S. J. Cantrill, W. B. Turnbull, J. F. Stoddart, Multivalency and cooperativity in supramolecular chemistry, *Acc. Chem. Res*. 38 (2005) 723-732.

114) G. M. Whitesides, B. Grzybowski, Self-Assembly at All Scales, *Science*, 295 (2002) 2418-2421.

115) J.-M. Lehn, Perspectives in Chemistry—Steps towards Complex Matter, *Angew. Chem. Int. Ed.* 2013, 52, 2836-2850.

116) J. A. Pelesko, *Self Assembly: The Science of Things That Put Themselves Together*, Taylor & Francis, (2007).

117) A. C. Mendes, E. T. Baran, R. L. Reis, H. S. Azevedo, *Wiley Interdisciplinary Reviews: Nanomedicine and Nanobiotechnology*, 5 (2013) 582-612.

118) H.-J. Schneider, Binding mechanisms in supramolecular complexes, *Angew. Chem. Int. Ed*. 48 (2009) 3924-3977.

119) D. S. Goodsell, *The Machinery of Life*, Copernicus Books, (2009).

120) Whitesides GM, Mathias JP, Seto CT. Molecular self-assembly and nanochemistry—a chemical strategy for the synthesis of nanostructures. *Science* 1991, 254:1312–1319.

121) Z. Liu, J. Qiao, Z. W. Niu, Q. Wang, Natural supramolecular building blocks: from virus coat proteins to viral nanoparticles. *Chem Soc Rev*, 41 (2012) 6178–6194.

122) A. Ciesielski, M. El Garah, S. Masiero, P. Samorì, Self-assembly of Natural and Unnatural Nucleobases at Surfaces and Interfaces, 12 (2015) 83-95.

123) https://filestore.aqa.org.uk/resources/chemistry/AQA-7405-TN-BIOCHEMISTRY.PDF

124) M. R. Villarreal, https://www.ck12.org/biology/phospholipidbilayer/lesson/Phospholipid-Bilayers-BIO/

125) M. Enciso, Hydrogen bond models for the simulation of protein folding and aggregation, (2012) 7.

126) Virus capsid, https://en.wikipedia.org/wiki/Capsid.

127) J. W. Steed JW. *Core Concepts in Supramolecular Chemistry and Nanochemistry*. Chichester: John Wiley & Sons, Ltd, (2007).

128) N. V. Bhagavan. *Medical Biochemistry*. San Diego: Academic Press; 2002.

129) J. Berg, J. Tymoczko, L. Stryer, *Protein Structure and Function*, New York: W.H Freeman, (2002) 117-118.

130) R. V. Ulijn, A. M. Smith, Designing peptide based nanomaterials, *Chem. Soc. Rev*. 37 (2008) 664-675.

131) D. Mandal, A. Nasrolahi Shirazi, K. Parang, Self-assembly of peptides to nanostructures, *Org. Biomol. Chem.* 12 (2014) 3544-3561.

132) M. Zelzer, R. V. Ulijn, Next-generation peptide nanomaterials: molecular networks, interfaces and supramolecular functionality, *Chem. Soc. Rev.* 39 (2010) 3351-3357.

133) M. R. Ghadiri, J. R. Granja, R. A. Milligan, D. E. McRee, N. Khazanovich, *Nature*, 366 (1993) 324-327.

134) D. T. Bong, T. D. Clark, J. R. Granja, M. R. Ghadiri, Self-assembling organic nanotubes based on a cyclic peptide architecture, *Angew. Chem. Int. Ed*., 40 (2001)988-1011.

135) S. Zhang, Fabrication of novel biomaterials through molecular self-assembly, *Nat. Biotechnol*., 21 (2003)1171-1178.

136) Z. Luo, S. Zhang, Designer nanomaterials using chiral self-assembling peptide systems and their emerging benefit for society, *Chem. Soc. Rev*. 41 (2012) 4736-4754.

137) W. Kabsch, C. Sander, Dictonary of protein secondary structure – pattern-recognition of hydrogen-bonded and geometrical features, *Biopolymers*, 22 (1983) 2577-2637.

138) J. Garner, M. M. Harding, Design and synthesis of alpha-helical peptides and mimetics, *Org Biomol Chem*. 5(2007) 3577-85

139) J. M. Scholtz, R. L. Baldwin, The Mechanism of Alpha-Helix Formation by Peptides, *Annu. Rev. Biophys. Biomol. Struct*. 21 (1992) 95-118.

140) E. G. Baker, G. J. Bartlett, M. P. Crump, R. B. Sessions, N. Linden, C. F. J. Faul, D. N. Woolfson, Local and macroscopic electrostatic interactions in single alpha-helices. *Nat. Chem. Biol.* 11 (2015), 221-U92.

141) J. Walshaw, D. N. Woolfson, Open-and-shut cases in coiled-coil assembly: alpha-sheets and alpha-cylinders. *Prot. Sci.* 10 (2001) 668-673.

142) S. Potekhin, T. Melnik, V. Popov, N. Lanina, A. Vazina, P. Rigler, A. Kajava, De novo design of fibrils made of short α-helical coiled coil peptides. *Chem. Biol.* 8 (2001), 1025–1032.

143) W. D. Kohn, R. S. Hodges, De novo design of α-helical coiled coils and bundles: models for the development of protein-design principles, Trends Biotechnol. 16 (1998) 379-389.

144) D. N. Woolfson, The design of coiled-coil structures and assemblies, *Adv. Prot. Chem*. 70 (2005), 80-106.

145) D. Papapostolou, A.M. Smith, E.D.T. Atkins. S. J. Oliver, M.G. Ryadnov, L.C. Serpell, D.N. Woolfson, Engineering nanoscale order into a designed protein fiber. *Proc. Natl. Acad. Sci. USA.* 104 (2007) 10853–10858.

146) J.F. Ross, A. Bridges, J. M. Fletcher, D. Shoemark, D. Alibhai, H.E.V. Bray, J. L.Beesley, W.M. Dawson. L.R. Hodgson, J. Mantell, P. Verkade, C. M. Edge, R.B. Sessions, D. Tew, D.N. Woolfson, Decorating self-assembled peptide cages with proteins. *ACS Nano*. 11 (2017) 7901–7914.

147) H. Dong, S.E. Paramonov, J. D. Hartgerink, Self-assembly of α-helical coiled coil nanofibers, *J. Am. Chem. Soc*.130 (2008) 13691–13695.

148) Y. Wu, J. H. Collier, α-Helical Coiled Coil Peptide Materials for Biomedical Applications, *Wiley Interdiscip Rev Nanomed Nanobiotechnol*. 9 (2017).

149) S. Bera, E. Gazit, Self-assembly of Functional Nanostructures by Short Helical Peptide Building Blocks, *Protein Pept Lett*. 26 (2019) 88–97.

150) J. M. Fletcher, R. L. Harniman, F. R. H. Barnes, A. L. Boyle, A. Collins, J. Mantell, T. H. Sharp, M. Antognozzi, P. J. Booth, N. Linden, M. J. Miles, R. B. Sessions, P. Verkade, D. N. Woolfson, Self-Assembling Cages from Coiled-Coil Peptide Modules. Science, 340 (2013), 595–599.

151) Alpha-helix, https://commons.wikimedia.org/wiki/File:AlphaHelixProtein.jpg; coiled coil https://en.wikipedia.org/wiki/Coiled_coil.

152) L. Pauling, R. B Corey, Configurations of Polypeptide Chains with Favored Orientations around Single Bonds - 2 New Pleated Sheets. *Proc. Natl. Acad. Sci. U. S. A.* 37 (1951) 729-740.

153) M. R. Caplan, P. N. Moore, S. G. Zhang, R. D. Kamm, D. A. Lauffenburger, Self-assembly of a beta-sheet protein governed by relief of electrostatic repulsion relative to van der Waals attraction, *Biomacromolecules*, 1 (2000), 627-631.

154) O. Khakshoor, J. S. Nowick, Artificial β-Sheets: Chemical Models of β-Sheets, *Curr Opin Chem Biol*. 12 (2008) 722–729.

155) S. G. Zhang, T. Holmes, C. Lockshin, A. Rich, Spontaneous assembly of a self-complementary oligopeptide to form stable macroscopic membrane, *Proc. Nat. Acad. Sci. U. S. A.* 90 (1993), 3334-3338.

156) Z. Luo, X. Zhao, S. Zhang, Structural Dynamic of a Self-Assembling Peptide d-EAK16 Made of Only D-Amino Acids, *PLoS One*. 3(2008) e2364.

157) C. J. Bowerman, B. L. Nilsson, Review self-assembly of amphipathic beta-sheet peptides: Insights and applications. *Biopolymers*, 98 (2012), 169-184.

158) S. Zhang, Discovery and design of self-assembling peptides, *Interface Focus* 7 (2017) 20170028.

159) S. Zhang, X. Zhao, Design of molecular biological materials using peptide motifs, *J. Mater. Chem*. 1 4 (2004) 2082–2086.

160) H. Yokoi, T. Kinoshita, S. G. Zhang, Dynamic Reassembly of Peptide Rada16 Nanofiber Scaffold. *Proc. Natl. Acad. Sci. U. S. A.* 102 (2005) 8414-8419.

161) R. Wang, Z. Wang, Y. Guo, H. Li, Z. Chen, Design of a RADA16-based self-assembling peptide nanofiber scaffold for biomedical applications, J. Biomater. Sci. Polymer Edition, 30 (2019) 713-736.

162) Y. Li ,F. Wang, H. Cui, Peptide-based supramolecular hydrogels for delivery of biologics, *Bioeng Transl Med*. 1 (2016) 306-322.

163) β- sheet: https://en.wikipedia.org/wiki/Antiparallel_(biochemistry); β-hairpin: https://en.wikipedia.org/wiki/Beta_hairpin.

164) W. F. DeGrado, J. P. Schneider, Y. Hamuro, The twists and turns of beta-peptides, *J Pept Res*. 54(1999) 206-17.

165) J. P.Schneider, D. J. Pochan, B. Ozbas, K. Rajagopal, L. Pakstis, J. Kretsinger, Responsive hydrogels from the intramolecular folding and self-assembly of a designed peptide, J *Am. Chem. Soc.* 124 (2002) 15030-15037.

166) B. Ozbas, J. Kretsinger, K. Rajagopal, J. P. Schneider, D. J. Pochan, Salt-Triggered Peptide Folding and Consequent Self-Assembly into Hydrogels with Tunable Modulus, *Macromolecules*, 37 (2004)7331-7337.

167) C. M. Nair, M.Vijayan, Y. V. Venkatachalapathi, P. Balaram, X-ray crystal-structure of pivaloyl-D-Pro-L-Ala-N-Methylamide – observation of a consecutive beta-turn conformation, *J. Chem. Soc.-Chem. Commun.* 24 (1979) 1183-1184.

168) L. Haines-Butterick, K. Rajagopal, M. Branco, D. Salick, R. Rughani, M. Pilarz, M. S. Lamm, D. J. Pochan, J. P. Schneider, Controlling hydrogelation kinetics by peptide design for three-dimensional encapsulation and injectable delivery of cells, *Proc Nat Acad Sci U S* A. 104 (2007) 7791–7796.

169) H. G. Cui, M. J.Webber, S. I. Stupp, Self-Assembly of Peptide Amphiphiles: From Molecules to Nanostructures to Biomaterials. *Biopolymers*, 94 (2010), 1-18.

170) I. Hamley, Self-assembly of amphiphilic peptides, *Soft Matter*, 7 (2011) 4122-4138.

171) A. Dasgupta, D. Das, Designer Peptide Amphiphiles: Self-Assembly to Applications, *Langmuir* 35 (2019) 10704-10724.

172) M. P. Hendricks, K. Sato, L. C. Palmer, S. I. Stupp, Supramolecular Assembly of Peptide Amphiphiles, *Acc. Chem. Res*. 50 (2017) 2440-2448.

173) P. Berndt, G. B. Fields, M. Tirrell, Synthetic lipidation of the peptides and amino-acids – monolayer structure and properties. J. Am. Chem.Soc. 117 (1995) 9515-9522.

174) J. Li, R. Xing, S. Bai, X. Yan, Recent advances of self-assembling peptide-based hydrogels for biomedical applications, Soft Matter, 15 (2019) 1704-1715

175) J. D. Hartgerink, E. Beniash, S. I. Stupp, Peptide-amphiphile nanofibers: A versatile scaffold for the preparation of self-assembling materials. *Proc. Natl. Acad. Sci. U. S. A.* 99 (2002) 5133-5138.

176) J. D. Hartgerink, E. Beniash, S. I. Stupp, Self-assembly and mineralization of peptide-amphiphile nanofibers. *Science* 294 (2001), 1684-1688.

177) S. E. Paramonov, H.-W. Jun and J. D. Hartgerink, Self-Assembly of Peptide−Amphiphile Nanofibers: The Roles of Hydrogen Bonding and Amphiphilic Packing, *J. Am. Chem. Soc*., 128 (2006) 7291-7298.

178) S. Lee, T. H.T. Trinh, M. Yoo, J. Shin, H. Lee, J. Kim, E. Hwang, Y-b. Lim, C. Ryou1, Self-Assembling Peptides and Their Application in the Treatment of Diseases, *Int J Mol Sci.* 20 (2019) 5850.

179) D. G. Fatouros, D. A. Lamprou, A. J. Urquhart, S. N. Yannopoulos, I, S. Vizirianakis, S. Zhang, Sotirios Koutsopoulos, Lipid-like Self-Assembling Peptide Nanovesicles for Drug Delivery, *ACS Appl. Mater. Interfaces*, 6 (2014) 8184-8189.

180) G.von Maltzahn, S. Vauthey, S. Santoso, S. Zhang, Positively Charged Surfactant-like Peptides Self-assemble into Nanostructures, *Langmuir*, 19 (2003)4332−4337.

181) A. Dehsorkhi,V. Castelletto, I. W. Hamley, J. Seitsonen, J. Ruokolainen, Interaction between a Cationic Surfactant-like Peptide and Lipid Vesicles and Its Relationship to Antimicrobial Activity. *Langmuir*, 29 (2013) 14246−14253.

182) V. Castelletto, R. M. Gouveia, C. J. Connon, I. W. Hamley, J. Seitsonen, A. Nykanen, J. Ruokolainen, Alanine-rich amphiphilic peptide containing the RGD cell adhesion motif: a coating material for human fibroblast attachment and culture. *Biomater. Sci.* 2014, 2, 362−369.

183) M. K. Fariya, A. K Jain, M. S. Nagarsenker, Bolaamphiphiles: a pharmaceutical review, *Ad. Pharm. Bull.* 4 (2014), 483-491.

184) T. Shimizu, M. Kogiso, M. Masuda, Vesicle assembly in microtubes, *Nature* 1996, 383, 487-488.

185) H. Matsui, S. Pan, B. Gologan, S. H. Jonas, Crystalline Glycylglycine Bolaamphiphile Tubules and Their pH-Sensitive Structural Transformation, *J. Phys. Chem. B.* 104 (2000) 9576-9579.

186) S. Ahmed, B. Pramanik, K. N. A. Sankar, Solvent Assisted Tuning of Morphology of a Peptide-Perylenediimide Conjugate: Helical Fibers to Nano-Rings and their Differential Semiconductivity. Sci. Rep. 7 (2017) 9485.

187) S. Ahmed, K. N. A. Sankar, B. Pramanik, K. Mohanta, D. Das, Solvent Directed Morphogenesis and Electrical Properties of a Peptide–Perylenediimide Conjugate, *Langmuir*, 34, 28 (2018) 8355-8364.

188) E. Gazit, Self-assembled peptide nanostructures: the design of molecular building blocks and their technological utilization, *Chem. Soc. Rev.* 36 (2007) 1263-1269.

189) S. Fleming, S. Debnath, P. W. J. M. Frederix, T. Tuttle, R. V. Ulijn, Aromatic peptide amphiphiles: significance of the Fmoc moiety, *Chem. Commun*., 49 (2013)10587-10589.

190) S. Fleming, R. V. Ulijn, Design of nanostructures based on aromatic peptide amphiphiles, *Chem. Soc. Rev*.43(2014) 8150-8177.

191) M. Reches, E. Gazit, Casting metal nanowires within discrete self-assembled peptide nanotubes, *Science* 300(2003) 625-7.

192) C. G. Pappas, R. Shafi, I. R. Sasselli, H. Siccardi, T. Wang V. Narang, R. Abzalimov, N. Wijerathne, R. V. Ulijn Dynamic peptide libraries for the discovery of supramolecular nanomaterials. *Nat Nanotechnol*. 11(2016) 960-967.

193) X. Du, J. Zhou, J. Shi, B. Xu Supramolecular Hydrogelators and Hydrogels: From Soft Matter to Molecular Biomaterials, *Chem Rev.* 115(2015) 13165–13307.

194) M. Ma, Y. Kuang, Y. Gao, Y. Zhang, P. Gao, B. Xu, Aromatic−Aromatic Interactions Induce the Self-Assembly of Pentapeptidic Derivatives in Water To Form Nanofibers and Supramolecular Hydrogels, *J. Am. Chem. Soc.* 132 (2010) 8, 2719-2728.

195) J. Li, X. Du, S. Hashim, A. Shy, B. Xu, Aromatic–Aromatic Interactions Enable α-Helix to β-Sheet Transition of Peptides to Form Supramolecular Hydrogels, *J. Am. Chem. Soc.* , 139 (2017)1, 71-74.

196) H. Wang, Z. Yang, D. J. Adams, Controlling peptidebased hydrogelation, *Materials Today*, 15 (2012) 500-507.

197) I. W. Hamley The Amyloid Beta Peptide: A Chemist's Perspective. Role in Alzheimer's and Fibrillization, *Chemical Reviews*. 112 (2012) 5147–92.

198) W. Pulawski, U. Ghoshdastider, V. Andrisano, S. Filipek, Ubiquitous amyloids. *Applied Biochemistry and Biotechnology*. 166 (2012) 1626–43.

199) R. N. Rambaran, L. C. Serpell, Amyloid fibrils, *Prion*, 2(2008) 112–117.

200) L. C. Serpell, Alzheimer's amyloid fibrils: structure and assembly, *Biochimica et Biophysica Acta- Molecular Basis of Disease*, 1502 (2000) 16-30.

201) P. C. Ke, M-A. Sani, F. Ding, A. Kakinen, I. Javed, F. Separovic, T. P. Davis, R. Mezzenga, Implications of peptide assemblies in amyloid diseases, *Chem. Soc. Rev*. 46 (2017) 6492-6531.

202) G. Chen, T. Xu, Y. Yan, Y. Zhou, Y. Jiang, K. M. & H E. Xu , Amyloid beta: structure, biology and structure-based therapeutic development, *Acta Pharmacol Sin* 38 (2017) 1205–1235.

203) E. Gazit, A possible role for pi-stacking in the self-assembly of amyloid fibrils, *FASEB J*, 16 (2002) 77-83.

204) C. H. Go¨rbitz, The structure of nanotubes formed by diphenylalanine, the core recognition motif of Alzheimer's β-amyloid polypeptide, *Chem. Commun*. (2006) 2332–2334

205) R. Vegners, I. Shestakova, I. Kalvinsh, R. M. Essell and P. A. Janmey, Tuneable mechanical properties in low molecular weight gels, *J. Pept. Sci.*1 (1995) 371–378.

206) R. N. Mitra, D. Das, S. Roy, P. K. Das, Structure and properties of low molecular weight amphiphilic peptide hydrogelators. *J. Phys. Chem. B*, 111 (2007) 14107-14113.

207) S. Debnath, A. Shome, D. Das, and P. K. Das, Hydrogelation Through Self-Assembly of Fmoc-Peptide Functionalized Cationic Amphiphiles: Potent Antibacterial Agent, *J. Phys. Chem. B*, 114 (2010) 4407–4415.

208) A. Mahler, M. Reches, M. Rechter, S. Cohen, and E. Gazit, Rigid, Self-Assembled Hydrogel Composed of a Modified Aromatic Dipeptide, *Adv. Mater*. 18 (2006) 1365–1370.

209) J. Raeburn, C. Mendoza-Cuenca, B. N. Cattoz, M. A. Little, A. E. Terry, A. Z. Cardoso, P. C. Griffiths and D. J. Adams, The effect of solvent choice on the gelation and final hydrogel properties of Fmoc– diphenylalanine, *Soft Matter* 11 (2015) 927-935

210) M. D. Segarra-Maset, V. J. Nebot, J. F. Miravet, B. Escuder, Control of molecular gelation by chemical stimuli, *Chem. Soc. Rev*. 42 (2013) 7086-7098.

211) A. Martin, J. Wojciechowski, A. Robinson, et al. Controlling self-assembly of diphenylalanine peptides at high pH using heterocyclic capping groups. *Sci Rep* 7, (2017) 43947.

212) C. Tang, A. M. Smith, R. F. Collins, R. V. Ulijn, Alberto Saiani, Fmoc-Diphenylalanine Self-Assembly Mechanism Induces Apparent pKa Shifts, *Langmuir*, 25 (2009), 9447–9453.

213) E. R. Draper, D. J. Adams, Controlling the Assembly and Properties of Low-Molecular-Weight Hydrogelators, *Langmuir* 35 (2019) 6506−6521.

214) L. Chen, S. Revel, K. Morris, L. C. Serpell, D. J. Adams, Effect of Molecular Structure on the Properties of Naphthalene-Dipeptide Hydrogelators, *Langmuir*, 26 (2010), 13466–13471.

215) Z. Yang, G. Liang, M. Ma, Y. Gao, B. Xu, Conjugates of naphthalene and dipeptides produce molecular hydrogelators with high efficiency of hydrogelation and superhelical nanofibers. J. Mater. Chem. 17 (2007) 850–854.

216) D. J. Adams, M. F. Butler, W. J. Frith, M. Kirkland, L. Mullen, P. Sanderson, A new method for maintaining homogeneity during liquid–hydrogel transitions using low molecular weight hydrogelators, *Soft Matter*, 2009,5, 1856-1862 .

217) Y. I. González, E. W. Kaler, Fibrous Assemblies and Water Gelation in Mixtures of Lysine with Sodium Alkyl Sulfates. *Langmuir*, 21 (2005) 7191–7199.

218) G. Verma, V. K. Aswal, P. Hassan, pH-Responsive self-assembly in an aqueous mixture of surfactant and hydrophobic amino acid mimic. *Soft Matter*, 5 (2009) 2919.

219) M. Yang, W. J. Song, Diverse protein assembly driven by metal and chelating amino acids with selectivity and tunability. *Nat Commun* 10 (2019) 5545.

220) J. Yang, F. Xu, C-R. Han, Metal Ion Mediated Cellulose Nanofibrils Transient Network in Covalently Cross-linked Hydrogels: Mechanistic Insight into Morphology and Dynamics, *Biomacromolecules* 18 (2017) 1019-1028.

221) C. M. Micklitsch, P. J. Knerr, M. C. Branco, R. Nagarkar, D.J. Pochan and J. P. Schneider, Zinc-Triggered Hydrogelation of a Self-Assembling β-Hairpin Peptide *Angew. Chem., Int. Ed*. 50 (2011) 1577–1579.

222) P. J. Knerr, M. C. Branco, R. Nagarkar, D. J. Pochan and J.P. Schneider, Heavy metal ion hydrogelation of a self-assembling peptideviacysteinyl chelation, *J. Mater. Chem*., 22 (2012) 1352–1357.

223) S. Roy, N. Javid, P. W. J. M. Frederix, D. A. Lamprou, A. J. Urquhart, N. T. Hunt, Pe. J. Halling, R. V. Ulijn, Dramatic Specific-Ion Effect in Supramolecular Hydrogels, *Chem. Eur. J.* 18 (2012) 11723 – 11731.

224) D. Das, A. Dasgupta, S. Roy, R. N. Mitra, S. Debnath and P.K. Das, Water Gelation of an Amino Acid-Based Amphiphile, *Chem.–Eur. J.* 12 (2006) 5068–5074.

225) S. Roy and P. K. Das, Antibacterial hydrogels of amino acid-based cationic amphiphiles, *Biotechnol. Bioeng*. 100 (2008) 756–764.

226) A. Shome, S. Debnath and P. K. Das, Head Group Modulated pH-Responsive Hydrogel of Amino Acid-Based Amphiphiles: Entrapment and Release of Cytochrome c and Vitamin B12, *Langmuir*, 24 (2008) 4280–4288.

227) R. N. Mitra, D. Das, S. Roy and P. K. Das, Structure and properties of low molecular weight amphiphilic peptide hydrogelators, *J. Phys. Chem. B*, 111 (2007) 14107–14113.

228) M. R. Caplan, P. N. Moore, S. Zhang, R. D. Kamm, D.A. Lauffenburger, Self-Assembly of a β-Sheet Protein Governed by Relief of Electrostatic Repulsion Relative to van der Waals Attraction Biomacromolecules, 1 (2000) 627–631.

229) B. Ozbas, J. Kretsinger, K. Rajagopal, J. P. Schneider, D. J. Pochan, Salt-Triggered Peptide Folding and Consequent Self-Assembly into Hydrogels with Tunable Modulus, *Macromolecules* 37 (2004) 7331-7337.

230) J. Shi, Y. Gao, Y. Zhang, Y. Pan, B. Xu, Calcium Ions to Crosslink Supramolecular Nanofibers to Tune the Elasticity of Hydrogels over Orders of Magnitude, *Langmuir*, 27 (2011) 14425–14431.

231) P. Sharma, H. Kaur, S. Roy, Inducing Differential Self-Assembling Behavior in Ultrashort Peptide Hydrogelators Using Simple Metal Salts, *Biomacromolecules*, 20, (2019) 2610-2624.

232) Z. Yang, G. Liang and B. Xu, Enzymatic Hydrogelation of Small Molecules, *Acc. Chem. Res*. 41 (2008) 315–326.

233) Y. Gao, Z. Yang, Y. Kuang, M.-L. Ma, J. Li, F. Zhao and B. Xu, Enzyme-instructed self-assembly of peptide derivatives to form nanofibers and hydrogels, *Biopolymers*, 94 (2010) 19–31.

234) R. J. Williams, R. J. Mart, R. V. Ulijn, Exploiting Biocatalysis in Peptide Self-Assembly, *Pept. Sci*. 94 (2009) 107-117.

235) S. Toledano, R. J. Williams, V. Jayawarna, R. V. Ulijn, Enzyme-Triggered Self-Assembly of Peptide Hydrogels via Reversed Hydrolysis, *J. Am. Chem. Soc*., 128, (2006) 1070–1071.

236) Z. Yang, B. Xu, Using Enzymes to Control Molecular Hydrogelation, *Adv. Mater*., 18(2006) 3043–3046

237) R. J. Williams, A. M. Smith, R. Collins, N. Hodson, A. K. Das and R. V. Ulijn, Enzyme-assisted self-assembly under thermodynamic control. Nat. Nanotechnol., 4 (2008) 19–24.

238) Z. Yang, H. Gu, D. Fu, P. Gao, J. K. Lam and B. Xu, Enzymatic Formation of Supramolecular Hydrogels, *Adv. Mater*.16 (2004) 1440–1444.

239) Z. Yang, G. Liang, L. Wang and B. Xu, Using a Kinase/Phosphatase Switch to Regulate a Supramolecular Hydrogel and Forming the Supramolecular Hydrogel in Vivo, *J. Am. Chem. Soc*., 128 (2006) 3038–3043.

240) T. E.L. Douglas, P. B. Messersmith, S. Chasan, A. G. Mikos, E. L.W. de Mulder, G. Dickson, D. Schaubroeck, L. Balcaen, F. Vanhaecke, P. Dubruel, J. A. Jansen, S. C. G. Leeuwenburgh, Enzymatic mineralization of hydrogels for bone tissue engineering by incorporation of alkaline phosphatase, *Macromol Biosci*. 12 (2012) 1077–1089.

241) Y. Kuang, J. F. Shi, J. Li, D. Yuan, K. A. Alberti, Q. B. Xu, B. Xu, Pericellular Hydrogel/Nanonets Inhibit Cancer Cells. *Angew. Chem. Intl. Ed*. 53. (2014) 8104-8107.

242) Z. Yang, P.-L. Ho, G. Liang, K. H. Chow, Q. Wang, Y. Cao,Z. Guo, B. Xu, Using beta-lactamase to trigger supramolecular hydrogelation, *J. Am. Chem. Soc*. 129 (2007) 266–267

Chapter 2

Materials and Methodology

This chapter describes the synthetic protocols and characterization techniques used for the design and development of peptide based hydrogels and assessment of their functional behavior. The basic principle of the peptide synthesis and their characterization will be covered in this chapter. In particular, this chapter is further classified into four major sections including 1) peptide synthesis and characterization, 2) hydrogel preparation and 3) physicochemical characterization of the peptide hydrogels using different spectroscopic as well as microscopic techniques and 4) biological assays with peptide hydrogels to evaluate their biocompatibilities as well as their potential applications in cell culture studies.

2.1 Peptide synthesis and characterization:

2.1.1 Materials:

All the chemicals used in the research work were purchased from Sigma-Aldrich, Merck, Hi-media with high purity (≥90%).

All required N-terminal Fmoc-protected amino acids, N-terminal Boc-protected amino acids, C-terminal methyl ester protected amino acids, C-terminal ter-butyl protected amino acids, piperazine, diisopropyl carbodiimide (DIC), N, N-Diisopropylethylamine (DIPEA), HBTU (O-(Benzotriazol-1-yl)-N,N,N′,N′-tetramethyluronium hexa-fluoro-phosphate), 1,2- Ethanedithiol (EDT), anisole, thioanisole were obtained from Sigma-Aldrich with > 99% purity.

Trifloroacetic acetic acid, Acetonitrile (HPLC and LCMS grade), Dimethyl formamide (DMF), Dichloromethane (DCM), Diethyl ether, Rinkamide-MBHA resin were purchased from Merck. All chemicals were stored at conditions as mentioned for each chemical.

Cell culture reagents such as DMEM (Dulbecco's Modified Eagle's Medium), FBS (foetal bovine serum), antibiotic solution (penicillin-streptomycin), Dulbecco's Phosphate buffer saline, cell culture grade DMSO, MTT salt, Alamar blue salt, dyes for fluorescence and immunofluorescence studies were obtained from Hi-Media.

2.1.2 Peptide synthesis:

Standard synthesis protocols were used for the synthesis of peptides. [1, 2]The synthesis reactions were carefully controlled by using N-terminal or C-terminal protected amine acids, as required. Peptides can be synthesized through two methods: Solid phase peptide synthesis and liquid phase peptide synthesis. Both methods have their own advantages over each other. Liquid synthesis can be used for large scale synthesis. However, the synthesis of long peptides would be extremely difficult and time consuming with liquid phase synthesis. In contrast to this, solid phase synthesis can easily produce long sequences in a short span of time, with high purities. However, the solid phase synthesis is more expensive and can be used for small scale synthesis only. Therefore, we adopted solid phase peptide synthesis to synthesize pentapeptide sequences based of laminin and collagen inspired peptides, studied during our work. While, the ultra short dipeptide sequences were synthesized using liquid phase synthesis. Standard protocols for both methods are described below:

2.1.2.1 Solid Phase Peptide Synthesis (SPPS):

To synthesize our designed peptides, the amino acids were sequentially coupled one by one from C-terminal to N-terminal. The first Fmoc-protected amino acid is coupled to insoluble polymer support (resin) to protect the coupling reaction at C-terminal. After each coupling reaction, the Fmoc- protecting group is cleaved in the presence of basic solutions such as piperazine/piperidine, which allows the next amino acid to couple. The schematic representation of solid phase peptide synthesis is shown in figure 2.2.

Meanwhile, the carboxylic group of the second amino acid was activated to produce intermediate reactive species. One cycle of synthetic reaction involves deprotection, activation and coupling steps, which are repeated at the joining of each amino acid. In the end, the insoluble polymeric support is detached from the peptide sequence by dissolving the product in cleavage cocktail solution. At this step, all the protecting side chain protecting groups were also cleaved and the target peptide with native primary structure is obtained by filtration. The filtrate solution was precipitated in chilled ether to obtain the crystallized peptide. The cleavage cocktail solution comprised of trifluoroacetic acid (90% v/v), Thioanisole (5% v/v), EDT (3% v/v) and anisole (2% v/v). [3]

Solid Support: The solid support is required to provide physical stability to the synthesized peptides and to allow the rapid filtration of liquids. These supports are inert to the solvents/reagents used during SPPS and must have the capability to swell in the solvents used so that it can allow the penetration of the reagents for facilitating the attachment of the first amino acid. The choice of solid support resins for a synthesis reaction depends upon requirement of the type of product's C-terminal i.e. whether a carboxylic acid or amide C-terminal is desired. The Wang resin was, most commonly used resin for peptides with C-terminal carboxylic acids while Rinkamide is widely used for generating amide C-terminal. [4]

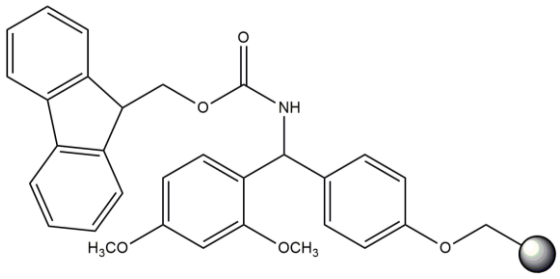

Figure 2.1 *Schematic representation of Fmoc rinkamide resin (adapted from ref 5)*

Protecting groups: During peptide synthesis, the use of N-terminal and side chain protecting groups is important to avoid the undesirable side reactions for eg. self-coupling of the activated amino acid can lead to polymerization, reducing the yield of desired peptides. Two commonly used protecting group schemes that are used in solid-phase peptide synthesis: Boc/Bzl and Fmoc/tBu approaches. The TFA-labile N-terminal Boc protection along with side chain protection are utilized by Boc/Bzl strategy while base-labile Fmoc N-terminal protection is used in Fmoc/tBu SPPS. Other protecting groups include Benzyloxy-carbonyl (carboxybenzyl), Alloc, etc. Apart from these protecting groups, other external hydrophobic groups can be attached to the peptides at N-terminal through amide coupling followed by Fmoc/Boc

deprotection. These groups may include aromatic hydrophobic moieties (such as Napthoxy acetic acid, pyrene butyric acid, indoleacetic acid, etc) or aliphatic carbon chains (decanoic acid, myristic acid, palmitic acid, etc) or some small groups like acetyl group. The groups are mainly incorporated to modulate the hydrophilic-lipophilic balance of the peptides.

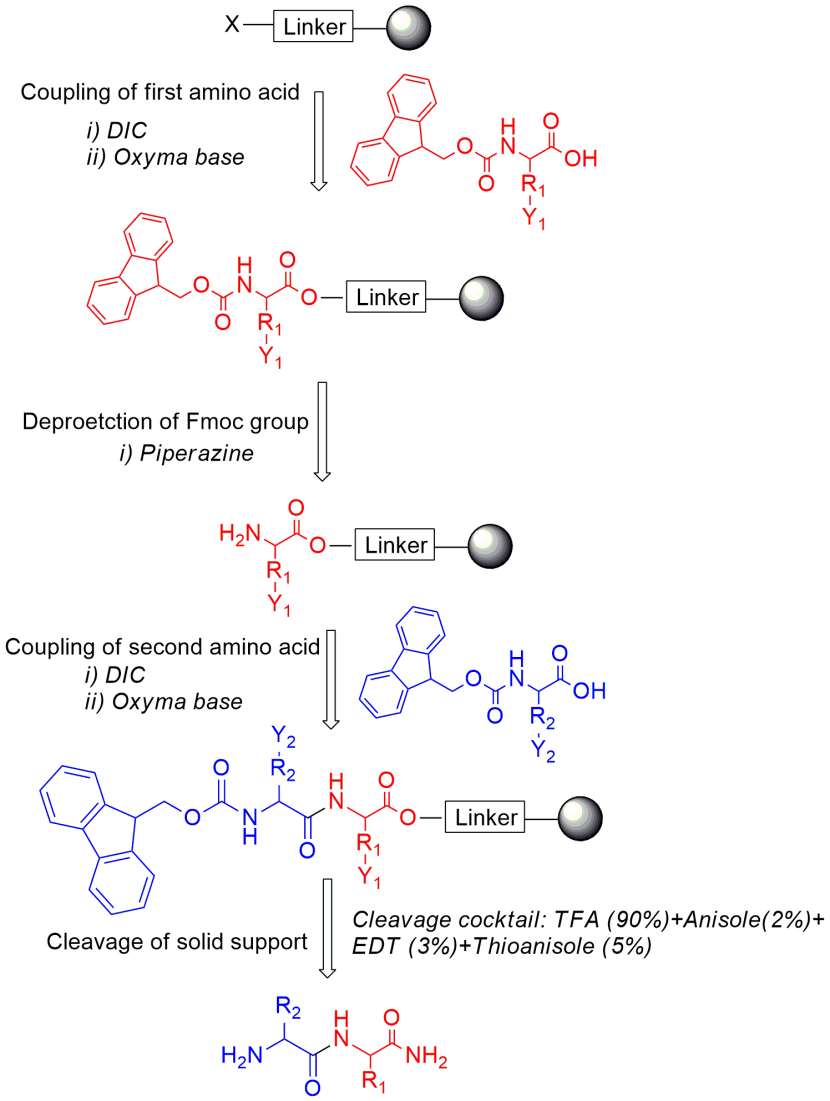

Figure 2.2 *Schematic representation of solid phase synthesis (adapted from ref 2)*

After synthesis and cleavage, the obtained peptide is purified using preparative HPLC to obtain ~100% pure product. The principle and working of HPLC is discussed in detail below.

2.1.2.2 Liquid phase peptide synthesis (LPPS):

Liquid phase synthesis is carried out by dissolving two amino acids in DMF, the free carboxylic group of N-terminal protected amino acid reacts with free amine group of C-terminal protected amino acid. Both amino acids are reacted in the presence of coupling agents such as HBTU and DIPEA. The coupling agents activate the carboxylic group of N-terminal protected

amino acid and allow its reaction with free amino group of C-terminal protected amino acid. The produced peptide was separated from the DMF through precipitation and sequential steps of aqueous/organic phase separation. The volatile organic solvent is removed with rotary evaporator and dried product was obtained. The product was purified through column chromatography to separate the unreacted reagents from the product, after each coupling reaction. Further, the deprotection step was carried out, as required. It is noteworthy that the cleavage conditions of C- and N- terminal should be different, to avoid cleavage of both ends before second coupling reaction. For example, Fmoc and methyl ester group are cleaved under basic environment and Boc and tert-butyl esters are cleaved under acidic conditions. Since all the reagents are in dissolved condition that's why it is called liquid synthesis (figure 2.3). [6,7]

In solution phase synthesis, each coupling and deprotection step is followed by TLC (thin layer chromatography). [8] It is a separation technique, which uses solvents of two different polarities and relies on the separation of compound based on their relative affinities towards both the phases. The compounds spotted over the stationary moves along with the mobile phase move over the surface of the stationary phase. The compounds having higher affinity towards stationary phase move slowly while the other compounds having more affinity towards solvent travel faster, resulting in the separation of the mixture. At the end of the separation process, the individual components of mixture appear as spots/bands at respective levels on the plates. Suitable detection techniques can be applied to identify their character and nature. Generally, the stationary phase is composed of alumina, cellulose, or silica gel coated over the surface of aluminium, glass or plastic sheets. The mobile phase may be composed of different proportions (0.5-10%) of more polar (eg. methanol) and a less polar (eg. chloroform) solvent mixture, depending upon the polarity of compound synthesized. The distance travelled by each system is measured and retention factor (R_f) is calculated:

Rf = dist. travelled by sample / dist. travelled by solvent ….Equation 2.1

The Fmoc-protected dipeptides generally involve single step coupling reactions of Fmoc N-terminal protected amino acid with tert-butyl C-terminal protected amino acid followed by deprotection of tert-butyl groups in acidic media (TFA).

However, in case of extension at N-terminal, generally, Boc N-terminal protected amino acid is coupled with methyl ester C-terminal protected amino acid. The Boc protecting group from N-terminal is cleaved in the presence of acidic environment (TFA), resulting in free amino group, which can be further coupled with other amino acid or hydrophobic moieties having free carboxyl terminal. Later, C-terminal methyl ester can be cleaved in basic environment (THF/NaOH) to result in free carboxyl end.

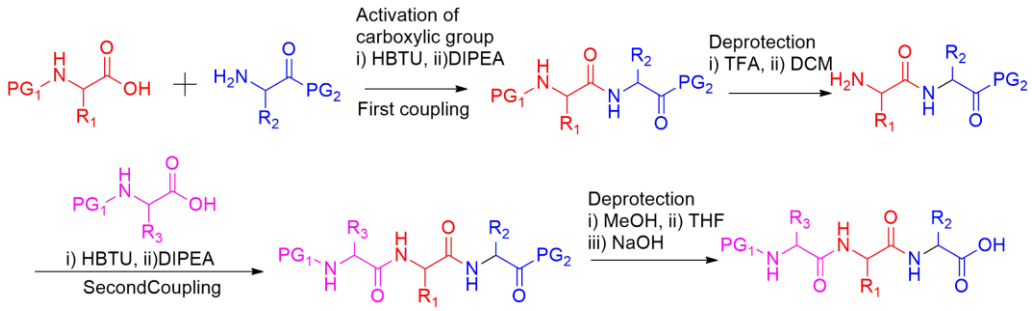

Figure 2.3 *Schematic representation of liquid phase peptide synthesis.*

2.1.2.3 Characterization of synthesized peptides:

Both SPPS and LPPS are not 100% efficient. There are high chances that some unreacted amino acids might be present as impurities and sometimes due to incomplete coupling, slight batch to batch variation is possible, which makes it important to analyze the purity of peptides.

Reverse phase high performance liquid chromatography (RP-HPLC)*:*

It is an important tool for the analysis and purification of synthesized peptides. A HPLC system primarily consists of two parts: a stationary phase (column) and a mobile phase (solvent). The injected sample is carried by the mobile phase through the column. The differential affinity of sample towards stationary phase and mobile phase causes the separation of components of sample. In case of reverse phase HPLC, the nature of stationary phase is non-polar which attracts hydrophobic components and shows longer retention times. While less hydrophobic components are eluted earlier with the polar mobile phase. This method separates the sample on the basis of their polarity. The separated components of the sample then pass through the detector where it is quantified and reported as the intensity of peak at different retention times. Then each eluent from the detector can be collected and dried separately. [9]

Typically, for the analysis peptides we used the C18 column with dimensions of 250 mm length and 4.6 mm internal diameter (id), which is packed with 5µm fused silica particles. The flow rate of 1ml/min is usually used with a gradient solvent system consisting of acetonitrile (0.1% TFA) and water (0.1% TFA). Addition of TFA is important because it controls pH (buffering), complexes with oppositely charged ions to enhance RP retention (ion pairing) and it suppresses the adverse ionic interactions of peptides and silanol groups of silica. The UV based PDA detector is commonly used for the detection of samples.

HPLC is also used to separate and purify the target compounds from a solution mixture after a synthesis reaction or from natural extracts that are called preparative or semi-preparative HPLC. An HPLC preparative system differs from a normal analytical system in their capabilities to separate large scale compounds by using high flow rates and high pressures. The separated fractions at different time points are collected and dried to obtain the products.

***Mass spectroscopy (MS)*:**

Mass spectroscopy was carried out as a molecular identification tool to detect the mass of the synthesized peptides, which can either work in harmony with the HPLC system for simultaneous detection of masses of each separated peak or can be used separately. In a typical mass spectroscopy, the sample molecules are first ionized by bombarding electrons, which may break the sample into fragment or produces the molecular ion without fragmentation. The selection of methods for ionization is important and depends upon the nature of sample. For liquid and solid samples, electrospray ionization or matrix-assisted laser desorption/ionization (MALDI) methods are commonly used. These methods are called as soft ionization techniques because they impart less residual energy on the sample molecules that result in little fragmentation of the molecule. These charged ions are then accelerated in a vacuum tube, supplied with electric or magnetic fields, where they are separated based on their mass-to-charge ratio. The charged molecules are captured by the detecting element such as electron multiplier and the integrated signals are displayed as a function of mass/charge ratio. [10]

NMR Spectroscopy

NMR is an important technique to analyse the structure and stereochemistry of synthesized chemical molecules mainly organic compounds that are composed of carbon, hydrogen and oxygen. The NMR experiments are based on three major steps that involve placement of sample in a static magnetic field, excitation of the sample nuclei with a radio frequency pulse and frequency measurement of the emitted signals. Typically the NMR active nuclei in the sample resonate at different resonance frequencies which are affected by the local atomic environment. The electrons, protons, and neutrons spin on their axes. In spin paired atoms like 12C, lack of overall spin makes them inactive towards radio frequency. Therefore, the atoms that possess an overall spin (I) are active, such as 1H and 13C.

In the external magnetic field, the electrons interact with the magnetic field and begin to circulate around the nucleus, depending on their spin. These spinning electrons generate a magnetic field opposite to the applied field. Due to this, the electrons shield the nucleus from the applied magnetic field and the difference between the two fields is termed the nuclear shielding, which can be measured in parts per million (ppm). The chemical shift is defined as the ratio of the change in magnetic field with respect to the magnetic field that is required to bring unshielded nuclei into resonance. The size of chemical shift is susceptible to neighbouring atoms. Frequencies of NMR signal are measured in Hertz (Hz –cycles per second) or Megahertz (MHz). All the sample frequencies are measured with respect to a reference and tetramethylsilane $Si(CH_3)_4$ (TMS) is the most commonly used reference for 1H NMR and its peak is taken as a reference of zero.

The magnetic interaction between neighboring protons causes splitting of NMR signals like two protons can combine and exist in three possible magnetic states as a result of spin orientation. An NMR spectrum is plotted between signal frequency versus signal intensity. The frequency gives the qualitative information about the local atomic environment and the intensity provides quantitative information as the integral of the peak which is directly related to the number of nuclei contributing to a resultant signal at a particular frequency. [11, 12]

^{13}C NMR ^{1}H NMR follows the same principles and identifies carbons and hydrogen in organic molecules. TMS is also used as the reference (0 ppm), however, the chemical shift range for ^{13}C NMR is approximately 20 times larger than that of ^{1}H NMR. In this thesis, the ^{1} NMR and ^{13}C NMR are used to analyze the dipeptides synthesized for the preparation of hydrogels. [13]

2.2 Hydrogel preparation

Different methods of molecular self-assembly have been employed to access diverse nanostructures depending upon the nature of the peptide building blocks through different methods of hydrogels preparation.

2.2.1 Solvent mediated gelation: In this method, the stock solution of peptide is prepared in an organic solvent such as ACN, DMSO, methanol etc. in which peptide shows good solubility. The peptide gelator remains in monomeric state in the solubilized form and exhibited higher gelator-solvent interactions. As soon as, the poor solvent such as water is added, the solubility of peptide is reduced, increasing gelator-gelator interaction, probably, due to high surface tension of water. Due to hydrophobic effects organic solvent eventually moves to the hydrophobic pockets. The enhanced gelator-gelator interactions trigger self-assembly of the molecules resulting in their gelation.

However, the utilization of organic solvents creates gels, which might be less favorable for biological applications. Therefore, to make these gels more biocompatible, the solvent exchange method is employed to remove the traces of organic solvents. The pre-formed gels are immersed in water or other aqueous solvents, which replaces the organic solvents entrapped with the gel networks. The supernatant aqueous media is changed multiple times to ensure the complete removal of organic solvent. The removal of solvents can further be detected by spectroscopic techniques such as FTIR. [14]

2.2.2 pH triggered gelation: It is most widely studied method to trigger self-assembly. Changing pH can vary the ionization state of the peptides that helps in their dissolution in aqueous solvent. The N-terminal modified short peptides have free carboxylic groups at C-terminal, which are deprotonated at high pH and get further protonated when pH is reduced to physiological pH. The charged C-terminal facilitates solubilization of the gelator molecules in water and a further decrease in pH reduces the solubility with enhanced gelator-gelator interactions resulting in gelation. pH control is extremely important for charged peptides, due to their inherent sensitivity to pH and their role in regulating electrostatic interactions. We used NaOH (0.1N) to dissolve the hydrophobically modified peptide amphiphiles until a clear solution is obtained. Further, the pH is lowered to neutral pH by adding HCl (0.1N).

2.2.3 Temperature triggered gelation: The hydrophobic peptides tend to show less solubility in water at higher concentrations and room temperatures. Heat-cool cycle facilitates the dissolution of hydrophobic peptides at higher concentrations and cooling to lower temperature reduces solubility, thus driving the self-assembly of the gelator into fibrillar structures by induction of non-covalent interactions. A competition between intermolecular interactions and Brownian motion of the peptide monomer dictates its propensity to self-assemble. In this method, the

peptide was dispersed in aqueous solvents such as water or PBS and allowed to heat at temperature ranging from 60-80^{0}C until the complete peptide was dissolved. Vortexing was used intermittently to produce a uniform dispersion. Following complete dissolution, the solution was kept undisturbed at room temperature to form a self-supporting three dimensional hydrogels.

2.3 Physicochemical Characterization of Hydrogels

2.3.1 Oscillatory Rheology

Viscoelastic materials are those which exhibit the properties of both, viscous liquids as well as pure solid. The basic principle of an oscillatory rheometer involves the induction of sinusoidal shear deformation in the sample and measuring resultant stress response. A typical rheology experiment requires the sample to be placed between two parallel plates as shown in figure 2.4. One plate remains stationary, while the other rotates to impost a time dependent strain on the sample. [15, 16]

The strain applied is denoted by the equation below:

$$\gamma(t) = \gamma \cdot \sin(\omega t) \qquad \text{...Equation 2.2}$$

Where, γ=*strain,* ω=*oscillation frequency,* t=*time.* At the same time, the time dependent stress is measured by torque imposed by the sample on the stationary plate. Temperature control can be provided by Peltier element.

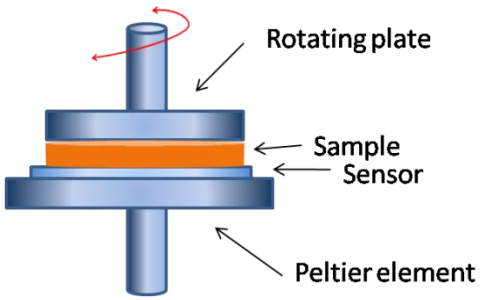

Figure 2.4 *Schematic representation of a typical oscillatory rheology setup with sample placed between the two parallel plates (adapted from ref 17).*

Initially, the amplitude sweeps are performed to find out the linear viscoelastic region (LVR) that determines the range of strain where the material is independent of the extent of deformation. Further, the LVR is used to perform the frequency sweeps. In oscillatory shear measurements, the shear storage modulus (G′), loss modulus (G″) and loss factor (tan δ) are critical parameters monitored against time, frequency, and strain. Storage modulus, G′ indicates the deformation energy stored during the shear process (i.e. the solid like the behavior of the material) while loss modulus, G″ signifies the energy dissipated during shear (i.e. the liquid-like or flow behavior of the material). When the G′ > G″ (tan δ < 1), the sample behaves more like an elastic solid while, conversely, G″ > G′ (tan δ > 1), the sample behaves more like a viscous liquid like. [18]

In the research work carried out in this thesis, Anton Parr Rheometer MCR 302 instrument was used for rheological measurements and thixotropic measurements.

2.3.1.1 Thixotropy measurement: Time-dependent shear thinning property is termed as thixotropy. In thixotropy, there is a decrease in the apparent viscosity under constant shear force, which is followed by a gradual recovery on the removal of shear. [19] Thixotropic behavior is an important quality characteristic tool for products like paints, coatings, gels, etc. Thixotropy testing can be performed with a viscometer or rheometer in either rotation or oscillation mode. The thixotropic behavior can be analyzed using step test that consists of three intervals and is therefore called "3 intervals thixotropy test (3ITT)". It can be performed in 2 ways: a controlled shear rate (CSR) mode and in a controlled shear stress (CSS) mode. In CSR mode the shear rate or rotational/oscillation speed is preset, whereas the shear stress or torque is preset on the rheometer in CSS mode. [20] The test is performed at two different speeds/shear rates. The first and last intervals are performed at a low shear rate and the second interval is performed at a high shear rate. The third interval of the 3ITT test is used for analyzing the thixotropic behavior of the sample by calculating the recovery percentage after a given time.

2.3.2 Microscopic characterization:

These methods mainly include atomic force microscopy (AFM) and transmission electron microscopy (TEM). These methods facilitate the direct imaging of peptide nanostructure morphology.

2.3.2.1 Atomic Force Microscopy: AFM is a scanning probe microscopic technique, which scans the sample surface using a sharp tip positioned on a cantilever and provides a three dimensional image of a sample. The basic concept of AFM is shown in figure 2.5. The attractive or repulsive forces between the sample surface and tip make the positive or negative deflections in the cantilever. These deflections are measured by the laser beam, which falls on the backside of the cantilever and collected in photodiode. Cantilevers are generally made up of silicon (Si) or silicon nitride (Si_3N_4). [21, 22]

An AFM can be operated in different modes such as tapping, contact, non-contact modes, etc. The choice of mode for analysis depends upon the interatomic force (like van der Waals) between the sample and the cantilever. For contact mode, the repulsive forces must be predominant because the distance between tip and sample is very close (~10^{-10} m), while in non contact mode, inter-atomic forces must have attractive nature because of larger distance (in the order of 10 -100Å) between the tip and sample. However, the intermediate fluctuating distance can be observed in non-tapping mode. Generally, tapping mode tips are preferred for soft biological samples ad hard materials are studied using contact mode. [23]

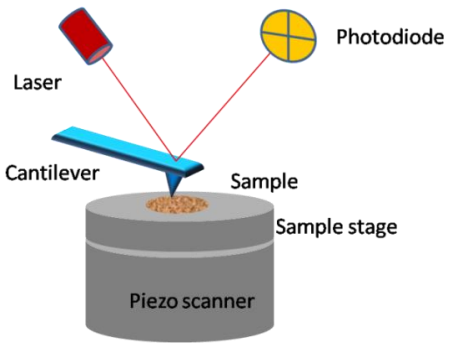

Figure 2.5 *Schematic diagram of working of atomic force microscope. (adapted from ref 24)*

The samples, either in the form of solution or dried film on the planar solid substrate such as mica or silicon can be used for imaging. Apart from morphology imaging, AFM can also be used to study the mechanical properties of protein structures and assemblies. In this thesis, Bruker Multimode 8 scanning probe microscope with a NanoScope controller and a J-scanner was used. Tapping mode tips were used with silicon cantilever obtained from Bruker (RTESP-150) with force constant 5 Nm^{-1}. The samples for imaging were drop-casted on a silicon wafer and dried before scanning. [25]

2.3.2.2 Electron Microscopy: In this thesis, transmission electron microscopy is used for studying the morphology of peptide nanostructures. TEM is based on principle of simple light microscope, but instead of light it uses high energy electron beam that can pass through the sample and determines the microstructure of the materials with the resolution of the atomic scale. The electrons emitted from the radiation source travel through the column in vacuum (as shown in figure 2.6). The accelerated electrons give the wavelengths in a much smaller range than that of light, thus facilitating a higher resolution. The resolution limit using visible light was proposed by Ernst Abbe's, which is approximately about 200nm. The resolution limit, d, is given as Abbe's equations (Equation 2.3), where λ and NA correspond to the wavelength of light and numerical aperture, respectively. [26-28]

$$d = \frac{1.22\lambda}{2\mathrm{NA}} \qquad \text{....Equation 2.3}$$

So, another equation is used to achieve the resolution in nm range for a electron source. According to Louis de Broglie, the wavelength of electron is related to its kinetic energy, which is given in the below equation 2.4.

$$\lambda_e \frac{h}{\sqrt{2m_o E\left(1+\frac{E}{2m_o c^2}\right)}} \qquad \text{....Equation2.4}$$

here, h = Planck constant, m_0 = electron rest mass, E= kinetic energy of electrons and c = speed of light. The variable resolution can be accessed by applying different accelerating voltages. Generally, for biological samples, lower accelerating voltages that are in the range of 80-120 kV are used while for other materials higher voltages can be used.

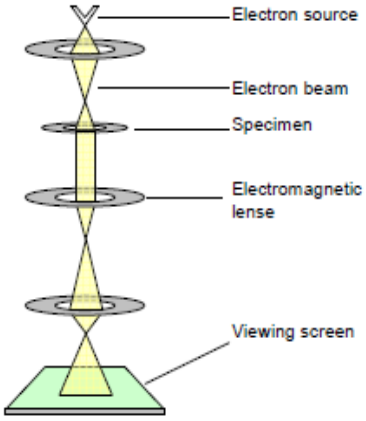

Figure 2.6 *Schematic representation of transmission electron microscope (adapted from ref 29.)*

The electrons are focused using electromagnetic lenses to produce a very thin beam that can penetrate through the specimen. However, the polymeric or biological samples are composed of elements, which weakly scatter the electrons and have little spatial variations in the electron density, resulting in poor contrast. To overcome this, the negative stain is used to stain such samples. These stains are composed of heavy metal ions such uranyl acetate, which are attached to the samples and enhance the contrast. Depending on the density of the sample, the electrons hitting the sample surface are scattered and lost from the beam. While the unscattered electrons hit a fluorescent screen below and provides a image that is the shadow of the specimen displaying different parts with varied contrast, as per their density. The image can be directly obtained on the screen. [26-28]

In this thesis, TEM has been used to study the morphology of peptide assemblies. The instrument used is JEOL JEM 2100 with a tungsten filament at an accelerating voltage of 200kV. The samples were placed on the carbon coated copper grids in the form of dried films. Peptides are poorly scattering, therefore, uranyl acetate salt (1-2%w/v) has been used to stain the sample before studying under microscope. [30]

2.3.3 Spectroscopic Characterization

2.3.3.1 Circular Dichroism: CD is one of the primary techniques to characterize the secondary structure of polypeptides and proteins. CD spectroscopy is a light absorption spectroscopy that measures the differential absorption of left and right circularly polarized light. In the UV region, the electronic CD is sensitive to the presence of chiral groups in organic molecules. Basically, the fingerprint spectra of different structural elements of peptide lie in the far UV region in the range of 190-250 nm. Some of the commonly occurring structures are shown in figure 2.7. The near UV region can provide information about aromatic residues having absorption features in the range of 250-310 nm. For α-helix, the characteristic minima are observed at 208 and 222 nm while β-sheet shows a broad minimum in the range at 218nm and a maximum in the range of 195-200nm. The disordered structures have a broad negative band at ~195-200 nm. [31-32]

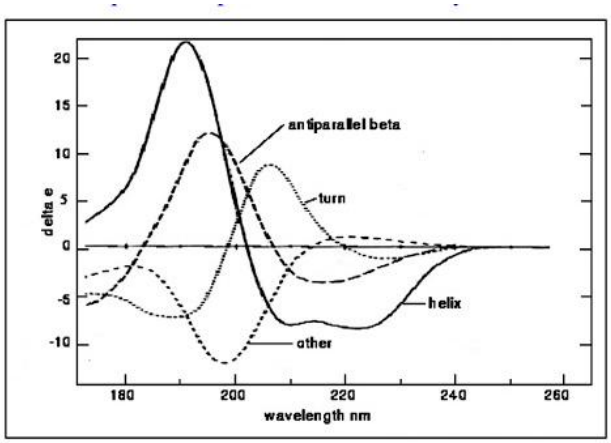

Figure 2.7 *Representative CD spectra showing common secondary structures of peptides. (adapted from ref 33)*

The CD signals are measured in terms of ellipticity that is defined as the tangent of the ratio of the minor to major elliptical axis. The other unit of denoting CD results is ΔE, which is the difference in absorbance of E_R and E_L by an asymmetric molecule. The molar ellipticity [θ] is related to the difference in extinction coefficients by [θ] = 3298ΔE having units in deg. · cm^2/dmol. Ellipticity is denoted as:

$$[\theta] = \frac{\theta}{10cl} \qquad \text{....Equation 2.5}$$

Here, *[θ]* is the molar ellipticity, *θ* is the measured CD signal amplitude in millidegrees (mdeg), *c* is the molar concentration and *l* is the path length of the cuvette in cm.

Proteins contain three types of chromophores that can absorb in the UV range, the peptide bond; the amino acid side-chains, and any prosthetic groups (aromatic moieties). The n → π* transition is the lowest energy transition in the peptide chromophore observed at 210-220 nm with very weak intensity. A much stronger absorption band centered at 190 nm is responsible for the majority of the peptide bond absorbance that occurs due to p →π* transition. [34]

This thesis mainly describes the secondary structures formed by the self-assembly ultrashort peptides mainly varying from dipeptides to pentapeptides. Jasco J-1500 CD spectrophotometer has been used for the measurements with 0.1mm quartz cells. The temperature was maintained at 20^0C through a water circulator. The recorded data is analyzed using Spectra Manager software.

2.3.3.2 Fourier Transform Infrared Spectroscopy (FTIR): FTIR is a powerful analytical technique for investigating protein secondary structure and local conformational changes. In electromagnetic spectrum, IR radiation ranges between 700 nm to 1 mm wavelength. Moreover, the entire range can be divided into 3 regions, near IR 12500-4000 cm^{-1} (0.8–2.5 μm), mid IR 4000-400 cm^{-1} (2.5–25 μm) and far IR 400-10 cm^{-1} (25–1000 μm). IR spectroscopy is associated with the molecular vibrations. The IR radiations of specific wavelengths are absorbed by the molecules, which results in a change of dipole moment of the molecule. When

the absorbed radiation frequency matches with the vibrational frequencies a characteristic peak is observed the IR region. [35, 36]

A typical protein IR spectrum often contains nine amide bands resulting from the vibrational contributions of both peptide bonds in protein backbone and amino acid side chains. Among which, Amide I and Amide II hold particular significance in elucidating the protein structure. The Amide I bands are associated with C=O stretching that ranges between 1600-1700 $cm^{-1}$and Amide II bands due to N-H bending. Since both C=O and N—H bonds participate in the hydrogen bonding that takes place between different moieties of secondary structure, the positions of both bands (Amide I & Amide II) are sensitive to the secondary structure composition of the protein.

A band typically in the range between1620-1640cm^{-1} is associated with the β-sheets. A band in the range of 1648-1657 cm^{-1} is expected to arise from α-helix structure while the disordered peptides show the characteristic bands in the range between 1642-1650cm^{-1}. The narrow band observed at 1675-1695cm^{-1} is assigned to antiparallel arrangements of β-sheets. However, there is a controversy regarding this assignment and *ab initio* studies suggest that this band is due to vibration coupling of carbamate moieties. The measurements are preferred in samples prepared in D_2O, to avoid the spectral overlap with water absorption that is also observed at ~1650cm^{-1}. [37, 38]

In the present thesis work, Agilent Cary 620 FTIR spectrophotometer and Bruker Vertex 70 ATR spectrophotometer were used for sample analysis. The samples used for the analysis were either in the form of lyophilized gels or wet gels prepared in D_2O. The spectra were collected in the range between 4000 to 400 cm^{-1} with a resolution of 1cm^{-1}. The final spectrum was the averaged spectra of 64 scans.

2.3.3.3 Fluorescence spectroscopy: Fluorescence spectroscopy is a type of luminescence spectroscopy that is caused by electronic excitation from ground state (S_0) to excited state (S_1 or S_2), after absorbing photons. When the excited molecule returns to the ground state it emits a lower energy photon than the absorbed photon. The lower energy is associated with longer wavelengths of the emission band than that of excitation band. The transition of electrons between different electronic levels occurring due to absorption and emission of light is classically explained by the Jablonski diagram (figure 2.8). Following absorption, there are probabilities for several processes that can occur. [39, 40]

Fluorescence is mainly observed when emission of photon takes place from the lowest vibrational level of singlet excited state (S_1). The intensity of emission, the wavelength of energy of the emitted photons and time for which the molecule remained in the excited state i.e. lifetime are extremely important in understanding the phenomenon of fluorescence. The average lifetime of fluorescence process is ~10^{-8} s. The fluorescence of the molecules is dependent on various factors such as temperature, pH, local polarity, aggregation, or surrounding molecules that can quench the energy of the molecules under observation.

Two more non-radiative decay processes take place that competes with the fluorescence: internal conversion and intersystem crossing. A molecule undergo internal conversion when it

passes from the lowest vibrational level of the upper state (S_2) to a higher vibrational level of a lower excited state (S_1), which is having the same energy. When the molecule is passed from excited singlet state to triplet state, it is known as intersystem crossing, which results in the phosphorence phenomenon. The average lifetime of phosphorescence ranges between 10^{-4}- 10^{4} s.

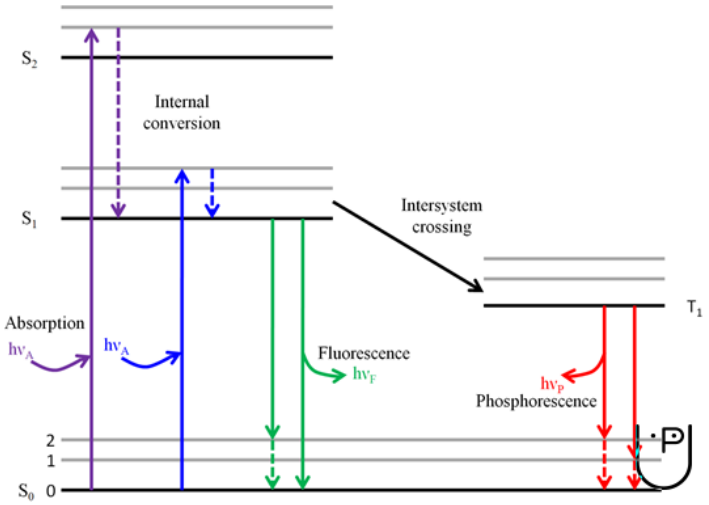

Figure 2.8 *The Jablonski diagram showing possible electronic transitions giving rise to absorption and emission. S_0, S_1, S_2, and T_1 denote the singlet ground, first, and second and first triplet electronic states respectively (taken from ref 41)*

Fluorescence spectroscopy has crucial role in studying protein conformations and interactions. Proteins are unique biomaterials because of their inherent fluorescence owing to aromatic amino acids such as tryptophan, phenylalanine and tyrosine. Interestingly, intrinsic protein fluorescence is the highly sensitive to local environment and changes in emission spectra in response to conformational transitions, substrate binding, denaturation or subunit association are highly useful. In context with short peptide amphiphiles, fluorescence spectroscopy is an important tool in predicting role of aromatic interactions in molecular self-assembly. [42, 43]

In this thesis, steady state spectrofluorometer (FS5) from Edinburgh Instruments has been used to perform fluorescence measurements. During work, the intrinsic fluorescence of amino acids as well as aromatic moieties were explored to investigate their self-assembly process. In our work, the change in the fluorescence intensity from solution to gel state was studied, to depict the hydrophobic environment in the self-assembled structures. In addition to this, external fluorescent dyes such as thioflavin T was used to check the formation of amyloid like fibrillar structures rich in β-sheet conformations.

2.3.3.3.1 Thioflavin T fluorescence assay: Thioflavin T (ThT) is an external fluorescent probe having benzothiazole ring, which is widely used for the identification and quantification of *in vitro* amyloid fibril formation. Free ThT exhibits weak fluorescence in an aqueous environment, but when it is bound to amyloid fibrils, it gives a strong fluorescence signal at ~482 nm when excited at 450 nm. The proposed mechanism of fluorescence enhancement of ThT upon binding to amyloids has been attributed to the rotational immobilization of the central C–C bond that

connects the benzothiazole and aniline rings. It results in high quantum yield of fluorescence due to preserved excited state, which otherwise is quenched upon free rotation in aqueous solvent. It has been reported that Th T has been used to measure the critical aggregation concentration (cac) of amyloid peptides. Th T fluorescence can also be used to study the kinetics of fibril formation by amyloid peptides and peptide amphiphiles. In addition to quantification of amyloid fibril formation, ThT fluorescence can also be used to visualize the fibrillar structures formed by self-assembly, using fluorescence microscope. [44-47]

Th T can also act as a molecular rotor. The fluorescent properties of Th T are susceptible to change in viscosity which is often associated with formation of amyloid-like fibrils. The enhancement in Th T emission intensity with the progression of self assembly provides an insight to understand the molecular mechanism of supramolecular assembly. As the self-assembly proceeds towards higher order, the viscosity of the peptide solution tends to increase to eventually form gels. The higher viscosity of peptide solutions restricts the torsional movement of Th T molecules in space and avoids non-radiative decay of excited state. The increase in fluorescence intensity depicts that the rigidity of Th T local environment has been increased indicating gelation. [48]

2.3.4 Powder X-ray diffraction (XRD):

XRD is another technique employed for the analysis of supramolecular order of gelling peptides. When an X-ray beam falls incident on a crystalline sample, it gets diffracted into many specific directions. The measurement of the angles and intensities of these diffracted beams produces a three-dimensional picture of the density of electrons within the crystal. This electron density depicts the mean positions of the atoms in the crystal, their chemical bonding, crystallographic disorder and various other information. The amorphous peptides can form crystalline structures after self-assembly which can diffract the x-rays and give characteristic peaks. [49, 50]

The diffraction of x-rays was explained as 'reflections' from different planes of crystals, firstly by W.L. Bragg. These reflections satisfy the following equation, known as Bragg's equation:

$$n(\lambda) = 2d \sin\theta \qquad \text{....Equation 2.6}$$

Here, n is a positive integer (1,2,3,...n), λ is the wavelength, d is the distance between the atomic planes, and θ is the angle of incidence of the X-ray beams. The long d spacing attained from XRD depicts the longest repeat distance in the ordered self assembled structures, which may provide information about the packing of small molecules in the fibrillar structures that can be either in an extended or a bent conformation.

In this thesis, Bruker D8 Advance X-ray diffractometer instrument equipped with Cu Kα radiation source (λ = 1.541 Å) was used under the accelerating voltage of 40 kV and 25 mA. The 2θ range used for recording the XRD pattern of peptide assemblies was 5^0 to 60^0. The lyophilized gel samples were used for analysis. XRD can provide the information regarding π-π stacking interactions and antiparallel β-sheet conformations by the characteristic peaks at ~3.8Å and 4.6 Å respectively. The intensity of signals can also be correlated with the extent of packing

i.e. the tightly packed β-sheets lead to the formation of more ordered structures having intense XRD signals. [51]

2.4 Biological characterization

2.4.1 *In vitro* cell culture: Cell culture involves culturing of cells in artificial environment (*in vitro*), which are conducive for their survival and/or proliferation. The artificial environment should be composed of necessary nutrients and provide controlled conditions such as temperature, humidity, gases, pH, etc. The selection of appropriate culture media is very crucial for *in vitro* cultivation of cells. The growth/culture media can be liquid or gel, which can support mammalian cells, plant cells, or micro-organisms. The basic composition of culture media includes inorganic salts, glucose, amino acids, vitamins, and serum as a source of growth factors, hormones, and attachment factors. In addition to nutrients, the growth media helps to maintain the pH and osmolarity. Generally, cells were cultured in culture media containing 10% serum (foetal bovine serum, FBS), and 1% antibiotic solution (penicillin-streptomycin). The cultures were incubated in humidified chamber with 5% CO_2 at 37^0C. [52]

2.4.1.1 Trypsinization: The isolated cells are cultured in the tissue culture flasks, which are made up of polystyrene with treated surfaces to promote cell attachment. To remove the adhered cells from the culture surface, Trypisn/EDTA solution (0.025% -0.5%) is used, depending on the trypsin activity or potency, incubation times; and cell lines. Trypsin hydrolyzes the proteins that provide anchorage to the cells and detaches them from culture surface. Trypsin can be deactivated by serum and divalent cations such as calcium and magnesium, therefore serum or media containing serum is usually added to the container once cells have detached, which is confirmed by observation under microscope. Trypsinization is often performed to transfer cells to a new container, observation for experimentation, or reducing the degree of confluency in the flask by removing some percentage of the cells. [53]

2.4.1.2 Cell counting: Prior to cell seeding for any experimentation, the cell counting was done using haemocytometer (contains the counting chamber). For cell counting, trypan blue stain is used, which can penetrate the dead cells but not the living cells. The stained cells were then gently expelled on to the hemocytometer under the coverslip and observed under a microscope. Cells were then counted within a given number of squares and total cell density of the suspension was calculated by using the given formula.

$$Total\ no.cells/ml = \frac{total\ \ cells\ \ counted}{number\ \ \ of\ squares} \times dilution\ factor \times 10{,}000 cells/ml \quad \ldots Equation\ 2.7$$

2.4.1.3 2 D cell cultures: 2D cell culture systems are meant to grow cells on flat surfaces, typically made of plastic. The coated surfaces provide two dimensional space for the cultured cells to adhere and spread. However, the 2D cultures poorly imitate the in vivo cell environment, but still, it is the most common method used by researchers and offers several advantages like simple, less expensive, easy cell observations and measurements. The 2D cultured cells on stiff plastic plate surfaces may lack cell-cell and cell-matrix interactions, which can affect other cellular processes. [54] But we believe that the 2D cultures over gel surfaces provides relatively flexible surface with tunable mechanical strength and distinct topography. In

addition to this, the functional epitopes on the nanostructures provide sites for cell-matrix interactions and promote cell-cell interactions.

In 2D culture with hydrogels, the gels are placed as a layer in wells of a culture plate or over the coverslips. The gels were allowed to adhere on the surface of plastics. Prior to cell culture, the gels were checked for their stability and integrity in the presence of culture media. This also helps to equilibrate the solvents present in gels and exchange them with cell culture media. Later, the cell suspension was added on the top of gel surface and cells were allowed to adhere and proliferate.

2.4.2 Metabolic activity assay: The MTT assay has been commonly used to assess cell viability. The principle of MTT assay is based on the cellular reduction of soluble tetrazolium salts to their insoluble formazan crystals. MTT is 3-[4, 5-dimethylthiazole-2-yl]-2, 5-diphenyltetrazolium bromide that is catalyzed by mitochondrial succinate dehydrogenase and serves as an indicator of mitochondrial respiration. MTT assay is a colorimetric assay, as the reduction of MTT is associated with color change from yellow salt solution to purple colored formazan crystals, which are dissolved in acid/alcohol or DMSO. Further, the converted formazan is quantified in terms of optical density using multiwell scanning spectrophotometer (ELISA plate reader) at 500-600nm. The optical density of treated cells was compared with that of control cells and results are reported as percentage cell survival, by using the following formula. [55-57]

$$\%\ viability = \frac{abs_{\ tretaed} - abs_{\ blank}}{abs_{\ control} - abs_{\ blank}} \qquad \text{.... Equation 2.8}$$

In this thesis, 0.5mg/ml of final concentration of MTT was added to each well under observation and incubated for 4 hrs, at 37^0C and 5% CO_2. At the end of incubation, the solution from each well is removed and 100µl of DMSO was added in each well to dissolve the insoluble formazan crystal. Later, the absorbance was measured at 495nm. The peptides were used in solution phase as well as gel phase to check their effect on metabolic activities of different types of cells. The duration for treatment was varied from 4hrs to 24 hrs, 48 hrs and 72hrs.

2.4.3 Cell Proliferation assay: Cell proliferation assays are meant to monitor actively dividing cells, which leads to an increase in number of cells. Alamar Blue based cell proliferation assay is a rapid, sensitive, and economical method to quantify cell proliferation. Alamar Blue is a resazurin salt, which is highly water-soluble, stable in the cell culture medium, and can penetrate through cell membranes. Unlike MTT, it is non-toxic and permits continuous monitoring of cells in culture. Alamar Blue is a fluorometric as well as colorimetric growth indicator based on detection of metabolic activity of cells. The dye behaves as an intermediate electron acceptor in the cellular electron transport chain, without affecting the inherent electron transfer. This accepted electron reduces the non-fluorescent blue color solution to fluorescent pink state. The reduced product is resorufin salt, which can be either detected by spectrophotometric method by measuring the absorbance at 570 and 600nm or fluorimetric method using 530-560nm and 590nm as excitation and emission wavelengths, respectively.

In this thesis, 100ul of 10% Alamar blue solution is added to the cultured cells and incubated for 4 hrs. At the end of incubation the supernatant solution from each well is separated in another

96-well plate for measuring their absorbance or fluorescence using micro plate reader (Tecan Infinite M Plex). To avoid any interference by peptides, the Alamar blue assay protocol was applied to blank gels (without cells) also and the readings were subtracted from the corresponding sample measurements. [58-60]

2.4.4 Live/Dead Assay: Live/dead assays are the fluorescent based method to simultaneously detect the live and dead cells by their differential labeling with two different dyes. In principle, cellular and membrane integrity is one of the important criteria that distinguish between viable and dead cells. It is assumed that viable cells are having intact and tight cell membranes, which does not allow some dyes to penetrate, whereas the dead cells are considered to have disrupted or broken membranes, which allows the penetration of dyes. However, some dyes like Calcein AM have high lipophilicity, which facilitates their permeabilization into cells and they stain the cytosolic region of the cells. Most of the dyes staining dead cells are nucleic acid binding dyes and stains the nuclear region. The differentially stained cells can later be analyzed by microscopy or flow cytometry. [61-63]

In our work, $DiOC_{18}$ (3) and PI (propidium iodide) were used as live and dead staining dyes respectively. The fluorescence excitation and emission maxima of $DiOC_{18}$ (3) were known to be 484 nm and 501 nm, respectively (when measured in methanol) and no appreciable changes in the spectra can be observed upon association with membranes. While, PI that binds to nucleic acids has a fluorescence excitation and emission maxima at 536 nm and 617 nm, respectively. The concentration of working solution of $DiOC_{18}$ (3) was 15μM and PI was 7.5 μM.

2.4.5 Confocal microscopy: Confocal microscopy is also known as 'confocal laser scanning microscopy (CLSM)'. It is a widely used technique for not only fluorescence imaging of samples but also for real time imaging and 3D screening of samples. The optical sectioning of sample helps in creating three dimensional images by capturing multiple two-dimensional images at different depths in a sample. [64, 65]

The principle of confocal fluorescence laser scanning microscopy is diagrammatically represented in Figure 2.9. The idea besides the working of confocal microscope involves point-by-point illumination of the sample and elimination of out-of-focus light. Coherent light emitted by the light source (laser system) passes through a pinhole aperture that is situated in a confocal plane with an objective near the specimen and another pinhole aperture placed in front of the photomultiplier detector. The laser reflected through a dichroic mirror falls across the sample in a defined focal plane that causes the emission of secondary fluorescence from points on the specimen (in the same focal plane). This emitted light is then passed back through the dichroic mirror and is focused at the detector pinhole aperture. The confocal imaging provides an advantage of high resolution and contrast attributed to the arrangement of spatial pinhole to block out-of-focus light in image formation. However, the increased resolution by blocking of light at pinhole was achieved at the cost of reduced signal intensity, which necessitates long exposure to reduce the signal to noise ratio. [66- 68]

Confocal microscopy allows the visualization of morphological structures and cellular processes through five simple steps. The first two steps involve the labeling and mounting of specimens for imaging, followed by image optimization, collection, and analysis. In this thesis, Zeiss

LSM880 confocal microscope (Carl Zeiss) was used for live-dead cell imaging (using $DiOC_{18}$ (3) and PI) and assessment of cell marker expression (using β-III tubulin and DAPI). In both cases, a set of two different dyes was used, which were excited at different wavelengths and separate emission signals were recorded to create a combined image. The confocal microscopy for imaging 2D cell cultures over hydrogel is important because the non-uniform gel surfaces provide different focal planes, which makes it difficult to analyze them through a simple fluorescence microscope.

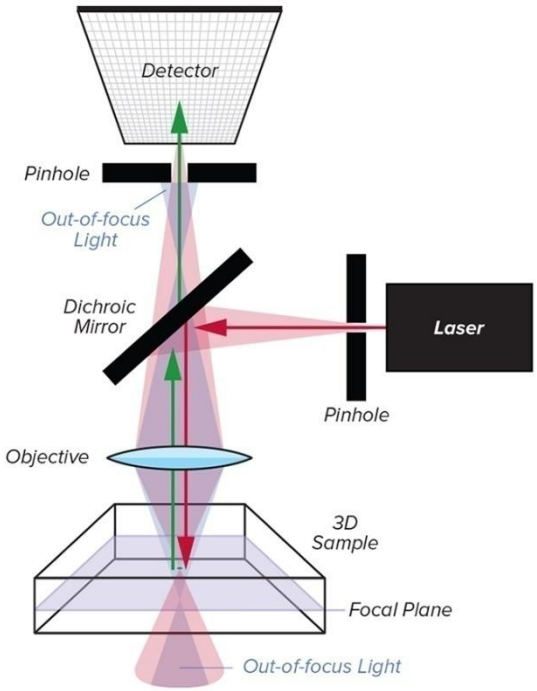

Figure 2.9 *Schematic representation of the working principle of confocal microscope. (taken from 67)*

2.4.6 Immunofluorescence staining: Immunofluorescence is a technique used for visualization of a specific protein or antigen in cells/tissue sections by the binding of a fluorescent dye conjugated specific antibody. Two types of immunofluorescence staining methods are majorly used: 1) direct immunofluorescence staining in which the primary antibody is tagged with fluorescence dye, and 2) indirect immunofluorescence staining in which a secondary antibody conjugated with fluorescent moiety and is used to recognize a primary antibody. The immunofluorescence staining can be done with fixed cells or tissue sections. Fluorescence microscope or confocal microscope was used to examine immunofluorescence stained samples. [69]

The basic steps involved in the immunofluorescence staining of adherent cells are cell preparation, fixation, permeabilization, blocking, immunostaining, and mounting. For preparing samples, cells were seeded (2-5x10^4 cells on the coverslips placed in each 35mm culture dishes) with 1mL of culture medium. The cells were incubated at 37°C at 5% CO_2 for the required time (24–48 hours) post cell seeding following which the cell culture medium was removed and cells

were rinsed 3 times using 1mL of 1X PBS. The cells were fixed using 4% paraformaldehyde (pH 7.4) and washed 3 times with 1mL of 1X PBS. After this, the cells were permeabilized using 0.1% - 0.5% Triton X-100 in 1X PBS and incubate the cells at room temperature. After the removal of Triton-X-100, the cells were washed 3 times with 500 µL of 1X PBS. Further, the blocking was performed by adding 500 µL of 2-5% BSA in 1X PBS and the cells were incubated at room temperature for 60 min. Ultimately, the immunostaining was performed by adding primary antibody at 1:500 dilution in dilution buffer (composed of 1% BSA, 0.1 % Triton X-100 in 1X PBS) and incubated at 4^0C for overnight. After the incubation, cells were washed thrice with the dilution buffer, and then secondary antibodies were added at 1: 1000 dilution, incubated for 1 hr at room temperature. After removal of secondary antibodies, the samples were washed thrice with the dilution buffer. After the complete protocol, other stains such as DAPI, etc. can be added to co-localize other cell organelles. At last, the coverslips were mounted with the help of the mounting medium (80% glycerol) and stored under dark until visualized under microscope. [70]

2.4.7 Flow cytometry for cell cycle analysis: Flow cytometry is an analytical tool to detect and measure physical and chemical characteristics of a cell or particle population. [71,72] It is widely used for cell counting, cell sorting, biomarker detection, determining cell characteristics, and diagnose the cell health. In this process, suspended cells or particles are injected into the flow cytometer instrument where each cell in the sample is individually focused through a laser beam, where the characteristic light scattering is measured. Light scattering at different angles is explored to distinguish differences in size and internal complexity of the samples, whereas wide array of cell surface and cytoplasmic antigens can be detected and analyzed by using light emitted from fluorescently labeled antibodies (figure 2.10). This approach makes flow cytometry a powerful tool for analyzing complex sample populations in detail, within a short span of time. [73, 74]

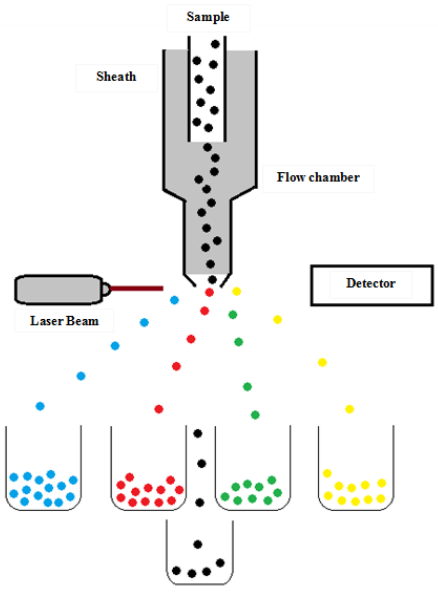

Figure 2.10 *Working principle of flow cytometer (taken from ref 73)*

Cell cycle analysis by flow cytometry is based on univariate analysis of cellular DNA content which is determined by the staining with propidium iodide (PI) or 4′,6′-diamidino-2-phenylindole (DAPI), followed by the deconvolution of the cellular DNA content frequency histograms. This approach determines the distribution of cells in three major phases of the cell cycle (G1 vs S vs G2/M) and also makes provides the information regarding apoptotic cells as indicated by their fractional DNA content. The other approaches may include bivariate analysis of DNA content and proliferation-associated proteins and BrdU labeling of the DNA-replicating cells. [75] In this thesis, PI based cell cycle analysis was performed using BD biosciences Flow Cytometer. The recoded results were analyzed using Flowjo v9 software.

2.5 References

1. R. B. Merrifield, Solid Phase Peptide Synthesis. I. The Synthesis of a Tetrapeptide, *J. Am. Chem. Soc.*, 85 (1963) 2149-2154.
2. N. Sewald and H.-D. Jakubke, Peptides: Chemistry and Biology, Wiley-VCH (2002) ISBN: 978-3-527-31867-4.
3. M. M. D. Jaradat, Thirteen decades of peptide synthesis: key developments in solid phase peptide synthesis and amide bond formation utilized in peptide ligation. *Amino Acids*, 50 (2017): 39–68.
4. P. H. H.Hermkens, H. C. J. Ottenheijm, D. C. Rees, Solid-phase organic reactions II: A review of the literature Nov 95–Nov 96, *Tetrahedron*, 53 (1997), 5643-5678.
5. Rinkamide resin structure https://www.sigmaaldrich.com/catalog/product/mm/855001?lang=en&region=IN.
6. C. A. Montalbetti, V. Falque, Amide bond formation and peptide coupling, *Tetrahedron*, 61 (2005) 10827–10852.
7. E. Bayer & M. Mutter, Liquid Phase Synthesis of Peptides, Nature, 237 (1972) 512–513.
8. Harry W. Lewis & Christopher J. Moody, Experimental Organic Chemistry: Principles and Practice (Illustrated ed.). WileyBlackwell, (1989) 159–173. ISBN 978-0-632-02017-1.
9. F. Rouessac and A. Rouessac, *Chemical Analysis: Modern Instrumentation Methods and Techniques*, John Wiley & Sons (2000).
10. D. J. Burdick, J. T.Stults, Analysis of peptide synthesis products by electrospray ionization mass spectrometry, *Methods Enzymol.* 289 (1997) 499-519.
11. *Avance. Beginners Guide. Version 003*, Bruker Biospin GmbH (2003).
12. R. J. Anderson, D. J. Bendell and P. W. Groundwater, *Organic Spectroscopic Analysis*, Royal Society of Chemistry (2004).
13. J. Keller, *Understanding NMR spectroscopy*, http://www-keeler.ch.cam.ac.uk/, *accessed in March, 2020*.
14. J. Raeburn, C. Mendoza-Cuenca, B. N. Cattoz, M. A. Little, A. E. Terry, A. Z. Cardoso P. C. Griffiths, D. J. Adams, The effect of solvent choice on the gelation and final hydrogel properties of Fmoc–Diphenylalanine, *Soft Matter* 11 (2015) 927-935
15. J. W. Goodwin and R. W. Hughes, *Rheology for Chemists: an introduction*, RSC (2000) ISBN 978-0-85404-616-4.

16. W. Macosko, Rheology: Principles, Measurements and Applications, Wiley-VCH, New York (1994) ISBN: 978-0-471-18575-8
17. Rheology basics, http://www.mate.tue.nl/~wyss/home/resources/publications/2007/Wyss_GIT_Lab_J_2007.pdf.
18. A. Y. Malkin, A. I. Isayev, *Rheology: Concepts, Methods, and Applications, 2nd Edition,* ChemTec Publishing (2011) ISBN: 9781895198812
19. J. Mewis, N. J.Wagner, "Thixotropy". Advances in Colloid and Interface Science. (2009)147-148, 214-227.
20. Mezger, T.G.: Applied Rheology (2018) (5th edition)
21. G. Binnig, C. F. Quate, C. Gerber, Atomic Force Microscope, *Physical Review Letters*. 56 (1986) 930–933.
22. F. J. Giessibl, *Advances in atomic force microscopy*, *Rev. Mod. Phys.* 75 (2003) 949-983.
23. Y. F. Dufrêne, T. Ando, R. Garcia, D. Alsteens, D. Martinez-Martin, A. Engel, C. Gerber, D. J. Müller, Imaging modes of atomic force microscopy for application in molecular and cell biology, *Nat. Nanotech.* 12 (2017) 295–307.
24. AFM schematics, https://en.m.wikipedia.org/wiki/File:AFM_schematic_(EN).svg.
25. J. Adamcik, R. Mezzenga, Study of amyloid fibrils via atomic force microscopy. Curr Opin Colloid Interface Sci 17 (2012) 369–376.
26. B. Fultz, J. Howe, *Transmission Electron Microscopy and Diffractometry of Materials*. Springer (2007) ISBN 978-3-540-73885-5.
27. D. B. Murphy, *Fundamentals of Light Microscopy and Electronic Imaging*. New York: John Wiley & Sons (2002) ISBN 9780471234296.
28. B. Alberts, *Molecular biology of the cell* (5th ed.) New York: Garland Science (2008) ISBN 978-0815341116.
29. TEM schematic, http://getdrawings.com/microscope-drawing-and-label#microscope-drawing-and-label-53.jpg, accessed in February, 2020.
30. J. Nebesářová1, M. Vancová, How to Observe Small Biological Objects in Low-Voltage Electron Microscope, Microscopy and Microanalysis. 13 (2007) 248–249.
31. R. W. Woody, Circular dichroism, *Methods Enzymol* 246 (1995) 34–71.
32. W. C. Johnson, Protein secondary structure and circular dichroism: A practical guide. *Proteins: Structure, Function, and Genetics*, 7 (1990) 205–214.
33. S. Brahms, J. Brahms, Determination of protein secondary structure in solution by vacuum ultraviolet circular dichroism, J. Mol. Biol. 138 (1980), 149-178.
34. N. J. Greenfield, Using circular dichroism spectra to estimate protein secondary structure, *Nat Protoc*. 1 (2006) 2876–2890.
35. W. K. Surewicz, H. H. Mantsch, D. Chapman, Determination of protein secondary structure by Fourier transform infrared spectroscopy: a critical assessment. *Biochemistry*, 32 (1993) 389–394.
36. H. Hiramatsu, T. Kitagawa, FT-IR approaches on amyloid fibril structure. *Biochim Biophys Acta* 1753 (2005) 100–107.
37. P. Haris, D. Chapman, The conformational analysis of peptide using Fourier transform IR spectroscopy. *Biopolymers* 37, (1995) 251–263.

38. J. Seo1, W. Hoffmann, S. Warnke1, X. Huang, S. Gewinner, W. Schöllkop, M. T. Bowers, G. von Helden, K. Pagel, An infrared spectroscopy approach to follow β-sheet formation in peptide amyloid assemblies, *Nat. Chem.* 9 (2017) 39-44.
39. S. Ladokhin, Fluorescence Spectroscopy in Peptide and Protein Analysis, Encyclopedia of Analytical Chemistry, 2006.
40. L.B. Berlman, Handbook of fluorescence spectra in aromatic molecules, Academic Press, New York, Vol. 1 (1965), Vol. II (1971).
41. Jablonski diagram, https://www.urbanpro.com/upsc-exams/upsc-chemistry-jablonski-diagram, accessed in February, 2020.
42. M. R. Liyanage, K. Bakshi, D. B. Volkin, C. R. Middaugh, Fluorescence Spectroscopy of Peptides. Methods in Molecular Biology, 1088 (2014) 237-246.
43. J. R. Lakowicz, Protein Fluorescence, Principles of Fluorescence Spectroscopy (2006) Springer, Boston, MA.
44. H. Levine H, Thioflavine T interaction with synthetic Alzheimer's disease β-amyloid peptides: detection of amyloid aggregation in solution. *Protein Sci*. 2 (1993) 404–410
45. C. Xue, T. Y. Lin, D. Chang, Z. Guo, Thioflavin T as an amyloid dye: fibril quantification, optimal concentration and effect on aggregation, *R. Soc. open sci.* 4 (2016) 160696.
46. S. A. Hudson, H. Ecroyd, T. W. Kee, J. A. Carver, The thioflavin T fluorescence assay for amyloid fibril detection can be biased by the presence of exogenous compounds, *FEBS J.* 276 (2009) 5960–5972
47. S. Marchesan, K. E. Styan, C. D. Easton, L. Waddington, A. V. Vargiu, Higher and lower supramolecular orders for the design of self-assembled heterochiral tripeptide hydrogel biomaterials, *J. Mater. Chem. B,* 3 (2015) 8123—8132.
48. V. I. Stsiapura, A. A. Maskevich, V. A. Kuzmitsky, V. N. Uversky, I. M. Kuznetsova K. K. Turoverov, Thioflavin T as a molecular rotor: fluorescent properties of thioflavin T in solvents with different viscosity, *J Phys Chem B.* 112 (2008) 15893-902.
49. X. Du, J. Zhou, J. Shi, B. Xu, Supramolecular Hydrogelators and Hydrogels: From Soft Matter to Molecular Biomaterials, *Chem. Rev.* 115 (2015) 13165−13307.
50. C. G. Pope, X-Ray Diffraction and the Bragg Equation, *J. Chem. Educ.* 74 (1997) 129-131.
51. O. S. Makin, L. C. Serpell, Structures for amyloid fibrils. *FEBS J*, 272 (2005) 5950–5961.
52. J. W. Pollard, J. M. Walker, Basic Cell Culture Protocols, 2nd ed. *Methods in Molecular Biology*, 75 (1997), Humana Press, US.
53. H. L. Huang, H.W. Hsing, T. C. Lai, Y. W. Chen, T. R. Lee, H. T. Chan, P. C. Lyu, C. L.Wu, Y. C. Lu, S. T. Lin, C. W. Lin, C. H. Lai, H. T. Chang, C. H. Chou, H. L. Chan, Trypsin-induced proteome alteration during cell subculture in mammalian cells, *J. Biomed. Sci.* 17 (2010) 36.
54. M. Kapałczyńska, T. Kolenda, W. Przybyła, M. Zajączkowska, A. Teresiak, V. Filas, M. Ibbs, R. Bliźniak, Ł. Łuczewski, K. Lamperska, 2D and 3D cell cultures – a comparison of different types of cancer cell cultures, Arch Med Sci. 14 (2018) 910–919

55. J. C. Stockert, R. W. Horobin, L. L Colombo, A. Blázquez-Castro,. Tetrazolium salts and formazan products in Cell Biology: Viability assessment, fluorescence imaging, and labeling perspectives. *Acta Histochemica,* 20 (2018) 159-167.
56. M. V. Berridge, P. M. Herst, A.S. Tan, Tetrazolium dyes as tools in cell biology: new insights into their cellular reduction. *Biotechnology Annual Review*, 11 (2005) 127-152
57. T. Mosmann, Rapid colorimetric assay for cellular growth and survival: application to proliferation and cytotoxicity assays, *Journal of Immunological Methods*, 65 (1983) 55–63.
58. S. N. Rampersad, Multiple Applications of Alamar Blue as an Indicator of Metabolic Function and Cellular Health in Cell Viability Bioassays, *Sensors (Basel).* 12 (2012) 12347–12360.
59. R.D. Fields, M. V. Lancaster, Dual attribute continuous monitoring of cell proliferation cytotoxicity. *American Biotechnology Laboratory*, 11 (1993) 48-50.
60. S.Al-Nasiry, N. Geusens, M. Hanssens, C. Luyten and R. Pijnenborg, The use of Alamar Blue assay for quantitative analysis of viability, migration and invasion of choriocarcinoma cells, *Human Reproduction*, 22 (2007) 1304–1309.
61. B. J. Kroesen, G. Mesander, J. G. ter Haar, T. H. The, L. de Leij, Direct visualisation and quantification of cellular cytotoxicity using two colour fluorescence, *J Immunol Methods* 156 (1992)47-54.
62. LIVE/DEAD® Cell-Mediated Cytotoxicity Kit (L7010), Molecuar Probes, Invitrogen detection technologies (2004)
63. O. Ozdemir, Evaluation of human mast cell-mediated cytotoxicity by DiOC18 target cell labeling in flow cytometry, *J. Immunol. Methods*. 319 (2007) 98-103.
64. J. B. Pawley, *Handbook of Biological Confocal Microscopy* (3rd ed.), (2006), Berlin: Springer. ISBN 0-387-25921-X.
65. J. C. Stockert, A. Blázquez-Castro, Fluorescence Instrumental and Techniques, *Fluorescence Microscopy in Life Sciences*. (2017) Bentham Science Publishers, 180–184. ISBN 978-1-68108-519-7
66. D. Semwogerere, E. R. Weeks, Confocal microscopy, *Encyclopedia of Biomaterials and Biomedical Engineering, Biomaterials, Biomedical Engineering*, (2005), DOI: 10.1081/E-EBBE-120024153
67. T. J. Fellers, M. W. Davidson, Introduction to Confocal Microscopy. Olympus *Fluoview Resource Center*. (2007). National High Magnetic Field Laboratory.
68. Confocal microscope schematic, https://www.laser2000.co.uk/applications/confocal-microscopy.
69. J. G. Donaldson, Immunofluorescence Staining, *Curr Protoc Cell Biol.* 69 (2015) 4.3.1-4.3.7.
70. Immunocytochemistry and immunofluorescence protocol, https://www.abcam.com/protocols/immunocytochemistry-immunofluorescence-protocol.
71. J. Picot, C. L. Guerin, C. Le Van Kim, C. M. Boulanger, Flow cytometry: retrospective, fundamentals and recent instrumentation. *Cytotechnology*. 64 (2012) 109–30.
72. M. Brown, C. Wittwer, Flow Cytometry: Principles and Clinical Applications in Hematology, Clinical Chemistry 46 (2000) 1221–1229.

73. Flow cytometry fundamental principle, How FACS works, https://www.bosterbio.com/protocol-and-troubleshooting/flow-cytometry-principle.
74. Flow cytometry, https://www.thyrocare.com/Fluorescence-flow-cytometry,
75. P. Pozarowski, Z. Darzynkiewicz, Analysis of Cell Cycle by Flow Cytometry, In: Schönthal A.H. (eds) *Checkpoint Controls and Cancer*. Methods in Molecular Biology, 281, Humana Press (2004).

Chapter 3

Differential self-assembly of Laminin derived short peptides using solvent mediated approach

3.1 Introduction

During the last few decades, self-assembling peptides have attracted extensive attention owing to their integral role in many biological processes. [1-4] Peptide or protein misfolding and their anomalous aggregation in to cross-β amyloid fibrils play a crucial role in several neurodegenerative diseases, like Alzeimer's, Parkinson's disease etc. [5, 6] The rapidly growing interest in identifying amyloid like short peptide fragments and understanding their self-assembling mechanism have developed a new class of functional materials for various biomedical applications. [7, 8]

One of the most studied short peptide sequence is diphenylalanine, which is the core recognition motif of β-amyloid peptide, Aβ-42. [9, 10] These short sequences are known to self-assemble into diverse structures like nanotubes, nanofibers, nanowires depending up on their self-assembling conditions, which undergo further hierarchical organization resulting in supramolecular gels. [11-13] Self-assembling peptides have been extensively explored towards their ability to form supramolecular gels under specific environmental conditions. [14-18] However, the investigation of the differential material properties in the final gel-phase materials as induced by different self-assembly pathways have attracted attention of the researchers only in recent years. [19- 24] In this context, it would be extremely interesting to note that the different gelation methods those were reported for Fmoc FF, the most explored member of the amyloid like short-peptide family, clearly resulting into diverse gels showing significant differences in their material properties. [25-28]

In this framework, one of the key regulators is solvent, which may play a crucial role in controlling the supramolecular gelation and material properties. [29] To this direction, Mahler et al. first time demonstrated the preparation of Fmoc FF gels by dissolving Fmoc FF in water-miscible solvent and further diluting it with water, leading to formation of one-dimensional structures transforming to supramolecular gels. [30] Such solvent triggered approach was further used by Adams and coworkers to show that the mechanical properties of the gels are highly susceptible to the differential mixture of DMSO and water. [31]

In a similar line, Hamley and co-workers have demonstrated that the short peptide fragments, derived from β-amyloid peptide, AAKLVFF exhibited distinct structural differences depending on the solvent polarity. [32] The transformation of nanotubes to filamentous tapes was reported as a result of competitive hydrogen bonding in water/methanol mixture. These studies clearly indicated the precise role of solvents towards controlling the self-assembly behaviour of the peptides in terms of promoting either gelator-gelator or gelator-solvent interactions to achieve the controlled nanostructure with desired function. [32]

To this end, laminins, the heterotrimeric glycoproteins, which are one of the major components of basement membrane, were found to be over-expressed in Alzeimer's disease. [33, 34] Several short peptide sequences have been identified from laminin protein, including Ile-Lys-Val-Ala-Val (IKVAV) and Tyr-Ile-Gly-Ser-Arg (YIGSR), which can mimic certain biological functions of the laminin protein. [35] IKVAV, present on long arm of A-chain of laminin, promotes neurite growth whereas YIGSR, found on B1- chain, controls neuronal cell-substrate adhesion and migration. [36, 37] To this direction, M. Nomizu's group working extensively towards identifying the amyloidogenic sequences based on the laminin protein, experimentally showed the formation of amyloid like-fibrils from Ile-Lys-Val-Ala-Val (IKVAV)-containing laminin A chain peptides. [34] These peptide derivatives promoted cell attachment and neurite outgrowth which clearly indicated the scope of utilizing these laminin derived peptide sequences in designing bioactive scaffold. Several scientists explored these bioactive peptide sequences for functionalization of different polymeric hydrogels or tethered it to a longer peptide amphiphiles to induce self-assembly to generate amyloid β-type fibrillar network. [38-43]

In order to broaden the spectrum of these laminin peptides, the detailed understanding of the self-assembling behavior of these short peptide sequences at the molecular level and their propensity to form the aggregated structure at different self-assembling conditions will be highly desirable. [12] These short peptide sequences (IKVAV and YIGSR) inherently fail to form hierarchical structures, which prevent the formation of supramolecular gels owing to the insufficient interactions within these peptide building blocks. Only a very few reports available in the literature clearly demonstrated that the hydrophobic modifications with a long alkyl chain or additional hydrophobic peptide sequence can only induce supramolecular gelation within these laminin derived peptide amphiphiles. [45] For example, Stupp et al., showed the self-assembly of two bioactive peptide (containing IKVAV and YIGSR ligands in a 13-mer sequence) amphiphile molecules into nanofibers by electrostatic attraction, over a wide pH range. [44] Williams et. al. reported the formation of supramolecular hydrogels by Fmoc-IKVAV at very high pH (~12), which was further tuned by chemical modification through incorporation of aspartic acid residues in IKVAV, resulting the gelation to occur at physiological pH. [45] However, such limited exploration of laminin derived peptides as supramolecular gelators relies on the traditional design paradigm where the differential nanostructures and material properties are fully encoded in to the molecular design of the peptide building blocks while the different self-assembly pathways to induce differential gelation behavior remain unexplored in this regime. The exploration of diverse self-assembly pathways through changes in local environment would eliminate the synthetic challenges while designing a gelator.

In this study, we focused on the creation of differential nanostructures from the laminin derived β-amyloid peptide sequence, IKVAV and YIGSR, which are less explored as self-assembling peptide gelators. The differential environmental conditions to tailor their self-assembling properties were obtained by using solvents of different polarity. For the first time, we have demonstrated the effect of solvent's nature on the differential self-assembling behavior among series of peptide analogues, which otherwise has been shown in single peptides, so far. The solvent triggered approach provides an access to more homogenous gels with lesser defects and higher reproducibility. Our approach relies on the solubility of the peptide building blocks in suitable solvents, and their exposure from a highly soluble to a poorly soluble environment to induce their self-assembly. Moreover, we derived a correlation between the solvent polarity and self-assembling properties of the peptides, which was quite general throughout the library and was evident through morphology, mechanical stiffness, thermoreversibility, thixotropy as well as through differential secondary structures. Such differential environment is expected to create structures, which are 'out of equilibrium' and hence the final gel phase properties can be tuned in a single gelator domain.

3.2 Experimental Section

3.2.1 Materials

All Fmoc protected amino acids, piperazine, diisopropyl carbodiimide(DIC), and cleavage solution reagents were purchased from Sigma-aldrich. The solid support Fmoc- Rink amide MBHA resin, Oxyma, Dimethylformamide (DMF) and Trifluoroacetic acid were purchased from Merck.

3.2.2 Peptide synthesis

Microwave Automated Solid Phase Peptide Synthesizer (Liberty Blue CEM, Matthews, NC, USA) was used to synthesize the laminin derived peptide sequences using standard fluorenyl-methyloxycarbonyl (Fmoc)-solid phase peptide chemistry. Fmoc-protected amino acids were coupled on a rinkamide resin. Fmoc-Rink Amide MBHA Resin was placed in the peptide synthesis reactor for 30 minutes with sufficient dimethylformamide for swelling. Fmoc deprotection was completed using 20% piperazine in dimethylformamide containing 10% ethanol in microwave. Each Fmoc-amino acid coupling step was achieved by heating in microwave with 0.5M N, N'-Diisopropylcarbodiimide (DIC) as activator and 1M Oxyma as activator base. Fmoc-deprotection was done using 10% piperazine in DMF. The peptides were cleaved from resin by using a mixture of 90% trifluoroacetic acid, 5% thioanisole, 3% 1, 2-ethanedithiol and 2% anisole for 3 hours. The product was recovered by precipitating the filterate in cold ether, followed by centrifugation and drying under vacuum. The dried product

was purified by preparative scale reverse phase high performance liquid chromatography (Waters).The mobile phase used was acetonitrile and water with 0.1% trifluorocetic acid. Pure peptide containing fractions were mixed and lyophilized, and stored under vacuum until use. The peptide identity was confirmed using mass spectrometry. Similarly, scrambled peptide sequence, Fmoc VVIAK was synthesized as control. However, a shorter amyloid based peptide was synthesized using method as solution phase synthesis. [46] The C log P values of the IKVAV and YIGSR backbones were calculated using Chem Draw Ultra 12.0 software.

3.2.3 Hydrogel formation in different solvent environment

The requisite amount of peptide was added to a screw-capped vial with an internal diameter of 10 mm, which was then dissolved using different solvent systems

i) ACN/water: Peptides were dissolved in half the total volume of acetonitrile followed by addition of equal amount of water (containing 0.1% trifluoroacetic acid) using alternate vortexing and sonication. The peptide solutions were left undisturbed to self-assemble and form gels.

ii) DMSO/water: The peptides were dissolved in 10% v/v of DMSO followed by addition of 90% water (containing 0.1% TFA) and allowed to self-assemble to form gel.

iii) PBS: Gels were formed using phosphate buffer saline (pH 6). In this method, peptide was dissolved in PBS and heated in a Stuart digital waterbath (SWD15D) maintained at 80°C, having temperature range from 25 °C to 99.9 °C and temperature stability of ± 0.5 °C. The peptides formed gel immediately after cooling to room temperature.

The gels were used for further characterization after the incubation of 24 hrs.

3.2.4 Hydrophobicity measurement

The surface hydrophobicity of the peptide nanostructures formed after self-assembly was estimated through contact angle using Drop shape analyser (DSA25E, Kruss). Contact angle was measured in two ways:

Method1- In the absence of solvent: The gels were drop casted on the glass slide and dried to make a thin film. After drying, a droplet of water was placed on the surface and angle between the surface and water droplet was measured.

Method 2- In the presence of solvent: The gel droplet was dropped from the needle on the clean glass slide surface and angle was measured.

3.2.5 Morphological Characterization

3.2.5.1 Atomic Force Microscopy (AFM)

The samples were prepared by diluting the peptide gels (at MGC) to 10 times. Then, 10 μL of diluted gel solution was mounted on a silicon chip (4” diameter diced silicon wafer cleaned in

methanol/ acetone by sonication for 25 min beforehand) and the sample was air dried. The atomic force microscopic (AFM) images were obtained by scanning the silicon wafer surface in air under ambient conditions using Bruker Multimode 8 scanning probe microscope operated in tapping mode with Nanoscope V controller and a J-scanner.

3.2.5.2 Transmission Electron Microscopy (TEM)

The diluted peptide gels (at MGC) were allowed to adsorb for 3 min on the carbon coated copper TEM grids. Excess sample was wicked off with the filter paper. It was followed by the addition of 2% (w/v) uranyl nitrate with incubation of 5 minutes and wicking off the excess stain. Samples were then kept in the desiccator under vacuum. TEM micro-graphs were recorded with a JEOL JEM 2100 with a Tungsten filament at an accelerating voltage of 200 kV.

3.2.6 Material Property Analysis

3.2.6.1 Mechanical Properties

To verify the mechanical properties of the resulting hydrogels, dynamic frequency sweep experiments were carried out on a strain-controlled rheometer (Anton Parr MCR302) using 50mm parallel plate geometry. The samples were prepared at 40 mM concentration and incubated at room temperature for 24 h before measurement. The storage (G') and loss (G") moduli of the gels were recorded as a function of frequency sweeps between 0.1 and 18 Hz. To ensure that the measurements were made in the linear regime, an amplitude sweep was performed with strain ranging from 0.01-100% and optimum strain value was obtained from the linear viscoelastic region (the results showed no variation in elastic modulus (G′) and viscous modulus (G″) up to a strain of 1%). The experiments were performed using a solvent trap to prevent any kind of solvent loss due to evaporation, at 20^0C and temperature was controlled with an integrated electrical heater. The measurements were repeated for three times to ensure reproducibility, with the average data shown.

3.2.6.2 Mechanoresponsive behavior studies

To explore self-healing behavior of the peptide gels, thixotropic studies have been performed. Gels prepared at 40 mM concentration were used for this study. Before performing the step - strain rheology, we checked the recovery properties by mechanical shaking, which transforms the gel material into solution (sol) and its recovery into the self-supporting gel state upon resting. However, the recovery varies in both peptides in different solvent environment. The thixotropic nature of the gels was confirmed with step-strain rheology experiments, by putting the strain values within linear viscoelastic (LVE) region. The stress was consecutively applied to the gels, due to which they lose their solid-like behavior ($G' < G''$) and as soon as the stress is reduced, they began to transform into semi-solid gel like state. During experiment, the gel

samples were subjected to pre-shear stress interval with 0.1% strain (equivalent to its LVE range strain) at frequency of 1Hz, to obtain the initial values of modulus for 100 s. Then a high shear stress with a strain of 100% for 200 s was applied. This is then followed by the recovery of gel state from sol state by reducing the strain to 0.1%, for 800s.The frequency, is fixed to 1Hz for both deformation and recovery process. Three consecutive cycles were applied on the hydrogels to compare the extent of gel strength recovery.

The microscopic analysis of deformed gels and their recovered state was carried out using AFM. The samples collected at different phases of cycle were diluted and drop casted on silicon wafer. After 3 minutes, the excess sample was wicked off using filter paper and the silicon substrate was air dried. Finally each sample was visualized under AFM to capture morphological changes.

3.2.6.3 Thermo-reversible property assessment

To assess the thermoreversible property, the gels were prepared at concentration of 30 mM using ACN/water mixture with 0.1% TFA and PBS. After 24 hrs, the mechanical stiffness of the gels prepared in both solvent systems was measured using oscillatory rheology. The gel melting temperature (T_m) of all the gels was determined by heating the hydrogels in Stuart digital waterbath (SWD15D) having temperature range from 25 °C to 99.9 °C and temperature stability of ± 0.5 °C. The temperature was increased from 25 °C to 95 °C in steps of 2 °C and hydrogels were stabilized for 10 minutes at each temperature. The temperature at which gel transforms to sol is recorded as its gel melting temperature. In ACN/water, Tm of Fmoc IKVAV was ~95°C, myristyl IKVAV was ~ 90°C and acetyl IKVAV was~75°C and in PBS, ~80°C for all the three peptides. Similarly, for Fmoc YIGSR and myristyl YIGSR, Tm was found to be around ~80°C in ACN/water for both and ~85°C for both, in PBS, respectively.

Depending upon the gel melting temperatures, the gels were subjected to heating in a water bath maintained at specific temperature, until the gels get melted. During melting, the vials were tightly sealed capped to avoid any solvent loss by evaporation. The melted gels were allowed to recover by keeping them at room temperature. After 3 hours, the mechanical strength of reformed gels was measured. The strain used for both the measurements was obtained from the linear viscoelastic region of amplitude sweep graph and was found to be 0.1%. The storage (G') and loss (G") moduli of the gels were recorded as a function of frequency sweeps between 0.1 and 100Hz.

3.2.7 Spectroscopic characterization

3.2.7.1 Circular dichroism

CD measurements of all peptides (30 mM) were performed using Jasco J-1500 CD spectrophotometer. Spectra for all peptides were obtained between a wavelength of 195-320 nm with 1 s integrations with a step size of 1 nm and a single acquisition with a slit width of 1 nm. A 0.1 mm quartz cuvette was used in which three repeat scans were compiled to generate the average spectra. The results were analyzed using the Jasco Spectra Manager.

The CD melting studies was performed by recording the temperature scans in the range of 25^0C to 80^0C with temperature increasing at the rate of 2.5^0C per minute. The gels at 30 mM concentration were used. The CD was recorded, in the range of 195-320 nm, at rise of every 5^0C.

3.2.7.2 FTIR spectroscopy

FT-IR spectra were recorded on an Agilent Cary 620 FTIR spectrophotometer. The spectra were taken in the region between 400 and 4000 cm^{-1} with a resolution of 1 cm^{-1} and averaged over 25 scans. Spectra were background subtracted to correct for atmospheric interference. Samples were analyzed by mixing about 10% of lyophilized gels (30 mM) with KBr powder to form pellets. The background was collected using blank KBr pellet.

3.2.7.3 Fluorescence Spectroscopy

Fluorescence experiments were undertaken using an Edinburgh Instruments spectrofluorometer (FS5). Excitation and emission wavelength were set as 280 and 320 nm respectively. Emission spectra (excitation at 290 nm for Fmoc-group) were acquired at 25^0C in the 300–550 nm range using FLUORACLE software. Gels prepared at a concentration of 30 mM, which were transferred to quartz cuvette after preparation with a path length of 1cm and analyzed for the initial emission intensity, then kept overnight for further analysis.

3.2.7.4 Thioflavin T assay for β-sheet determination

The fluorescence spectroscopy was performed on the Edinburgh spectrofluorometer (FS5) in a 1.0cm quartz cuvette. ThT stock solution (8mg in 10 ml PBS pH7.4 buffer) was freshly prepared and filtered through 0.2 mm syringe filters. The working solution was prepared by diluting stock solution (1ml to 50ml) with PBS pH 7.4. The fluorescence intensity was measured for 1ml of working solution by excitation at 440 nm (slitwidth 1 nm) and emission at 482 nm (slitwidth 1nm) with an average intensity of 8 accumulations. For measuring the fluorescence intensity of peptide hydrogels (30 mM), 1ml of working solution was titrated with 20µl of peptide hydrogels/solutions. For each sample the spectra was recorded from 450 to 600 nm, at room temperature. The final intensity for each sample was plotted after subtracting the ThT spectrum in PBS.

3.2.8 Fluorescence Microscopic Imaging

The diluted peptide gels were mixed with Th T working solution (as prepared for Th T fluorescence spectroscopy) in 2:1 ratio and allowed to incubate for 5 min. 50µl of mixture was added on a glass slide and covered with coverslip. The image was observed by the Olympus BX53 fluorescence microscope and captured using Q-Capture Pro 7 software. The 20X lens was used to capture bright field images and the fluorescence images with the help of FITC emission filters (an excitation wavelength of 490 nm).

The self-assembly mechanism was studied by adding the Th T (10ul of working solution) to the peptide solution (at 2 mM), immediately after dissolution. Then 10ul mixture of peptide and Th T solution was drop casted on slide and fixed by coverslip. The images were recorded at different time points starting from initial, 0 min, 10 min, 20 min, 60 min and 90 min. No further change in the structures was observed after 90 min, due to drying, at further time points.

3.2.9 XRD analysis

The Fmoc IKVAV and Fmoc YIGSR gels were prepared at a concentration of 30 mM in different solvents as described in hydrogels preparation method. The gels were air dried to form powder. The powdered sample was placed on glass holder. The spectra was recorded in the 2θ range of 5^0 to 60^0 using Bruker D8 Advance X-ray diffractometer instrument equipped with Cu Kα radiation source (λ = 1.541 Å) under the accelerating voltage of 40 kV and 25 mA.

3.2.10 *Generality of solvent mediated approach in controlling peptide self-assembly*

To generalize the concept, self-assembly of control peptides was studied in different solvent conditions. A classical amyloid dipeptide Fmoc FF was used as a positive control and a scrambled laminin peptide, Fmoc VVIAK was utilized as a negative control. Synthesis of Fmoc FF was done by liquid phase peptide synthesis. [46] While Fmoc VVIAK was synthesized by solid phase synthesis as reported above. Further, both the peptides were dissolved in 50% ACN/water (0.1% TFA), 10% DMSO in water (0.1% TFA) and PBS (pH 6) and allowed to self-assemble at concentrations ranging from 5 mM to 20 mM. For rheology measurement, Fmoc FF gels were prepared at 10 mM concentration and Fmoc VVIAK gels at 20 mM in all three solvent systems. For each gel, the frequency sweep was performed in the linear regime of viscoelastic region with 0.1-0.5% strain for Fmoc FF and 0.05% strain for Fmoc VVIAK peptides, using 50 mm parallel plate. To study the morphological changes, AFM was performed for gels prepared in different solvents, diluted upto 20 times in water.

3.2.11 Solvent Exchange

Fmoc IKVAV gels prepared at 5mM concentration in ACN/water and DMSO/water. After 24 hrs of gelation, 1ml of milli-Q water was added at the top of the gel and allowed to perfuse for 2 hrs. After 2 hrs the supernatant water is replaced by fresh water. Similar procedure was repeated

upto 4 cycles. After this the DMSO gel was lyophilized to carry out FTIR analysis. Similarly, the media was added in place of water and mechanical strength was checked using rheometer. [31]

3.3 Results and Discussion

3.3.1 Design and synthesis of peptides

The library of structurally related penta-peptides derived from laminin was designed to demonstrate the differential self-assembly behavior in different solvent systems (Figure 3.1). To understand the trend of gelation behavior in different solvents, both hydrophobic as well as hydrophilic analogues were designed. The design of the peptides was based on the two functional sequences of laminin protein identified as IKVAV and YIGSR. The C log P values of IKVAV and YIGSR were calculated to be as 0.42 and -3.218, respectively, which also indicates the more hydrophobic character of IKVAV in comparison to YIGSR. However, both the sequences lack the ability to self-assemble in to three dimensional supramolecular gels. Therefore, the sequences were further capped with different hydrophobic modifications at N-terminal ranging from aromatic Fmoc (N-(fluorenyl-9-methoxycarbonyl); C-14 aliphatic chain, myristyl; and a small aliphatic group, like acetyl (figure 3.1).

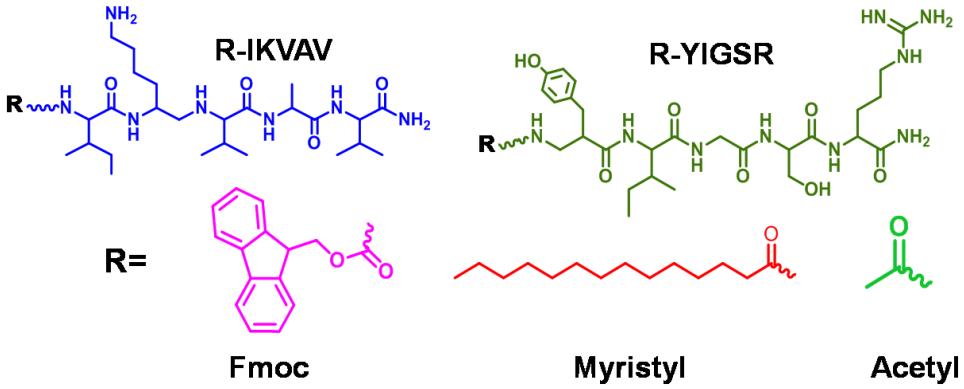

Figure 3.1 *Molecular design of the library of hydrophobically modified self-assembling laminin derived peptides based on pentapeptide sequences IKVAV and YIGSR along with the hydrophobic cappings such as Fmoc, Myristyl and Acetyl.*

These simple modifications are expected to induce balanced intermolecular interactions in the form of π-π interactions, hydrophobic interactions and H-bonding interactions in peptide backbone of these short peptide sequences, which would likely to result in gelation. [47- 49] However, these modifications do not always results into formation of gels. In this context, Orbach et al., demonstrated a library of Fmoc based di-, tri- and tetra- peptides which self-assembles to form distinct morphologies and physical properties, but only a few peptides forms

gel while others failed to undergo gelation. [50] Therefore, a proper hydrophobic-hydrophillic balance within a peptide molecule is critical while designing a new peptide gelator, in the absence of which highly hydrophobic modifications fail to induce gelation. The designed peptides were synthesized using standard solid phase synthesis protocol. The purity of peptides was assessed using LC-MS (shown in Table 3.1).

***Table 3.1**. m/z of different laminin derived peptides from Chemdraw (Ultra 12.0) and LCMS.*

Peptides	Molecular Formula	m/z	
		Predicted (Chem Draw)	Calculated (LC-MS)
IKVAV	$C_{27}H_{49}N_7O_5$	527.38	527.34
Fmoc IKVAV	$C_{40}H_{59}N_7O_7$	749.45	749.41
Myristyl IKVAV	$C_{39}H_{75}N_7O_6$	737.58	737.54
Ac IKVAV	$C_{27}H_{50}N_7O_6$	569.39	569.36
YIGSR	$C_{25}H_{41}N_9O_7$	593.66	593.54
Fmoc YIGSR	$C_{41}H_{53}N_9O_9$	815.40	815.38
Myristyl YIGSR	$C_{40}H_{69}N_9O_8$	803.53	803.53
Ac YIGSR	$C_{28}H_{45}N_9O_8$	635.34	635.34

3.3.2 Solvent induced self-assembly of designed peptides

It is likely that solvent environment has remarkable effect on the self-assembly behavior of the peptides and getting an insight of solvent gelator interaction would be highly beneficial. The differential assembling behavior of peptides in particular solvent can be determined by using Hansen solubility parameter. [16, 51, 52] The solvents can be categorized as good solvents which have the capability to dissolve the gelator while bad solvent has poor solubility for the gelator. For inducing gelation, a balanced solubility and insolubility is required. [53] It is quite obvious that the hydrophobic peptides require a organic solvent (good solvents), which aid to dissolve the peptide monomer, while charged peptide sequences dissolve easily in acidic/basic environment, depending on the pH required for protonation or deprotonation. So, considering our design of hydrophobic, basic nature peptide sequences, we have chosen the solvents of different polarity varying from highly polar phosphate buffer saline (pH 6) to 10% DMSO/water (0.1% TFA) and comparatively weakly polar 50% ACN/ water (0.1% TFA). [52, 54, 55] The final pH of the aqueous-organic mixture gels was found to be nearly 2, due to presence of 0.1% TFA, while for PBS gels, pH was nearly 5. The acidic pH of the solvents plays an important role in ionization and dissolution of peptides containing basic amino acid (Lys- and

Arg-). In addition to this, the acidic pH also promotes the aggregation of β-amyloid peptides. [52] To confirm the role of TFA in self assembly, the gelation of peptides was tried with solvents without TFA which resulted the pH of medium~7. Interestingly, no gelation was observed in solvents without TFA, but self-assembly occurred which was evident from the microscopy of corresponding peptide solutions (figure 3.2 a and b). It was also crucial to know critical concentration of TFA required in inducing self-assembly and gelation within the peptides. To this direction, we used 0.01% & 0.05% TFA, resulting into peptide solution with pH ~6 and ~4 respectively. It was observed that no gelation resulted with 0.01% TFA, whereas weak gel has been obtained in presence of 0.05% TFA (figure 3.2 c and d).

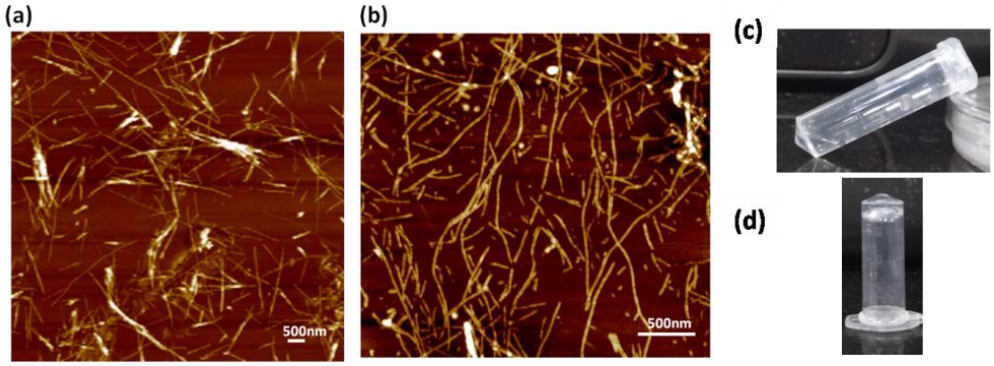

Figure 3.2 *AFM mages of Fmoc IKVAV (5mM) in (a) ACN/water and (b) DMSO/water without any TFA in solvent (inset showing the optical images of peptide solution), (c and d) Optical images of Fmoc IKVAV in ACN/water with 0.01% TFA and ACN/water with 0.05% TFA.*

The effect of solvent parameters is clearly reflected in minimum gelation concentration (MGC) of peptides. As shown in table 3.2 and figure 3.3, the minimum gelation concentration (MGC) of Fmoc IKVAV in ACN/water was 5 mM which increases to 15 mM in PBS, the polar counter part, whereas, Ac IKVAV was found to gelate at 30 mM concentration in ACN/water which decreases to 25 mM in PBS. This indicates that in order to reduce contact with polar environment, the hydrophobic peptide molecules interact with each other through strong π-π or hydrophobic interactions, at lower MGC. [56, 57] While, the peptides having smallest hydrophobic modification can be easily dissolved in aqueous solvent and the self-assembly induced by hydrophobic effects resulted in their gelation (figure 3.4).

Table 3.2 *Minimum gelation concentrations (MGC) of laminin peptides in different solvents as measured by inverted vial method.*

Peptides \ Solvents		ACN/ water (50:50)	DMSO/ water (10: 90)	PBS (100mM, pH 6)
		MGC (mM)		
IKVAV	Fmoc	5	5	15
	Myristyl	5	10	25
	Acetyl	30	35	25
YIGSR	Fmoc	20	20	10
	Myristyl	15	15	10
	Acetyl	--	--	--

On the contrary, lesser hydrophobic YIGSR analogues, Fmoc YIGSR and myristyl YIGSR, the MGC observed was 20 mM and 15 mM respectively, in both ACN/water and DMSO/water which decreases to 10 mM in PBS for both the peptides (table 3.2 and figure 3.3). It was observed that in aqueous-organic mixture, the Fmoc and myristyl analogues of YIGSR showed higher MGC in comparison to corresponding IKVAV analogues due to lower solubility of hydrophillic YIGSR derivatives in organic solvents leading to weaker hydrophobic interactions. This also results in increased exposure of gelator molecules towards solvent. Addition of ACN ($\epsilon\sim$ 37) and DMSO ($\epsilon\sim$ 47) to water ($\epsilon\sim$80) reduces the dielectric constant of water, which induces self-assembly due to hydrophobic effects. [49, 58] Moreover, the molecules having aromatic or hydrophobic interactions, shows faster self-assembly kinetics. [58] In the similar context, the least hydrophobic Ac-YIGSR fail to gelate in any of the solvent because of improper hydrophobic-hydrophilic balance. [59] As discussed, unmodified peptides IKVAV and YIGSR failed to form gels in both aqueous and non-aqueous solvent mixtures owing to the weak intermolecular association of the peptide building blocks. Our results corroborates with the previous studies stating that organic solvent (ACN) interferes with the gelator-water H-bonding, thus promoting gelator-gelator interactions. [58] Such differential behaviour of the laminin derived peptides in different solvent systems would be highly interesting for molecular level understanding of the mode of self-assembly and thus tune their physical properties leading to different nanostructures for further biotechnological applications.

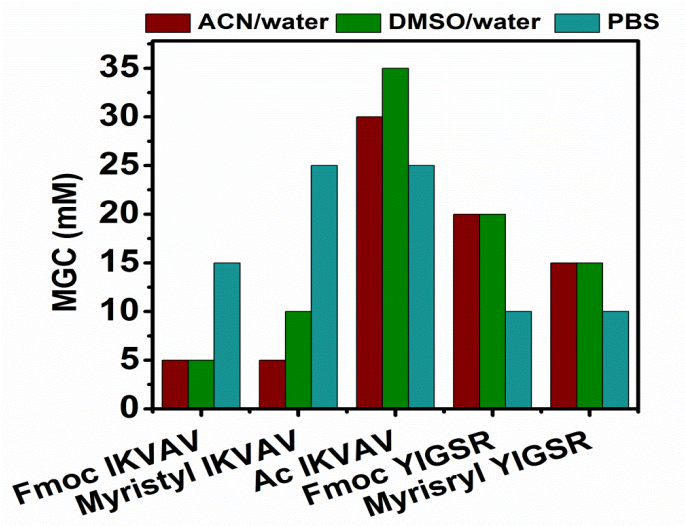

Figure 3.3 *Minimum gelation concentrations of gelator peptides in different solvents.*

Further, the gelation studies revealed that aqueous-organic mixtures are more favourable for inducing hierarchial self-assembly in more hydrophobic peptide derivatives by promoting hydrophobic and aromatic interactions between gelator moieties, which otherwise could not be possible in aqueous solvent due to their poor solubility (figure 3.4 a and b). [59] While, the aqueous solvents favours the self-assembly of less hydrophobic analogues by promoting gelator-gelator interaction. However, it is extremely difficult to find the major determinant for controlling self-assembly, among various solvent parameters like, polarity, hydrogen bond acceptor or donor ability, surface tension, dielectric constant. [60] According to Meijer's report, the organic solvent (ACN) behaves as a good solvent and peptides tend to remain in monomeric dissolved state, avoiding the polymerization. In the presence of ACN and DMSO, the gelator-solvent interaction dominates, avoiding self-assembly. [58] As soon as, the poor solvent i.e. water is added, the gelator-gelator interaction is enhanced, probably, due to high surface tension of water, eventually moving organic solvent to the hydrophobic pockets. [59, 60] The Hansen solubility parameters also favour the similar explanation that hydrophobic IKVAV derivatives requires solvents with low solubility parameters i.e δ_p and δ_h (δ_p for polarity parameter and δ_h for hydrogen bonding parameter), while, the YIGSR derivatives having more polar groups (-OH groups of tyrosine and serine and –NH2 group of aginine) requires high δ_p and δ_h. The gelation was triggered by the addition of water to the solublized peptides, which promotes the intermolecular amide-amide H-bonding in the gelator molecules, in addition to hydrophobic and aromatic π interactions. On the other hand, YIGSR derivatives showed preferred gelation in water which suggested that binding strength of gelator-gelator hydrogen bonding (amide-amide and hydroxyl) is higher than the solvent-gelator H-bonding interactions and thus supports

gelation of hydrophilic derivatives. [61, 62] The self-assemblies were further strengthened by aromatic π-π interactions and hydrophobic interactions (aromatic moieties or aliphatic carbon chain) by the hydrophobic effect of aqueous solvents.

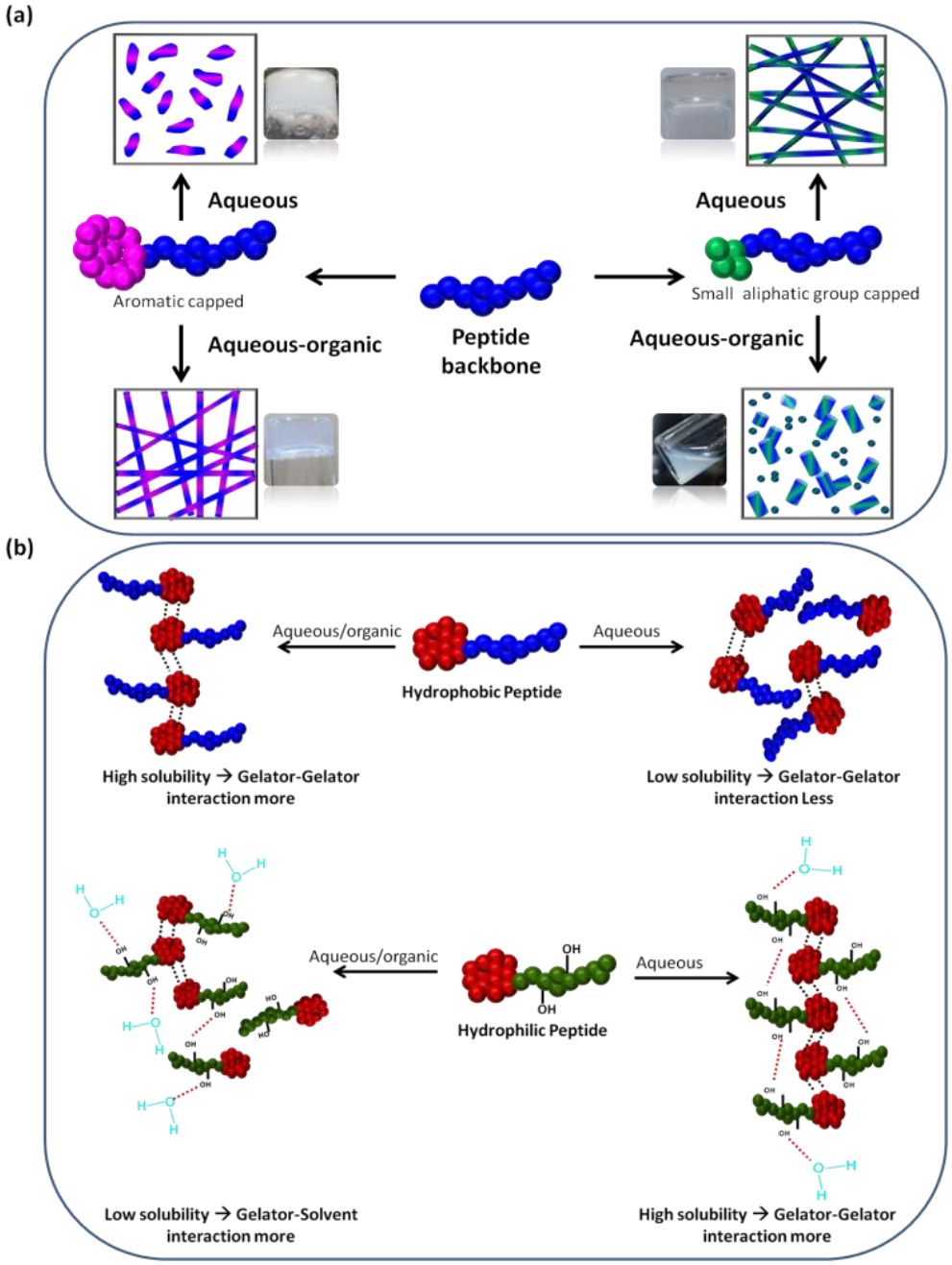

Figure 3.4 *(a) Schematic representation of the differential self-assembling behaviour of peptides in aqueous and aqueous-organic mixture of solvents. Modification of peptide backbone with larger hydrophobic groups forms sheet like structures in aqueous solvent and nanofibrous network in aqueous-organic mixture. In contrast, smaller group favours entangled fibrous*

network in aqueous solvent and coexisting spherical aggregates and short fibers like morphologies in aqueous-organic mixture. (b) Highlighting the aqueous and aqueous-organic solvent interactions with Fmoc modified hydrophobic IKVAV and hydrophilic YIGSR peptides. For IKVAV, higher solubility of gelator leading to greater gelator-gelator interactions in aqueous-organic mixture while poor solubility in aqueous solvent leads to weaker gelator-gelator interactions forming less ordered structures. On the other hand hydrophilic YIGSR exhibits prominent intermolecular gelator-gelator H-bonding in aqueous solvent due to higher solubility while gelator-solvent H-bonding may dominate due to poor solubility of hydrophilic peptides in aqueous-organic solvent.

3.3.3 Surface hydrophobicity

It was noteworthy that different polarity of solvents would lead to differential arrangement of the peptides, which could result in different surface hydrophobicity. Investigation of surface hydrophobicity would give deeper insight into the solvent effects on the molecular packing within the nanostructures. [63, 64] To check the surface hydrophobicity of these self-assembled nanostructures, contact angle measurements were performed. [65] Contact angle measurement is one of the commonly used methods to determine the surface hydrophobicity of the materials. If contact angle between the surface and the droplet is greater than 90^0, it is considered as hydrophobic. However, in contrast to this, in case of hydrogels, water being the major component, the contact angle observed was below 90^0, indicating their hydrophilic nature.

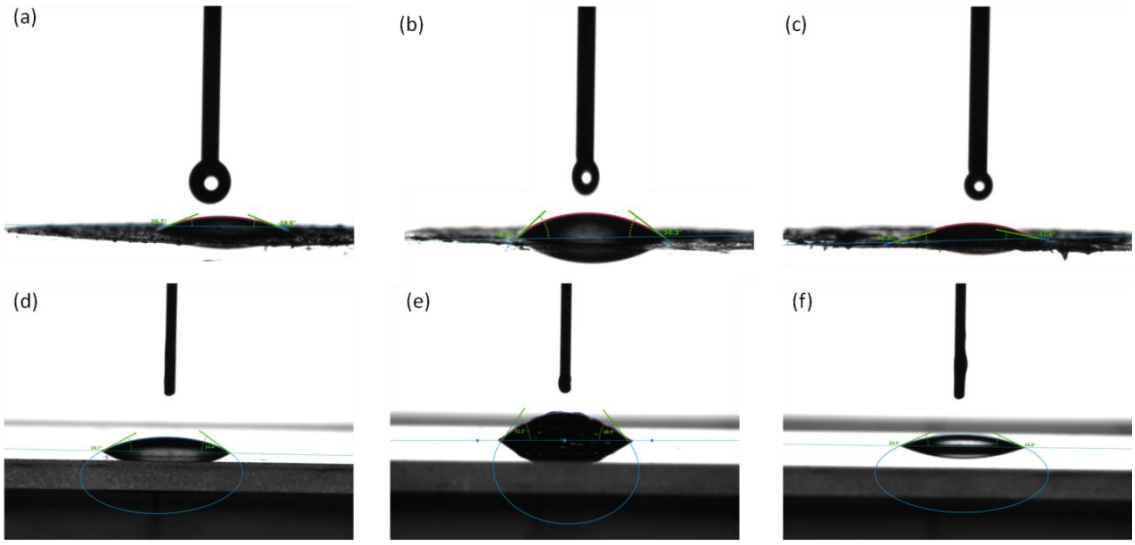

Figure 3.5 *Contact angle measurement by dropping water droplet on the dried film of Fmoc IKVAV gels (method 1) prepared in (a) ACN/water, (b) DMSO/water, (c) PBS and contact*

angle of gel droplet prepared in (d) ACN/water, (e) DMSO/water and (f) PBS with that of glass slide surface (method 2).

We have measured the contact angle in two different ways: one of the methods focuses on the investigation in absence of solvent which includes preparation of the dried film of gels on the surface of glass slide and measuring its contact with water droplet. While other method demonstrated the contact of peptide gel droplet with glass surface i.e. presence of solvents (figure 3.5). In both the methods, the Fmoc IKVAV gels prepared in 10% DMSO/water showed the higher contact angle of ~40.45^0 with method 1 and 50.6^0 with method 2. However, gels prepared in ACN/water and PBS showed much lower contact angles 19.8^0 (method1) and 31.55^0 (method 2) in ACN/water and 12.75^0 (method 1) and 24.6^0 (method 2) in PBS, indicating their hydrophilic nature (table 3.3). Also the literature suggests that the relative polarity of acetonitrile is more i.e. ~0.46 than DMSO i.e. ~0.44, which might be the reason for more hydrophilic nature of ACN/water gels. [66]

Table 3.3 *Contact angle measurement of the laminin derived peptide hydrogels prepared in different solvents by using two different ways.*

Solvent system	Method 1*	Method 2**
ACN/water	19.8^0	31.55^0
DMSO/water	40.45^0	50.6^0
PBS	12.75^0	24.6^0

**Method 1: dropping a water droplet over the dried hydrogel film and measuring the contact angle between the two.*

***Method 2: placing the hydrogel as a droplet and measuring its contact angle with glass surface.*

3.3.4 Morphological investigations of self-assemblies

Accessing diverse nanostructures from single gelator, depending upon their dissolution memory, reduces the synthetic challenges of creating huge peptide libraries. We expected that differential solubility of peptides in variable solvents, triggers different self-assembly pathway leading to the differential molecular packing, which can be microscopically observed as diverse nanostructures. The structural variations with respect to solvent polarity was investigated using atomic force microscopy (AFM) which showed a clear correlation between the solvent polarity and the peptide hydrophobicity at the nanoscale. The more hydrophobic IKVAV analogues were found to be more susceptible to solvent variation and showed prominent structural

differences. In aqueous-organic mixture, Fmoc IKVAV showed more homogenous fibrillar structures of ~32±10 nm which changes to shorter heterogenous thicker fibers of diameter ~82±12 nm in PBS (figure 3.6 a-c and 3.10 c). More prominent structural variations could be observed with myristyl IKVAV, which showed a clear transformation of long network of nanofibers in ACN/water to short length fibers in DMSO/water and finally sheet like structures in PBS (figure 3.6 d-f). [67- 69] In corroboration to comparatively higher MGC values, the least hydrophobic analogue in the series i.e. Ac IKVAV followed different pattern from its more hydrophobic analogues. It showed coexistence of spherical aggregates and short fibers in ACN /water, which transforms to well-defined fibrillar network in PBS. The diameters of the fibers were also reduced from 84±11 nm in ACN/water to 53±11 nm in PBS with improved hierarchical order of the nanostructures.

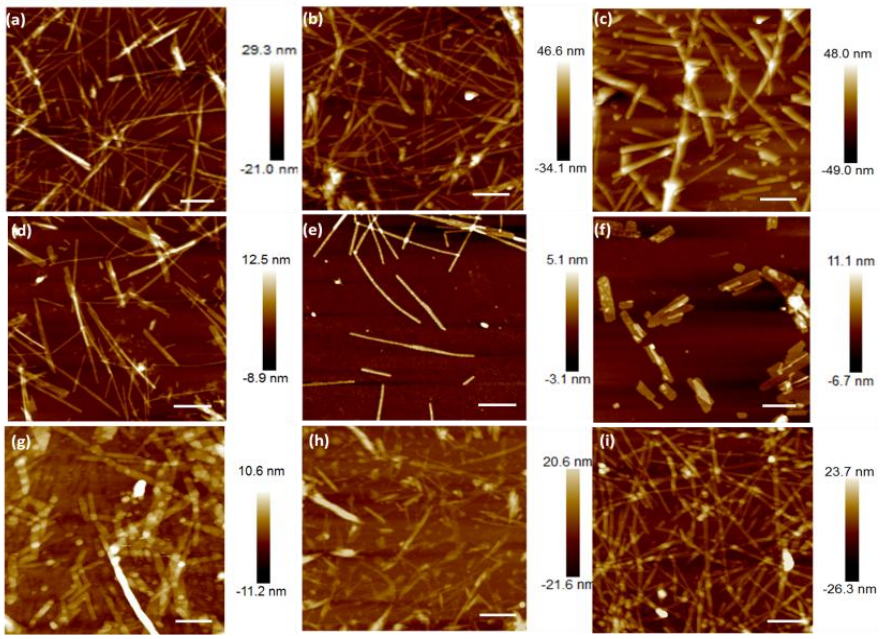

Figure 3.6 *AFM images of IKVAV derived peptide gels with (a-c) Fmoc IKVAV, (d-f) Myristyl IKVAV and (g-i) Acetyl IKVAV at MGC in ACN/water, DMSO/water and PBS, respectively. Scale bar is 500nm for each image*

The solvent effect was less pronounced in YIGSR derived supramolecular structures in comparison to more hydrophobic IKVAV sequences. However, the Fmoc and myristyl YIGSR showed more homogenous and dense network in PBS along with aggregation of fibers at some places (figure 3.7 a- i). The diameter of Fmoc YIGSR and myristyl YIGSR in ACN/water was found to be 60±12 nm and 49±11 nm, which was reduced to 20±2 nm and 25±5 nm in PBS, respectively (figure 3.10 d). The involvement of H-bonding between gelator-gelator molecules

might be the plausible reason of exhibiting lesser fiber diameter in aqueous solvent. Interestingly, the least hydrophobic peptide analogue of our library i.e Ac YIGSR, which did not form gel irrespective of the solvent, showed a significant variation from aggregates to highly ordered fibrillar network when solvent polarity has been increased from ACN/water to PBS (figure 3.7 g-i). This suggests the intriguing effect of solvent environment is still persistent even at sub-gelation state. It also clearly indicates that although greater extent of gelator-gelator interactions in aqueous solvent exist which tends to induce self-assembly in Ac YIGSR, however the absence of sufficient hydrophobic interaction as well as π-π stacking makes it fail to gelate. As expected, the unmodified IKVAV and YIGSR being a non-gelator showed the formation of the spherical aggregates owing to the absence of sufficient intermolecular interactions, irrespective of the solvent (figure 3.8). The morphological analysis results suggested that less polar solvents are favorable for inducing complex hierarchical assembly in hydrophobic peptides, whereas the vice versa holds true for hydrophilic peptides.

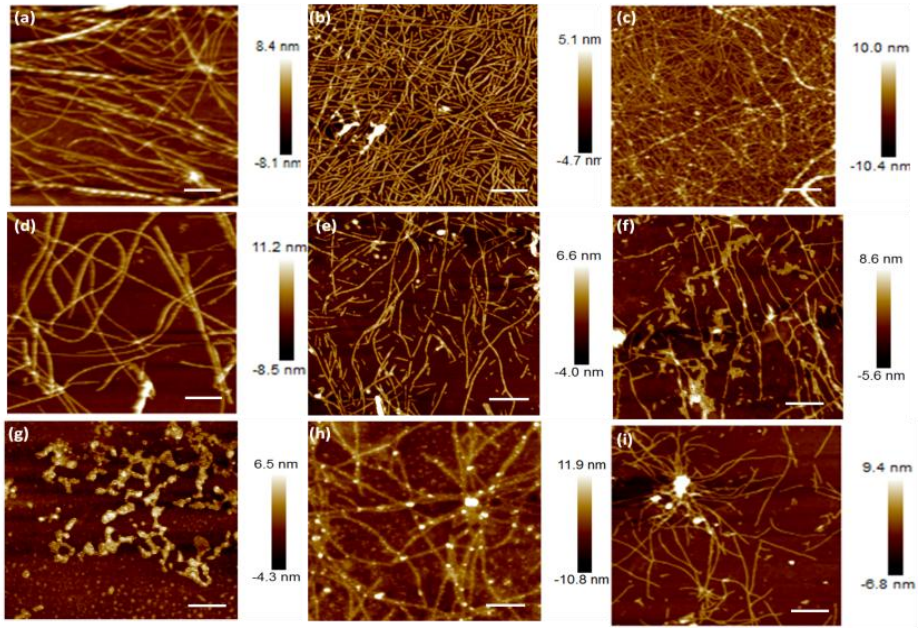

Figure 3.7 *AFM images of YIGSR derived peptide gels with (a-c) Fmoc YIGSR, (d-f) Myristyl YIGSR and (g-i) Acetyl YIGSR at MGC in ACN/water, DMSO/water and PBS, respectively. Scale bar is 500 nm for each image.*

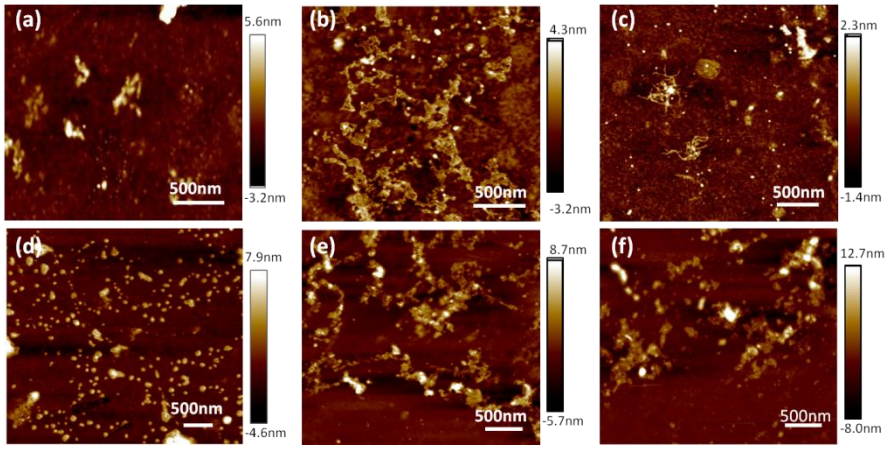

Figure 3.8 *AFM images of unmodified laminin peptides (a-c) IKVAV and (d-f) YIGSR in ACN/Water, DMSO/Water with 0.1%TFA and PBS, respectively.*

The nanoscale morphologies of the structure underpinning the formation of the gels were further assessed by Transmission Electron Microscopy (TEM). [70] TEM of peptide gels prepared with ACN/water also demonstrated nanofibrous morphology for these peptide gels and

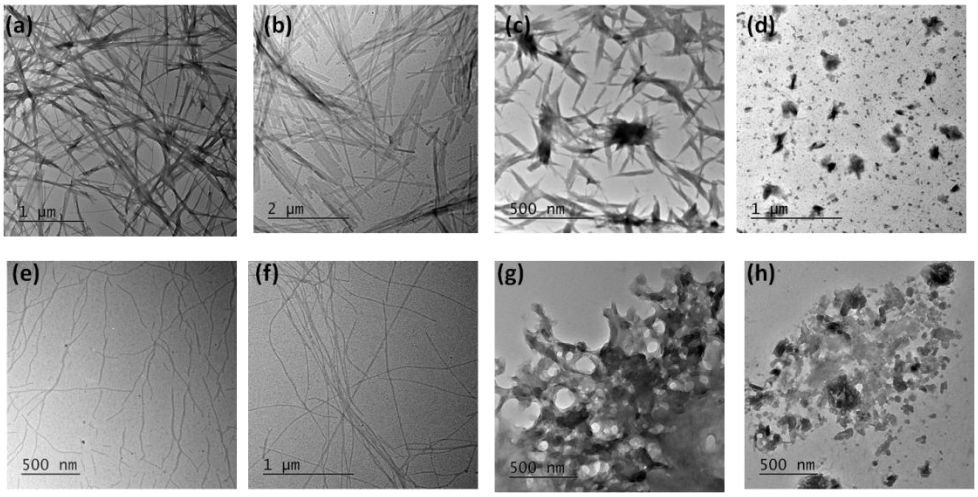

Figure 3.9 *TEM images of different laminin peptide gels/solutions (a) Fmoc-IKVAV, (b) Myristyl -IKVAV, (c) Ac-IKVAV, (d) IKVAV, (e) Fmoc-YIGSR, (f) Myristyl-YIGSR, (g) Ac-YIGSR and (h) YIGSR after 24 hr of incubation in ACN/water with 0.1% TFA as a solvent system.*

showed close resemblance with AFM (figure 3.9).Thus, using this unique solvent mediated approach for controlling variable supramolecular nanoarchitechtures could be an effective way to design dynamic assembly of gel-phase soft materials. [71]

3.3.5 Viscoelastic measurements of self-assembled gels

The mechanical properties of these gels with respect to different solvents were then probed by oscillatory rheology (Figure. 3.10 a & b). The differential solubility of peptides in different solvents leads to the formation of different structural network, owing to variable interactions. For all gels (at 40 mM concentration), the storage modulus (G') was found to be an order of magnitude higher than the loss modulus (G'') indicating their viscoelastic nature. The mechanical strength of these gels was found to be significantly affected by the solvent

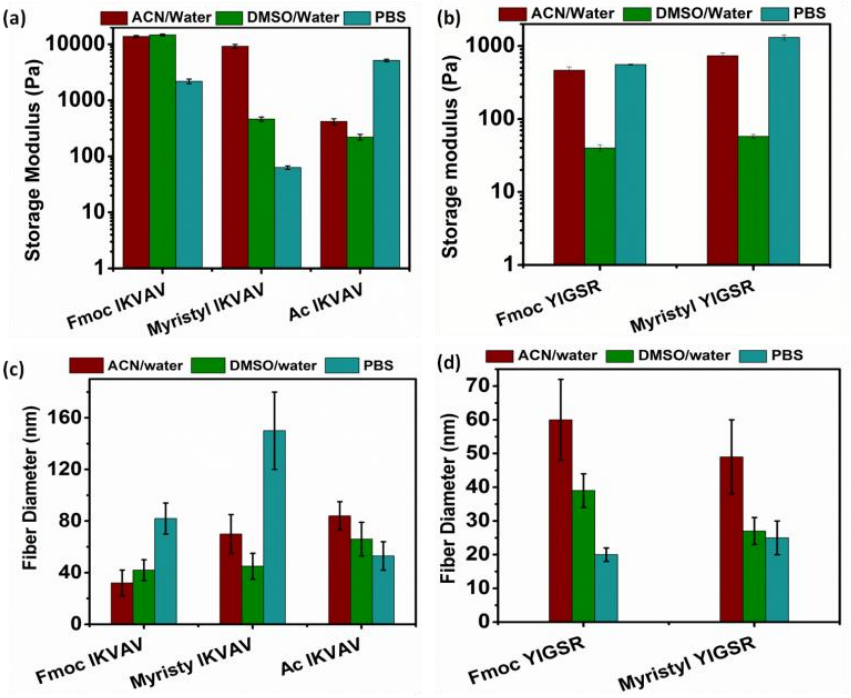

Figure 3.10 *Mechanical strength investigation of laminin peptide (a) IKVAV based and (b) YIGSR based gels in different solvents (ACN/water, DMSO/water, PBS) and (c & d) comparison of fiber dimensions of IKVAV and YIGSR gels, respectively, obtained from AFM.*

environment (Figure 3.10 a and b). [72] The close observation clearly depicted that the hydrophobic derivatives of IKVAV like Fmoc, myristyl showed higher mechanical strength of gels prepared in aqueous-organic mixture in comparison to those prepared in aqueous PBS. As evident from the results, Fmoc-IKVAV has stiffness in the similar range with storage modulus of 13.8±0.56 KPa and 14.7±0.51KPa in ACN/water and DMSO/water, respectively. However, the gel stiffness significantly decreased in aqueous PBS buffer, 2±0.21 KPa, which is in corroboration with higher MGC of Fmoc IKVAV peptides in aqueous solvent (figure 3.10 a). Fmoc capping was found to induce extensive intermolecular interactions which were more favored in aqueous-organic mixture and trigger the formation of highly ordered supramolecular structures resulting in the formation of the strongest gels. [73] Moreover, myristyl IKVAV, showed less rigid network than Fmoc IKVAV which might be due to lack of π-π interactions, thus inducing formation of relatively weaker gels than Fmoc IKVAV. The hydrophobic interactions of myristyl-IKVAV showed significant variation in the presence of different solvent leading to the gels of variable storage modulus, ranging from 9.2±0.7 KPa in ACN/water to 0.5±0.04 KPa in DMSO/water and 0.06±0.004 KPa in PBS. The solvent dependent reduction in gel strength was possibly due to lower solubility of myristyl IKVAV in aqueous solvent, which hinders gelator-gelator interactions. [21] Interestingly, Ac-IKVAV gels showed reversed physical behavior in PBS, as it exhibits highest strength in aqueous solvent in comparison to aqueous-organic solvent mixture. The results clearly depicts an order of mangnitude difference in storage moduli of Ac-IKVAV in PBS than in the other two solvents, which was found to be 0.4±0.05 KPa in ACN/water, 0.2±0.03 KPa in DMSO/water and the highest strength was observed in PBS i.e. 5±0.3 KPa. This change is attributed to increased H-bonding between gelator-gelator molecules leading to stronger gel. [74]

3.3.6 Mechanoresponsive behavior of gels

Interestingly, these gels were found to be thixotropic. The mechanoresponsive property was found to be highly susceptible to the solvent memory where it has been dissolved. The gels (40 mM) were subjected to high shear strain of 100% for 200 s due to which they lose their solid-like behaviour followed by subsequent reduction of strain to 0.1% (equivalent to LVE range strain value) for 800s resulting in recovery of gel state from sol state (figure 3.11). [46, 75] However the extent of recovery is different for Fmoc IKVAV and Fmoc YIGSR in aqueous and aqueous- organic solvent environments (Fig. 3.11 a-b). The step-strain rheology curves for Fmoc IKVAV showed a significant difference in the gel recovery in different solvents varying from 90±8%, 45±5% and 3±1.6% structure recovery, in ACN/water, DMSO/water and PBS, respectively, within 60s. Whereas, the Fmoc YIGSR showed comparatively higher recovery in

all three solvents with recovery percentage varying from 72±5% in ACN/water, 87±8% in DMSO/water and 99±4% within 60s. [24] The probable reason for this differential recovery might be that the less polar solvents are expected to promote hydrophobic as well as π- π interactions in hydrophobic IKVAV derivatives, thereby inducing a faster recovery through

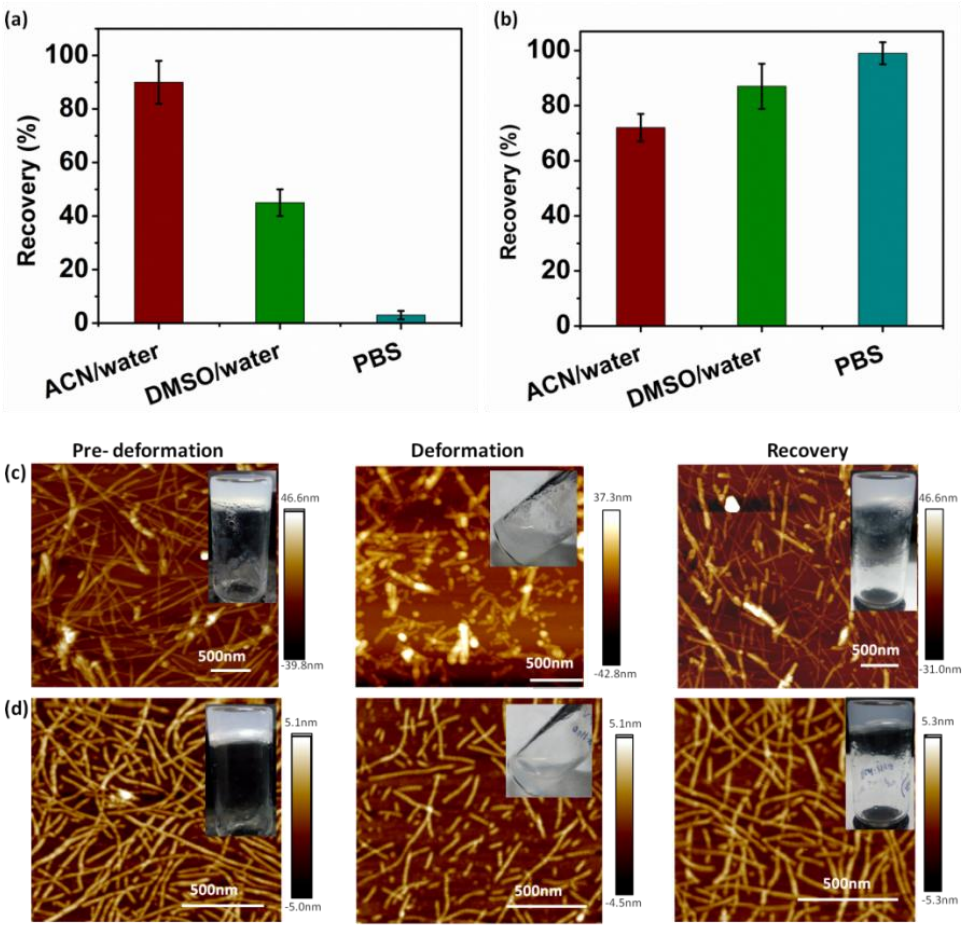

Figure 3.11 *Thixotropic studies of (a) Fmoc IKVAV and (b) Fmoc YIGSR peptides in different solvent system showing different percentages of recovery after stress followed by AFM images at different stages of pre-deformation, after deformation and after recovery of (c) Fmoc IKVAV and (d) Fmoc YIGSR. Inset shows the macroscopic thixotropic transition with optical images of gel and sol.*

facilitating gelator-gelator interactions, which is clearly indicated by our thixotropic results. [76] The weak gelator, YIGSR showed a better recovery profiles compared to strong gelator IKVAV. [77] However, the reverse pattern can be observed in Fmoc YIGSR, where the structure recovery ratio is higher in PBS (~100%) than in ACN/water (72±5%). This thixotropic behaviour was further visualized under AFM, which clearly showed the nanofibers were broken to give rise to the shorter fibers under stress, however on resting, the shorter fibers rejoined and formed the fibers of same dimension (Fig. 3.11 c and d). This change in nanostructure is responsible for gel-sol-gel transition observed macroscopically. Thus, solvent environment has a significant role in regulating the intermolecular interactions during self-assembly of peptide building blocks into supramolecular gels.

3.3.7 Thermoreversible property

Another interesting property shown by these gelators was the thermoreversible behavior, which extends their potential in several fields. [78] The thermoreversibility of all the gels (30 mM) were checked in least polar (ACN/water) and most polar (PBS) solvent systems (figure 3.12). The results revealed that all the gels were able to recover their gel strength after melting (table 3.4). Initially during gel melting studies, the temperature at which macroscopic appearance of gel melting for all gels was observed to be higher than 80^0C, which was higher than boiling point of ACN (82^0C), except for Ac IKVAV (~75^0C). The results showed that all IKVAV and YIGSR peptide gels exhibited higher mechanical strengths in ACN/water after recovery. The probable reason for this increment in mechanical strength was due to the exclusion of condensed solvent after recovery. The storage modulus of Fmoc IKVAV, myristyl IKVAV and acetyl IKVAV were 7.2±1.2 KPa, 3.2±1.6 KPa and 0.31±0.05 KPa initially, interestingly upon resting at room temperature, gel recovery took place and it regained its strength (Table 3.4). However, an enhancement was observed in the gels strength values which are 1.03±0.45 KPa, 2.5±0.76 KPa and 0.28±0.031 KPa, respectively, in ACN/water. Also, it was observed that IKVAV analogues showed enhanced strength in PBS, after recovery. The mechanical stiffness of Fmoc IKVAV, myristyl IKVAV and acetyl IKVAV in PBS becomes 5.73±1.6 KPa, 0.8±0.3 KPa and 6.4±0.9 KPa from 3.7±0.86 KPa, 0.17±0.02 KPa and 3.4±0.2 KPa, respectively, after recovery. The probable reason for increment in strength after heating was that, the more ordered structures were formed due to heating during melting studies, which were otherwise formed as kinetically trapped structures.

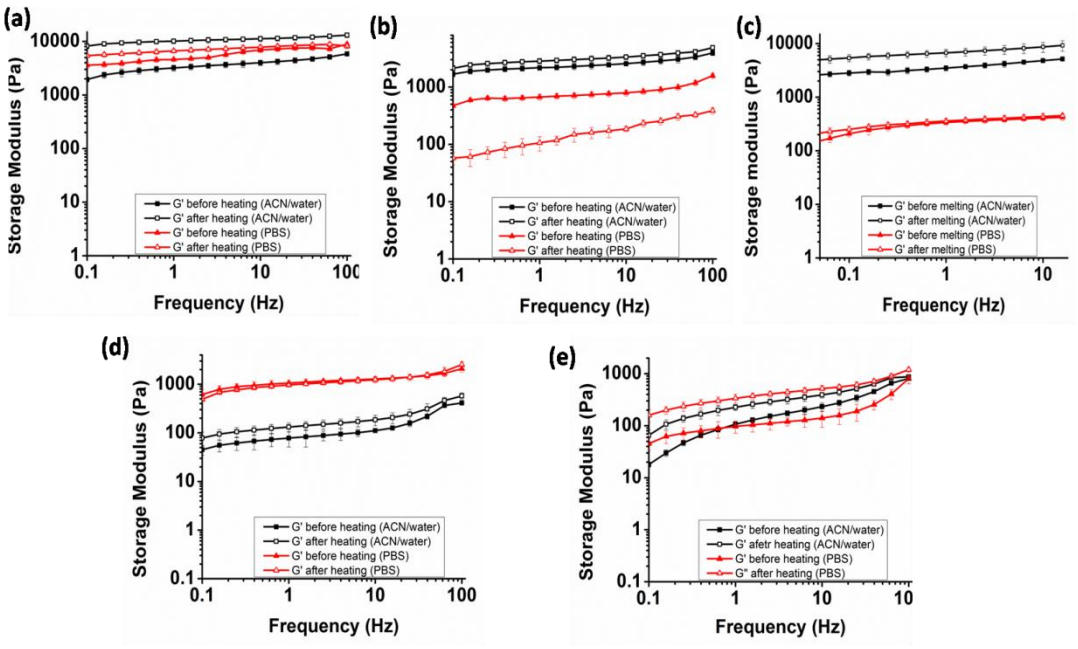

Figure 3.12 *Thermoreversibility studies comparing the storage modulus of (a) Fmoc IKVAV, (b) Myristyl IKVAV, (c) Ac IKVAV, (d) Fmoc YIGSR, and (e) Myristyl YIGSR gels before melting of the gels and gels after recovery from melting (recovery time=3 hrs), prepared in ACN/water with 0.1% TFA and PBS solvents. The peptide concentration was used as 30mM.*

As known from rheological studies, the YIGSR gels were relatively weak in comparison to IKVAV gels. The Fmoc YIGSR and myristyl YIGSR also observed a small increment in mechanical strength after recovery in ACN/water, while the strengths remained in the similar range in PBS.As observed, the G' of Fmoc YIGSR becomes 0.20±0.02 KPa from 0.13±0.01 KPa in ACN/water and 0.36±0.03 KPa from 0.24±0.14 KPa for myristyl YIGSR (figure 3.12 d & e). In PBS, the G' values for Fmoc YIGSR and myristyl YIGSR remained in the range of 1.18±0.43 KPa and 0.18±0.04 KPa before melting and 1.21±0.5 KPa and 0.5±0.03 KPa after recovery, respectively (table 3.4). This also suggested that different method of gelation, select differential self-assembly pathways to form diverse structures, but they regain similar structures after thermal and mechanical deformations, as evident by gel strength recovery, which indicated that possibly thermodynamic structures are formed for such systems. [68] Such differential mechanoresponsive and thermoreversible behaviour clearly indicated that the initial dissolution of the peptide followed by dilution with water basically interplay with intermolecular interactions, resulting in diverse gels accessible based on the single gelator domain. This reduces the synthetic challenges and showed the promise of overcoming non-reproducibility problem in the gel based systems and resulting in defect free structures with variable functions.

Table 3.4 *Thermoreversible studies: Comparison of storage modulus (G') of different IKVAV and YIGSR derived peptides in ACN/water and PBS before and after melting.*

Peptide	Solvent system	Before melting (kPa)	After melting (kPa)
Fmoc IKVAV	ACN/water	1.03± 0.45	7.2 ±1.2
	PBS	3.7± 0.86	5.73 ± 1.6
Myristyl IKVAV	ACN/water	2.5± 0.76	3.2 ±1.6
	PBS	0.17 ± 0.02	0.80 ± 0.3
Ac IKVAV	ACN/water	0.28±0.031	0.31±0.05
	PBS	3.4±0.2	6.4±0.9
Fmoc YIGSR	ACN/water	0.13± 0.01	0.20± 0.02
	PBS	1.18± 0.430	1.21± 0.5
Myristyl YIGSR	ACN/water	0.24± 0.014	0.36± 0.03
	PBS	0.18±0.04	0.50± 0.03

3.3.8 Molecular level investigations of laminin peptide self-assemblies

The secondary structure of the self-assembled peptide gels arising from the well-ordered and highly aligned hydrogen-bonded network were assessed using circular dichroism (CD), FT-IR spectroscopy and fluorescence spectroscopy.

3.3.8.1 CD spectroscopy: The supramolecular ordering of the nanofibers has been previously shown to give pronounced CD signal owing to the supramolecular organization of the peptide monomers rather than their inherent molecular chirality. [70] The effect of solvent on extent of secondary structure formation can be clearly assessed by CD spectra which can be directly correlated to the suitability of particular solvent for peptide self-assembly (figure 3.13). The amide region (195-230 nm) of the self-assembled peptides showed transition typically indicating the presence of β-sheet structure, which is further evident from the FT-IR spectra. The peak at 196-200 nm is associated with π-π* transition while that at 218-222 nm denotes an n- π* transition. [79] The IKVAV analogues majorly showed the signature of the β-sheet structures in highly ordered peptide assemblies while non-gelator peptides showed formation of random coils (figure 3.13a). On comparing the self-assembled structures of Fmoc and myristyl IKVAV in different solvents, the reduction in relative intensity of the CD signals has been observed with increasing polarity of the solvent (figure 3.13a). This also supports the morphological observations which show disruption of fibrillar structures along with reduction in β-sheet structures on enhanced solvent polarity. The probable reason for such transformations in secondary structures in different solvents is their altered molecular configuration and intermolecular interactions. [80] In corroboration to morphological and mechanical properties,

Ac-IKVAV showed relatively enhanced CD signal in PBS as compared to aqueous-organic mixture. In both the gelator YIGSR derivatives (Fmoc and myristyl) the characteristic CD signal corresponding to β-sheet was observed (figure 3.13 b). CD spectra of the Fmoc-capped peptides in both IKVAV and YIGSR series of peptides showed a transition in the region 230-280 nm, arising from the supramolecular ordering between the fibrils in a lateral alignment. [75] Further supramolecular organization of the fluorenyl groups in the Fmoc-peptides exhibited an additional peak at 303 nm owing to the induced supramolecular chirality of the Fmoc- groups associated with the fluorenyl absorption. [68] The non-assembling peptides, such as, IKVAV, YIGSR and Ac YIGSR gives a weak CD signal with IKVAV showing a minimum at 196 nm indicative of random coil structure, suggesting insufficient intermolecular interactions that can support β-sheet assembly.

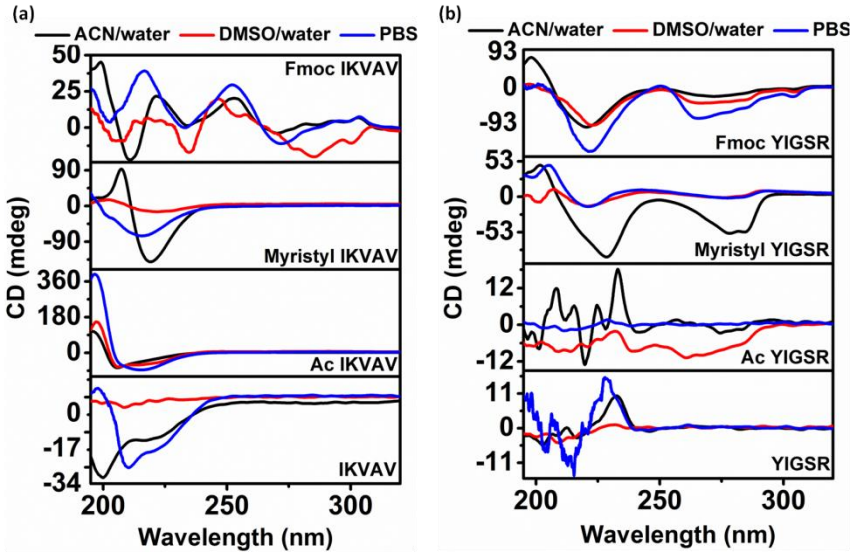

Figure 3.13 *Secondary structure investigation through CD spectra of (a) IKVAV and (b) YIGSR derived peptides in different solvents (ACN/water, DMSO/water and PBS).*

3.3.8.2 FTIR spectroscopy: FT-IR spectra of hydrophobically modified IKVAV gelators (30 mM) in aqueous-organic mixture showed a peak at 1627 cm^{-1}, which is typically assigned to β-sheet conformation (figure 3.14 a). [81] In contrast to IKVAV, for YIGSR derived peptides (30 mM) in ACN/water, the spectra looks quite different, the Fmoc and myristyl YIGSR showed a very weak peak at ~1630 cm^{-1} along with a broad maxima around 1640-1650cm^{-1} assigned primarily to the formation of the random coil structure (figure 3.14 b). [82] In corroboration to above discussed results, it also suggested that aqueous-organic solvent mixture favours the self-assembly of hydrophobic peptides as indicated by major peaks at ~1627cm^{-1} while less

hydrophobic YIGSR derived peptides majorly showed the presence of random coils in aqueous-organic solvent. Additionally, a dominant peak was observed at around 1670-1680 cm^{-1} for IKVAV derived peptides, which can be attributed to the presence of TFA. The FTIR and CD confirmed the presence of β-sheet structures in the hydrophobic self-assembling peptides, while random coil structures for relatively less hydrophobic derivatives.

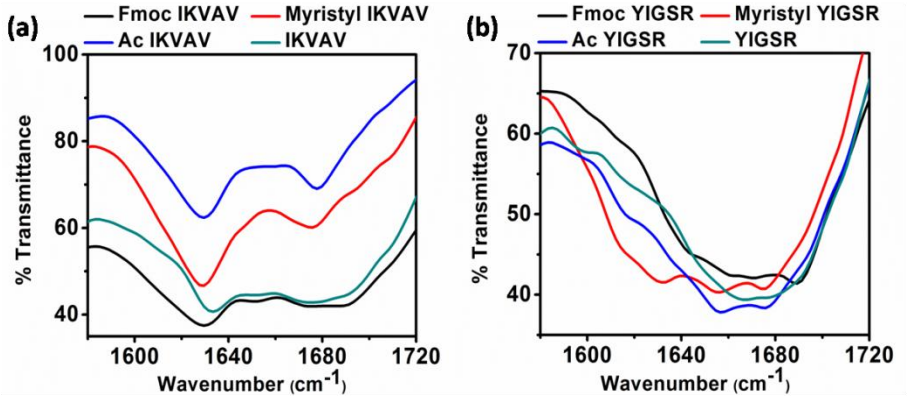

Figure 3.14 *Secondary structure investigation of (a) IKVAV and (b) YIGSR derived peptides using FTIR spectroscopy in ACN/water.*

3.3.8.3 Thioflavin T fluorescence assay: Formation of the β-sheet structure of the self-assembled nanofibrous network of synthetic laminin peptide derivatives, which closely resembles the amyloid like fibrils were further investigated through the binding of these nanofibers with Thioflavin T (Th T). Th T is a positively charged dye, which is widely used to monitor and detect the formation of amyloid like fibrils. Th T shows enhanced fluorescence signals at 480 nm when bound to amyloid like fibrils. A very weak emission of Th T was observed at 486 nm in phosphate buffer up on excitation at 440 nm. [83, 84] A significant enhancement in the fluorescence intensity was observed when Th T is added to the laminin peptides capped with Fmoc and myristyl group at the N-terminal end (Figure 3.15 a and c). Such remarkable effect of enhanced fluorescence strongly indicates the binding of Th T with amyloid like fibrillar network formed by the Fmoc and myristyl derivative of IKVAV and YIGSR. However, the extent of enhancement in the fluorescence intensity was found to be comparatively higher in IKVAV than YIGSR derivatives in ACN/water mixture indicating stronger intermolecular interactions in hydrophobic analogues. In contrast, the soluble pentapeptides or the weak gelator with acetyl capping or unmodified peptide derivative showed weak fluorescence intensity (figure 3.15 b and d). The bright-field microscopic images were used to visualize the fibrillar structures (figure 3.15 e and g) The fluorescence microscopic images of Fmoc IKVAV and Fmoc YIGSR with ACN/water gels after Th T binding clearly demonstrated the enhancement in fluorescence intensity, indicating the presence of β-sheet

structures (figure 3.15 f and h). However, the relative intensity in the microscopic images of Fmoc IKVAV was found to be higher than Fmoc YIGSR (figure 3.15 f and h) indicating the higher extent of β-sheet structure as evident from CD analysis. [85]

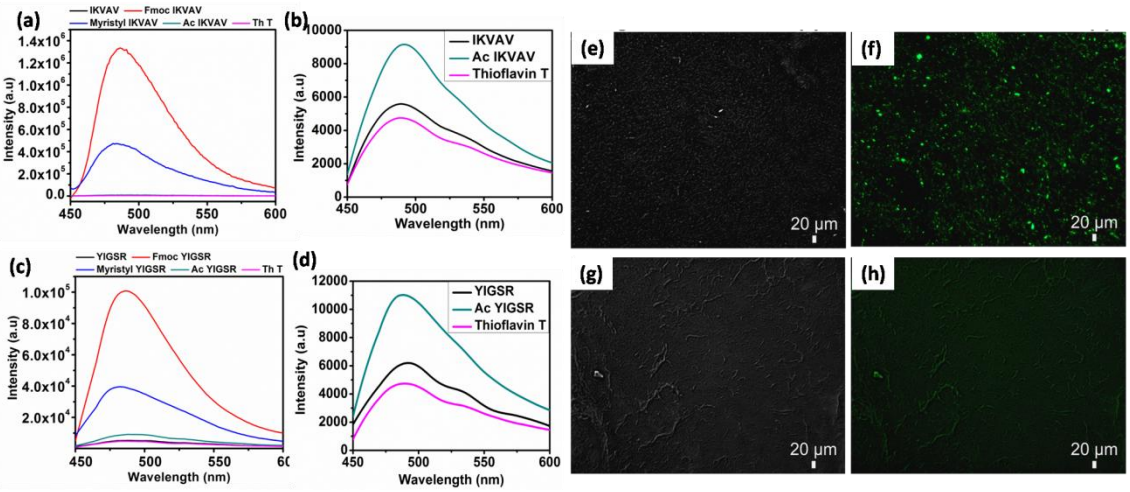

Figure 3.15 *Fluorescence spectra of Thioflavin T and its interaction with different (a) IKVAV and (c) YIGSR peptides along with magnified spectra of (b) IKVAV and (d) YIGSR derived weak gelators and bright-field microscopic images and fluorescence microscopic images of (e &f) Fmoc IKVAV and (g & h) Fmoc YIGSR after binding with Thioflavin T in ACN/water.*

3.3.8.4 Fluorescence spectroscopy: In order to acquire deeper insights at the molecular level, in presence of different solvents, the Fmoc-capped peptide gels were further analysed through fluorescence spectroscopy as Fmoc moiety has intrinsic fluorescence. The principal molecular interactions driving the self-assembly of these Fmoc-IKVAV and Fmoc-YIGSR peptides at are weak hydrophobic forces leading to π-π stacking between the fluorenyl chromophore along with the hydrogen-bonding between the peptide backbones. [86] A report by Wilson's group states that decrease in emission intensity of fluorescence indicates the π-stacking between the closely located molecules. [87] Fluorescence emission spectroscopy principally monitors the emission of the Fmoc-groups, which displayed the characteristic monomeric peak at 320 nm in the solution state irrespective of the solvent systems. The relative intensity of the monomeric emission was found to be significantly dependent on the peptide building blocks as well as solvent environment of the Fmoc-groups in the gel state. The intensity of the monomeric emission was found to be quenched in the gel state for Fmoc-IKVAV (30 mM) in both aqueous as well as aqueous-organic solvent mixture (figure 3.16). This was accompanied by a significant red shift of the emission maxima for Fmoc IKVAV in aqueous-organic mixture, indicating an extremely hydrophobic environment created by favourable π-π interactions. In contrast, less hydrophobic sequence Fmoc-YIGSR (30 mM) showed extensive quenching of monomeric emission only in

aqueous PBS buffer indicating more ordered supramolecular structures owing to the intermolecular association while less extent of quenching of emission intensity was observed in presence of ACN/water, however showing a slight red shift in emission maxima resulting from gelation which indicates the involvement of intermolecular interactions. The analysis of fluorescence emission spectra provided clear evidence of formation of extended π-π stacking interactions between the fluorenyl moieties, which is more pronounced for hydrophobic peptide sequence inducing more ordered π-β structures. Interestingly, such interactions were found to be significantly promoted in aqueous environment for even hydrophilic peptide sequence, like, Fmoc-YIGSR.

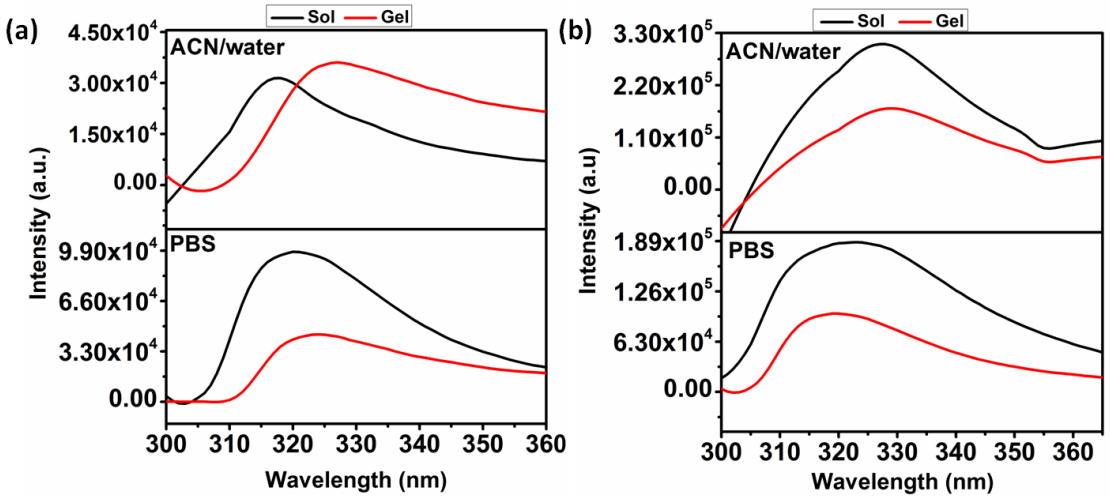

Figure 3.16 *Fluorescence emission spectra of (a) Fmoc-IKVAV and (b) Fmoc-YIGSR in ACN/water and PBS solvent systems.*

3.3.8.5 X-ray diffraction: X-ray diffraction pattern was obtained for laminin derived peptide gels (30 mM) in different solvents to understand the supramolecular packing of gelator molecules. The XRD spectrum of representative Fmoc IKVAV and Fmoc YIGSR were recorded in the 2 theta angle range of 5^0 to 60^0 using air dried gels (figure 3.17). The report by A. Banerjee and group suggested that the wet and dried gels showed similar β-sheet arrangement. [88] The peptide gels with Fmoc IKVAV in ACN/water and PBS showed distinct peaks 2θ= ~19^0 with d-spacing= 4.6Å which corresponds to β-sheet arrangement. However, the peak at 2θ= ~23^0 with d-spacing of 3.8 Å corresponding to π -π stacking between aromatic residues is more prominent in ACN/water in comparison to broad hump like signal in PBS. On the other hand, Fmoc YIGSR showed distinct peak at 2θ= ~19^0 with d-spacing= 4.6Å in PBS and a weak broad signal in ACN/water, while a sharp π -π stacking signal (2θ= ~23^0 with d-spacing of 3.8 Å) can be observed in ACN/water in contrast to PBS. [89] The XRD results suggested that organic-aqueous mixture of solvents favour π -π stacking in both hydrophobic

peptide IKVAV and hydrophilic peptides, YIGSR, but the more ordered structures are favored in aqueous solvents for hydrophilic peptides, due to higher solubility. The XRD results also provide the evidences for preferred molecular interactions, as hypothesized in figure 3.3.

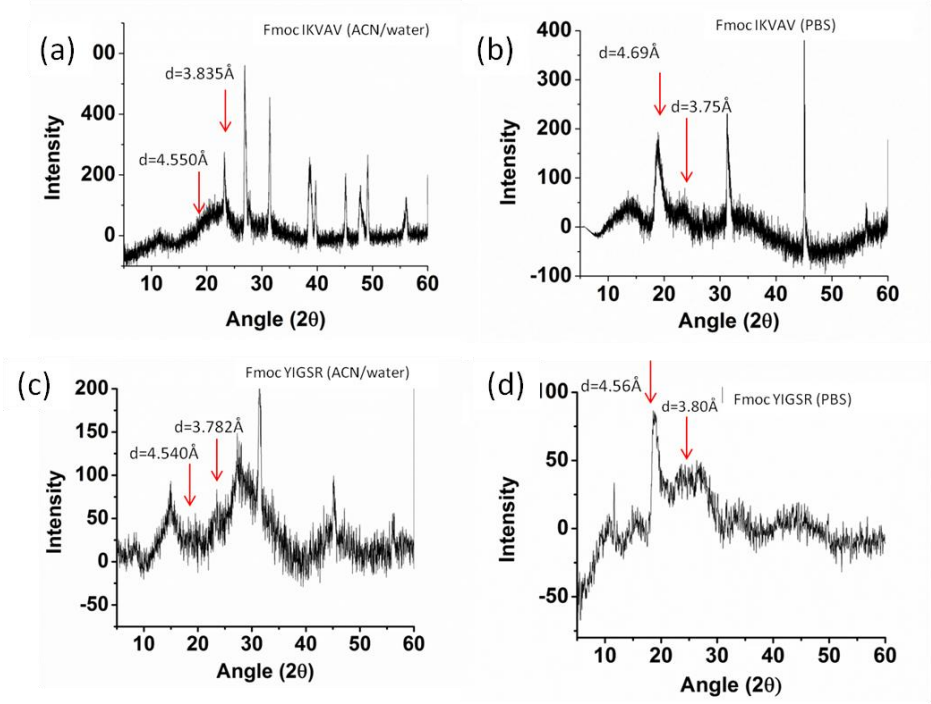

Figure 3.17 *XRD analysis of laminin derived peptide gels in different solvent systems (a) Fmoc IKVAV in ACN/water, (b) Fmoc IKVAV in PBS, (c) Fmoc YIGSR in ACN/water, (d) Fmoc YIGSR in PBS.*

3.3.9 Thermodynamic stability of self-assembled structures

The different morphological and spectroscopic studies clearly depicted that utilization of different solvents for gelation leads to nanostructures with variable thermodynamic stability via different self-assembly routes. It is known from the literature, that the supramolecular assemblies are based on non-covalent interactions, they offer lesser energy barrier for the inter-conversion. Such non-significant energy difference led the thermodynamic equilibrium of the supramolecular systems can be easily influenced by the assembly pathways. Such phenomenon further leads to the formation of kinetically trapped structures. Several factors like pH, temperature, ionic strength, salt concentration, solvent polarity etc are responsible to control the kinetics of molecular self assembly. This also suggests that the thermodynamic equilibrium states generally reside in the global minima of the free energy landscape while kinetically trapped structures are confined to the local minima. However, the kinetic factors induces competitive interactions between different non-covalent interactions leading to variable self-

assembly pathways. These different pathways results in the formation of distinct morphology and functions of the self-assembled structures. [19, 90]

In order to assess the stability of structures formed using different solvent mediated routes, thermal melting studies using CD was performed in the temperature range of 25^0C to 80^0C. [91, 92] The complete CD spectra were collected in the range of 195 nm to 320 nm. The characteristic supramolecular chirality signal of Fmoc at 303 nm was chosen to mark the disassembly of self-assembled structures. The melting temperatures (Tm) of Fmoc IKVAV gels prepared in ACN/water and DMSO/water were found to be at ~65^0C and ~60^0C respectively (figure 3.18 a and b). However, due to low solubility of Fmoc IKVAV in PBS, the thermodynamic stability behaviour showed deviation in the trend owing to its routes of self-assembly which differ from aqueous-organic mixture. The initial heating of the peptide solution in PBS leads to the formation of more ordered self-assembled structures as shown by the rise in curve in figure 3.18c, which upon further heating, melts at ~75^0C. Such differential route of self-assembly created the exception in the trend. This can be explained as the difference in kinetically trapped structures and thermodynamically stable structures is not very high and the supply of small amount of energy favours the switching between two energy states. However, the differential trend is persistent in hydrophilic Fmoc YIGSR, which tends to form highly organized structures in PBS, showing T_m at ~65^0C and with increasing non-polar nature of the solvent the Tm tends to decrease to 60^0C and 50^0C in DMSO/water and ACN/water, respectively, owing to the formation of less stable structures in aqueous-organic mixtures (figure 3.18 d -f). We believe that higher temperature is required to melt more stable structures and the correlation of Tm with respect to different solvents for each peptide is in close association with the results obtained with other spectroscopic and microscopic techniques. This confirms that solvent switch can lead to the formation of diverse nanostructures from same peptide with different thermodynamic minima.

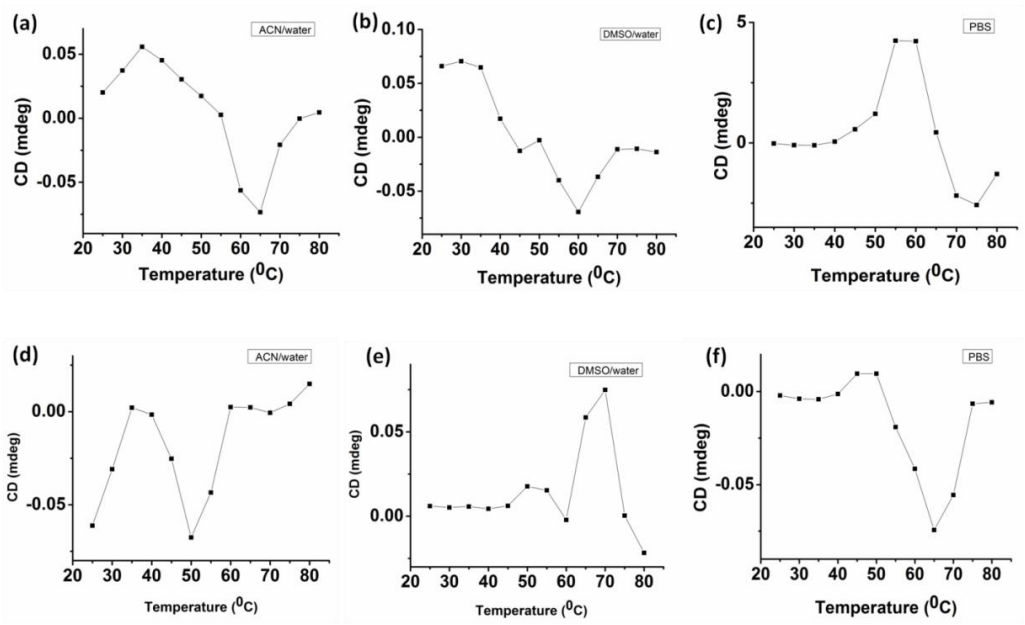

Figure 3.18 *CD melting studies of (a-c) Fmoc IKVAV and (d-f) Fmoc YIGSR gels prepared in different solvents with first derivative of normalized CD signal at 303 nm plotted against temperature.*

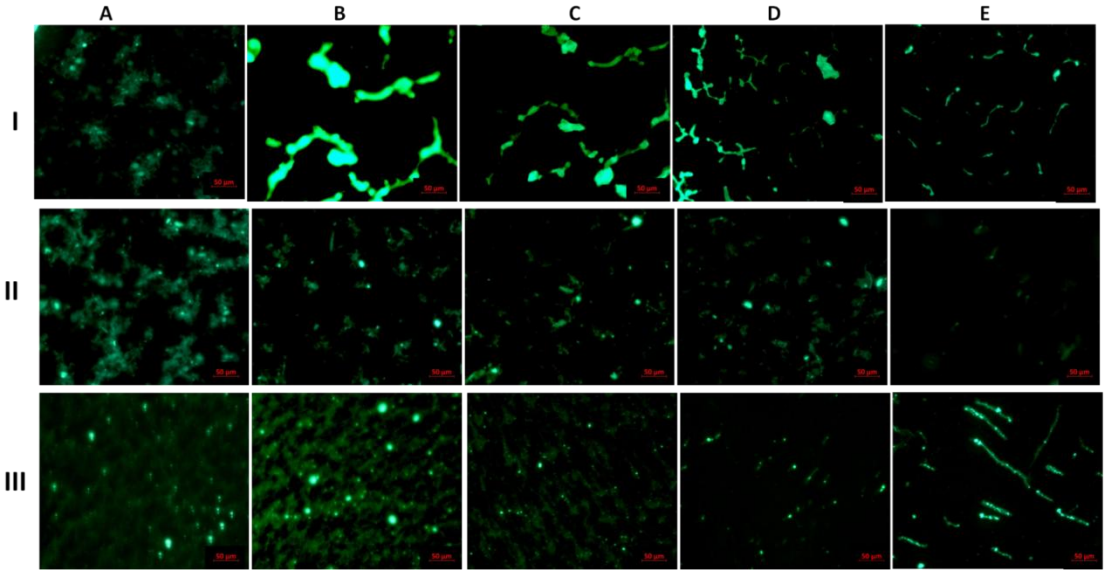

Figure 3.19 *ThT fluorescence microscopic images of Fmoc IKVAV showing progress of self assembly process at different time intervals of (A) 0 min, (B) 10 min, (C) 20 min, (D)60min and (E) 90 min in different solvent (I) ACN/water, (II) DMSO/water, (III) PBS.*

3.3.10 Solvent dependence of self-assembly kinetics

The molecular self-assembly initiates through nucleation followed by growth of the nanostructures. It is obvious that solvent environment will affect the nucleation and growth events during self-assembly. We explored Th T fluorescence to elucidate the self-assembly mechanism of peptides in solvents of different polarity. The growth of fibers from spherical aggregates was demonstrated in Fmoc IKVAV (2 mM) and Fmoc YIGSR (2 mM) peptides, through their binding ability with Th T, at different time points in different solvents (figure 3.19 and 3.20). The concentrations lower than MGC was used to visualize the process closely and avoid overcrowding of structures. The results also revealed the mechanism of Th T binding with the β-sheet rich regions. Initially, at 0 min time point, as the self-assembly proceeds, these spherical aggregates, which acts as nucleating point for further growth, combine to form fibrous structures and as a result, the intensity of Th T emission was enhanced. In Fmoc IKVAV, quick domains of ordered structures appears in aqueous organic mixture, within 10 min only, which transforms into more compact and uniform diameter fibers within 1.5 hrs. However, the fluorescence of final fibrous structures might diminish due to drying of sample, within duration of 1.5 hrs and which also prevents to extend the studies for further duration. In corroboration to above studies, Fmoc YIGSR showed delayed initiation of self-assembly in aqueous-organic mixture, in comparison to PBS, where it showed fluorescent assembled structure within 20 min. The enhanced intensity of Th T provides the evidences for the formation of ordered self-assembled structures.

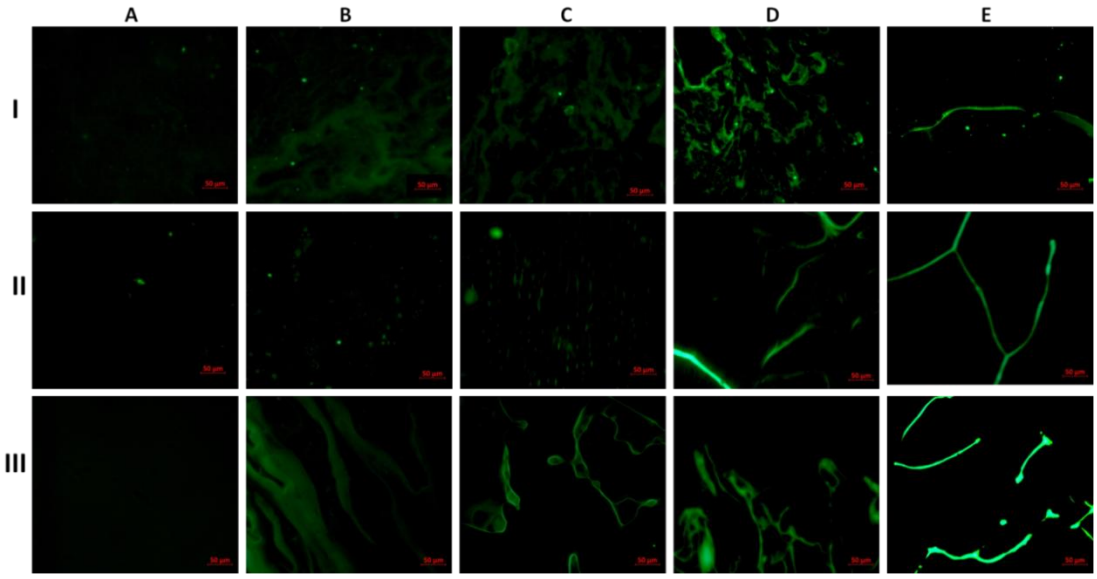

Figure 3.20 *ThT fluorescence microscopic images of Fmoc YIGSR showing progress of self assembly process at different time intervals of (A) 0 min, (B) 10 min, (C) 20 min, (D)60min and (E) 90 min in different solvent (I) ACN/water, (II) DMSO/water, (III) PBS.*

To support the above observations, we have also checked the growth mechanism of Fmoc IKVAV (20mM) in ACN/water and PBS through AFM (figure 3.21). The AFM images of Fmoc IKVAV in ACN/water revealed that very short fibrillar structures along with some longer fibers arises at 1 min interval only while in PBS the spherical aggregates dominates along with a few short fibrous structures after 1 min. [93] The images clearly showed the progressive increase in the length of the fibers with time. After 30 min, negligible change in lengths of fibers was observed. At similar concentration, the fiber length and density was lesser in PBS than ACN/water at all time points. Also, spherical aggregates can also be seen in PBS along with fibers, after 30min (figure 3.21 a and b). The morphology of structures obtained after 30 min were consistent with morphological studies of Fmoc IKVAV in ACN/water, which reports dense fibrous network with thinner fiber diameters in comparison to that in PBS. The AFM and Th T fluorescence microscopic images clearly revealed the effect of solvent on nucleation and growth processes of the individual peptide.

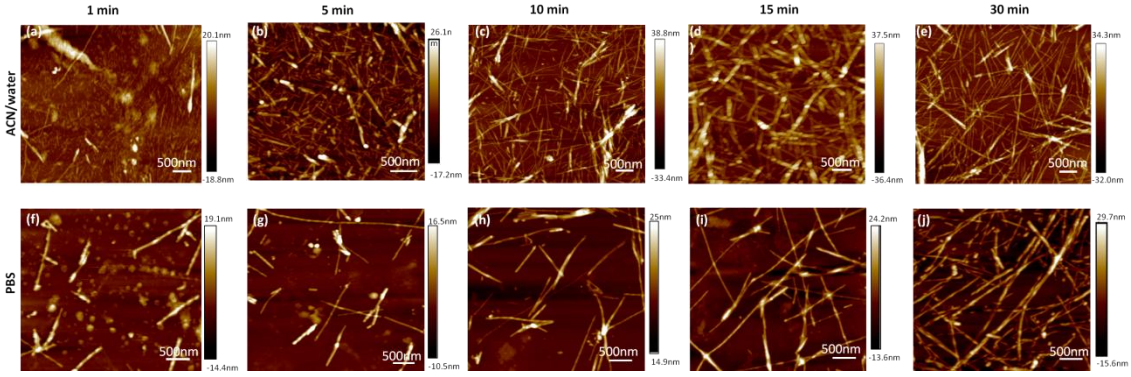

Figure 3.21 *Time dependent morphological analysis of Fmoc IKVAV using AFM images in (a-e) ACN/water and (f-j) PBS after 1 min, 5 min, 10 min, 20 min and 30 min, showing nucleation and growth of peptide structures during molecular self-assembly.*

3.3.11 Generality of Approach

To demonstrate the widespread applicability of solvent mediated approach in controlling self-assembly pathways, we analysed control peptides for their self-assembly in different solvents. To provide the evidence that the solvent dependent properties are not sequence specific, we applied similar approach with a classical amyloid based dipeptide, Fmoc FF, and a scrambled laminin peptide, Fmoc VVIAK. [94] The Fmoc FF was synthesized by liquid phase synthesis. The gelation of Fmoc FF was tried in three different solvent systems: 50% ACN/water (with

0.1% TFA), 10% DMSO/water (with 0.1% TFA) and PBS at 10 mM peptide concentration. It was observed that Fmoc FF in ACN/water failed to form gel upto the concentration of 30mM and results in clear transparent solution (table 3.5). However, Fmoc FF in DMSO/water and PBS results into gel formation at 10 mM concentration. These gels were further characterized for their morphology and mechanical stiffness. The rheology of DMSO/water and PBS gels was measured in the frequency range of 0.1 to 100 Hz with strain of 0.1% and 0.5% (as obtained by amplitude sweep) for DMSO/water and PBS gels, respectively (figure 3.21 b). For both the gels storage modulus (G') was magnitude higher than loss modulus (G") indicating stable gel structure (figure 3.22a). The storage modulus of PBS gels (1.1±0.078 kPa) was comparatively higher that than DMSO/water gels (0.86±0.081 kPa). The AFM analysis of Fmoc FF supports rheology results (figure 3.22 b-e). The Fmoc FF solution in ACN/water revealed the sheet like morphologies, which suggested that sheets were unable to entrap water to form three dimensional networks. Similarly, DMSO/water gels showed network like structures formed by the entanglement of short fibers and fibrillar structures were observed with PBS, which supports the stable gels. The probable reason for failure of gelation of Fmoc FF in ACN/water could be the higher solubility of peptide in ACN which competes with gelator-gelator interactions. However, Fmoc FF formed strong gel with 10% ACN/water having mechanical stiffness in range of 10.3±1.2 kPa showing thin fibrous morphology (figure 3.22 a and d).

Table 3.5*: Gelation studies of Fmoc FF in different solvent system.*

Solvent	Gelation Status
50% ACN/water 10% ACN/water	Sol Gel
DMSO/water	Gel
PBS	Gel

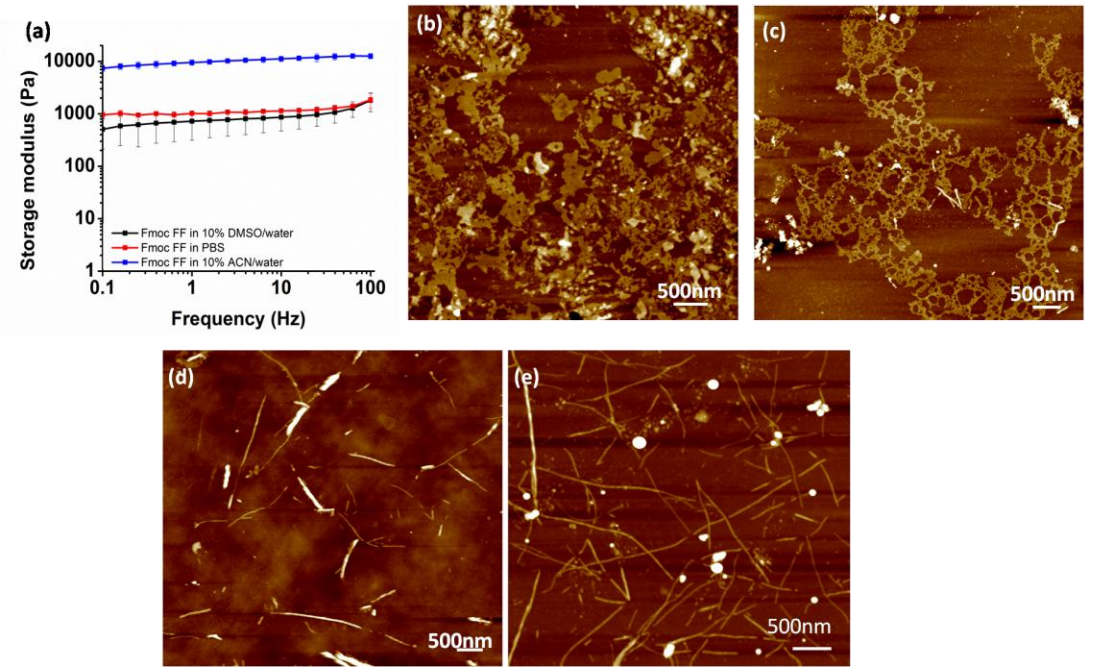

Figure 3.22 *Gelation studies of β-amyloid peptide, Fmoc FF in different solvents at 10mM concentration with (a) Rheology studies of Fmoc FF gels in 10% DMSO/water PBS (pH 6) and10% ACN/water, and AFM images of Fmoc FF solution/gel in (b) 50% ACN/water, (c) 10% DMSO/water and (d) PBS and (e)10% ACN/water.*

For negative control, Fmoc VVIAK peptide was synthesized using solid phase synthesis. The purity of synthesized peptide was confirmed by LC-MS (figure 3.23 a and b). The C log P value of scrambled IKVAV i.e. VVIAK was found to be same as IKVAV i.e. 0.42. The gelation studies of the scrambled IKVAV peptide were performed in all three different types of solvents. Although, the C log P was same, but MGC of Fmoc VVIAK was found to be significantly higher. In comparison to 5 mM Fmoc IKVAV in ACN/water and DMSO/water, it increased to 15 mM, while in PBS it remained same i.e. 15 mM (table 3.6). The differential solvent effect was also observed on the mechanical strength and morphology of the scrambled peptides (figure 3.23 c-f).

Table 3.6 *Gelation studies of Fmoc VVIAK peptide in different solvent systems*

Solvent	Gelation Status			
	5mM	10mM	15mM	20mM
ACN/water	Sol	Sol	Weak Gel	Gel
DMSO/water	Sol	Sol	Weak Gel	Gel
PBS	Sol	Sol	Gel	Gel

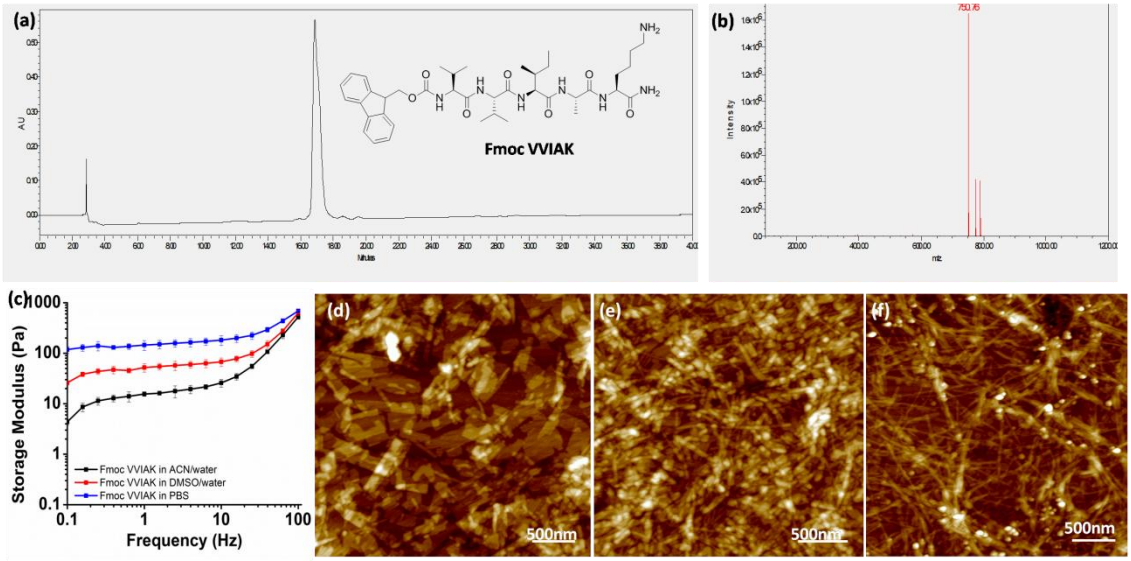

Figure 3.23 *Scrambled IKVAV peptide synthesis, gelation and characterization: (a and b) HPLC chromatogram along with the molecular structure and LCMS spectra of Fmoc VVIAK peptide, (c) Storage modulus of Fmoc VVIAK peptide gels at concentration of 20mM in different solvents, measured at 0.1% strain (LVE range) in the frequency range of 0.1 to 100Hz and (d-f) AFM images showing different morphologies of Fmoc VVIAK formed in 50% ACN/water, 10% DMSO/water and PBS respectively.*

The gel strength has shown a reversal of behavior compared to that of Fmoc IKVAV in differential solvent environment and showed the higher strength (~0.22±0.03 kPa) in PBS in comparison to that in ACN/water (~0.070±0.008 kPa). The reason for lower mechanical strength of Fmoc VVIAK in ACN/water can be correlated to its sheet like morphology. However, in DMSO/water it showed short fibrillar structures and in PBS dense fibrillar network can be observed. The probable reason for the increased MGC and lower strength in organic-aqueous mixture might be the altered hydrophobic interactions because of the presence of

charged lysine residue at the C-terminal, which might also be responsible for the improved solubility of the peptide in aqueous solvent. The control studies suggested that, nature of solvent could affect the self-assembling properties of a peptide, irrespective of the peptide sequence and its length (dipeptide or pentapeptide). And it entirely depends on the overall hydrophobicity of the peptide and also the surface functionality exposed to a particular solvent. This can, in turn, control the gelator-gelator or solvent-gelator interactions. The choice of solvent can be an effective means to modulate self-assembly pathways and achieve diverse nanostructures.

3.3.12 Implications in biological applications

The presence of solvents and lower pH of the solvent can be detrimental towards some biological applications like cell culture and drug delivery, etc. However, the tunability achieved using solvent switch is highly appreciable. Therefore, to eliminate the deleterious effects of solvents and pH, we considered solvent exchange method post-gelation, which was earlier shown by Dave Adams and co-workers. [31] The Fmoc IKVAV gels (5mM) were initially prepared in ACN/water and DMSO/water according to the procedure described. Post-gelation, 1ml of milli-Q water was added gently at the top of the gel and allowed to exchange with the solvent entrapped in gel network for 2 hrs. The supernatant aqueous layer was removed without disturbing the gel. Subsequently, the similar exchange was done three more times, until the pH increases to ~6. The gels remain intact after the four cycles of solvent exchange. Similarly, the exchange with culture media was also performed and after 4 cycles the media colour remained red which means the gels were no more acidic. We also confirmed the removal of DMSO through FTIR. After exchange, the sulfoxide peak ~1020 cm^{-1} got diminished, indicating the reduction in quantities of DMSO in the gels (figure 3.24 a). [31] It was important to evaluate the effect of solvent exchange on the mechanical strength of the gels, so we carried out rheology of Fmoc IKVAV gels in ACN/water and DMSO/water with and without solvent exchange (figure 3.24 b and c). An order of mangnitude difference in the gel strength was observed for both the ACN/water and DMSO/water gels, but the integrity of gels was maintained. However, the loss of mechanical properties is expected to be reduced by increasing the concentration of gels, as this study was done at MGC only. Since, we propose the utility of these biofunctional laminin based gels in cell culture applications, the assessment of the mechanical strength after exchange with media is important (figure 3.24 d). The media was perfused through the gels in the similar manner, as done with water. After media exchange, the mechanical strength was decreased to 1.5 ± 0.3 kPa from 4.7± 0.9 kPa. Hence, the desirable mechanical properties can be achieved by altering the concentration of peptides with purely aqueous media. This could be highly beneficial approach for developing bio-applications suited gels from peptides which require

organic solvent for their solubilisation. This would inevitably improve the bicompatability of the materials as a next generation scaffold for bio-medical applications. [31]

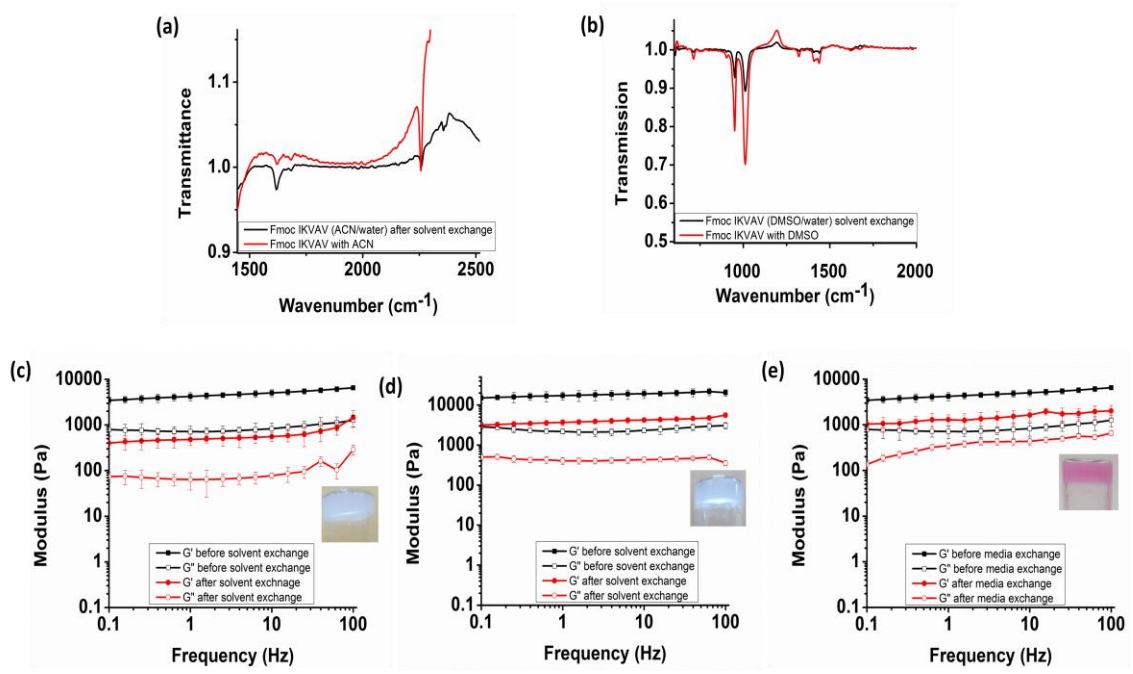

Figure 3.24 *FTIR spectra of Fmoc IKVAV gels before and after solvent exchange in (a) ACN/D_2O and (b) DMSO/D_2O showing the reduced peak of nitrile (CN) at 2250cm^{-1} and diminished peak of sulfoxide at 1020cm^{-1} after exchange. Rheology measurements of Fmoc IKVAV gels in (c) ACN/water and (d) DMSO/water before and after solvent exchange at concentration of 5mM and (e) Fmoc IKVAV gel in ACN/water before and after media exchange.*

3.4 Conclusions

In summary, we have successfully demonstrated a versatile and facile approach of using both aqueous and aqueous-organic solvent mixture to induce differential supramolecular gelation in a single gelator domain. To find out that the effect is general, a library of laminin derived peptide amphiphiles were employed. The diverse nanostructures were accessed using solvent switch throughout the library of hydrophobically modified short laminin peptides, which otherwise are forming a single type of nanostructures depending upon their molecular architecture, which corresponds to lowest energy structure and represents thermodynamic minima. The solvent mediated approach of controlling self-assembling pathways can find applicability with wide range of gelator molecules ranging from amyloid based dipeptides to oligopeptide amphiphiles. We showed that solvent environment greatly affects the intermolecular interactions of gelator molecules and thus leading to the formation of various non-equilibrium nanostructures corresponding to local minima in the free energy landscape. The hydrophobic peptide

derivatives face difficulty in dissolution with aqueous solvents. Therefore, incorporation of organic solvent facilitated dissolution which proceeds towards self-assembly after dilution with aqueous solvent. We report that choice of solvent affects significantly the minimum gelation concentration of the modified peptides which is translated in to the differential mechanical and morphological properties of the final gel phase materials. We have also demonstrated the differential mode of self-assembly through various spectroscopic techniques. Thus, selection of solvent plays a crucial role in determining the final gel phase material properties and expanding their potential utility in various fields. We envisage that the solvent triggered access of diverse nanostructures corresponding to the differential energy level of the free energy landscape could represent a simple and elegant method of bottom up nanofabrication which could overcome the synthetic challenges.

Note:

- ✓ The permission has been granted by authors and corresponding author of the published paper prior to its adoption in the present thesis. The publication associated with this work is:

  Rashmi Jain, Sangita Roy, Tuning the gelation behavior of short laminin derived peptides via solvent mediated self-assembly, *Mater. Sci. Eng. C*, 108 (2020) 110483 doi.org/10.1016/j.msec.2019.110483.

3.5 References

1. H. Cui, M. J. Webber, S. I. Stupp, Self-Assembly of Peptide Amphiphiles: From Molecules to Nanostructures to Biomaterials, Biopolymers 94 (2010) 1-18.
2. L. Adler-Abramovich and E. Gazit, The physical properties of supramolecular peptide assemblies: from building block association to technological applications, Chem. Soc. Rev. 43 (2014) 6881-6893.
3. P. Singh, S. K. Brar, M. Bajaj, N. Narang, V. S. Mithu, O. P. Katare, N. Wangoo, R. K. Sharma, Self-assembly of aromatic α-amino acids into amyloid inspired nano/micro scaled architects, Mater. Sci. Eng. C 72 (2017) 590–600.
4. X. Du, J. Zhou, J. Shi, and B. Xu, Supramolecular Hydrogelators and Hydrogels: From Soft Matter to Molecular Biomaterials, Chem. Rev. 115 (2015) 13165−13307.
5. S. Y. Qin, Y. Pei, X.J. Liu, R. X. Zhuo and X. Z. Zhang, Hierarchical self-assembly of a β-amyloid peptide derivative, J. Mater. Chem. B 1 (2013) 668-675.

6. M. J. Krysmann, V. Castelletto, A. Kelarakis, I. W. Hamley, R. A. Hule, and D. J. Pochan, Self-Assembly and Hydrogelation of an Amyloid Peptide Fragment, Biochemistry 47 (2008) 4597-4605.
7. T. P. J. Knowles and R. Mezzenga, Amyloid Fibrils as Building Blocks for Natural and Artificial Functional Materials, Adv. Mater. 28 (2016) 6546–6561.
8. S. Bera, E. Gazit, Self-assembly of Functional Nanostructures by Short Helical Peptide Building Blocks, Protein Pept. Lett. 26 (2019) 88-97.
9. M. Reches and E. Gazit, Casting metal nanowires within discrete self-assembled peptide nanotubes, Science 300 (2003) 625-627.
10. D. Martí, E. Mayans, A. M. Gil, A. Díaz, A. I. Jimenez, I. Yousef, I. Keridou, C. Cativiela, J. Puiggali, and C. Alemán, Amyloid-Like Fibrils from a Diphenylalanine Capped with an Aromatic Fluorenyl, Langmuir 34 (2018) 15551–15559.
11. Y. Wang, J. Chou, Y. Sun, S. Wen, S. Vasilescu, H. Zhang, Supramolecular-based nanofibers, Mater. Sci. Eng. C, 101 (2019), 650-659.
12. G. Fichman and E. Gazit, Self-assembly of short peptides to form hydrogels: Design of building blocks, physical properties and technological applications, Acta Biomater. 10 (2014) 1671-1682.
13. D. M. Raymond, B. L. Abraham, T. Fujita, M. J. Watrous, E. S. Toriki, T. Takano, B. L. Nilsson, Low-Molecular-Weight Supramolecular Hydrogels for Sustained and Localized in Vivo Drug Delivery, ACS Appl. Bio Mater. 2 (2019) 2116−2124.
14. W. Liyanage, W. W. Brennessel, and B. L. Nilsson, Spontaneous Transition of Self-assembled Hydrogel Fibrils into Crystalline Microtubes Enables a Rational Strategy To Stabilize the Hydrogel State, Langmuir, 31 (2015) 9933−9942.
15. Q. Jin, L. Zhang, and M. Liu, Solvent-Polarity-Tuned Morphology and Inversion of Supramolecular Chirality in a Self-Assembled Pyridylpyrazole-Linked Glutamide Derivative: Nanofibers, Nanotwists, Nanotubes, and Microtubes, Chem. Eur. J. 19 (2013) 9234 – 9241.
16. A. R. Hirst and D. K. Smith, Solvent Effects on Supramolecular Gel-Phase Materials: Two-Component Dendritic Gel, Langmuir 20 (2004) 10851-10857.
17. P. Zhu, X. Yan, Y. Su, Y. Yang and J. Li, Solvent-Induced Structural Transition of Self-Assembled Dipeptide: From Organogels to Microcrystals, Chem. Eur. J. 16 (2010) 3176 – 3183.

18. P. Sharma, H. Kaur, S. Roy, Inducing differential self-assembling behaviour in ultrashort peptide hydrogelators using simple metal salts, Biomacromolecules, 207 (2019) 2610-2624.
19. J. Wang, Kai Liu, R. Xing and X. Yan, Peptide self-assembly: thermodynamics and kinetics, Chem. Soc. Rev. 45 (2016) 5589-5604.
20. N. A. Dudukovic, B. C. Hudson, A. K. Paravastuc and C. F. Zukoski, Self-assembly pathways and polymorphism in peptide-based nanostructures, Nanoscale 10 (2018) 1508-1516.
21. Y. Li , L. Yan , K. Liu , J. Wang , A. Wang , S. Bai and X. Yan, Solvothermally Mediated Self-Assembly of Ultralong Peptide Nanobelts Capable of Optical Waveguiding, Small 1 (2016) 2575–2579.
22. J. Raeburn, A. Z. Cardoso and Dave J. Adams, The importance of the self-assembly process to control mechanical properties of low molecular weight hydrogels, Chem. Soc. Rev. 42 (2013) 5153-5156.
23. S. Debnath, S. Roy, Y.M. Abul-Haija, P.W. J. M. Frederix, S. M. Ramalhete, A. R. Hirst, N. Javid, N. T. Hunt, S. M. Kelly, J. Angulo, Y. Z. Khimyak, R. V. Ulijn, Tunable Supramolecular Gel Properties by Varying Thermal History, Chem. Eur. J. (2019) https://doi.org/10.1002/chem.201806281.
24. X. Zhang, Y. Wang, Y. Hua, J. Duan, M. Chen, L. Wang and Z. Yang, Kinetic control over supramolecular hydrogelation and anticancer properties of taxol, Chem. Commun. 54 (2018) 755-758.
25. E. Mayans, G. Ballano, J. Sendros, M. Font-Bardia, J. L. Campos, J. Puiggal, C. Cativiela, and C. Alemán, Effect of Solvent Choice on the Self-Assembly Properties of a Diphenylalanine Amphiphile Stabilized by an Ion Pair, ChemPhysChem, 18 (2017) 1888 – 1896
26. X. Yan, P. Zhua and J. Li, Self-assembly and application of diphenylalanine-based nanostructures Chem. Soc. Rev. 39 (2010) 1877–1890.
27. E. Çelik, C. Bayram, R. Akçapınar, M. Türk, E. B. Denkba, The effect of calcium chloride concentration on alginate/Fmoc-diphenylalanine hydrogel networks, Mater. Sci. Eng. C 66 (2016) 221–229.
28. W. Helen, P. de Leonardis, R. V. Ulijn, J. Gougha and N. Tirelli, Mechanosensitive peptide gelation: mode of agitation controls mechanical properties and nano-scale morphology, Soft Matter, 7 (2011) 1732–1740.

29. K. Ma, W. Chen, T. Jiao, X. Jin, Y. Sang, D. Yang, J. Zhou, M. Liu and P. Duan, Boosting the circularly polarized luminescence of small organic molecules via multi-dimensional morphology control, Chem. Sci. 10 (2019) 6821–6827.
30. A. Mahler, M. Reches, M. Rechter, S. Cohen, and E. Gazit, Rigid, Self-Assembled Hydrogel Composed of a Modified Aromatic Dipeptide, Adv. Mater. 18 (2006) 1365–1370.
31. J. Raeburn, C. Mendoza-Cuenca, B. N. Cattoz, M. A. Little, A. E. Terry, A. Z. Cardoso, P. C. Griffiths and D. J. Adams, The effect of solvent choice on the gelation and final hydrogel properties of Fmoc– diphenylalanine, Soft Matter 11 (2015) 927-935.
32. I. W. Hamley, D. R. Nutt, and G. D. Brown, Influence of the Solvent on the Self-Assembly of a Modified Amyloid Beta Peptide Fragment. II. NMR and Computer Simulation Investigation, J. Phys. Chem. B 114 (2010) 940–951.
33. S. Kasai, S. Urushibata, K. Hozumi, F. Yokoyama, N. Ichikawa, Y. Kadoya, N. Nishi, N. Watanabe, Y. Yamada and M. Nomizu, Identification of Multiple Amyloidogenic Sequences in Laminin-1, Biochemistry 46 (2007) 3966-3974.
34. M. Yamada,Y. ichi Kadoya, S. Kasai, K. Kato, M. mi Mochizuki, N. Nishi, N. Watanabe, H. K. Kleinman,Y. Yamada and M. Nomizu, Ile-Lys-Val-Ala-Val (IKVAV)-containing laminin K1 chain peptides form amyloid-like fibrils, FEBS Letters 530 (2002) 48-52.
35. J. H. Miner, Laminins and Their Roles in Mammals, Microsc. Res. Tech. 71 (2008) 349–356.
36. S. Ali, J. E. Saik, D. J. Gould, M. E. Dickinson, and J. L. West, Immobilization of Cell-Adhesive Laminin Peptides in Degradable PEGDA Hydrogels Influences Endothelial Cell Tubulogenesis, BioResearch 2 (2013) 241-249.
37. X. Li, X. Liu, B. Josey, C. J. Chou, Y. Tan, N. Zhang and X. Wen, Short Laminin Peptide for Improved Neural Stem Cell Growth, Stem Cells Transl. Med. 3 (2014) 662–670.
38. K. Tashiro, G. C. Sephel, B. Weeks, M. Sasakig, G. R. Martinn, H. K. Kleinman, and Y. Yamada, A Synthetic Peptide Containing the IKVAV Sequence from the A Chain of Laminin Mediates Cell Attachment, Migration, and Neurite Outgrowth, J. Biol. Chem. 264 (1989) 16174-16182.
39. S. Chen, M. Zhang, X. Shao, X. Wang, L. Zhang, P. Xu, W. Zhong, L. Zhang, M. Xing and L. Zhang, A laminin mimetic peptide SIKVAV-conjugated chitosan hydrogel

promoting wound healing by enhancing angiogenesis, re-epithelialization and collagen deposition J. Mater. Chem. B 3 (2015) 6798-6804.

40. B. He, J. Zhao, Y. Ou, D. Jiang, Biofunctionalized peptide nanofiber-based composite scaffolds for bone regeneration, Mater. Sci. Eng. C, 90 (2018), 728-738.
41. Y. H. Yang, Z. Khan, C. Ma, H. J. Lim, L. A. S. Callahan, Optimization of adhesive conditions for neural differentiation of murine embryonic stem cells using hydrogels functionalized with continuous Ile-Lys-Val-Ala-Val concentration gradients, Acta Biomater. 21 (2015) 55–62.
42. S. Sur, E. T. Pashuck, M. O. Guler, M, Ito, S. I. Stupp and T. Launey, A hybrid nanofiber matrix to control the survival and maturation of brain neurons, Biomaterials 33 (2012) 545–555.
43. K. Luder, K. Kulkarni, H. W. Lee, R. E. Widdop, M. P. Del Borgo and M-I. Aguilar, Decorated self-assembling b3-tripeptide foldamers form cell adhesive scaffolds, Chem. Commun. 52 (2016) 4549-4552.
44. K. L. Niece, J. D. Hartgerink, J. J. J. M. Donners, and S. I. Stupp, Self-Assembly Combining Two Bioactive Peptide-Amphiphile Molecules into Nanofibers by Electrostatic Attraction, J. Am. Chem. Soc. 125 (2003) 7146-7147.
45. A. L. Rodriguez, C. L. Parish, D. R. Nisbet and R. J. Williams, Tuning the amino acid sequence of minimalist peptides to present biological signals via charge neutralised self assembly, Soft Matter 9 (2013) 3915-3919.
46. R. Jain, G. Khandelwal, S. Roy, Unraveling the Design Rules in Ultrashort Amyloid-Based Peptide Assemblies toward Shape-Controlled Synthesis of Gold Nanoparticles, Langmuir, 35 (2019) 5878-5889.
47. J. Zhan, Y. Cai, S. Ji, S. He, Y. Cao, D. Ding, L. Wang, and Z. Yang, Spatiotemporal Control of Supramolecular Self-Assembly and Function. ACS Appl. Mater. Interfaces 9 (2017) 10012−10018.
48. D. J. Welsh, P. Posocco, S. Pricl and D. K. Smith, Self-assembled multivalent RGD-peptide arrays – morphological control and integrin binding, Org. Biomol. Chem. 11 (2013) 3177–3186.
49. N. R. Lee, C. J. Bowerman, B. L. Nilsson, Sequence Length Determinants for Self-Assembly of Amphipathic β-Sheet Peptides, Pept. Sci., 100 (2013) 738-750.
50. R. Orbach, L. Adler-Abramovich, S. Zigerson, I. Mironi-Harpaz, D. Seliktar, and E. Gazit, Self-Assembled Fmoc-Peptides as a Platform for the Formation of Nanostructures and Hydrogels Biomacromolecules 10 (2009) 2646–2651.

51. H. Wang, C. Yang, M. Tan, L. Wang, D. Kong and Z. Yang, A structure–gelation ability study in a short peptide-based 'Super Hydrogelator' system, Soft Matter 7 (2011) 3897–3905.
52. C-L Shen and R.M Murphy, Solvent Effects on Self-Assembly of β-Amyloid Peptide Biophys. J. 69 (1995) 640-651.
53. K. Chen, T. Jiao, J. Li, D. Han, R. Wang, G. Tian, and Q. Peng, Chiral Nanostructured Composite Films via Solvent-Tuned Self- Assembly and Their Enantioselective Performances, Langmuir 35 (2019) 3337−3345.
54. C. C. Horgan, A. L. Rodriguez, R. Li, K. F. Bruggeman, N. Stupka, J. K. Raynes , L. Day, J. W. White, R. J. Williams and D. R. Nisbet, Characterisation of minimalist co-assembled fluorenylmethyloxycarbonyl self-assembling peptide systems for presentation of multiple bioactive peptides. Acta Biomater. 38 (2016) 11–22.
55. C. K. Rouse, A. D. Martin, C. J. Easton and P. Thordarson, A Peptide Amphiphile Organogelator of Polar Organic Solvents, Sci. Rep. 7 (2017) 43668.
56. F. T. Senguen, N. R. Lee, X. Gu, D. M. Ryan, T. M. Doran, E. A. Anderson and B. L. Nilsson, Probing aromatic, hydrophobic, and steric effects on the self-assembly of an amyloid-β fragment peptide, Mol. BioSyst. 7 (2011) 486–496.
57. N. F. A. van der Vegt and D. Nayar, The Hydrophobic Effect and the Role of Cosolvents, J. Phys. Chem. B, 121 (2017) 9986-9998.
58. R. P. M. Lafleur, X. Lou, G. M. Pavan, A. R. A. Palmans, E. W. Meijer, Consequences of a cosolvent on the structure and molecular dynamics of supramolecular polymers in water, Chem. Sci. 9 (2018) 6199–6209.
59. X. Liu, J. Fei, A. Wang, W. Cui, P. Zhu, and J. Li, Transformation of Dipeptide-Based Organogels into Chiral Crystals by Cryogenic Treatment, Angew. Chem. Int. Ed., 56 (2017) 2660 –2663.
60. R. Huang, W. Qi, R. Su, J. Zhao, Z. He, Solvent and surface controlled self-assembly of diphenylalanine peptide: from microtubes to nanofibers, Soft Matter 7 (2011) 6418–6421.
61. M. Raynal, L. Bouteiller, Organogel formation rationalized by Hansen solubility parameters, Chem. Commun. 47 (2011) 8271–8273.
62. J. Zhu, R. Wang, R. Geng, X. Zhang, F. Wang, T. Jiao, J. Yang, Z. Bai and Q. Peng A facile preparation method for new two component supramolecular hydrogels and their performances in adsorption, catalysis, and stimuli response, RSC Adv. 9 (2019) 22551–22558.

63. X. Du, J. Zhou, and B. Xu, Supramolecular Hydrogels Made of Basic Biological Building Blocks, Chem. Asian J. 9 (2014) 1446 – 1472.
64. R. J. Betush, J. M. Urban, B. L. Nilsson, Balancing hydrophobicity and sequence pattern to influence self-assembly of amphipathic peptides Pept. Sci. (2018) 110:e23099. https://doi.org/10.1002/bip.23099.
65. C. Zhu, Y. Gao, H. Li, S. Meng, L. Li, J. S. Francisco, X. C. Zeng, Characterizing hydrophobicity of amino acid side chains in a protein environment via measuring contact angle of a water nanodroplet on planar peptide network PNAS, 113 (2016) 12946–12951.
66. C. Reichardt, T. Welton, Solvents and Solvent Effects in Organic Chemistry, Fourth Edition, 2010, DOI: 10.1002/9783527632220.
67. D. Mandal, S. Dinda, P. Choudhury, and P. K. Das, Solvent Induced Morphological Evolution of Cholesterol Based Glucose Tailored Amphiphiles: Transformation from Vesicles to Nanoribbons, Langmuir, 32 (2016) 9780−9789.
68. S. Wu, J. Gao, T. J. Emge and M. A. Rogers, Influence of solvent on the supramolecular architectures in molecular gels, Soft Matter, 9 (2013) 5942–5950.
69. J. Wang, K. Liu, Linyin Yan, A. Wang, S. Bai, and X. Yan, Trace Solvent as a Predominant Factor To Tune Dipeptide Self-Assembly, ACS Nano 10 (2016) 2138−2143.
70. V. Castelletto, I.W. Hamley, Influence of the Solvent on the Self-Assembly of a Modified Amyloid Beta Peptide Fragment. I. Morphological Investigation, J. Phys. Chem. B, 113 (2009) 9978–9987.
71. P. Zhu, X. Yan, Y. Su, Y. Yang, and J. Li, Solvent-Induced Structural Transition of Self-Assembled Dipeptide: From Organogels to Microcrystals Chem. Eur. J. 16 (2010) 3176 – 3183.
72. R. Orbach, I. Mironi-Harpaz, L. Adler-Abramovich, E. Mossou, E. P. Mitchell, V. T. Forsyth, E. Gazit, and D. Seliktar, The Rheological and Structural Properties of Fmoc-Peptide-Based Hydrogels: The Effect of Aromatic Molecular Architecture on Self-Assembly and Physical Characteristics, Langmuir, 28 (2012) 2015−2022.
73. H. Huang, A. I. Herrera, Z. Luo, O. Prakash, and X. S. Sun, Structural Transformation and Physical Properties of a Hydrogel-Forming Peptide Studied by NMR, Transmission Electron Microscopy, and Dynamic Rheometer, Biophys. J. 103 (2012) 979–988.

74. J. Nanda, A. Biswas and A. Banerjee, Single amino acid based thixotropic hydrogel formation and pH-dependent morphological change of gel nanofibers, Soft Matter 9 (2013) 4198–4208.
75. N. Hou, R. Wang, R. Geng, F. Wang, T. Jiao, L. Zhang, J. Zhou, Z. Bai and Q. Peng, Facile preparation of self-assembled hydrogels constructed from poly-cyclodextrin and poly-adamantane as highly selective adsorbents for wastewater treatment, Soft Matter, 15 (2019) 6097-6106.
76. J. N. Israelachvili, Intermolecular and Surface Forces, Academic Press, San Diego, 3rd edn, 2011, pp. 151–167.
77. C. Yan, A. Altunbas, T. Yucel, R. P. Nagarkar, J. P. Schneiderk, D. J. Pochan, Injectable solid hydrogel: mechanism of shear-thinning and immediate recovery of injectable b-hairpin peptide hydrogels, Soft Matter, 6 (2010) 5143–5156.
78. H. Yan, A. Saiani, J. E. Gough and A. F. Miller, Thermoreversible Protein Hydrogel as Cell Scaffold, Biomacromolecules 7 (2006,) 2776-2782.
79. A. R. Hirst, S. Roy, M. Arora, A. K. Das, N. Hodson, P Murray, S. Marshall, N. Javid, J. Sefcik, J. Boekhoven, J. H. van Esch, S. Santabarbara, N. T. Hunt and R. V. Ulijn, Biocatalytic induction of supramolecular order Nat. Chem. 2 (2010) 1089-1094.
80. R. Xing, C. Yuan, S. Li, J. Song, J. Li, and X. Yan, Charge-Induced Secondary Structure Transformation of Amyloid-Derived Dipeptide Assemblies from β-Sheet to a-Helix, Angew. Chem. Int. Ed. 57 (2018) 1537 –1542.
81. S. Roy, N. Javid, P. W. J. M. Frederix,D. A. Lamprou, A. J. Urquhart, N. T. Hunt, P. J. Halling, and R. V. Ulijn, . Dramatic Specific-Ion Effect in Supramolecular Hydrogels Chem. Eur. J. 18 (2012) 11723-31.
82. S. Fleming, P. W. J. M. Frederix, I. R. Sasselli, N. T. Hunt, R. V. Ulijn, T. Tuttle, Assessing the Utility of Infrared Spectroscopy as a Structural Diagnostic Tool for β-Sheets in Self-Assembling Aromatic Peptide Amphiphiles, Langmuir 29 (2013) 9510−9515.
83. M. Biancalana and S. Koide, Molecular mechanism of Thioflavin-T binding to amyloid fibrils, Biochim Biophys Acta 180 (2010), 1405–1412.
84. M. J. Krysmann, V. Castelletto, I. W. Hamley, Fibrillisation of hydrophobically modified amyloid peptide fragments in an organic solvent, Soft Matter 3 (2007) 1401–1406.

85. S. Marchesan, K. E. Styan, C. D. Easton, L. Waddington and A. V. Vargiu, Higher and lower supramolecular orders for the design of self-assembled heterochiral tripeptide hydrogel biomaterials, J. Mater. Chem. B, 3 (2015) 8123-8132.
86. M. Ma, Y. Kuang, Y. Gao, Y. Zhang, P. Gao, and B. Xu, Aromatic-Aromatic Interactions Induce the Self-Assembly of Pentapeptidic Derivatives in Water To Form Nanofibers and Supramolecular Hydrogels, J. Am. Chem. Soc. 132 (2010) 2719–2728.
87. N. S. S. Kumar, M. D. Gujrati and J. N. Wilson, Evidence of preferential p-stacking: a study of intermolecular and intramolecular charge transfer complexes, Chem. Commun. 46 (2010) 5464-5466.
88. J. Naskar, G. Palui, A. Banerjee, A. Tetrapeptide-Based Hydrogels: for Encapsulation and Slow Release of an Anticancer Drug at Physiological pH, J. Phys. Chem. B 113 (2009) 11787- 11792.
89. D. Ke, C. Zhan, A. D. Q. Li, and J. Yao, Morphological transformation between nanofibers and vesicles in a controllable bipyridine-tripeptide self-assembly, Angew. Chem. Int. Ed. 50 (2011) 3715 –3719.
90. Y. Yan, J. Huang, B. Zhong Tang, Kinetic trapping – a strategy for directing the self-assembly of unique functional nanostructures, Chem. Commun. 52 (2016) 11870.
91. P. W. J. M. Frederix, J. Ide, Y. Altay, G. Schae¨ffer, M. Surin, D. Beljonne, A. S. Bondarenko, T. L. C. Jansen, S. Otto, and S. J. Marrink, Structural and Spectroscopic Properties of Assemblies of Self-Replicating Peptide Macrocycles, ACS Nano, 11 (2017) 7858−7868.
92. L. Yao, M. He, D. Li, H. Liu, J. Wua and J. Xiao, Self-assembling bolaamphiphile-like collagen mimetic peptides, New J. Chem. 42 (2018) 7439-7444.
93. J. Wang, C. Yuan, Y. Han, Y. Wang, X. Liu, S. Zhang, and X. Yan, Trace Water as Prominent Factor to Induce Peptide Self-Assembly: Dynamic Evolution and Governing Interactions in Ionic Liquids, Small, 13 (2017) 1702175.
94. A. J. Matsuoka, Z. A. Sayed, N, Stephanopoulos, E. J. Berns, A. R. Wadhwani, Z. D. Morrissey, D. M. Chadly, S. Kobayashi, A. N. Edelbrock, T. Mashimo, C. A. Miller, T. L. McGuire, S. I. Stupp, and J. A. Kessler, Creating a stem cell niche in the inner ear using self-assembling peptide amphiphiles, PLoS One. 12 (2017) e0190150.

Chapter 4

Laminin conjugate hydrogels for controlling neuronal cell behavior

4.1 Introduction

As discussed in Chapter 1 and 3, supramolecular self-assembly is an attractive route of fabricating biomimetic materials with controlled physical and chemical properties. [1, 2] The synthetic biomimetic materials offer several advantages but, at the same time, present significant challenges in terms of their real applications in biology. [3] These challenges can be considered as crucial parameters for their biocompatibility and biodegradability and provides an inspiration to explore nature's toolbox for fabricating biomimetic materials. [4] Peptides have gained huge interest as a building block for biomimetic materials due to their chemical diversity and biological functionality. [5, 6] Self-assembling peptides have the capability to generate various types of nanostructures like fibers, tubes, vesicles, micelles etc, but fibrous structures, in particular, have received great interest due to their close similarity with the nano-architecture of natural extracellular matrix. [7-9] Apart from structural similarity, the biologically relevant peptide design has the potential to regulate cell growth and regeneration, by providing biochemical and mechanical cues. [10, 11]

Recently, the research interest is being shifting towards simulation of native cellular milieu, which can facilitate the regulation of cellular processes *in vitro* and in developing in depth understanding of cell response towards physical and biological cues *in vivo*. [12, 13] So far in the literature, several functional peptide sequences derived from ECM proteins are known, which includes fibronectins (RGD), Collagen (GXY), Laminin (IKVAV & YIGSR), Elastin like peptides (VPG) etc, which have significant impact on cellular processes like adhesion, differentiation, proliferation and migration. [14-20] A recent report mentioned that in last few decades, majority of studies reported on cell-adhesive peptides used RGD based sequences (~89%), while laminin was the other commonly used peptide to impart cell-adhesiveness (~10%) and remaining sequences comprise < 1% of the literature. [14, 15-26] In most of the instances, the functional short peptide derivatives lack the self-assembling capability and are used with other self-assembling polymers or peptide amphiphiles. [21, 22, 27] However, bio-functionalization of self-assembling peptides or polymers proposes synthetic challenges like uncontrolled epitope density, disruption of mechanical stiffness of self-assembling peptide amphiphiles and reproducibility issues. [28] Therefore, it is highly desirable to incorporate functional peptide sequences within our rational design of bioactive peptides, which can inherently self-assemble to form nanofibrous scaffolds.

As already mentioned in chapter 3, a bioactive peptide, laminin holds an important status owing to its diverse biological roles. [29] Laminin is a heterotrimeric protein, present in abundance in the basement membrane of native ECM. Two short functional laminin derivatives i.e. IKVAV and YIGSR are widely known in the literature. IKVAV is located on long arm of A-chain of laminin and promotes neurite growth whereas YIGSR, present on B1- chain, controls neuronal cell-substrate adhesion and migration. [30, 31] However, these short peptide sequences (IKVAV and YIGSR) lack sufficient interaction to support hierarchical assembly and fail to form supramolecular gels. In this context, full length laminin protein and its derivatives (IKVAV and YIGSR) are widely incorporated for developing biomimetic hydrogels with cell interactive properties. [32-37] A report by Arulmoli's group demonstrated the improved neurite outgrowth in neural stem cell with interpenetrating hyaluronic acid (HA) and fibrin network decorated with full laminin. In this work, thiol modified HA was used to readily combine with laminin. [38] In context with short laminin derivatives, L. Zhang's group reported CSIKVAV conjugated-chitoan hydrogels for skin regeneration and successfully demonstrated the wound healing in vivo through angiogenesis, re-epithelialisation, and collagen deposition. [39] The peptide conjugation with chitosan involved maleimide covalent chemistry. In the similar line, Luder *et al*, demonstrated the decoration of self-assembling N-acetylated β-tripeptides with cell adhesion molecule, IKVAV and RGD, which exhibited improved cellular responses. [5] The authors used solid phase synthesis approach to functionalize β-peptide monomers. The above examples clearly showed that covalent approaches were more common in the previous reports, which may offer synthetic challenges.

So far, very few reports are available in the literature which described the design of self-assembling laminin derived peptides. [24, 40-42] These self-assembly in the laminin derived peptides can be induced through hydrophobic modifications with a long alkyl chain, aromatic groups or additional hydrophobic peptide sequences, that makes them capable of forming supramolecular gels. In this context, a report by K. L. Niece and group demonstrated self-assembly of the C-16 alkyl chain modified IKVAV and YIGSR sequences with 13- mer amphiphile. [24] In this communication, gelation was induced by the addition of oppositely charged peptide amphiphiles. Similarly, Rodriguez *et al*. suggested a minimalist peptide design using Fmoc aromatic group, which forms hydrogels at very high pH (~12). This was further tuned by chemical modification through the incorporation of aspartic acid residues in IKVAV, resulting the gelation to occur at physiological pH. [40] In our previous work, we have developed a library of hydrophobically modified laminin derivatives. [41] The differential gelation behavior

of these peptides were found to be highly susceptible to the surrounding solvent environment. The design incorporates only the pentapeptide backbone (IKVAV and YIGSR) with simple hydrophobic ligands, without using any polymeric network or large self-assembling peptidic backbone. The above examples suggested that attempts were made to develop short laminin peptide based hydrogels, but these sequences were further not been assessed for their biological activities. However, this limited exploration of bioactivities of IKVAV and YIGSR peptides with minimalist modifications suggest the way to explore new class of self-assembling laminin derived peptides.

Moreover, the regulation of cell proliferation and differentiation is an extremely sophisticated process that involves multiple ligand-receptor interactions. A scaffold with single type of peptide epitope may have limited ability to control complex biological functions of the cells. Incorporation of more than one inherent bioactive motifs of a native protein in single scaffold can create a closer biomimetic scaffold, which is expected to broaden the functional spectrum of such scaffolds. In addition to this, the diverse nanostructures created by self-assembling peptide motifs provide unprecedented opportunities to recapitulate the natural niche for the cells. In case of laminin protein, IKVAV and YIGSR are the intrinsic peptide motifs and both together regulate the functional activity of basement membrane protein. A versatile strategy to expand the boundaries of scaffold design beyond the conventional single component bioactive scaffold still remains a challenge. At this point, simple mixing approach of two or more functional peptide sequences can be an effective strategy to create multicomponent microenvironment for controlling cell behavior. Through such co-assembly, we expect that multiple bioactive domains can be presented for controlling cell adhesion, proliferation and migration, mediated through interaction with different types of receptors. The integrin binding IKVAV peptides and YIGSR peptides binding with laminin receptors mediate the intracellular functions in response to extracellular biochemical and mechanical cues. [42, 43] To the best of our knowledge, this is the first attempt to demonstrate the co-assembly approach for combining the inherent laminin bioactive motifs for improved physiochemical and biological properties of the supramolecular hydrogels without relying on the covalent attachment in a polymeric network or additional peptide segment. [3]

In this study, we have illustrated the formation of composite network of self-assembling laminin derived peptides, which were designed in our previous work (chapter 3). [41] The idea behind the design of composite synthetic scaffold was to embed both functional motifs of native laminin protein in the same matrix. The two pentapeptides IKVAV and YIGSR, appended with Fmoc

modification, vary greatly in their hydrophobicity and provide an excellent control over the modularity of the system, in combined gels. Majorly, this work elucidates the physiochemical properties of modified self-assembling IKVAV and YIGSR peptides in combination. We have explored these laminin derived scaffolds towards controlling neuronal cell behavior using C6 glial cells and SHSY5Y neuroblastoma cells. In this work, we tried to mimic the biological roles of native laminin protein, using its shortest possible functional derivatives. The designer scaffolds were found to induce significant proliferation rates and supporting cell adhesion upto 5 days indicating the characteristics of a potent scaffold. Their properties of promoting cellular functions were marked by neurite extension, neuronal marker (βIII-tubulin) expression and normal cell cycle behavior. The results clearly revealed that the designed laminin peptide scaffolds were highly biocompatible and promote normal cellular responses, which were better in comparison to control TCPS (tissue culture polystyrene). This work enables us to compare the role of each peptide scaffold individually towards regulating neuronal cell behavior and how the cell-matrix interactions would be affected when the two peptides were used in combination as a gel scaffold. Moreover, the simple co-assembly approach provides a facile route for developing multifunctional scaffolds. Based on our observations, we hypothesize that such bioactive scaffolds can be promising materials for emerging biotechnological applications like tissue engineering and drug delivery.

4.2 Experimental Section

4.2.1 Materials and methods

All Fmoc protected amino acid, coupling reagents, like, Piperazine, Diisopropyl carbodiimide (DIC), and cleavage cocktail reagents like Anisole, EDT (1,2-ethanedithiol), Thioanisole, TFA (Trifluoroacetic acid), Myristic acid were purchased from Sigma-Aldrich. The solid support Fmoc- Rink amide MBHA resin,2-napthoxy acetic acid, Oxyma, Dimethylformamide (DMF) and Diethyl ether were purchased from Merck.

4.2.2 Synthesis of Peptides

Fmoc IKVAV and Fmoc YIGSR were synthesized using standard Fmoc-chemistry through solid phase synthesis. [41, 44] Microwave assisted automated Solid Phase Peptide synthesizer (Liberty Blue CEM, Matthews, NC, USA) was used for the synthesis at a scale of 0.1mM. For both the peptides, Fmoc-rinkamide resin was allowed to swell for 30 minutes in DMF, followed by Fmoc-amino acids coupling in the presence of DIC (0.5M) as activator and oxyma (1M) as

activator base. Fmoc deprotection, before each coupling was completed using 10% piperazine in dimethylformamide containing 10% ethanol, with no Fmoc-deprotection after final coupling. The peptides were cleaved from resin by using a mixture of 90% trifluoroacetic acid, 5% thioanisole, 3% 1, 2-ethanedithiol and 2% anisole for 3 hours. The product was recovered by precipitating the filtrate in cold ether, followed by centrifugation and drying under vacuum. The dried product was purified by preparative scale reverse phase high performance liquid chromatography (Waters). The mobile phase used was acetonitrile and water with 0.1% trifluorocetic acid. Pure peptide containing fractions were mixed and lyophilized and stored under vacuum until use. The peptide identity was confirmed using mass spectrometry. Similarly, Myristyl IKVAV and Nap IKVAV were synthesized by attaching myristyl and napthoxy group at N-terminal, in place of Fmoc group.

4.2.3 Solubility Measurement

To determine the solubility of peptides, initially, the calibration curve of Fmoc IKVAV and Fmoc YIGSR were prepared. The peptide stock of 1mg/ml was prepared in water using 50µl of methanol as a solubilizing aid, followed by dilution to different concentrations ranging from 0.01mg/ml to 0.2 mg/ml in water. The absorbance of each peptide dilution was measured at 260nm. The absorbance of each peptide dilution was plotted against concentration. The data points were fitted linearly and the intercept and slope of the plot was calculated. Then to determine the solubility of peptide in PBS and water, an excess (10mg) peptide was dissolved in 1ml of solvent. Then the supernatant with dissolved peptide was measured and its absorbance at 300 nm was recorded. The concentration corresponding to that absorbance was calculated by extrapolating the standard calibration curve.

4.2.4 Gel Formation

The heat-cool method was employed to form gels using the designed peptides. The prerequisite amount, equivalent to 20 mM of peptide (in case of individual peptide gels) was added in to PBS (100mM, pH 6). While for composite hydrogels, Fmoc IKVAV and Fmoc YIGSR were mixed in 1:1 ratio i.e. 10mM of each peptide, keeping the total concentration of peptides fixed at 20mM. The peptide suspension was kept in a water bath, which was maintained at 90^0C, until the peptides were dissolved completely. The time for dissolution of peptides may vary from ~30 min for Fmoc YIGSR to ~2 hrs for Fmoc IKVAV. After complete dissolution, the peptide solutions were allowed to self-assemble, at room temperature and form self-supporting hydrogels. [41] Similarly, gelation of Myristyl IKVAV and Nap IKVAV was carried out.

4.2.5 Morphological assessment of the hydrogel network

4.2.5.1 Atomic Force Microscopy: Gels were prepared at 20mM concentration and diluted upto 10 times before drop casting over the silicon wafer. The sample was allowed to adsorb on the surface of wafer and excess solution was removed by the wicking action of filter paper. The samples were air dried and scanned under ambient conditions using Bruker Multimode 8 scanning probe microscope operated in tapping mode with Nanoscope V controller and a J-scanner. The AFM probe used was RTESPA-300 with the resonating frequency of 300 kHz.

4.2.5.2 Transmission Electron Microscopy: The peptide gels prepared at concentration of 20mM were diluted and drop casted over the carbon coated copper grids. The samples were allowed to adsorb for 3 min and the excess sample was removed. Freshly prepared and filtered uranyl acetate solution (2% w/v, 5µl) was added on the grid and allowed to stain the gel samples for 5min. The samples were vacuum dried before imaging. TEM micro-graphs were recorded at an accelerating voltage of 200 kV using JEOL JEM 2100 with a Tungsten filament.

4.2.6 Mechanical Strength Evaluation

Oscillatory rheology was performed to measure the viscoelastic properties of the nanofibrous laminin derived peptide hydrogels. The measurements were done using 50mm parallel plate geometry (Anton Parr MCR302). The hydrogel samples (1ml) of 20mM concentrations were prepared and incubated for 24 hrs before measurements. Amplitude sweep was performed to obtain the optimum strain values in the linear viscoelastic region. Further, the frequency sweep was performed in the range of 0.1 to 100 Hz to record storage (G') and loss modulus (G"). Solvent trap was used to prevent any drying affect, and temperature was maintained at 20^0C with an integrated electrical heater. The measurements were repeated 3 times to ensure reproducibility, with the average data shown. To study the effect of concentration of peptides on the mechanical properties of the hydrogels, gels were prepared at 30mM and 40mM concentrations and evaluated for the rheological properties.

4.2.7 Thixotropic Studies

Step-strain rheology was performed to study the mechano-responsive behavior of the laminin derived hydrogels. Initially, thixotropic behavior was checked through inversion vial method, in which gels (20mM) were subjected to mechanical shaking, which transforms the gel material into solution (sol) and it recovers into the self-supporting gel state upon resting. However, the time of reformation may vary depending up on the nature of the network of the monomer as

well as the composite monomers.. The initial strain values were fixed within linear viscoelastic (LVE) region as 0.1 %, followed by deformation strain of ~50 %, which transforms it to sol, as indicated by G′ < G″. The gel like character is restored on the removal of stress (strain 0.1%). The frequency was fixed at 1Hz, during, both, deformation and recovery cycles. Each cycle having 200s deformation phase and 800s recovery phase. The measurements were repeated three times.

4.2.8 Secondary Structure Investigation

4.2.8.1 Circular Dichroism (CD): A Jasco J-1500 CD spectrophotometer with 0.1 mm quartz cuvette was used for the measurement of CD spectra of laminin peptide hydrogels. Spectra were recorded between a wavelength range of 195-320 nm with signal integrations of 1 s and a step size and slit width of 1 nm, respectively. Three repeated scans were compiled to generate the average spectra. Jasco Spectra Manager software was used to analyze the spectra. Baseline correction was done by subtracting the spectrum in PBS, without peptides. Composite gels were prepared at different ratios of Fmoc IKVAV and Fmoc YIGSR and studied for characteristic resultant CD signals.

4.2.8.2 Fourier Transform Infrared Spectroscopy (FTIR)*:* Bruker Vertex 70 ATR spectrophotometer was used to record FT-IR spectra. The spectra were recorded in the range of 400 and 4000 cm^{-1} with a resolution of 1 cm^{-1} and averaged for 64 scans. Spectra were background subtracted using each solvent system to correct for atmospheric interference. Samples were analyzed in gel state by keeping the 20µl of gels (20mM) on the top of diamond crystal.

4.2.9 In vitro Cell Culture Experiments

Cell culture experiments were performed with C6 glioma cells and SHSY5Y neuroblastoma cells. DMEM media with 10% foetal bovine serum (FBS), and 1% penicillin-streptomycin antibiotic solution was used to culture the cells. Cultured cells were incubated at humidified chamber with 5% CO_2 at 37^0C.

4.2.10 2D culture

Prior to 2D cultures, the peptide gels were washed and perfused with media, which helps to determine the stability of gels in culture media for longer durations. The gels were prepared at 20 mM concentrations and placed on coverslips which were sterilized under UV. Media was

perfused through the gels to exchange PBS and provide uniform environment to the cells. The sub-confluent monolayer of cells were trypsinized using trypsinase (0.25%)–EDTA (0.02%) solution and re-suspended in complete media. The cell density was counted using haemocytometer. Then 1ml of cell suspension, having 50,000 cells/ml was added in each well of 6 well-plate. The cells were maintained at 37 ^{0}C with 5% CO_2 and allowed to adhere.

4.2.11 Metabolic activity assay

MTT assay was carried out to assess the initial contact cytotoxicity of laminin derived short peptides and quantify cell survival in the presence of peptides. Each well of 96well plate was seeded with 5000 cells and allowed to adhere for 24 hrs. Peptide stock solutions of 5mg/ml concentration in PBS (100mM, pH 6) were prepared using heat cool method of gelation and were sterilized before treatment. Diluted peptide stocks (100µg/ml, 500µg/ml and 1000µg/ml with DMEM media) were added to the adhered cells. For each peptide, experiments were done in triplicates. The control cells were treated with same volumes of PBS (pH 6) in DMEM media. MTT salt (3-(4, 5-dimethylthiazol-2-yl)-2,5-diphenyltetrazolium bromide) dissolved in PBS (10µl of 5mg/ml stock in each well) was added to the cells after 4 hrs of peptide treatment, with 100µl of fresh media. MTT is a colorimetric assay reagent which converts into purple colored insoluble formazan upon activity with metabolically active cells and gives the relative number of viable cells. Supernatant media was removed, after 4 hrs of MTT addition. Formazan crystals were dissolved in DMSO (100µl). Absorbance was recorded at 495nm wavelength using plate reader. The percentage viability of treated cells was calculated with respect to control cells. Similarly, MTT assay was carried after 24 and 72 hrs, to assess the long term cytotoxicity of the peptide hydrogels. For this study, the MTT assay was performed on 2D cultured cells. The gels (75ul) were placed in 96 well plate and perfused with culture media. Further, the cell suspension was added on the top of gels in each well. The cells were allowed to adhere and grow on the gel surface for 24 hrs and 48 hrs, before adding MTT. After 4 hrs of MTT addition, the insoluble formazan crystals were dissolved in DMSO. To eliminate any interruption with peptide gels in absorbance measurement, blank peptide gels were incubated with same concentration of MTT and DMSO and their absorbance were subtracted from the samples.

4.2.12 Live/Dead Staining

Live dead staining studies were performed after 2 and 5 days of cell culture over hydrogels using standard protocol for Live/Dead cell mediated cytotoxicity kit (Invitrogen). 4µl of $DiOC_{18}$

(3) was diluted with 1ml of complete media (1:250 dilution) while 2µl of PI (propidium iodide) was diluted with 1ml of PBS buffer and filtered using 0.2µ filters. The cells were incubated with $DiOC_{18}$ (3) for 45 min in dark and then washed three times with PBS. Further, PI solution was added to wells and left for 20 min. At last, three washes with PBS were performed and plates were visualized under the confocal microscope under the green (480nm) and red (530nm) channels.

4.2.13 Cell Proliferation Assay

Proliferation of C6 cells and SHSY5Y cells were assessed by Alamar blue assay after 2 days and 5 days of treatment. Laminin gels were prepared at 20mM concentration and 100ul gel was placed in each well (100ul). The plates with gels were UV sterilized and allowed to stabilize overnight, after which media was perfused to exchange PBS. The cells were seeded with cell density of $3X10^3$ in each well of a 96 well plate over the gels. The plates were incubated at 37^0C, with 5% CO_2, in 95% humidified incubator, for different time durations. Each sample was incubated in triplicate. The cells cultured on tissue culture plastic surface were used as positive control. After 2 days and 5 days, fresh media (100µl) was added to each well with 10% Alamar blue reagent. After 4 hr of incubation, the 96-well plate was read by using micro plate reader (Tecan Infinite M Plex). The fluorescence intensity of alamar blue was determined by excitation/emission of 530nm/600nm. The peptide gels (without cells) were incubated with alamar blue and used as negative controls and their fluorescence intensity values were subtracted from the corresponding cell embedded peptides.

4.2.14 Neurite Extension Study:

The C6 cells were cultured on the top of the gels in a 6 well plate with the concentration of $1X10^4$ cells/ well. The cells were allowed to adhere for 24 hrs. Further the morphology of the cells were studied using bright field microscope (EVOS XL, Life Technologies) at magnification of 40X, after 24 and 48hrs. The length of longest neurite i.e. axons were measured using Image J software, as reported in previously available reports. The average axon length was calculated by taking an average of 30 cells, for each gels and control that are grown on plastic surface.

4.2.15 Immunofluorescence staining:

To carry out this study, the hydrogels were uniformly spread over the surface of coverslips placed in 35mm culture dishes. Cell suspension containing 10^4 cells/ml were added to each

culture dish and allowed to adhere. After 5 days, the cells were fixed using 4% paraformaldehyde for 20 min at room temperature and washed three times with PBS. Then the cells were permeabilized with 0.5% Triton X100 in PBS. The samples were incubated with bovine serum albumin (5%) for 1 hr at room temperature, to avoid any non-specific binding. The primary antibodies (monoclonal rabbit anti-βIII Tubulin, CST) at dilution of 1:500 in dilution buffer (composed of 1% BSA, 0.1 % TritonX-100 in 1X PBS) was added to the samples and incubated for overnight at 4^0C. After incubation, the cells were washed thrice with the dilution buffer, following which the secondary antibodies (anti-rabbit IgG Alexa Fluor 555 conjugate, CST) were added at 1: 1000 dilution for 1 hr at room temperature. After the removal of secondary antibodies, the samples were washed thrice with the dilution buffer. DAPI (1μg/ml) solution was added for 5 min to stain the nuclei and excess stain was washed 2 times using dilution buffer. The samples were then fixed using 80% glycerol on the glass slides and used for imaging under confocal microscope (Zeiss LSM880 confocal microscope, Carl Zeiss) at 63X magnification. [45]

4.2.16 Cell Cycle study:

Cell cycle analysis was done by quantifying the DNA content of the cells using Flow cytometry. The cells were cultured over the surface of hydrogels. Prior to fixation and staining, the cell growth was synchronised by keeping the adhered cells (~1X 10^6 cells) in culture media with 2% FBS for 24 hrs. Further, cells were harvested and fixed using 70% chilled ethanol at 4^0C for 30 min. The samples were washed with PBS, twice, at 850g by centrifugation. The cells were then treated with ribonuclease (50μl of 10μg/ml RNasestock) to ensure selective staining of DNA only, and not RNA. At last the cells were suspended in 200 μl of propidium iodide (50μg/ml stock solution). The samples were analysed using flow cytometer (BD Biosciences). [46]

4.3 Results and discussion

4.3.1 Peptide design and gelation

The strategy for design of peptides for generating a biomimetic scaffolds usually involve the incorporation of biochemical cues, in terms of designer sequence, which are inspired from inherent component of ECM protein. The design should incorporate the functional sequence that can induce cell adhesion as well as proliferation. The design of peptides was based on minimalist modification to the identified functional sequence of laminin protein i.e. IKVAV and YIGSR, as illustrated in our previous report. [41] The N-terminal modification with an aromatic

Fmoc-moiety is expected to transform non-assembling peptide sequences into self-assembling functional peptides (figure 4.1 a, b). [41] The molecular structure of peptide sequence suggests that IKVAV is more hydrophobic than YIGSR, which was further confirmed by their C log P values, calculated as 0.42 and -3.218, using Chem Draw software. The peptides were synthesized using solid phase peptide synthesis and HPLC and ESI-MS was employed to confirm of purity of peptides that was found to be of high purity followed by purification through preparative HPLC (figure 4.1 c-f). [47]

Owing to different C log P values, it was expected that these peptides would have different solubility in particular solvent. In order to select a suitable gelation method, we determined the solubilities of both peptides in water and PBS. Prior to solubility determination, calibration curve of both the peptides were developed, which was further used for the calculation of solubility of each peptide in different solvents (figure 4.2). [48] Due to hydrophilic nature of Fmoc YIGSR, it showed high solubility in PBS (21.5mg/ml) and water (6.6mg/ml). However, it resulted into gel formation in water as well as PBS, at an excess concentration of 10mg/ml, which makes it difficult to assess the accurate solubility of Fmoc YIGSR.

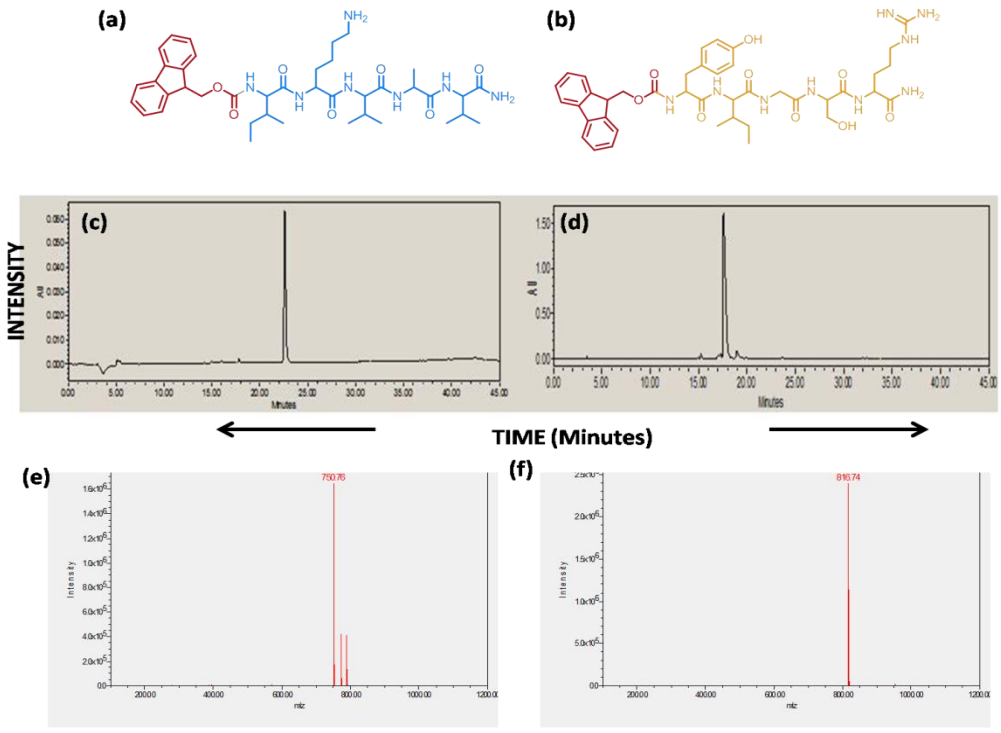

Figure 4.1 *Molecular structure of Laminin peptides (a) Fmoc IKVAV and (b)Fmoc YIGSR and corresponding HPLC chromatograms and mass spectra of (c, e) Fmoc IKVAV and (d, f) Fmoc YIGSR.*

Whereas, the higher hydrophobicity of Fmoc IKVAV makes it poorly soluble in aqueous solvent at room temperature (25^0C). Fmoc IKVAV showed solubility of ~0.02mg/ml in water and ~1.5mg/ml in PBS (pH 6). Therefore, heating method was chosen to enhance the solubility of Fmoc IKVAV in PBS to attain peptide concentration that could lead to gelation.

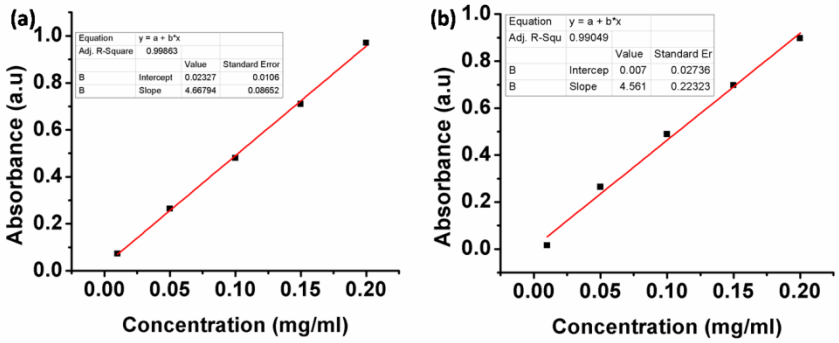

Figure 4.2 *Calibration curves of (a) Fmoc IKVAV and (b) Fmoc YIGSR.*

However, in previous chapter, we showed differential gelation behavior of these peptides in wide range of solvents, presence of organic solvents might limit their direct use in biomedical applications. Our previous work highlighted that the hydrophilic derivative, YIGSR showed more propensity to form highly entangled fibrous network in aqueous media, owing to enhanced gelator-gelator interactions compared to its hydrophobic counterpart, IKVAV. Furthermore, it is expected that aqueous solvent based gels would be more suitable for demonstrating cell-matrix interactions. Hence, the peptides were dissolved in PBS (100mM, pH 6) and subjected to heat-cool method to form hydrogels. [49] However, differential hydrophobicities of the peptides provide variable self-assembling behavior in aqueous solution (figure 4.3). The similar has been reflected in their minimum gelation concentration as well. The hydrophobic Fmoc IKVAV showed MGC at 15mM while relatively hydrophilic Fmoc YIGSR formed gel at 10mM concentration. The probable reason for differential MGC could be explained by the favored solubilization of Fmoc YIGSR in aqueous media than hydrophobic Fmoc IKVAV. The faster dissolution of hydrophilic peptide increases the local peptide concentration with enhanced solute-solute interactions, resulting in formation of primary self-assembled structures that further grow to form higher order network structures. However, for further studies, the gels at concentration above MGC i.e. 20mM were used for both the individual peptides, to yield stable gels for cell culture work. In case of composite hydrogel, 1:1 molar ratio of Fmoc IKVAV and Fmoc YIGSR result in a stable self-supporting gel, on simple mixing. Interestingly, composite gel was found to be stable at 10mM concentration of each of the peptides, thus enhancing the

propensity of these peptides to form composite network through enhanced intermolecular interactions. Upon mixing, Fmoc YIGSR immediately starts self-assembling at 10mM concentration which acts as a nucleating site for Fmoc IKVAV, thus facilitating the self-assembly of Fmoc IKVAV, at concentration below MGC.

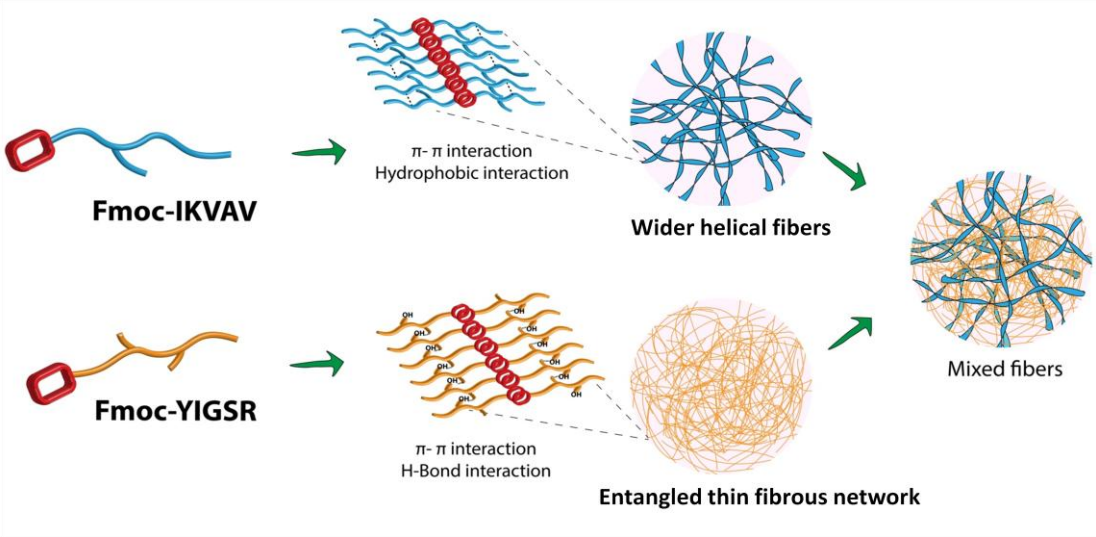

Figure 4.3 *Schematic representation of molecular self-assembly of laminin derived peptides showing differential fibrous morphology, while their composite gels showing coexistence of self-sorted fibrous morphology of both the peptides. The driving forces for self-assembly of IKVAV peptide is probably hydrophobic and aromatic π interactions and for YIGSR, H-bonding and aromatic π interactions are dominant in aqueous solvent environment.*

Another interesting way to control the self-assembly of short peptides is to vary the hydrophobicity of N-terminal ligand. The variable hydrophobicities of the ligands will dictate the differential self-assembly of non-gelator bioactive peptides such as IKVAV and YIGSR. In this context, we also tried to study the effect of hydrophobicities on the self-assembling behavior of IKVAV peptide. The IKVAV backbone was modified with another aromatic group, napthoxy and an aliphatic chain, myristyl. The comparison of log P values of these hydrophobic moieties suggests that Myristyl group having log P value of ~6.28 was the more hydrophobic than Fmoc (log P ~3.2) while napthoxy is less hydrophobic with log P values of ~2.02. The IKVAV sequence modified with these groups showed differential hydrophobicities, depending upon the hydrophobicities of these groups. These differences were confirmed by studying their gelation in aqueous solvent. The most hydrophobic Myristyl IKVAV showed the highest MGC in PBS of ~25mM in the series, which was also reported in our previous work. [41] While, the

least hydrophobic Nap showed lowest MGC of ~10mM, which was lesser than that of Fmoc IKVAV i.e. 15mM. This difference is probably due to their differential solubilities of these peptides in aqueous solvent. The effect of hydrophobicities on self-assembly of peptides in aqueous solvent was reflected in their mechanical stiffness as well. In comparison to storage modulus of Fmoc IKVAV i.e. ~1±0.17 kPa, Nap IKVAV showed storage modulus of ~1.7 ± 0.27 kPa and myristyl IKVAV in the range of ~0.008 ± 0.001 kPa (figure 4.4). The reason for higher mechanical stiffness of nap IKVAV can be correlated with higher strengths of Fmoc YIGSR in aqueous solvent which is probably due to their relatively higher solubilities in aqueous solvents leading to enhanced gelator-gelator interactions.

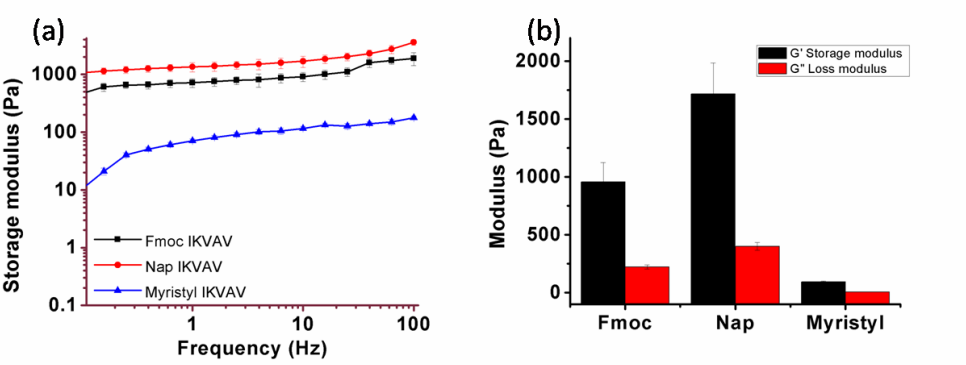

Figure 4.4 *Rheological measurements of IKVAV peptide with different N-terminal modifications with Fmoc, Nap, and Myristyl (a) showing change in storage modulus with respect to frequency for the hydrophobically modified IKVAV peptides and (b) comparing the average storage and loss modulus of each peptide.*

4.3.2 Morphology Assessment

The differential hydrophobicities of both the peptides i.e. Fmoc IKVAV and Fmoc YIGSR in aqueous solvent are expected to lead to differential molecular packing of the peptide building blocks, which may result in diverse nanostructures, which were studied using atomic force microscopy (AFM). [50] In corroboration to previous work, Fmoc IKVAV showed the presence of short helical fibers with lesser entanglement in comparison to dense, thinner fibrous network of Fmoc YIGSR (figure 4.5). [51] The diameter of Fmoc IKVAV was found to be in the range of ~30 ± 5nm, whereas, Fmoc YIGSR showed the fiber diameter in the range of 20 ± 6nm (table 4.1). Interestingly, the composite hydrogels showed self-sorted nanofibrous network, which was visible in figure 4.5c. The distinct intertwined network of two different fibers with wider fibers having diameter of ~85±14nm and thinner fibers having diameter ~ 32± 6.5nm can be clearly

observed. [52] It was assumed that the wider fibers represent the Fmoc IKVAV self-assembly while, the thinner ones indicate the self-assembly of Fmoc YIGSR, which can be correlated with that individual self-assembled peptide morphology at nanoscale. The probable reason for such self-sorting behavior could be the differential solubility of both peptides in aqueous environment. During gelation, the hydrophilic Fmoc YIGSR dissolves quickly on heating and starts early self-assembly in comparison to delayed self-assembly of Fmoc IKVAV, which takes 1-2 hrs to dissolve completely.

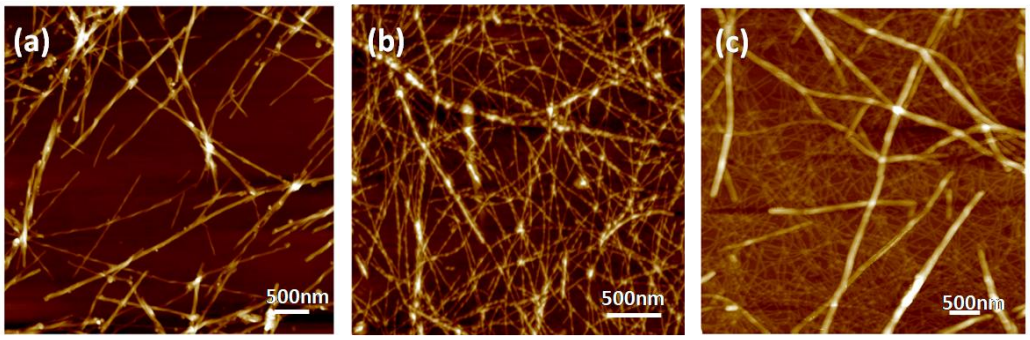

Figure 4.5 *Morphology analysis of (a) Fmoc IKVAV, (b) Fmoc YIGSR showing fibrous network and (c) Fmoc IKVAV+ Fmoc YIGSR peptides self-assembling to give rise to a mixed fibrous network structure, using AFM.*

The morphology attained due to self-sorting behavior of laminin derived peptides were further confirmed by TEM (figure 4.6). [53] The images clearly revealed the short nanofibrous morphology of Fmoc IKVAV which has diameter ~15±2.2nm (figure 4.6a). These fibers bundled together to form helical twisted fibers, which have wide diameters in the range of ~28±3.5nm. However, the Fmoc YIGSR hydrogels showed dense network of long nanofibers (figure 4.6b). The fibers have more uniform diameters in the range of 11.5±1.2nm. In corroboration to AFM results, the combined gels showed self-sorted network of two different diameters. The thinner, long fibers of diameter ~9.5±1.5nm appear in the background, which is overlaid by the wider fibers of diameter ranging ~28.3±2.5nm. The diameter of wider fibers was found to be nearly double of the individual Fmoc IKVAV fibers. The probable reason for this difference was adsorption of Fmoc IKVAV aggregates formed at concentration below MGC and Fmoc YIGSR fibers helps in the nucleation and growth of these aggregates, in composite gels. This was clearly evident from the magnified TEM image of composite gel (figure 4.6 d). The closely associated results of AFM and TEM revealed the differential morphology of different laminin derived peptides coexisting in the gel composite.

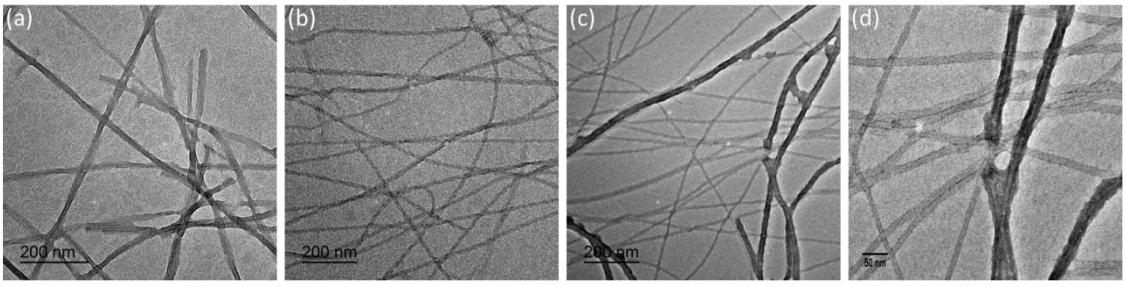

Figure 4.6 *TEM images of laminin derived peptides showing differential fibrous morphology formed by (a) Fmoc IKVAV, (b) Fmoc YIGSR, (c) combined self-sorted network of Fmoc IKVAV + Fmoc YIGSR and (d) magnified TEM image of composite gel.*

Table 4.1 *Fiber diameters of different laminin derived peptide hydrogels measured through AFM and TEM analysis through Image J software.*

Hydrogel composition	Diameter by AFM (nm)	Diameter by TEM (nm)
Fmoc IKVAV	30±5	15±2.2
Fmoc YIGSR	20±6	11.5±1.2
Fmoc IKVAV+Fmoc YIGSR	85±14 and 32±6.5	28.3±2.5nm and 9.5±1.9

4.3.3 Mixing Behaviour of Peptides in Composite Hydrogels

It is important to understand the mixing behavior of two components of composite gels, especially when they have different nature (hydrophobicities). Their mixing pattern will determine the resultant properties of the composite gels. To study the mixing behavior of Fmoc IKVAV and Fmoc YIGSR, time dependent microscopic studies were done using AFM (figure 4.7). The variable hydrophobicities of the two peptides lead to differential solubility. The Fmoc YIGSR being highly soluble in aqueous solvent showed quick self-assembly resulting into formation of dense fibrillar network within 5 min (figure 4.7 a). While Fmoc IKVAV, a poorly soluble peptide showed aggregate like structures in 5 min, which appear as patches on the preformed fibers of Fmoc YIGSR. It is expected that Fmoc YIGSR provides the nucleation sites for the Fmoc IKVAV aggregates. After 10 min, the density of these aggregates is increased and gradually extended over the length of the fiber, after 15 min (figure 4.7 b & c). Eventually, after 30 min and 1 hr, the network of two separate fiber diameters can be observed (figure 4.7 d & e). We believe that self-assembly of Fmoc IKVAV into aggregate like morphologies is due to their sub-gelation concentration in composite gels, which further grows into full length fiber, having Fmoc YIGSR fibers as their base. The adsorption of Fmoc IKVAV over the length of thin Fmoc

YIGSR fibers was also visible in the magnified TEM image of composite gel (figure 4.6 d). Therefore, this study reveals the mixing behavior of both peptides in composite gels, which predominantly depends upon their solubility in aqueous solvents.

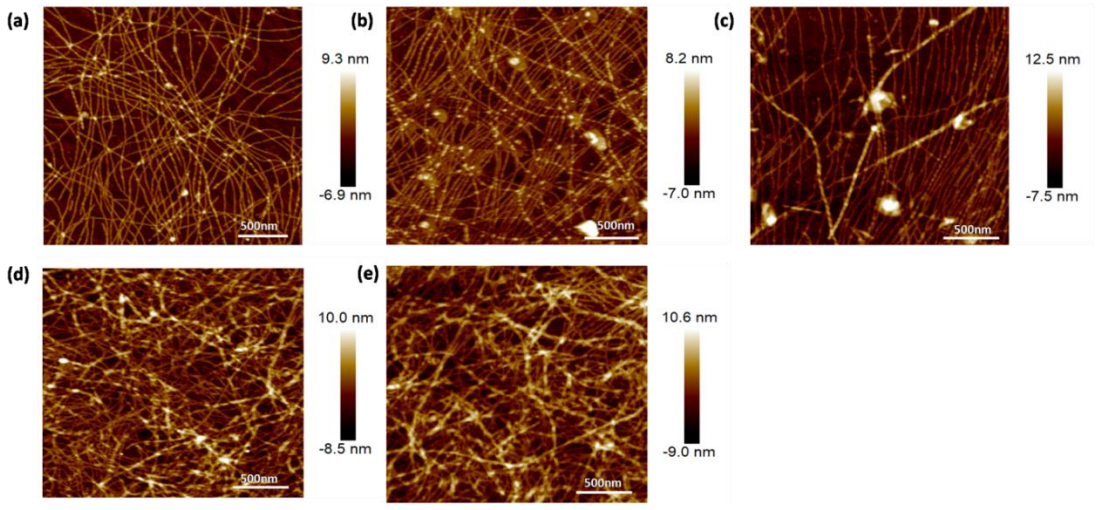

Figure 4.7 *AFM images of composite gels showing self-assembling behavior of individual peptides in mixture at different time points (a) 5 min, (b) 10 min, (c) 15 min, (d) 30 min and (e) 60 min.*

4.3.4 Mechanical Strength Evaluation

The differential morphologies will lead to variable strength of the resulting hydrogels. The mechanical strength of the hydrogels was measured by using oscillatory rheology. The storage modulus (G') was higher than loss modulus (G") for all the gels, which indicates the viscoelastic nature of the hydrogels. [54] Interestingly, the composite hydrogels exhibited highest strength of ~ 937±124 Pa in comparison to ~267± 47 Pa and ~674± 100 Pa of Fmoc IKVAV and Fmoc YIGSR, respectively (figure 4.8a & b). The difference between storage and loss modulus also indicates the stiffness of the gels, as more difference indicates higher mechanical stiffness. [28] This fact also confirms that the composite gels are relatively stronger, as their storage modulus was an order magnitude higher than its loss modulus (figure 4.8 b). The hydrophobic Fmoc IKVAV exhibited weaker hydrophobic interactions due to poor solubility in aqueous solvent, which lead to the formation of weaker hydrogels. Due to higher solubility of Fmoc YIGSR, it tends to form more entangled fibrous network, thus giving rise to stronger gel compared to Fmoc IKVAV. Further enhancement in the gel strength was observed in composite hydrogels, due to intertwined entangled fibrous network. It is expected that the self-assembly of laminin derived peptides involve hydrophobic interactions along with additional hydrogen

bonding interactions, which might be responsible for the higher strength of composite gels. [55] However, the intertwined entangled fibrous network imparts improved mechanical stiffness to the composite hydrogels. Interestingly, the mechanical stiffness of the designed gel matrices was found to be similar to that of native neural tissue ECM, which ranges from 0.1 to 1 kPa and is suitable to support neuronal cells. [28] These results suggested that the simple mixing of hydrophobic and hydrophilic peptides can be an effective means to tune the bulk properties of the resulting gel phase material, without changing the chemistry of the molecule. [56] At the same time, we anticipate that the composite hydrogel of these short laminin mimetic peptides would be a superior surrogate of native ECM protein since it incorporates essential functional sequences of the large basement membrane protein in the minimalist design of this single scaffold.

Moreover, peptide hydrogels offer the great advantage of high tunability. Their mechanical stiffness can be easily tuned by varying the gelator concentration. [57] The correlation between gel strength and peptide concentration would help to tune the mechanical stiffness of the scaffold in the required range. For both Fmoc IKVAV and Fmoc YIGSR, the increased elasticity of the hydrogels was observed with an increasing concentration of individual peptides (figure 4.8 c & d). For Fmoc IKVAV, the storage modulus was found to increase from ~0.3±0.05 kPa at 20mM, to ~1±0.07 kPa at 30mM and 2.2±0.3 kPa at 40mM concentration. Similarly, for Fmoc YIGSR, the storage modulus increases from ~0.6±0.03 kPa at 20mM to ~0.8±0.07 kPa at 30mM and ~1.5±0.2 kPa at 40mM. The reason for enhanced elasticity at higher concentration is the more number of intermolecular interactions that results in more rigid gels. It was interesting to note that varying the ratios of individual peptide components in composite gels, we can create diverse gels with variable mechanical properties. Keeping the total concentration of composite gels fixed (20mm), increasing the concentration of Fmoc IKVAV towards its MGC, significantly enhances the mechanical strength of composite gels. The storage modulus of 3:2 composite Fmoc IKVAV and Fmoc YIGSR gels showed stiffness of ~3.2 ± 0.3 kPa, while the peptides in 2:3 ratios resulted in gel strength of 1.4 ± 0.15 kPa (figure 4.8 e). The results suggested that simple mixing of different peptides in different ratios offers great flexibility of tuning the physical properties of the resulting gel-phase material.

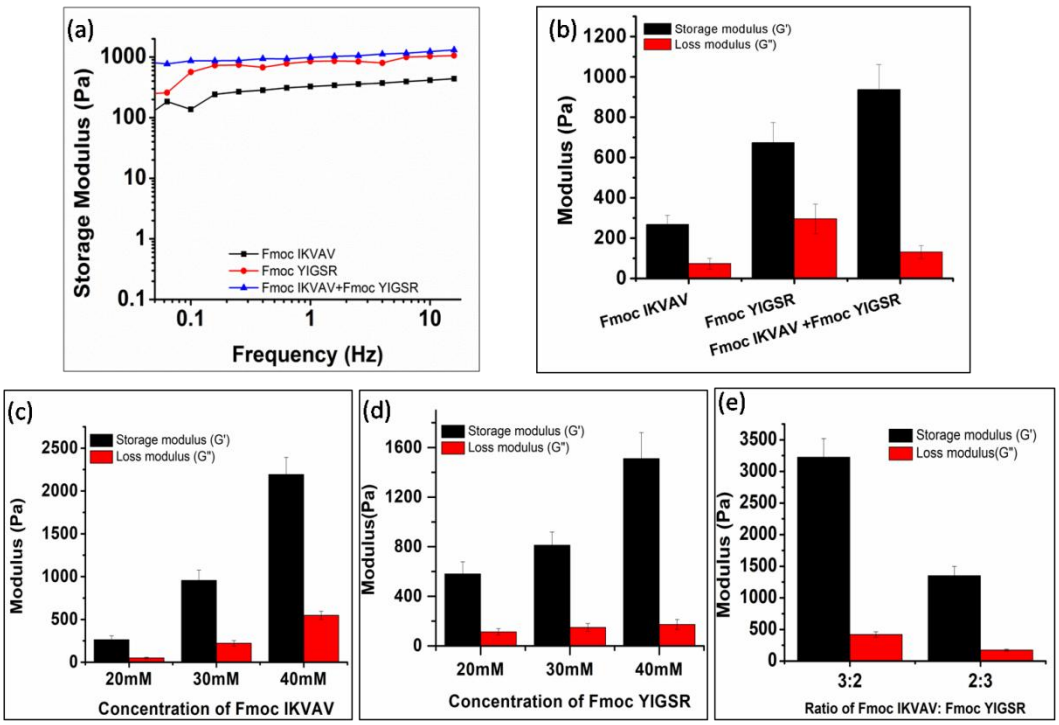

Figure 4.8 *Rheological studies showing (a) frequency sweep measurements, (b) comparison of storage modulus (G') and loss (G") modulus of individual laminin peptide as well as composite gels, (c and d) shows concentration dependent rheology of Fmc IKVAV and Fmoc YIGSR, respectively and (e) composite gels with variable ratios of Fmoc IKVAV and Fmoc YIGSR.*

4.3.5 Thixotropic Behaviour

To further explore the potential of these laminin mimetic peptides in biology, we were curious to find out an interesting property of these hydrogels, which is known as thixotropic nature of the gels. Thixotropic study involves the reversible gel-sol transformation upon application of mechanical stress and restoration of the gel phase upon resting. Initially, the thixotropic behavior was observed by the vial inversion method. [58, 59] All the hydrogels were converted to sol by vortexing for 2 min, which was allowed to stand undisturbed, to regain their gel state. It is to be noted that, during thixotropic recovery, these hydrogels do not require heating, as needed during gel formation. Step strain rheology was done to experimentally determine the thixotropic behavior of the laminin derived gels and their conjugate gel (figure 4.9). The peptides gels readily transformed into sol state, when strain higher than LVE range i.e. 100% with a frequency of 1Hz was applied, resulting in a drop of storage modulus (G') near to the value of loss modulus (G"). However, when the strain values were reduced to LVE range (~0.1%) at similar frequency (1Hz), the G' values started to regain its initial values, marked by

the transformation into semi-solid gel-like state. [7] The thixotropic behavior was studied consecutively for three cycles. We propose that highly soluble Fmoc YIGSR established their hydrophobic interactions and H-bonding interactions quickly in aqueous environment and showed fastest recovery of ~92% in initial 60sec. However, due to presence of hydrophobic Fmoc IKVAV in conjugate gels, the recovery is slightly delayed and observed ~70% recovery of initial strength within 60sec. The hydrophobic IKVAV, owing to its poor solubility showed slower recovery initially ~36% in 60sec (figure 4.9 d). The thixotropic behavior of individual peptides showed concentration dependence of the recovery values. It is worth mentioning that in our previous work, we found that the 40mM gels of Fmoc IKVAV and Fmoc YIGSR showed ~3% and ~100% recovery, respectively, in comparison to ~36% and 92% recovery of 20mM gels in this work. The scenario was little different at lower peptide concentrations, although trend remained same. The thixotropic properties of these laminin mimetic hydrogels showed great potential to be used as injectable gels for regenerative medicines and drug delivery.

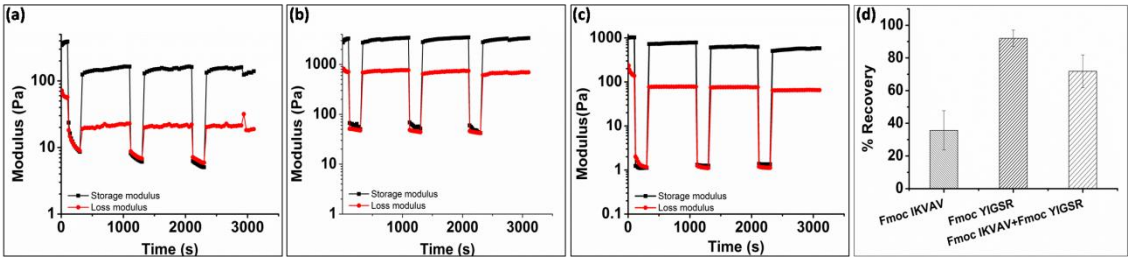

Figure 4.9 *Rheological analysis depicting thixotropic nature of laminin derived peptide hydrogels at a 20mM concentration of (a) Fmoc IKVAV, (b) Fmoc YIGSR and (c) Fmoc IKVAV+Fmoc YIGSR in 1: 1 molar ratio (10mM each) measured upto 3 consecutive cycles with deformation strain of 50% at frequency of 1Hz and (d) Percentage recovery of gel strength of laminin after 60sec.*

Analysis of morphological changes during thixotropic measurements:

The thixotropic behavior of these laminin derived gels was studied at microscopic level, through AFM (figure 4.10). A clear transformation of longer network into shorter fibrous networks can be observed, upon application of stress via vortexing and sonication for 5 min, which overcomes the intermolecular interactions leading to dissociation of the self-assembled network structure. Interestingly, upon resting, the reversal of broken fibers to intact fibers was observed, accompanied by sol-to gel transformation confirming the thixotropic behavior of gels. The differential recovery values of hydrophobic and hydrophilic peptides can be directly correlated

with morphology of recovered fibers. The morphology of recovered Fmoc IKVAV gel showed presence of broken fibers, along with longer length fibers, even 3 hrs after deformation (figure 4.10 b-d). While, the denser Fmoc YIGSR network has lesser effect of deformation, as it showed intact entangled network, just after deformation also. However, after 3 hrs of recovery, the network similar to that of before deformation was restored, indicating higher recovery percentages. In composite gels, both the self-sorted networks retain their individual deformation pattern (figure 4.10e-g). The wider Fmoc IKVAV fibers undergo more deformation and showed distorted structures over the less distorted Fmoc YIGSR network. After 3hr recovery, the Fmoc YIGSR network was found to be intact, while Fmoc IKVAV aggregates on the surface of Fmoc YIGSR (figure 4.10 h-j). The probable reason for the failure of Fmoc IKVAV to reassemble into fibrous structures might be the concentration lower than MGC, at which it initially formed fibers due to aid of Fmoc YIGSR nucleation sites. The results suggested that both peptides retain their nature in composite gels and adopt different self-assembly pathways in aqueous solvent, owing to their different hydrophobicities.

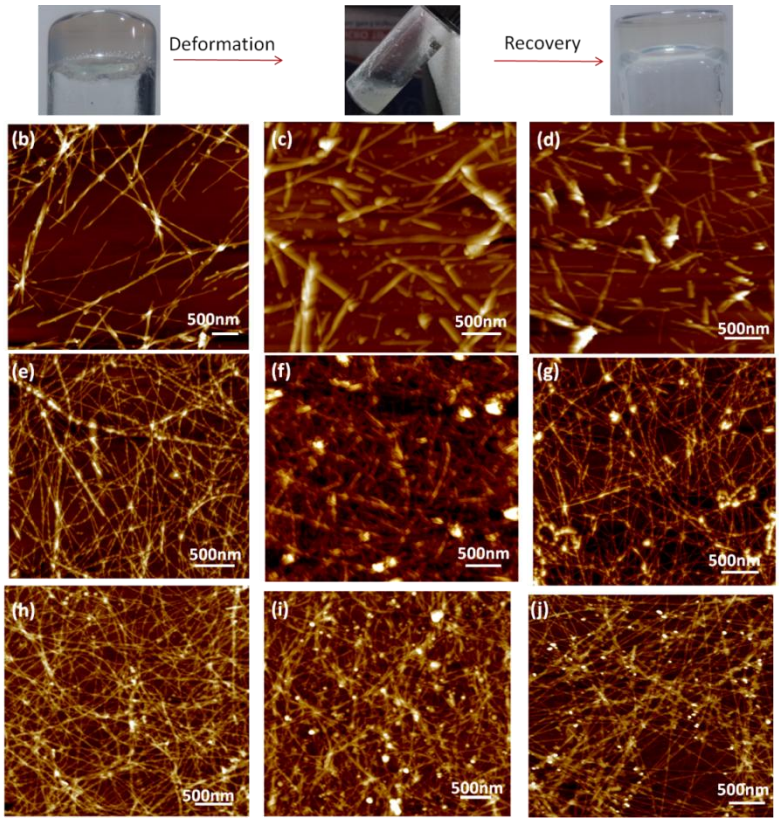

Figure 4.10 *Thixotropic measurements showing gel-sol-gel transformation after applying stress for 5 min and recovery after 3 hr. (a) Optical images of the macroscopic gel and sol transformations. AFM images of (b-d) Fmoc IKVAV, (e-g) Fmoc YIGSR and (h-j) Fmoc IKVAV*

+Fmoc YIGSR gels (20mM concentration) at different stages of thixotropy measurement i.e. before deformation, after deformation and after 3hrs of recovery.

4.3.6 Secondary Structure Analysis

4.3.6.1 CD Analysis: The supramolecular arrangements of peptide molecules during self-assembly were assessed by CD spectroscopy. The self-assembly of hydrophilic peptide i.e. Fmoc YIGSR showed the formation of β-sheet structures as evidenced by the characteristic positive peak at ~198nm (π-π*) and a negative peak at ~220nm (n-π*). [60] However, the hydrophobic IKVAV showed the characteristic signals of random coils indicated by negative band at ~205nm which accounts for the less ordered structures and weaker mechanical strength of Fmoc IKVAV hydrogels. Surprisingly, very weak characteristic signal of β-sheet can be observed in composite hydrogels. The reason for reduced signal intensity can be balancing out of the positive and negative band signals at ~220nm of Fmoc IKVAV and Fmoc YIGSR, respectively. [61] Also the supramolecular organization of peptide molecules imparts chiral molecular arrangements for Fmoc group which can be identified as characteristic CD signal at ~303nm, associated with absorption of fluorenyl group. [62] The Fmoc IKVAV and Fmoc YIGSR showed opposite chirality, as evident from the opposite handedness of peaks at 303nm, as a result of which the additive signal of composite gels do not show any supramolecular chirality peak. [61] Further, the evolution of residual signals in composite gels was confirmed by sequential variation of ratios of individual components (figure 4.11). The increase in concentration of one component with respect to other resulted in enhanced signals corresponding to that peptide. The characteristic β-sheet signal increases, when we increase the relative concentration of Fmoc YIGSR in a composite gel, indicated by enhanced intensity of negative peak at ~220nm (figure 4.11 c). This was supported by enhanced intensity of supramolecular chirality peak of Fmoc at ~303nm. However, the positive peak at ~220nm tends to increase with increasing concentration of Fmoc IKVAV in composite gels (figure 4.11b). Due to less ordered assembly of hydrophobic peptide (Fmoc IKVAV) in aqueous solvent, the supramolecular chirality peak of Fmoc is not prominent except in highest concentration ratio of Fmoc IKVAV in composite i.e. 9:1. These results indicated that CD signals in composite gels are the resultant of individual peptide signals and are concentration dependent.

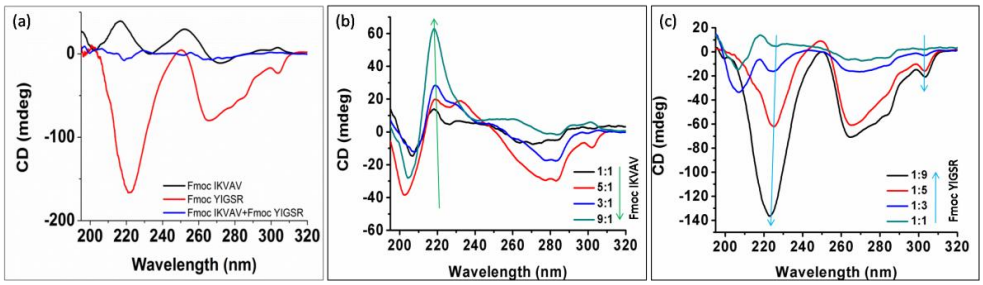

Figure 4.11 *(a) CD spectroscopic analysis of secondary structures of laminin inspired peptides and their composite hydrogels, and concentration dependence of resultant CD signals when (b) Fmoc IKVAV concentration is increased with respect to Fmoc YIGSR and (c) Fmoc YIGSR concentration is increased with respect to Fmoc IKVAV.*

4.3.6.2 FTIR Spectroscopy: FTIR is an important technique to investigate the peptide backbone intermolecular interactions that mainly includes H-bonding. The analysis of amide I region (1600-1700 cm^{-1}) of FTIR spectra revealed the characteristic peak at ~1635 cm^{-1} that indicated β-sheet arrangements for Fmoc YIGSR and composite hydrogel (figure 4.12). [63] Another broad peak extending between 1670-1690 cm^{-1}, corresponds to carbamate peak of Fmoc group. [64] However for Fmoc IKVAV, a broad weak signal extending from 1620 to 1650cm-1 was observed, which is indicative of random coil structures. [65] Also a sharp peak at ~1720cm^{-1} can be observed in Fmoc IKVAV, which corresponds to non H-bonded carbonyl carbamate of Fmoc group. [66]

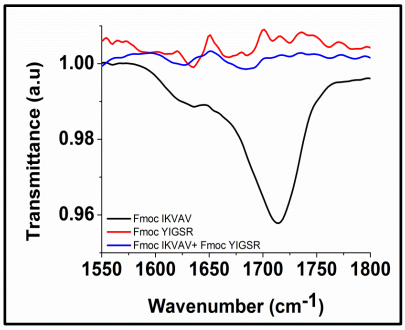

Figure 4.12 *FTIR spectra of individual laminin peptides as well as their composite peptide in 1:1 ratio.*

4.3.7 Thermodynamic Stability of Secondary structures

The differences in the morphological and spectroscopic properties of the self-assembled peptide nanostructures clearly indicated that different thermodynamic stable structures were formed via

different self-assembly pathways. [67] These different nanostructures would exhibit different extents of thermal stability which can be assessed by CD melting studies (figure 4.13). [68] It was evident from the CD melting studies that Fmoc YIGSR, having more organized self-assembled structures showed maximum melting temperature at ~75^{0}C. Following this, the composite hydrogels showed melting temperatures in the range of 65-75^{0}C. The broad range for composite hydrogels instead of specific temperature, also confirms the co-existence of differential structures in the composite hydrogels, where the individual peptides retain their structural integrity. However, in corroboration to previous results, Fmoc IKVAV showed the lower melting temperature ~60^{0}C, indicating less ordered nanostructures like random coils. This study supports the other spectroscopic data and morphological analysis of laminin derived hydrogels and provides an insight into stability of these gels at higher temperatures. [69]

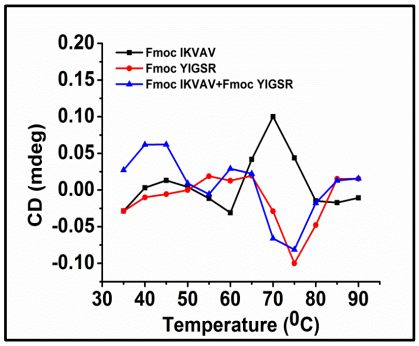

Figure 4.13 *CD melting temperature studies of individual laminin peptides as well as their composite peptide in 1:1 ratio.*

4.3.8 Evaluation of intact structure of hydrogels in cell culture media

The stability and integrity of hydrogels need to be assessed before culturing cells on these gels because media added along with cells may cause turbulence and damage the hydrogel scaffold. Therefore, the gels (20mM) were prepared and placed in a 96 well plate as well as on the coverslip in 6 well plate. The gels were allowed to self-assemble in the wells for 24 hrs. Cell culture media was added on the top of the gels and allowed to perfuse for 6 hrs. Then the media was changed and fresh media was added. The same cycle was repeated three times, each for 6 hrs. This ensures the stability of gels as well as exchanged the PBS in hydrogels with media, making hydrogel scaffolds more suitable for cell culture. [70, 71]

4.3.9 Metabolic activity assay

The inspiration for the design of laminin based short functional peptides were derived from the biological functions of native laminin protein. Before assessing different functional properties of the bioactive peptides, cytotoxicity studies are the pre-requisite. [72] To assess the initial contact cytotoxicity, metabolic activity analysis was performed after 4 hrs of treatment, using MTT colorimetric assay. [73] The MTT assay is a colorimetric method, which quantifies the metabolically active cells in control and treated groups. Due to biological implications of laminin in neural cell growth, the neuronal cell lines have been used to study cell-peptide matrix interactions. The rat glioma C6 cells and SHSY5Y human neuroblastoma cells were used throughout the studies to demonstrate the functional role of laminin derived peptides in controlling neural cell growth. Both the cell lines were seeded in 96 well plates at a concentration of 5X 10^3 cells/well and allowed to adhere for 24 hrs. The self-assembled peptides were diluted to three different concentrations i.e. 100µg/ml, 500µg/ml and 1000ug/ml. The control cells were treated with similar volumes of PBS (100mM, pH 6). The results suggested that the peptides showed concentration dependent effect and with increasing concentration, reduced percentage viability of cells was observed (figure 4.14 a & b). On comparing the effect of different peptides, it was found that Fmoc IKVAV showed relatively less biocompatibility of ~85% for C6 cells and ~70 % for SHSY5Y cells. While, Fmoc YIGSR and composite gels were relatively more biocompatible and showed ~100% and ~90 % viability of C6 cells and SHSY5Y cells, respectively. The probable reason for such behavior could be the less organized structures of Fmoc IKVAV, which may not provide uniform structures and surface for the adherence of cells. [74] While, Fmoc YIGSR was found to be the most biocompatible peptide, among all three self-assembled systems showing percentage cell viability of ~100%, owing to its long entangled fibrous network, which provides sufficient surface for the adherence of the cells. As expected, the cytocompatibility of composite gels was found to be intermediate between Fmoc IKVAV and YIGSR, which revealed that IKVAV, one of the crucial functional sequences of laminin peptide, can be used for cellular studies, through simply mixing with hydrophilic functional sequence of the laminin protein. The co-existence of both hydrophobic and hydrophilic peptides can reduce the detrimental effect of short fibrous network formed by IKVAV peptide, through formation of intertwined self-sorted network to enhance cellular adhesion. On comparing the response of laminin derived hydrogels towards both cell lines, C6 cells were found to be more metabolically active than SHSY5Y cells for the laminin derived short peptide hydrogels. However, the soluble laminin derived peptide nanostructures showed good biocompatibility, which inspires us to explore cell-matrix interactions further, through various biological assessments.

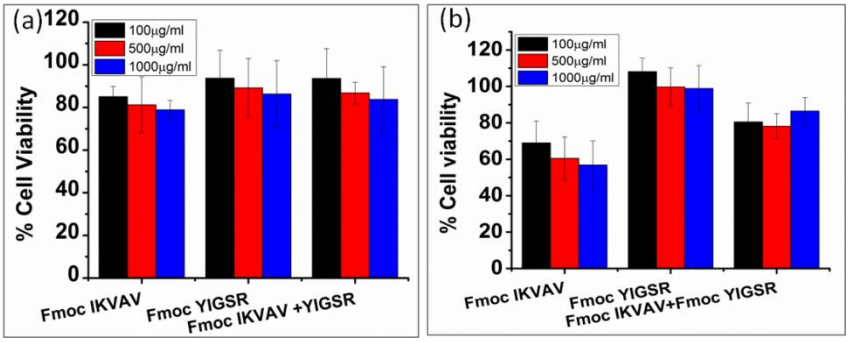

Figure 4.14 *Cytotoxicity studies using MTT assay with (a) C6 glial cells and (b) SHSY5Y neuroblastoma cells after 4 hrs of treatment, assessing initial toxicity of peptides in solution state.*

Following initial cytotoxicity studies, the gel phase biocompatibility was studied up to 72 hrs (figure 4.15). The cell viability of cells cultured over laminin derived peptide hydrogels, cultured for 24 hrs and 72hrs was assessed by MTT assay. For all the gels, the responses were similar to initial contact cytotoxicity results. Interestingly, the percentage of viable cells remained maintained upto 72 hrs, and in some cases increased viability was observed due to cell proliferation, promoted by functional hydrogel matrices. C6 cells were found to be more than 80% viable with hydrophilic Fmoc YIGSR and composite gels and more than 70% viability was observed with Fmoc IKVAV gels (figure 4.15 a). However, with SHSY5Y cells ~90% viability with Fmoc YIGSR, ~80% with composite gels and ~65% viability with Fmoc IKVAV was observed after 72 hrs (figure 4.15 b). The results indicate that the hydrophobic peptides, such as, IKVAV forming short nanofibrous structures can induce certain extent of cytotoxicity towards cells. However, that can be compromised after mixing them with a hydrophilic sequence, like YIGSR. This indicated that a proper hydrophillic-lipophillic balance is important for optimum biofuctionality.

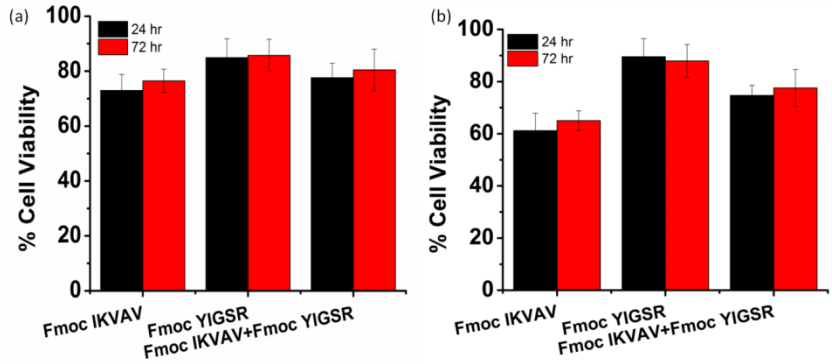

Figure 4.15 *Cytotoxicity studies through MTT assay with (a) C6 cells and (b) SHSY5Y cells after 24 hrs and 72hrs of culture over laminin derived peptide hydrogels and their conjugate hydrogels.*

4.3.10 Live-dead Cell Assessment

After the quantitative investigation of cytotoxicity by MTT assay, the microscopic evaluation was performed using live- dead staining. Live/dead staining helps out to directly visualize the live and dead cell population from the cells cultured over the hydrogel surface, which can be directly correlated to the biocompatibility, adhesion and proliferation of the cultured cells. The cell culture media perfused gels were seeded with cells ($5X10^4$) on the surface and allowed to adhere. The cells cultured over coverslips without hydrogels were used as control. The adhered cells were then visualized for adherence and morphology after every 24 hr upto 5 days, using optical microscope. The density of control cells increased progressively upto 4 days, while on the 5th day, the cells were stripped off from the control surface due to overgrowth of cells. However, the cells cultured over laminin derived peptide hydrogels remain adhered to healthy morphology, even after 5 days. It is expected that laminin functionality provides active sites for cell adhesion, by interacting with cell surface receptors. In addition to biofunctionality, modulated topography and mechanical strength of hydrogels also facilitate adhesion and proliferation of the cells. Moreover, the C6 cells were found to be completely adhered to elongated morphology within 24 hrs after seeding, as observed with optical microscope, (figure 4.16).

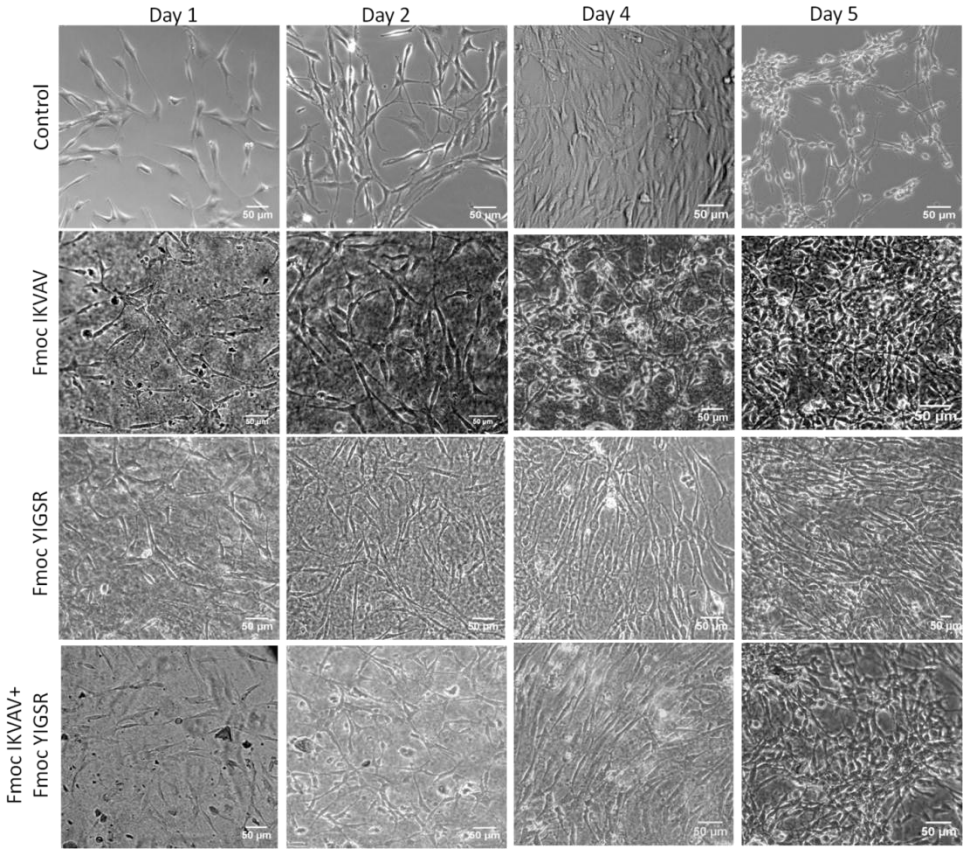

Figure 4.16 *Microscopic images of C6 cells cultured over Control (TCPS) and laminin derived peptide hydrogels based on Fmoc IKVAV, Fmoc YIGSR and composite Fmoc IKVAV+ Fmoc-YIGSR, at day 1, day 2, day 4 and day5.*

While, SHSY5Y cells were found to adhere on the hydrogel surfaces after 1 day, but remained in spherical shape. After 2 days, the cells have grown into cluster of cells with polyhedral cell morphology, which is their characteristic growth pattern. Interestingly, the cluster of cells was denser for the cells grown over laminin hydrogels in comparison to control cells and the density increased continuously, upto 5 days (figure 4.17).

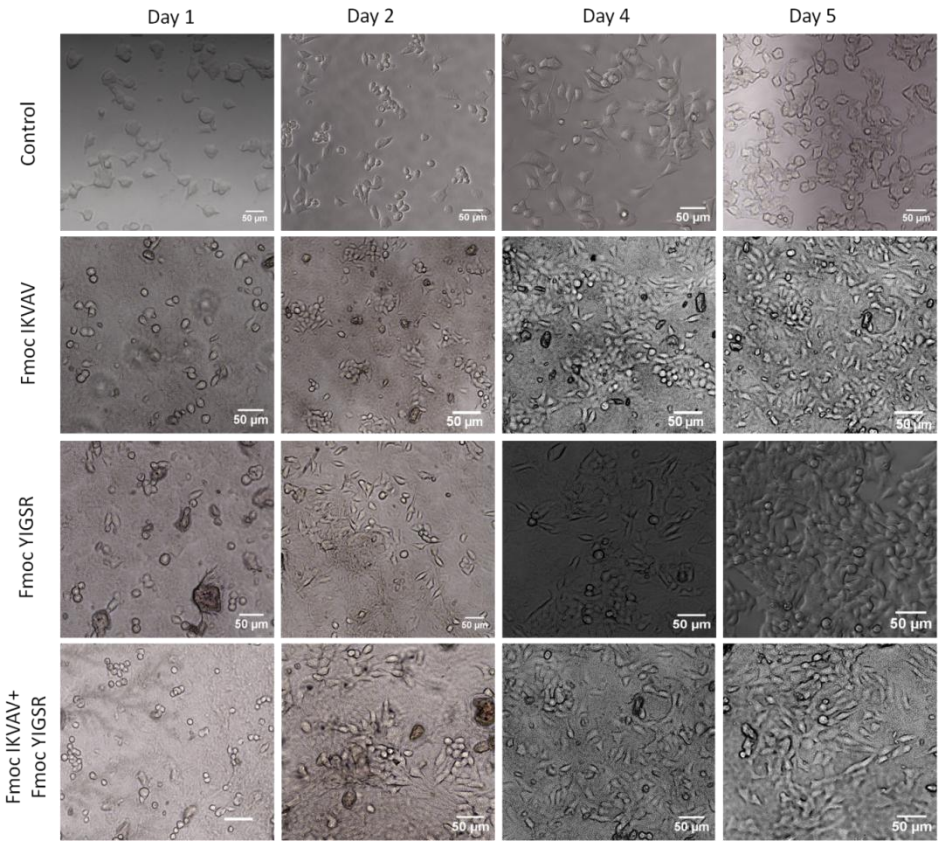

Figure 4.17 *Microscopic images of SHSY5Y cells cultured over Control (TCPS) and laminin derived peptide hydrogels based on Fmoc IKVAV, Fmoc YIGSR and composite Fmoc IKVAV+ Fmoc-YIGSR, at day 1, day 2, day 4 and day 5.*

Further, the cells were stained with two different dyes, $DiOC_{18}$ (3) staining live cells with green fluorescence and PI staining dead cells with red fluorescence and visualized under confocal microscope. The live/dead staining of cultured cells was done on 2nd day and 5th day, after seeding. The cell numbers cultured over hydrogels were comparable with that of control cells. Both C6 and SHSY5Y hardly showed the presence of dead cells, upto 5 days (Figure 4.18 and 4.19). In corroboration to biocompatibility results, Fmoc YIGSR showed the maximum growth of cells. It not only promoted the growth of C6 cells upto 5 days but also helped to align cells in particular direction. The composite gels demonstrated similar behavior with C6 cells, but showed relatively less alignment of cells in comparison to Fmoc YIGSR. However, in case of Fmoc IKVAV less stretched cell morphology was observed. The probable reason for such observation might be the weaker strength and less organized morphology of Fmoc IKVAV gels, which avoid cells to extend their appendages. [75]

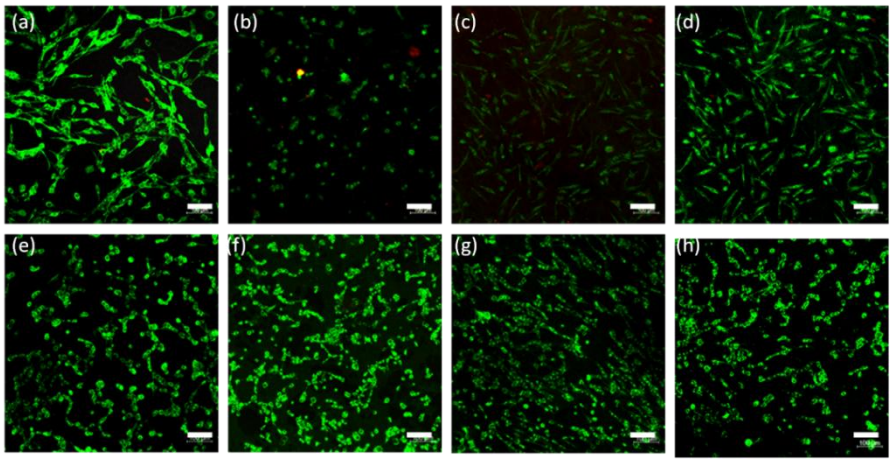

Figure 4.18 *Live dead staining assay of C6 glial cells cultured over (a, e) Control (TCPS), (b, f) Fmoc IKVAV, (c, g) Fmoc YIGSR and (d, h) conjugate hydrogel (Fmoc IKVAV+ Fmoc YIGSR), studied using DiOC3 and PI, after 2 days (panel 1) and 5 days (panel 2). Scale bar for images is of 100μm.*

Although, the SHSY5Y cell density was less after 2 days, for all three hydrogels, in comparison to control, but no appearance of dead cells was observed. However, after 5 days, nearly same cell density as that of control was observed, which indicated that these laminin derived scaffolds promote slower proliferation of SHSY5Y cells, initially. Moreover, in corroboration to cytotoxicity studies, both C6 and SHSY5Y cell density was relatively less after 2 days with Fmoc IKVAV gels, in comparison to control cells, which indicated relatively lesser biocompatibility, owing to its hydrophobicity. Thus live-dead staining results indicated that the laminin derived peptide hydrogels were highly biocompatible for 2D cultures of neural cells and have the potential to promote growth and adhesion of cells.

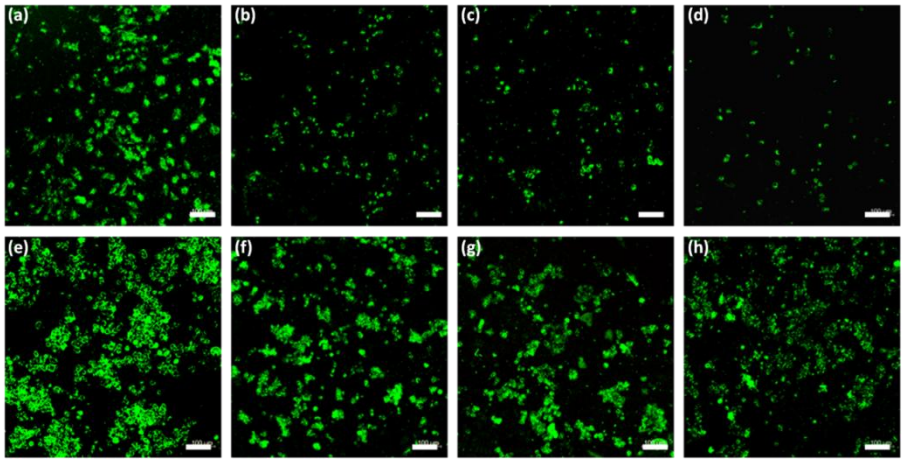

Figure 4.19 *Live dead staining assay of SHSY5Y neuroblastoma cells cultured over (a, e) Control (TCPS), (b, f) Fmoc IKVAV, (c, g) Fmoc YIGSR and (d, h) conjugate hydrogel (Fmoc IKVAV+ Fmoc YIGSR), studied using DiOC3 and PI, after 2 days (panel 1) and 5 days (panel 2). Scale bar for images is of 100μm.*

4.3.11 Proliferation studies

The live-dead staining studies clearly demonstrated the increase in cell number with time, which was the outcome of active proliferation of the cells. The proliferating C6 and SHSY5Y cells were quantified by using Alamar blue assay. Alamar blue reagent has the capability to get reduced into a pink colored, fluorescent resorufin product. [33, 76] The conversion of Alamar blue salt is directly proportional to the number of metabolically active cells. The cells cultured over peptide hydrogels and control cells were treated with Alamar blue salt after 2 days and 5 days. The salt was allowed to interact with the active cells for the duration of 4 hrs. At the end of this duration, the supernatant media with the converted Alamar reagent, which is pink in color, was collected and fluorescence intensity was measured at 600nm. [77] The results suggested that fluorescence intensity with hydrogel treated C6 cells was relatively less than control after 2days, was found to increase significantly within 5 days and reached nearly equal to the control cells, after 5 days (figure 4.20). Interestingly, the fluorescence intensity has been increased significantly in C6 cells cultured over composite gels, indicating enhanced proliferation with mixed functionality. Similar, results were obtained for SHSY5Y cells, but instead of composite gels, Fmoc YIGSR showed the highest proliferation rates, after 5 days, live-dead studies showed no signature of dead cells. The relatively lesser proliferation rates might be indicative of dominant growth phases, having more number of cells in resting phase than division phase, which will be further explained in detail in cell cycle studies. The results of proliferation studies were in close association with biocompatibility assay and live/dead 2D cell culture results. The results suggested that these laminin based scaffolds hold great potential to promote proliferation of neural cells.

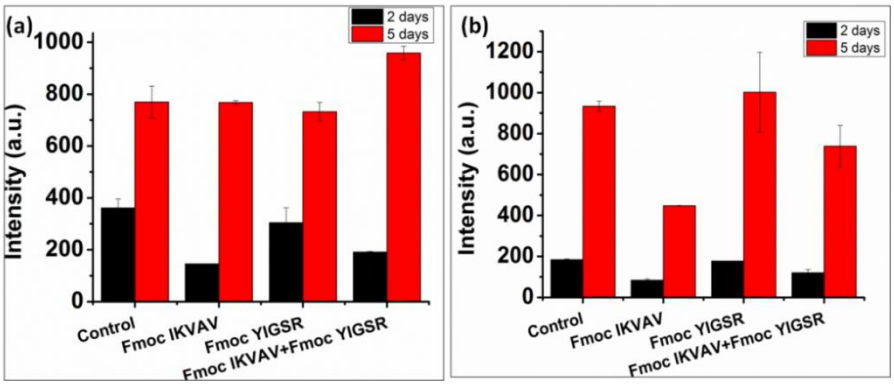

Figure 4.20 *Proliferation studies using Alamar blue assay with (a) C6 glial cells and (b) SHSY5Y neuroblastoma cells cultured over the surface of laminin derived peptide gels, after 2 days and 5 days.*

4.3.12 Neurite Extension

We further evaluated the effect of laminin peptide gel scaffolds on the growth and morphology of neuronal cells. The neuron structure is composed of two basic parts, cyton (cell body) and neurites (the extensions from cell body, including axon and dendrites). A recent report by A. de Campo provides the evidence for the role of IKVAV peptide motif in regulating the neurite outgrowth and extension in the neural progenitor cells; however the active IKVAV peptide was used as adhesive motif. [78] In the similar direction, we demonstrated the role both the laminin peptides i.e. IKVAV and YIGSR, and their combined scaffolds in promoting neurite extension through self-assembled supramolecular gels, made solely of these peptides. The morphology of the C6 cells cultured on the surface of laminin peptide hydrogels was studied and length of axon was compared with control cells. After 24 hrs, the length of axon for control cells was found to be ~33±8μm. Very interestingly, the axonal length exceeded >70 μm for cells grown on laminin hydrogels. In corroboration to other studies, Fmoc YIGSR and conjugate hydrogels showed the maximum average length of ~87±27μm and ~80±14μm, respectively. While, with Fmoc IKVAV, ~74±16μm average axonal length was observed. Over the period of time, a significant increase has been observed in the axon length, after 48 hrs. [79] These results implied that enhanced axon length promotes more cell-cell interactions, which is also one of the functions of YIGSR laminin peptides. For SHSY5Y cells, short spiny neurites are present in control cells which developed after 48 hrs. However, SHSY5Y cells grown over laminin hydrogels appears in rounded or pyramidal morphology upto 48 hrs (figure 4.21). Also the literature suggested that extended neurites indicate the differentiated cells, after which the proliferation is reduced. [80]

Therefore, the neurite extension parameter appears to be less important at early time durations of culture (24-48hrs), in case of SHSY5Y cells.

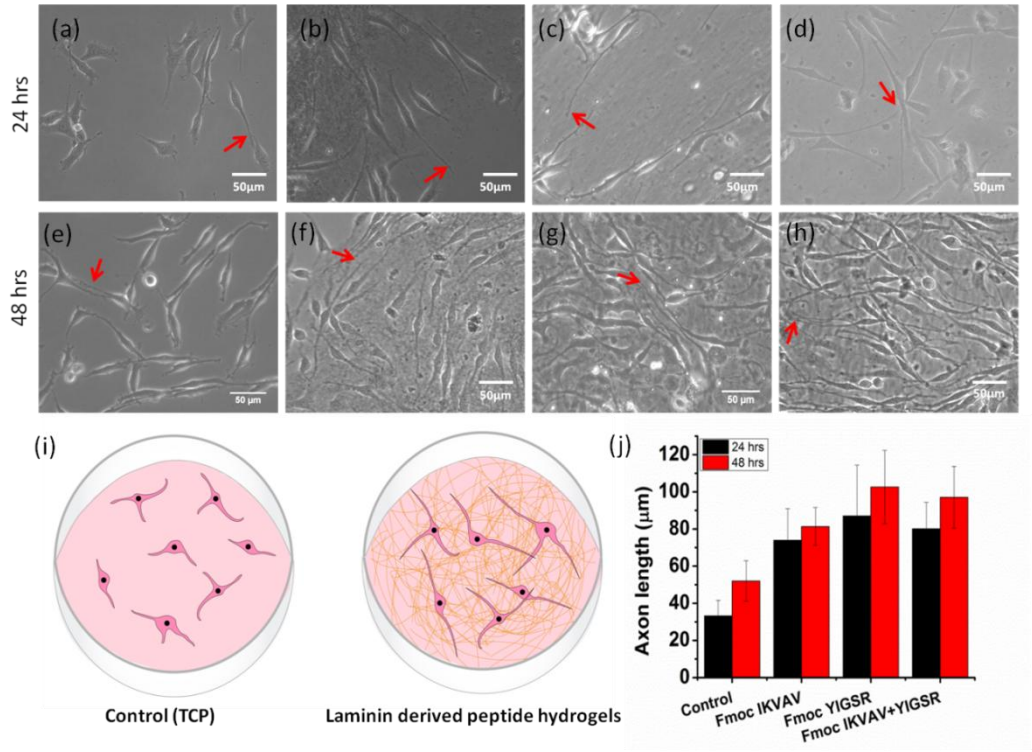

Figure 4.21 *Axon length measurement of C6 cells grown over (a, e) control (TCPS) and different laminin derived peptide (b, f) Fmoc IKVAV, (c, g) Fmoc YIGSR and (d, h) composite gels, after 24 hrs (row 1) and 48 hrs (row 2). Red arrows mark the ends of axons extending from cell bodies of the cells. (i) Schematic representation of differential extensions of neuronal cells in the absence and presence of laminin derived peptide hydrogels. (j) Average lengths of axons measured using Image J software by measuring 30 cells from each sample, after 24 and 48 hrs.*

4.3.13 Immunofluorescence staining for neuronal marker:

β-tubulins are the important structural component of micro-tubular compartment of the cells and have major roles in regulating cellular processes (mitosis, motility, etc). [(81)] Among different isoforms of β-tubulin, β-III tubulin expression is localized in neuronal cells and is used as a positive marker for normal neuronal activity. [(82)] In particular, β-III tubulin, have specific roles in neurogenesis, axon guidance and maintenance. [(83)] In similar line, we have explored the, β-III tubulin expression in the cells cultured over the laminin derived hydrogel matrix (Figure 4.22 and 4.23). [(45)]

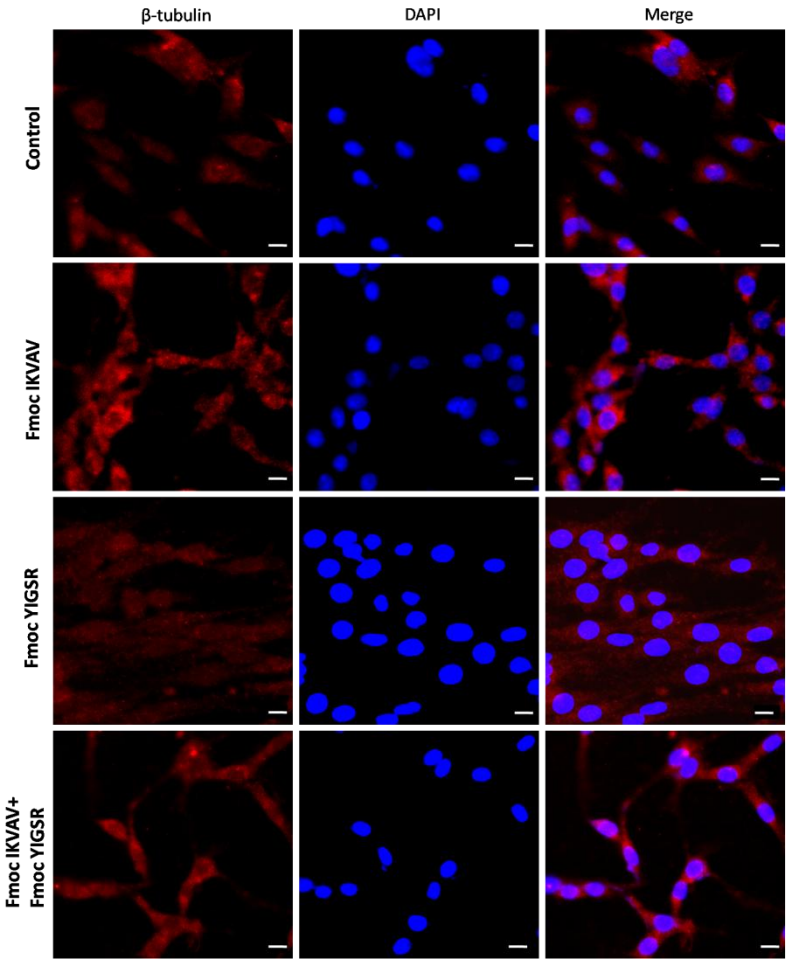

Figure 4.22 *Immunofluorescence staining of neuronal marker β-III tubulin expressed in C6 cells cultured over Control (TCPS), Fmoc IKVAV hydrogels, Fmoc YIGSR hydrogels and compoite Fmoc IKVAV and Fmoc YIGSR hydrogels, after 5 days. The red colour indicates the β-III tubulin stained with Alexa Fluor 555 and blue indicates nuclei stained with DAPI. Scale bar=10μm.*

The confocal imaging revealed nearly similar response towards β-III tubulin staining in control cells grown on coverslip surface and cells cultured over hydrogels, for both C6 cells and SHSY5Y cells. In corroboration to results, obtained from other studies, Fmoc YIGSR hydrogels showed a highly dense aligned population of cells, having elongated morphologies with β-III tubulin spread throughout the cell body and axons (figure 4.22). While less stretched, more number of multipolar cells were observed in control, Fmoc IKVAV and conjugate hydrogels. In contrast to this, SHSY5Y cells showed clustered growth in control as well as with hydrogel scaffolds (Figure 4.22). However, Fmoc IKVAV and Fmoc YIGSR showed more dense clusters of SHSY5Ycells in comparison to control cells (Figure 4.23). It was also observed that

SHSY5Y cells cultured over hydrogel scaffolds showed directional growth of cytoskeleton with nucleus centered at one end, while control cells showed nucleus positioned in the center of the cytoskeletal network. These results in conjugation with proliferation studies suggested that laminin hydrogels promote neuronal cell growth with normal cellular functioning. The studies also provide evidence to develop such bioactive scaffolds for neuronal differentiation of stem cells, which can be useful in the treatment of many nervous system disorders.

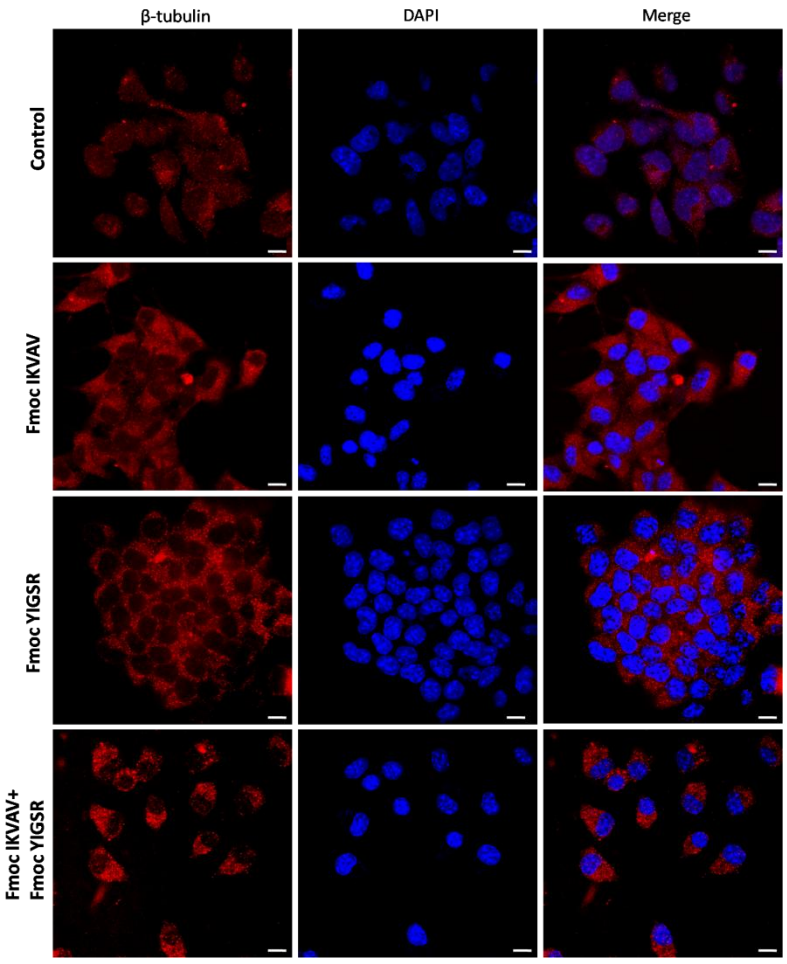

Figure 4.23 *Immunofluorescence staining of neuronal marker β-III tubulin expressed in SHSY5Y cells cultured over Control (TCPS), Fmoc IKVAV hydrogels, Fmoc YIGSR hydrogels and composite Fmoc IKVAV and Fmoc YIGSR hydrogels, after 5 days. The red colour indicates the β-III tubulin stained with Alexa Fluor 555 and blue indicates nuclei stained with DAPI. Scale bar=10μm.*

4.3.14 Cell Cycle analysis:

It is expected that cells interact with functional matrices through certain cell surface receptors and trigger intracellular responses. The analysis of cell cycle may give direct information about the cell health. [84] To assess the intracellular effect of the laminin derived peptide hydrogel scaffolds, cell cycle analysis was performed using flow cytometry. [85] The cell cycle analysis is based on the quantitation of DNA using DNA binding dyes like propidium iodide. The principle behind this study is that cells in S phase will have a relatively higher content of DNA and it will have greater fluorescence intensity than G0-G1 phase cells. While the cells in G2-M phase will have exactly double DNA content than G0-G1 phase cells and thus will have double fluorescence intensity. [86] The results indicated the normal cell cycle for both the cell types (C6 and SHSY5Y) cultured over laminin scaffolds, having phase distributions similar to that of control cells (figure 4.24).

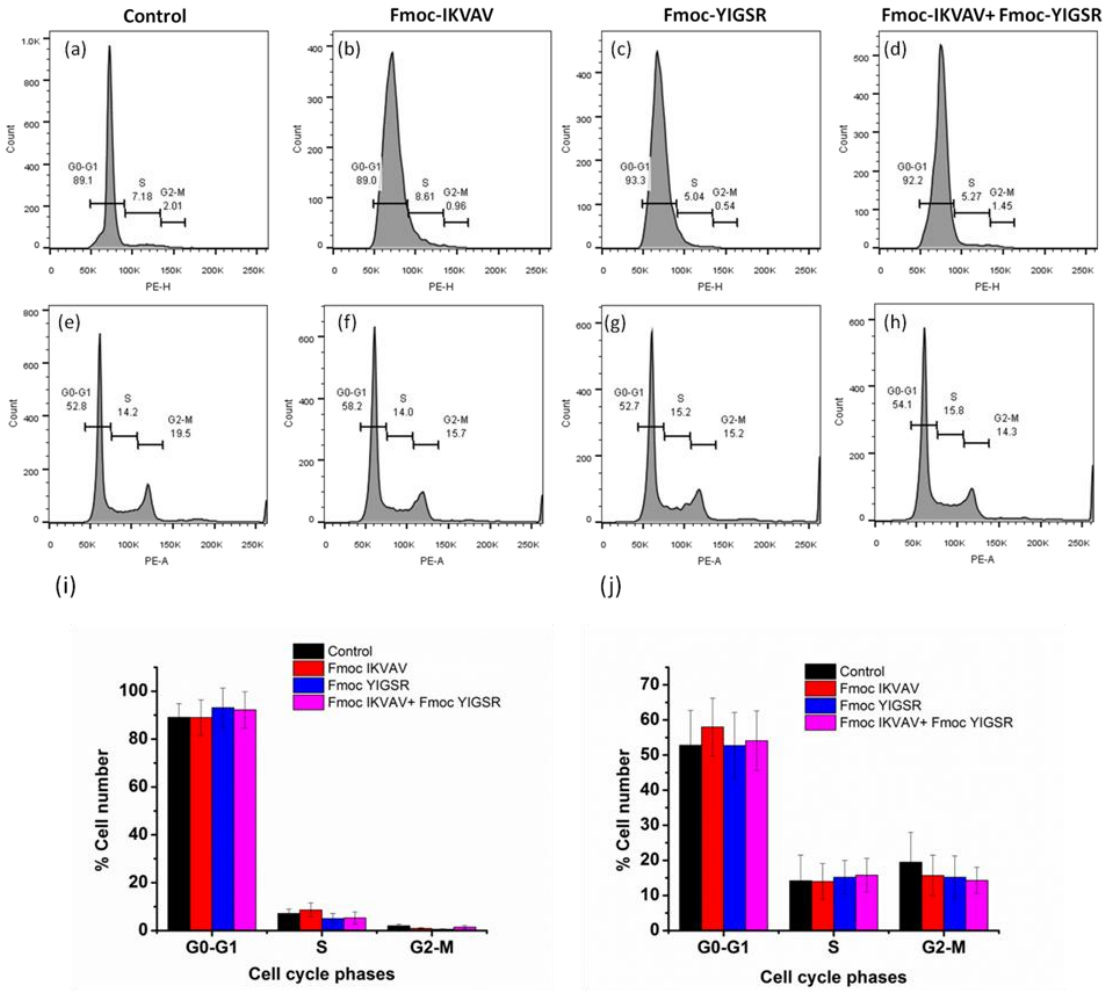

Figure 4.24 *Flow cytometry analysis of cell cycle in (a-d) C6 cells and (e-h) SHSY5Y cells, after the treatment with different laminin peptides hydrogels diluted upto the concentration of*

1000µg/ml, after 24 hrs. The percentage of cells present in different phases of cell cycle in (i) C6 cells and (j) SHSY5Y cells.

This implies that the scaffolds are highly biocompatible and do not cause cell cycle arrest in any of the phases. In addition to this, the proliferation results can be well correlated with the cell cycle analysis. The G0-G1 phase is elevated in cells cultured over Fmoc YIGSR and composite gels, which indicated dominant growth phase. The G2-M phase in composite gels was also found to be nearly equal to the control cells, which indicated active proliferation of C6 cells, which can be directly correlated with the higher proliferation rates with composite gels (figure 4.20 and figure S 4.24 a-d & i). However, lower intensity of G2-M phase in cells cultured over Fmoc IKVAV gels can be directly associated with their lower proliferation rates. However, in SHSY5Y cells, all peptide scaffolds exhibited lesser intensity of G2-M phase, which is indicative of almost equal or lesser proliferation rates than control cells. The Fmoc-IKVAV showed highest intensity G0-G1 phase, which marks the dominant growth phase and lower proliferation rates. The results depict the differential role of laminin derived scaffolds in controlling cell cycle through various intracellular pathways. In future, it would be interesting to gain in depth knowledge of intracellular responses by studying cell cycle specific markers, which would enhance the understanding of cell-matrix interactions and help to design more suitable biofunctional ECM mimics.

4.4 Conclusions

In this chapter, we have demonstrated the functional roles of laminin derived short peptides in controlling neuronal cell growth and proliferation. To the best of our knowledge, this is the first report on composite supramolecular hydrogels based on biologically relevant shortest laminin derived IKVAV and YIGSR peptides, without any polymeric scaffold. Such composite hydrogels offer the advantage of performing distinct functions of both laminin peptides by interacting with different receptors. Interestingly, the composite matrix showed the presence of self-sorted network of fibers, presenting both functional peptides for cell interaction, separately in a single scaffold. The entanglement of both networks strengthened the scaffold for inducing specific mechanical cues as well. Excellent recovery properties make them suitable candidates for their exploration as injectable gels. The short laminin derived peptide sequences were able to perform similar functions as that of laminin protein. The synthetic scaffold was highly biocompatible, promotes cellular proliferation and adhesion. The designer scaffolds were formed to demonstrate the crucial functions of whole native laminin protein and one of them is

neurite extension, which can be achieved by the short laminin peptide derived scaffolds. The results also suggested that laminin derived synthetic scaffolds do not hinder the normal functioning of cells, which was evidenced by the β-III tubulin expression and cell cycle analysis. However, Fmoc YIGSR hydrogels were found to show superior properties than that of Fmoc IKVAV, which was evident from the high stability of the gels and improved mechanical properties. This was further reflected in their biological properties as well. However, to develop a closer structural mimic of native laminin protein, we rely on mixing both bioactive motifs. The simple mixing can balance the overall hydrophobicities as well as can induce formation of highly entangled networks which could support adhesion and proliferation of biological cues, without relying on the covalent functionalization. We anticipate that simple co-assembly strategies will gain high importance in designing complex tunable bioactive materials, rather than complex covalent synthetic approaches. We speculate that many opportunities reside in such bioactive scaffolds to be developed for 3D encapsulation of cells within these gels. In future, such multifunctional bioactive scaffolds hold high potential to be explored in controlling stem cell differentiation and tissue regeneration.

Note:

- ✓ The permission has been granted by authors and corresponding author of the published paper prior to its adoption in the present thesis. The publication associated with this work is:

  Rashmi Jain, Sangita Roy, Controlling neuronal cell growth through composite laminin supramolecular hydrogels, *ACS Biomater. Sci. Eng.* (2020), *Just accepted*

4.5 References

1. J. Li, R. Xing, S. Bai, X. Yan, Recent advances of self-assembling peptide-based hydrogels for biomedical applications, Soft Matter, 15 (2019) 1704-1715.
2. Z. Yang, B. Xu, Supramolecular hydrogels based on biofunctional nanofibers of self-assembled small molecules, *J. Mater. Chem*. 17 (2007) 2385–2393.
3. H.Wang, Z. Yang, Short-peptide-based molecular hydrogels: novel gelation strategies and applications for tissue engineering and drug delivery, *Nanoscale*, 4 (2012) 5259–5267.
4. C. C. Horgan, A. L. Rodriguez, R. Li, K. F. Bruggeman, N. Stupka, J. K. Raynes, L. Day, J. W. White, R. J. Williams, D. R. Nisbet, Characterisation of minimalist co-

assembled fluorenyl-methyloxycarbonyl self-assembling peptide systems for presentation of multiple bioactive peptides, *Acta Biomater*. 38 (2016) 11–22.

5. K. Luder, K. Kulkarni, H. W. Lee, R. E. Widdop, M. P. Del Borgo, M-L. Aguilar, Decorated self-assembling b3-tripeptide foldamers form cell adhesive scaffolds, *Chem. Commun*. 52 (2016) 4549-4552.
6. Y. Loo, M. Goktas, A. B. Tekinay, M. O. Guler, C. A. E. Hauser, A. Mitraki, Self-assembled proteins and peptides as scaffolds for tissue regeneration, *Adv. Healthcare Mater*. 4 (2015) 2557–2586.
7. X. Yan, Y. Cui,Q. He, K. Wang, J. Li, W. Mu, B.Wang, Z. Ou-yang, Reversible transitions between peptide nanotubes and vesicle-like structures including theoretical modeling studies, *Chem. Eur. J.* 14 (2008) 5974 – 5980.
8. P. Makam, E. Gazit, Minimalistic peptide supramolecular co-assembly: expanding the conformational space for nanotechnology, *Chem Soc Rev*. 47 (2018) 3406–3420.
9. E. Radvar, H. S. Azevedo, Supramolecular nanofibrous peptide/polymer hydrogels for the multiplexing of bioactive signals, *ACS Biomater. Sci. Eng*. 5 (2019) 4646−4656.
10. E. Arslan, I. C. Garip, G. Gulseren, A. B. Tekinay, M. O. Guler, Bioactive supramolecular peptide nanofibers for regenerative medicine, *Adv. Healthcare Mater*., 3 (2014) 1357-76.
11. J. Li, R. Xing, S. Bai, X. Yan, Recent advances of self-assembling peptide-based hydrogels for biomedical applications, *Soft Matter*, 15 (2019) 1704—1715.
12. K. A. Kyburz, K. S. Anseth, Synthetic mimics of the extracellular matrix: how simple is complex enough? *Ann. Biomed. Eng*. 43 (2015) 489–500.
13. A. L. Rodriguez, C. L. Parish, D. R. Nisbet, R. J. Williams, Tuning the amino acid sequence of minimalist peptides to present biological signals via charge neutralised self assembly, *Soft Matter*, 9 (2013) 3915–3919.
14. N. Huettner, T. R. Dargaville, A. Forget, Discovering cell-adhesion peptides in tissue engineering: beyond RGD, Trends Biotechnol. 36 (2018) 372-383.
15. S. M. Yua, Y. Li, D. Kim, Collagen mimetic peptides: progress towards functional applications. *Soft Matter*, 7 (2011) 7927–7938.
16. R. Xing, T. Jiao, L. Yan, G. Ma, L. Liu, L. Dai, J. Li, Möhwald, H.,Yan, X., Colloidal gold−collagen protein core−shell nanoconjugate: one-step biomimetic synthesis, layer-by-layer assembled film, and controlled cell growth, *ACS Appl. Mater. Interfaces*, 7 (2015) 24733−24740.

17. S. Bhutani, A. L. Y. Nachlas, M. E. Brown, T. Pete, C. T. Johnson, A. J. Garc´ ía, M. E. Davis, Evaluation of hydrogels presenting extracellular matrix-derived adhesion peptides and encapsulating cardiac progenitor cells for cardiac repair, ACS *Biomater. Sci. Eng.* 4 (2018) 200−210.
18. D. Patel, R. Menon, L. J. Taite, Self-assembly of elastin-based peptides into the ECM: the importance of integrins and the elastin binding protein in elastic fiber assembly, *Biomacromolecules*, 12 (2011) 432–440.
19. S. Hamsici, G. Cinar, A. Celebioglu, T. Uyar, A. B. Tekinay, M. O. Guler, Bioactive peptide functionalized aligned cyclodextrin nanofibers for neurite outgrowth, *J. Mater. Chem.* B, 5 (2017) 517—524.
20. W. Zheng, Z. Wang, L. Song, Q. Zhao, J. Zhang, D. Li, S. Wang, J. Han, X-L. Zheng, Z. Yang, D. Kong, Endothelialization and patency of RGD-functionalized vascular grafts in a rabbit carotid artery model, *Biomaterials*, 33 (2012) 2880-2891.
21. S. Ali, J. E. Saik, D. J. Gould, M. E. Dickinson, J. L. West, Immobilization of cell-adhesive laminin peptides in degradable PEGDA hydrogels influences endothelial cell tubulogenesis. *BioResearch*, 2 (2013) 241-249.
22. E. Beniash, J. D. Hartgerink, H. Storrie, J. C. Stendahl, S.I. Stupp, Self-assembling peptide amphiphile nanofiber matrices for cell entrapment, *Acta Biomater*. 1 (2005) 387–97
23. G. A. Silva, C. Czeisler, K. L. Niece, E. Beniash, D. A. Harrington, J. A. Kessler, S. I. Stupp, Selective differentiation of neural progenitor cells by high-epitope density nanofibers. *Science*, 303 (2004) 1352–1355.
24. K. L. Niece, J. D. Hartgerink, J. J. J. M. Donners, S. I. Stupp, Self-assembly combining two bioactive peptide-amphiphile molecules into nanofibers by electrostatic attraction, *J. Am. Chem. Soc.* 125 (2003) 7146–7147.
25. C.E. Cimenci, G. Uzunalli, O. Uysal, F. Yergoz, E. K. Umay, M. O. Guler, A. B. Tekinay, Laminin mimetic peptide nanofibers regenerate acute muscle defect, *Acta Biomater*. 60 (2017) 190–200.
26. V. M. Tysseling-Mattiace, V. Sahni, K. L. Niece, D. Birch,C. Czeisler, M. G. Fehlings, S. I. Stupp, J. A. Kessler, Self-assembling nanofibers inhibit glial scar formation and promote axon elongation after spinal cord injury, *J. Neurosci*, 28 (2008) 3814–23.
27. H. Thakar, S. M. Sebastian, S. Mandal, A. Pople, G. Agarwal, A. Srivastava, Biomolecule-conjugated macroporous hydrogels for biomedical applications, *ACS Biomater. Sci. Eng.* 5 (2019) 6320−6341.

28. X. Z. Shu, K. Ghosh, Y. Liu, F. S. Palumbo, Y. Luo, R. A. Clark, G. D.Prestwich, Attachment and spreading of fibroblasts on an RGD peptide-modified injectable hyaluronan hydrogel, *J. Biomed. Mater. Res.*, 68A (2003) 365–375.
29. D. Barros, I. F. Amaral, A. P. Pêgo, Laminin-inspired cell-instructive microenvironments for neural stem cells, *Biomacromolecules*, (2020) https://doi.org/10.1021/acs.biomac.9b01319.
30. K. Tashiro, G. C. Sephel, B. Weeks, S. Sasaki, G. R. Martin, H. K. Kleinman, Y. Yamada, A synthetic peptide containing the IKVAV sequence from the a chain of laminin mediates cell attachment, migration, and neurite outgrowth, *J. Biol. Chem*., 264 (1989) 16174-16182.
31. Nomizu, M., Otakanll, A., Utani, A., Rollern, P. P., Yamada, Y., Assembly of synthetic laminin peptides into a triplet stranded coiled-coil structure, *J. Biol. Chem.* 269 (1994) 30386-30392.
32. J. P. Jung, A. K. Nagaraj, E. K. Fox, J. S. Rudra, J. M. Devgun, J. H. Collier, Co-assembling peptides as defined matrices for endothelial cells, *Biomaterials*, 30 (2009) 2400-2410.
33. X. Li, X. Liu, B. Josey, C. J. Chou, Y. Tan, N. Zhang, X. Wen, Short laminin peptide for improved neural stem cell growth, *Stem Cells Transl Med*. 3 (2014) 662–670.
34. R. Patel, M. Santhosh, J. K. Dash, R. Karpoormath, A. Jha, J. Kwak, M. Patel, J. H. Kim, Ile-Lys-Val-Ala-Val (IKVAV) peptide for neuronal tissue engineering, *Polym Adv Technol*. 30 (2019) 4–12.
35. K. Nam, J. P. Jones, P. Lei, S. T. Andreadis, O. J. Baker, Laminin-111 Peptides Conjugated to Fibrin Hydrogels Promote Formation of Lumen Containing Parotid Gland Cell Clusters, *Biomacromolecules*, 17 (2016) 2293−2301.
36. T-Y. M-H. Huang, T-W. Wang, Neural stem cells encapsulated in a functionalized self-assembling peptide hydrogel for brain tissue engineering, *Biomaterials*, 34 (2013) 2005-2016.
37. W. Sun, T. Incitti, C. Migliaresi, A. Quattrone, S. Casarosa, A. Motta, Viability and neuronal differentiation of neural stem cells encapsulated in silk fibroin hydrogel functionalized with an IKVAV peptide, *J Tissue Eng Regen Med*, 11 (2017) 1532–1541.
38. J. Arulmoli, H. J. Wright, D. T. T. Phan, U. Sheth, R. A. Que, G. A. Botten, M. Keating, E. L. Botvinick, M. M. Pathak, T. I.Zarembinski, D. S. Yanni, O. V, Razorenova, C. C. W. Hughes, L. A. Flanagan, Combination scaffolds of salmon fibrin,

hyaluronic acid, and laminin for human neural stem cell and vascular tissue engineering, *Acta Biomater*, 43 (2016) 122-138,

39. S. Chen, M. Zhang, X. Shao, X. Wang, L. Zhang, P. Xu, W. Zhong, L. Zhang, M. Xing, L. Zhang, A laminin mimetic peptide SIKVAV-conjugated chitosan hydrogel promoting wound healing by enhancing angiogenesis, re-epithelialization and collagen deposition. *J. Mater. Chem. B*, 3 (2015) 6798–6804.
40. A. L. Rodriguez, C. L. Parish, D. R. Nisbet, R. J. Williams, Tuning the amino acid sequence of minimalist peptides to present biological signals via charge neutralised self assembly. *Soft Matter*, 9 (2013) 3915-3919.
41. R. Jain, S. Roy, Tuning the gelation behavior of short laminin derived peptides via solvent mediated self-assembly, *Materials Science and Engineering: C*, 108 (2020) 110483,
42. I. Caniggia, J. Liu, R. Han, J. Wang, A. K. Tanswell, G. Laurie, M. Post, Identification of receptors binding fibronectin and laminin on fetal rat lung cells. *Am. J. Physiol-Lung Cell Mol Physiol.* 270 (1996) L459–L468.
43. S. P. Massia, S. S. Rao, J. A. Hubbell, Covalently immobilized laminin peptide Tyr-Ile-Gly-Ser-Arg (YIGSR) supports cell spreading and co-localization of the 67- kilodalton laminin receptor with a-Actinin and Vinculin, *J. Biol. Chem.* 268 (1993) 8053405-9.
44. N. Kapil, A. Singh, D. Das, Cross-β amyloid nanohybrids loaded with cytochrome c exhibit superactivity in organic solvents. *Angew Chem Int Ed Engl.* 54 (2015) 6492-6495.
45. E. M. Jouhilahti, S. Peltonen, J. Peltonen, Class III b-Tubulin Is a Component of the Mitotic Spindle in Multiple Cell Types, *J. Histochem. Cytochem*. 56 (2008) 1113–1119,
46. T. Blasi, H. Hennig, H. D. Summers, F. J. Theis, J. Cerveira, J. O. Patterson, D. Davies, A. Filby, A. E. Carpenter, P. Rees, Label-free cell cycle analysis for high-throughput imaging flow cytometry, *Nat. Commun*. 7 (2016) 10256.
47. F. A. Somaa, T-Y. Wang, J. C. Niclis, K. F. Bruggeman, J. A. Kauhausen, H. Guo, S. McDougall, R. J. Williams, D. R. Nisbet, L. H. Thompson, C. L. Parish, Peptide-Based Scaffolds Support Human Cortical Progenitor Graft Integration to Reduce Atrophy and Promote Functional Repair in a Model of Stroke, *Cell Reports*, 20 (2017) 1964–1977.
48. N. Singha, A. Srivastava, B. Pramanik, S. Ahmed, P. Dowari, S. Chowdhuri, B. K. Das, A. Debnath, D. Das, Unusual confinement properties of a water insoluble small peptide hydrogel, *Chem. Sci*. 10 (2019) 5920-5928.

49. Z. Wang, H. Wang, W. Zheng, J. Zhang, Q. Zhao, S. Wang, Z. Yang, D. Kong, Highly stable surface modifications of poly (3-caprolactone) (PCL) films by molecular self-assembly to promote cells adhesion and proliferation. *Chem. Commun*. 47 (2011) 8901–8903.
50. B. Dinesh, M. A. Squillaci, C. Ménard-Moyon, P. Samorì, A. Bianco, Self-assembly of diphenylalanine backbone homologues and their combination with functionalized carbon nanotubes, *Nanoscale*, 7 (2015) 15873–15879.
51. M. A. Elsawy, A. M. Smith, N. Hodson, A. Squires, A. F. Miller, A. Saiani, Modification of β sheet forming peptide hydrophobic face: effect on self-assembly and gelation, *Langmuir*, 32 (2016) 4917−4923.
52. R. Li, R., M. Boyd-Moss, B. Long, A. Martel, A. Parnell, A. J. C. Dennison, C. J. Barrow, D. R. Nisbet, R. J. Williams, Facile control over the supramolecular ordering of self-assembled peptide scaffolds by simultaneous assembly with a polysacharride, *Sci. Rep*. 7 (2017) 4797.
53. V. Castelletto, I. W. Hamley, Influence of the solvent on the self-assembly of a modified amyloid beta peptide fragment. I. morphological investigation, *J. Phys. Chem. B,* 113 (2009) 9978–9987.
54. R., Orbach, I. Mironi-Harpaz, L. Adler-Abramovich, E. Mossou, E. P. Mitchell, V. T. Forsyth, E. Gazit, D. Seliktar, The Rheological and Structural Properties of Fmoc-Peptide-Based Hydrogels: The Effect of Aromatic Molecular Architecture on Self-Assembly and Physical Characteristics, *Langmuir*, 28 (2012) 2015−2022.
55. B. Xing, C-W. Yu, K. H. Chow, P. L. Ho, D. Fu, B. Xu. Hydrophobic Interaction and Hydrogen Bonding Cooperatively Confer a Vancomycin Hydrogel: A Potential Candidate for Biomaterials, *J. Am. Chem. Soc*. 124 (2002) 14846-14847,
56. J. Raeburn, A. Z. Cardoso, D. J. Adams, The importance of the self-assembly process to control mechanical properties of low molecular weight hydrogels, *Chem. Soc. Rev*. 42 (2013) 5153-5156.
57. F. Koch, M. Müller, F. König, N. Meyer, J. Gattlen, U. Pieles, K. Peters, B. Kreikemeyer, S. Mathes, S. Saxe, Mechanical characteristics of beta sheet-forming peptide hydrogels are dependent on peptide sequence, concentration and buffer composition, *R. Soc. open sci.* 5 (2018) 171562.
58. N. Nandi, K. Gayen, S. Ghosh, D. Bhunia, S. Kirkham, S. K. Sen, S. Ghosh, I. W. Hamley, A. Banerjee, Amphiphilic Peptide-Based Supramolecular, Noncytotoxic,

Stimuli-Responsive Hydrogels with Antibacterial Activity, *Biomacromolecules,* 18 (2017) 3621−3629.

59. M. Abbas, R. Xing, N. Zhang, Q. Zou, X. Yan, Antitumor Photodynamic Therapy Based on Dipeptide Fibrous Hydrogels with Incorporation of Photosensitive Drugs, *ACS Biomater. Sci. Eng*. 4 (2018) 2046−2052.
60. A. R. Hirst, S. Roy, M. Arora, A. K. Das, N. Hodson, P. Murray, S. Marshall, N. Javid, J. Sefcik, J. Boekhoven, J. H. van Esch, S. Santabarbara, N. T. Hunt, R. V. Ulijn, Biocatalytic induction of supramolecular order, *Nat. Chem*. 2 (2010) 1089-1094.
61. Y. Luo, L. Wu, B.Yang, Y. Jin, K. Zheng, Z. He, A novel potential primary method for quantification of enantiomers by high performance liquid chromatography-circular dichroism, *Sci. Rep*. 8 (2018)7390.
62. S. Wu, J. Gao, T. J. Emge, M. A. Rogers, M. A., Influence of solvent on the supramolecular architectures in molecular gels, *Soft Matter*, 9 (2013) 5942–5950.
63. E. T. Pashuck, H. Cui, S. I. Stupp, Tuning supramolecular rigidity of peptide fibers through molecular structure, *J. Am. Chem. Soc*., 132 (2010) 6041- 6046.
64. S. Fleming, P. W. J. M. Frederix, I. R. Sasselli, N. T. Hunt, R. V. Ulijn, T.Tuttle, Assessing the utility of infrared spectroscopy as a structural diagnostic tool for β-sheets in self-assembling aromatic peptide amphiphiles, *Langmuir*, 29 (2013) 9510−9515.
65. S. Fleming,R. V. Ulijn, Design of nanostructures based on aromatic peptide amphiphiles, *Chem. Soc. Rev*. 43 (2014) 8150- 8177.
66. V. Singh, K. Snigdha, C. Singh, N. Sinha, A. K. Thakur, Understanding the self-assembly of Fmoc–phenylalanine to hydrogel formation, *Soft Matter*, 11 (2015) 5353-5364.
67. J. Wang, K. Liu, R. Xing, X. Yan, Peptide self-assembly: thermodynamics and kinetics, *Chem. Soc. Rev*. 45 (2016) 5589-5604.
68. P. W. J. M. Frederix, J. Ide,́, Y. Altay, G. Schae¨ffer, M. Surin, D. Beljonne, A. S. Bondarenko, T. L. C. Jansen, S. Otto, S. J. Marrink, Structural and spectroscopic properties of assemblies of self-replicating peptide macrocycles, *ACS Nano*, 11 (2017) 7858−7868.
69. L. Yao, M. He, D. Li, H. Liu, J. Wua, J. Xiao, Self-assembling bolaamphiphile-like collagen mimetic peptides, *New J. Chem*. 42 (2018) 7439-7444.
70. K. M. Hainline, F. Gu, J. F. Handley, Y. F. Tian, Y. Wu, L. de Wet, D. J. Vander Griend, J. H. Collier, Self-assembling peptide gels for 3D prostate cancer spheroid culture, *Macromol. Biosci*. 19 (2019)1800249.

71. M. Ghosh, M. Halperin-Sternfeld, I. Grigoriants, J. Lee, K. Tae Nam, L. Adler-Abramovich, Arginine-presenting peptide hydrogels decorated with hydroxyapatite as biomimetic scaffolds for bone regeneration, *Biomacromolecules*, 18 (2017) 3541−3550.
72. A. D. Martin, A. B. Robinson, P. Thordarson, Biocompatible small peptide super-hydrogelators bearing carbazole functionalities, *J. Mater. Chem. B*, 3 (2015) 2277–2280.
73. P. Gavel, D. Dev, H. S. Parmar, S. Bhasin, A. K. Das, Investigations of peptide-based biocompatible injectable shape-memory hydrogels: differential biological effects on bacterial and human blood cells, *ACS Appl. Mater. Interfaces*, 10 (2018) 10729-10740.
74. V. Jayawarna, A. Smith, J. E. Gough, R. V. Ulijn, Three-dimensional cell culture of chondrocytes on modified di-phenylalanine scaffolds, *Biochem. Soc. Trans*. 35 (2007) 535–537.
75. G. Bahcecioglu, N. Hasirci, V. Hasirci, Effects of microarchitecture and mechanical properties of 3D microporous PLLA-PLGA scaffolds on fibrochondrocyte and L929 fibroblast behavior, *Biomed Mater*. 13 (2018) 035005.
76. G. Damodaran, R. Collighan, M. Griffin, H. Navsaria, A. Pandit, Tailored laminin-332 alpha3 sequence is tethered through an enzymatic linker to a collagen scaffold to promote cellular adhesion, *Acta Biomater*. 5 (2009) 2441–2450.
77. P. Sharma, H. Kaur, S. Roy, Designing Tenascin-C inspired short bioactive peptide scaffold to direct and control cellular behavior, *ACS Biomater. Sci. Eng*., 5 (2019) 12, 6497-6510.
78. A. Farrukh, S. Zhao, J. I. Paez, A. Kavyanifar, M. Salierno, A. Cavalié, A. del Campo, In situ, light-guided axon growth on biomaterials via photoactivatable laminin peptidomimetic IK(HANBP)VAV, *ACS Appl. Mater. Interfaces*, 10 (2018) 41129−41137.
79. P. Brun, A. Zamuner, A. Peretti, J. Conti, G. M. L. Messina, G. Marletta, M. Dettin, 3D synthetic peptide-based architectures for the engineering of the enteric nervous system, *Sci. Rep*. 9 (2019) 5583.
80. S. Dwane, E. Durack, P. A. Kiely, Optimising parameters for the differentiation of SH-SY5Y cells to study cell adhesion and cell migration, *BMC Res. Notes*, 6 (2013) 366-377.
81. J. R. Menezes, M. B. Luskin, Expression of neuron-specific tubulin defines a novel population in the proliferative layers of the developing telencephalon, *J. Neurosci*. 14, (1994) 5399-5416.

82. S. Das, R. Kumar, N. N. Jha, S. K. Maji, Controlled exposure of bioactive growth factor in 3D amyloid hydrogel for stem cells differentiation, *Adv. Healthcare Mater*. 6 (2017) 1700368.
83. C. D. Katsetos, A. Legido, E. Perentes, S. J. Mörk, Class III β-tubulin isotype: a key cytoskeletal protein at the crossroads of developmental neurobiology and tumor neuropathology, *J. Child Neurol*. 18 (2003) 851-866.
84. V. J. Arellano, P. M. García, J. G. R. Plaza, M. T. L. Ortiz, G. Schreiber, R. Volkmer, E. Klipp, G. D. Rio, An Antimicrobial peptide induces FIG1-dependent cell death during cell cycle arrest in yeast, *Frontiers in Microbiology*, 9 (2018) 1240-1255.
85. N. Ashwanikumar, N. A. Kumar, P.S.S. Babu, K C. Sivakumar, M. V. Vadakkan, P. Nair, I. H. Saranya, S. A. Nair, G. S. V. Kumar, Self-assembling peptide nanofibers containing phenylalanine for the controlled release of 5-fluorouracil, *Int. J. Nanomed*. 11 (2016) 5583–5594.
86. M. G. Ormerod, B. Tribukait, W. Giaretti, Consensus report of the task force on standardisation of DNA flow cytometry in clinical pathology, *Anal Cell Pathol*. 17 (1998) 103–110.

Chapter 5

Designing a bi-functional synthetic extracellular matrix mimic from co-assembled collagen and laminin derived short peptides

5.1 Introduction

As discussed in previous chapters, the previous chapters provides the overview of the role of extracellular matrix (ECM), which is a complex extracellular environment that provides structural support to the cells and regulates several important functions like cell growth, cell-cell interactions and tissue organization. [1,2] Self-assembling hydrogels possess great potential to be developed as substitute for native ECM owing to its capability of providing desirable environment for cell survival and biodegradation. [3, 4] Hydrogels can be tailored to closely mimic the physical properties, stiffness, and topography matching to that of natural ECM, but inducing complex cell-ECM interactions still remains a challenge. [5, 6] This cell-ECM interaction encodes huge amount of information, which determines the cell fate. [7] Incorporation of bioactive cues majorly in the form of proteins derived from native ECM is the most versatile and facile strategy to promote cell-matrix interactions. [8]

In nature, bio-molecules have remarkable ability to self-assemble into highly ordered well-defined complex structures. [9] For example, collagen, the most abundant member of ECM protein family, has attracted considerable attention due to its functional significance, structural diversity and its excellent self-assembling properties. [10, 11] But, difficulties like thermal instability, relatively difficult isolation and specific modifications and possibility of contamination of collagen obtained from natural sources or by microbial expression have made synthetic collagen models a popular target of biomimetic design. [12] Inspite of having wide variety of structural organizations, all collagens shares a common primary structure. They are composed of distinct repetitive units of Gly-X-Y, where X and Y are usually proline and hydroxyproline. [13, 14] The characteristic triple helical structure of collagen is stabilized by the close packing of glycine and hydrogen bond formed between the amide proton of glycine and carbonyl group of nearby X-residue. [15] A classical report by Ramachandran and co-workers explained the role of hydroxyproline residues in stabilizing the collagen triple helix via additional H-bonding between hydroxyl group of hydroxyproline and water molecules. [16] Further, self-assembly of triple helices provides mechanical strength and structural integrity to the body. [15]

Crucial advancements have been made in replicating the multi-hierarchical self-assembly of collagen and towards understanding the fundamentals of design of native collagen. To this direction, collagen mimetic peptides (CMP) have been evolved as the potential biomaterial for biomedical applications, like, tissue engineering, drug delivery, diagnostics and therapy, etc. [17-21] Many approaches have been adapted to elucidate the driving forces of self-assembly in

synthetic systems mimicking the similar steps as that of natural collagen, but it still remains a challenge. [11] To overcome such challenge, researchers explored wide range of intermolecular interactions like electrostatic interactions, [11, 22, 23] π-π stacking, [24] hydrophobic interactions, [25] π-cation interactions, [26] metal-ligand interactions [27-31] and triple helical nucleation [32] and accessed diverse higher order structures. [33, 34] Hartgerink and co-workers designed a 36-mer CMP which can mimic each step of multi-hierarchical assembly of collagen. However, their smart design included classical intermolecular interactions like H-bonding complemented with salt bridges between lysine and aspartate residues. The electrostatic interactions stabilized the triple helix in a sticky end assembly. [11, 12]

Based on basic repeating sequence Gly-X-Y, extensive efforts have been made to overcome the synthetic challenge in designing a collagen inspired protein (CIP). However, only a few short collagen mimetic peptide amphiphiles have been developed that possess the ability to form supramolecular hydrogels. [35, 36] For example, the octapeptide library of collagen inspired supramolecular hydrogelator was developed by Z. Yang et. al., having random coil conformation. The gel strength was found to match that of the matrix of the fibroblast cells and hence they were suitable for the growth of 3T3 cells. [37] Another recent report by Teckinay's group demonstrated the collagen presenting scaffold based on octapeptide amphiphile having Pro-Hyp-Gly (POG) functional sequence, which forms β-sheets, were further explored for the prevention of progressive IVD (intravertebral disc) degeneration. [38] However, both these reports demonstrated self-assembling octapeptide sequences, which were the smallest length collagen mimetic peptides, reported so far. Hence, it would be extremely interesting to design even shorter peptides based on the native collagen structure (GXO), which would be easy to synthesize and can have the potential to achieve the similar structural complexity as well as functions of collagen. It was evident from earlier studies that attempts were directed to modify –X or –O positions with charged amino acids, inducing additional electrostatic interactions for stabilizing collagen mimetic oligopeptide sequences. [13] As mentioned in earlier reports, the cis-trans isomerization of prolines can have destabilizing effects on collagen assembly, so substitution of proline residues offers a target site for CIP modification and explore sequences, keeping the position of glycine and hydroxyproline residues constant. [39]

Moreover, the previous reports in the literature utilized single functional peptide sequence (collagen mimetic) to design a bioactive scaffold. [10-14] However, the complex hierarchical structure and composition of native ECM provide clues to incorporate multiple signals in a single homogenous scaffold which would provide synergistic cellular response. [40-43] Laminin is

another important class of extracellular matrix protein. Laminin is a heterotrimeric protein, mainly present in the basement membrane. As discussed in chapter 2 and 3, two most popular short peptide sequences, like, IKVAV which is present on the A-chain and YIGSR, present on the B-chain of native laminin protein, are identified to mimic the biological activity of the laminin protein. [44] Laminin has diverse biological roles including cell adhesion, migration, differentiation and growth. [44] However, a very few IKVAV and YIGSR based short laminin peptides showing classical role in controlling cell behavior. [44, 45] A report by Nisbet et. al., illustrated the minimalist Fmoc self-assembling peptide design using laminin derived IKVAV and YIGSR, along with fibronectin based RGD peptide for delivering cortical neural progenitor cells in mouse brain. [46, 47] In particular, the role of laminin peptides along with collagen IV has been widely studied for their nerve regeneration properties. [48-50] The role of multicomponent gels composed of isolated collagen, laminin, fibronectin and hyaluronic acid in neurite extension was shown by Schmidt et. al. [40] In the similar line, H. Iwata's group showed the development of hydrogels composed of collagen and laminin derived cell adhesive peptides isolated from microbial genetic engineering for improved survival of neural cell. [51] To the best of our knowledge, no synthetic co-assembled multi-component oligopeptide gels inspired by collagen and laminin peptides have been reported in the literature. [52] The previous studies clearly explained that synthetic oligopeptide sequences derived from collagen and laminin individually show promising biological applications, and therefore, in combination, can present an exclusive bioactive scaffold, which can provide a more realistic model of ECM mimetic biomaterials for tissue engineering. The combined matrix can provide the necessary biochemical and biomechanical cues to different cell types.

In this work, we take a step further to access the next hierarchical level of synthetic ECM. We have illustrated the design of Collagen inspired peptide (CIP), the shortest CIP sequence, containing only a single -GXO unit which makes it difficult to attain α-helical structures. However, this CIP structural mimic can self-assemble to form spherical aggregates but fails to induce higher order fibrillar network to form gel like structure. Interestingly, the incorporation of a very less quantity of laminin mimetic peptide (10% w/w) serves dual purpose. Initially, it acts as a nucleation center and induces gelation to the non-gelating self-assembling CIP through growth of organized nanostructures, in aqueous solvent. And secondly, it provides additional functionality to the scaffold for cell adhesion. The nanofibrillar structure of the co-assembled gels exhibited homogenous morphology, which indicates that the peptides formed co-assembled structures showing the β-turn like secondary structures. Further investigations were made to study the cell-matrix interactions which revealed that supramolecular co-assembled hydrogels

supported the adhesion, survival and proliferation of different types of cells. We aim to achieve the similar complexity of natural ECM within our designer self-assembled hydrogel domain, though they are the shortest CIP and LMP sequences designed so far which can mimic the functional attributes of large proteins. We envisage that this multicomponent co-assembled collagen and laminin mimetic peptide hydrogels based on molecular self-assembly can be developed as potential biocompatible platforms for presentation of biochemical functionality at nanoscale.

5.2 Experimental Section

5.2.1 Materials

Fmoc (9-Fluorenylmethoxycarbonyl) protected amino acids, DIC (diisopropyl carbodiimide), piperazine, EDT (1, 2-ethandithiol), Anisole, Thioanisole were purchased from Sigma-Aldrich. Fmoc-Rinkamide MBHA resin (200-400 mesh), TFA (trifluoro acetic acid), Oxyma, 2-Napthoxy-acetic acid, DMF (Dimethyl formamide) were purchased from Merck.

5.2.2 Peptide Synthesis

Designed collagen and laminin mimetic peptides were synthesized using standard Fmoc solid phase peptide chemistry by using Microwave Automated Solid Phase Peptide Synthesizer (Liberty Blue CEM, Matthews, NC, USA). Fmoc- protected amino acids were coupled on solid support Rinkamide resin at 0.1mmol scale. 2 equivalents of Fmoc-protected amino acids were coupled in the presence of 5 equivalents of DIC and 10 equivalents of oxyma. 20 % w/v piperazine/ DMF solution was used for Fmoc-group deprotection after each subsequent coupling. A cocktail mixture composed of TFA: Anisole: EDT: Thioanisole in the ratio of 95: 2:3:5 was added for 3 hrs to cleave peptides from resin. The purity of cleaved peptides was checked using HPLC and found to be >99% pure and molecular weights were confirmed by LC-MS analysis. The peptides were purified using preparative HPLC, using CAN/water gradients in mobile phase.

5.2.3 Critical aggregation concentration determination

Formation of self-assembled aggregates of CIP and LMP peptides were determined by the Thioflavin T (Th T) fluorescence assay. Th T stock of 2.5 mM was prepared by dissolving 8mg in 10ml water. 200µl of stock was further diluted upto 50 ml to produce 10 µM working solution of Th T. The peptide stocks were separately prepared at the concentration of 0.1mM and 0.5 mM, which were added in different volumes, to 100µl of Th T working solution, to attain different peptide concentrations for studying aggregation. Similarly, for studying co-

assembly, the Nap-FFGSO concentration was fixed at 5μM, to which different volumes of LMP stock solutions were added. The peptides were incubated for an hour with Th T, before the emission scan was recorded in the range of 450-600nm, using Tecan microplate reader with an excitation wavelength of 440nm.

5.2.4 Hydrogel Formation

Peptides were weighed individually and mixed in solid form and then dissolved in 10% DMSO of the total volume. After the complete dissolution of solid, the final volume was made up, by addition of MQ water. The mixture was vortexed and sonicated intermittently to form a uniform solution. The peptide solution was allowed to form gel and left undisturbed for 24 hrs, to ensure complete gelation. Throughout the studies, the collagen inspired peptide (Nap-FFGSO) was used at the concentration of 30mM along with 10% (3mM) of laminin mimetic peptides i.e Nap-IKVAV and Nap-YIGSR in biconjugate gels. The minimum gelation concentration (MGC) of the co-assembled gels was assessed by inverted-vial method.

5.2.5 Morphological Analysis

5.2.5.1 Atomic Force Microscopy (AFM): Silicon wafers were cleaned and dried. The self-assembled peptides were diluted upto 10 times and drop casted over the silicon wafer. After 3 min, the excess solution is removed by the wicking action of filter paper. The air dried samples were scanned under ambient conditions using Bruker Multimode 8 scanning probe microscope operated in tapping mode with Nanoscope V controller and a J-scanner. The AFM probe used was RTESPA-300 with the resonating frequency of 300 kHz.

5.2.5.2 Transmission Electron Microscopy (TEM): The diluted peptide gels were drop casted over the carbon coated copper grids and allowed to adsorb for 3 min. The excess sample was removed by using filter paper. 2% w/v uranyl acetate solution was used to stain the peptide nanostructures. The samples were then vacuum dried and TEM micro-graphs were recorded with a JEOL JEM 2100 with a Tungsten filament at an accelerating voltage of 200 kV.

5.2.6 Rheological Measurements

Viscoelastic properties of the nanofibrous co-assembled hydrogels were measured using oscillatory rheology with 50mm parallel plate geometry (Anton Parr MCR302). The co-assembled hydrogel samples with 30mM collagen inspired peptide and 3mM (in biconjugate system) and 1.5 mM (in tri-conjugate system) of each laminin mimetic peptide were prepared and incubated for 24 hrs before measurements. The optimum strain values were obtained in the linear viscoelastic region by performing the amplitude sweep.

Further, the storage (G') and loss modulus (G") was recorded as a function of frequency sweep in the range of 0.1 to 100 Hz. The experiments were performed using a solvent trap to prevent any drying effect, at 20^0C and temperature controlled with an integrated electrical heater. The measurements were repeated three times to ensure reproducibility, with the average data shown.

5.2.7 Thixotropic Studies

To explore the mechano-responsiveness of these co-assembled hydrogels, step-strain rheology was done. Before performing thixotropic measurements, we checked the recovery properties by mechanical shaking, which transforms the gel material into solution (sol) and its recovery into the self-supporting gel state upon resting, however, the time of reformation may vary for different peptide hydrogels. The initial strain values were fixed as 0.1 % within linear viscoelastic (LVE) region followed by 50 % strain which deforms the gel and transforms it to sol, as indicated by $G' < G''$. As soon as the stress is removed (strain 0.1%), the gel like character is recovered. Both, during deformation and recovery cycles, the frequency was fixed at 1 Hz. Three consecutive cycles each having 200 s deformation phase and 800 s recovery phase were carried out. The temperature was maintained at 20^0C throughout the measurement, through an automated temperature controller.

5.2.8 Secondary structure investigation

5.2.8.1 Circular Dichroism (CD): CD measurements of all peptides were performed using Jasco J-1500 CD spectrophotometer maintained at 20^0C through a water circulator. Spectra for all peptides were obtained between a wavelength of 195-310 nm with 1s signal integrations with a step size of 1 nm and a single acquisition with a slit width of 1 nm. A 0.1 mm quartz cuvette was used in which three repeated scans were compiled to generate the average spectra. The results were analyzed using the Jasco Spectra Manager. A baseline spectrum for 10% DMSO in water was recorded and subtracted from the observed CD spectra to find the actual resultant spectrum for each of the co-assembled gels.

5.2.8.2 Fourier Transform Infrared Spectroscopy (FTIR): FT-IR spectra were recorded on an Agilent Cary 620 FTIR spectrophotometer. The spectra were taken in the region between 400 and 4000 cm^{-1} with a resolution of 1 cm^{-1} and averaged over 64 scans. Spectra were background subtracted to correct for atmospheric interference. Samples were analyzed by mixing about 10% of lyophilized gels with KBr powder to form pellets. The background was collected using blank KBr pellet.

5.2.8.3 Thioflavin T binding assay: The fluorescence spectroscopy was performed on the Edinburgh spectrofluorometer (FS5) in a 1.0cm quartz cuvette, at 25^0C. Th T stock solution (8mg in 10 ml PBS pH7.4 buffer) was freshly prepared and filtered through 0.2 μm syringe filters. The working solution was prepared by diluting stock solution (1ml to 50ml) with PBS 7.4 pH. The fluorescence intensity was measured for 1ml of working solution by excitation at 440nm (slitwidth 1nm) and emission at 482nm (slitwidth 1nm) with an average intensity of 5 accumulations. For measuring the fluorescence intensity of peptide hydrogels, 1ml of working solution was titrated with 50μl of peptide hydrogels. For each sample, the spectra were recorded from 450 to 600nm, at room temperature. The final intensity for each sample was plotted after subtracting the ThT spectrum in 10% DMSO/water.

5.2.8.4 Fluorescence Microscopy of Th T binding: The diluted peptide gels were mixed with Th T working solution (as prepared for Th T fluorescence spectroscopy) in 2:1 ratio and allowed to incubate for 5 min. 50μl of mixture was added on a glass slide and covered with coverslip. The image was observed by the Olympus BX53 fluorescence microscope and captured using Q-Capture Pro 7 software. The 40X lens was used to capture bright field images and the fluorescence images with the help of FITC emission filters (an excitation wavelength of 490nm).

5.2.9 Evaluation of co-assembly

The Nap IKVAV peptide was fluorescently tagged with FITC (Fluorescein isothiocyanate) using standard coupling protocol. In the absence of free N and C terminal, the FITC was coupled with Lysine side chain of IKVAV, under basic conditions, in the presence of excess DIPEA. [53] The tagged Nap IKVAV peptide was mixed with untagged Nap-FFGSO to form co-assembled gel. The peptide solution was drop casted on a slide a co-assembly was visualized using fluorescence microscope.

5.2.10 Solvent Exchange

CIP/LMP co-assembled gels prepared at 30mM+3mM concentration in DMSO/water. After 24 hrs of gel formation, 1ml of milli-Q water was added at the top of the gel and allowed to perfuse for 2 hrs. After 2 hrs the supernatant water is replaced by fresh water. Similar procedure was repeated upto 3 cycles. After this, the DMSO gel was used for FTIR analysis using Vertex 70v FTIR spectrometer (Bruker). Similarly, the solvent exchanged gels were analyzed for mechanical strength using rheometer.

5.2.11 In vitro cell culture experiments

Cell culture experiments were performed with C6 glioma cells and L929 fibroblast cells. Cells were cultured using DMEM media with 10% foetal bovine serum (FBS), and 1% penicillin-streptomycin antibiotic solution and were incubated at humidified chamber with 5% CO_2 at 37^0C.

5.2.12 Metabolic activity assay

To assess the initial contact cytotoxicity of these peptides and quantify cell survival in the presence of peptides, an MTT (3-(4, 5-dimethylthiazol-2-yl)-2,5-diphenyltetrazolium bromide) assay was performed. For biocompatibility studies, 5000 cells were seeded in each well in a 96 well plate and allowed to adhere for 24 hrs. The peptide stock solutions were prepared of 5mg/ml (6.5mM) concentration in 10% DMSO/water. The peptide solutions were sterilized before treatment. Peptide stock solution was diluted upto 100µg/ml (0.13mM) and 1000µg/ml (1.3mM) with DMEM media, resulting in final DMSO concentration to 0.2% and 2% respectively, and added to the cells. The experiments were done in triplicates. For control, the cells were treated with 10% DMSO/water diluted with DMEM media upto 0.2% and 2% DMSO. After 4 hrs of treatment, the media was changed and MTT was added to the cells to check the viability of cells. MTT is a colorimetric assay reagent which converts into purple colored insoluble formazan upon activity with metabolically active cells. After 4 hrs of MTT addition, the supernatant media was removed and formazan crystals were dissolved in DMSO (100µl). The absorbance of each well was recorded using plate reader at 495nm wavelength. The % viability of treated cells was calculated with respect to control cells. To check the toxicity after long term treatment, the MTT assay was carried out after 24hrs, 48hrs and 72hrs, of treatment of 1000µg/ml (1.3mM) of peptide solution to both the cell lines.

5.2.13 2D culture

Prior to 2D cultures, the stability of gels was assessed for media exchange and long duration media perfusion. The gels were placed on coverslips and UV sterilized, after which the media was perfused to provide cells, a uniform environment. The sub-confluent monolayer cells were trypsinized using trypsinase (0.25%)–EDTA (0.02%) solution and resuspended in complete media. The cell density was counted using a haemocytometer. Then 1ml of cell suspension, having 10,000 cells/ml was added in each well of 6 well-plate. The cells were maintained at 37^0C with 5% CO_2 and allowed to adhere.

5.2.14 Live/Dead Staining

The standard protocol according to Live/Dead cell mediated cytotoxicity kit (Invitrogen) was used for differential fluorescent staining of live and dead cells. 4µl of $DiOC_{18}(3)$ was diluted with 1ml of complete media (1:250 dilution) while 2µl of PI (propidium iodide) was diluted with 1ml of PBS buffer and filtered using 0.2µ filters. The cells were incubated with $DiOC_{18}(3)$ for 45 min in dark and then washed three times with PBS. Further, PI solution was added to wells and left for 20 min. At last three washes with PBS were performed and plates were visualized under confocal microscope under the green (480nm) and red (530nm) channels.

5.2.15 Cell Proliferation Assay

Proliferation of C6 cells and L929 cells were assessed by Alamar blue assay after 24 hrs and 48 hrs of treatment. To perform this assay, both the types of cells were seeded in 96 well plates at the cell density of $5X10^3$. The gels were prepared according to the described procedure and diluted upto the concentration of 1000µg/ml (1.3mM) with culture media. The dispersed nanostructures were added to each well and incubated in 95% humidified incubator maintained at 37^0C, with 5% CO_2, for different time durations, with triplicates for each sample. The cells treated with blank 2% DMSO in media were used as negative control and the cells treated with Matrigel was considered as positive control. The media of each well was replaced with 100µl of fresh media with 10% Alamar blue reagent, after different time points (24 hrs, 48 and 72 hrs). The Alamar blue containing plates were further incubated for 4 hrs. At the end of the incubation, the 96-well plate was read by using micro plate reader (Tecan Infinite M Plex). The fluorescence intensity of Alamar blue was determined by excitation/emission of 530nm/600nm. The diluted solutions of peptide gel were used as controls and their fluorescence intensity values were subtracted from the corresponding cell embedded peptides. The data were statistically analysed by using GraphPad Prism 8.0 software. Two way-ANOVA test was applied on data obtained in triplicates (N=3) with 95% confidence level. The data was analysed using Bonferroni statistical test. The data having P values >0.01 were considered as non-significant.

5.2.16 In vitro scratch wound assay

Induction of wound healing ability of the bio-inspired peptide conjugates was tested by scratch wound assay, in vitro. L929 fibroblast cells and C6 glioma cells were passaged and diluted to the density of 10X103 and were seeded in a 24 well plate. The cells were allowed to adhere to and become 60-70% confluent. After that, a scratch was made and each well is treated with diluted peptide gels with 1000µg/ml concentration. The plates were placed in a microscope incubator (37^0C/ 5% CO_2). The plates were imaged using an upright Olympus microscope at 10X magnification, at different time points.

5.3 Results and Discussion

5.3.1 Peptide design

The scaffolds designed with combination of multiple signals offer a synergistic effect on cellular response. To mimic the co-existence of collagen and laminin in native extracellular matrix, we designed multi-component hydrogel scaffolds composed of collagen and laminin derived functional short peptide sequences. [54, 55] To the best of our knowledge, it is the first time we demonstrate the minimalist approach for co-assembly of two different bioactive short peptides resulting in supramolecular gels, without any polymeric network utilization. Most interestingly, these are the shortest peptide sequence designed, so far, attempting minimal modification to the functional known sequence. The design of collagen inspired peptide sequence i.e. Nap-FFGSO was based on incorporation of the basic collagen motif, Gly-X-O, with aromatic dipeptide gelator, Nap-FF (napthoxy-diphenylalanine) in figure 5.1. In our design, 2nd position 'proline' was mutated with aliphatic amino acid, serine, with an additional hydroxyl group, which can facilitate the extensive H-bonding interactions in the aqueous solvent. The aromatic dipeptide, Nap FF is an excellent gelator and its gelation properties were well explored in the literature. [56-58] The evidences for the presence of aromatic amino acid residues in the native collagen can be found in the literature, which catalyzes the formation of stable fibril formation. It was proposed that such type of short non-helical peptides flanked at the terminals of long chain triple helix confers rigidity and stability to the more flexible collagen fibrils. [59] Although, a few reports on short IKVAV and YIGSR based peptides forming gels are available in the literature, in conjugation with an aliphatic chain, or polymeric network or additional amino acid sequences. [44-47] However, in combination to collagen inspired peptide, the pentapeptide sequences i.e. IKVAV (A) and YIGSR (B), derived from native laminin protein, were also synthesized with 2-nathoxyacetic-acid attached at their N-terminal end (figure 5.1). The variable side chains in the peptide backbone give rise to the variable intermolecular interactions (aromatic π- π interactions, hydrophobic interactions and H-bonding) resulting in differential co-assembly, which further led to formation of different types of self-assembled structures. [60] The designed peptide sequences and their representative assembly mechanism is shown in figure 5.1 and 5.2. The peptides were synthesized using standard solid phase synthesis protocols. The purity of synthesized peptides was checked through HPLC and LC-MS. The compound was found to be >99% pure (table 5.1 and figure 5.1). [61]

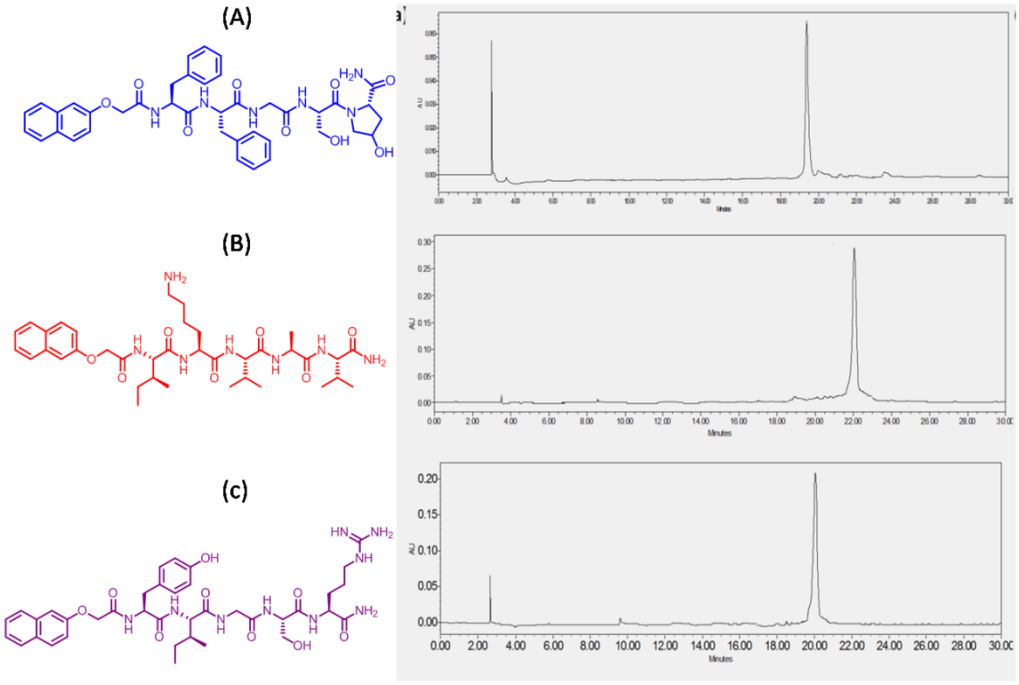

Figure 5.1 *Molecular structure of CMP (collagen inspired peptide) (A) Nap-FFGSO and LMP (laminin mimetic peptides) (B) Nap IKVAV and (C) Nap YIGSR and their corresponding HPLC chromatograms.*

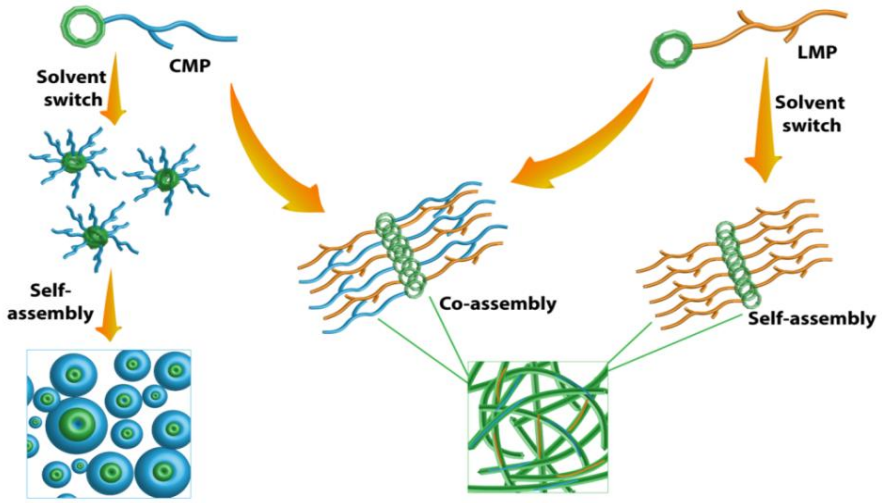

Figure 5.2 *Schematic representation of co-assembly of CIP and LMP using 10% DMSO/ water as a solvent switch.*

Table 5.1 *Mass analysis of synthesized peptides using LC-MS.*

Peptides	Calculated Mass (m/z) (Chem Draw)	Observed Mass (m/z) (LC-MS)
Nap-FFGSO	753.32	753.61
Nap-IKVAV	712.43	712.66
Nap-YIGSR	778.38	778.65

5.3.2 Gelation studies

It is expected that variable amino acid sequences in hydrophobic IKVAV i.e. A as well as hydrophilic YIGSR i.e. B, will induce differential intermolecular interactions (π-π, hydrophobic and H-bonding) with Nap-FFGSO, leading to differential co-assembly. These peptides were found to be insoluble in aqueous media owing to their extensive hydrophobicities, which prevent them from forming an organized network structure in water. Therefore, we employed a unique strategy of solvent switch to induce organized network in the peptide solution. This strategy involves the dilution of DMSO stock of peptides with water and the solution was vortexed until a uniform mixture was obtained. To investigate the differential self-assembling properties of collagen inspired peptide individually as well as their co-assembly with LMP, their critical aggregation concentration (cac) was determined using thioflavin T (Th T). [62] Th T is a fluorescent dye that binds to hydrophobic patches of amyloid fibrils. The intensity of Th T fluorescence is dependent on the concentration of aggregates. As the aggregation starts, more hydrophobic patches are exposed to the Th T dye and emission fluorescence intensity of Th T tends to increase. Addition of increasing concentration of peptides to a fixed 10μM concentration of Th T results in drastic increase in the fluorescence intensity, after a certain concentration, and that can be considered as cac. For individual peptides, the cac for Nap-FFGSO, Nap-IKVAV and Nap-YIGSR was found to be ~10μM, ~2.5μM and ~2.5μM respectively (figure 5.3 a-c). This indicates that LMPs have higher aggregation propensity than Nap-FFGSO, as LMP's aggregates at the lower concentrations. The induction of co-assembly after addition of LMP was assessed by adding the varying concentrations of LMP peptide to sub-aggregation concentration of Nap-FFGSO i.e. 5μM. It was observed that 1 μM of Nap-IKVAV and 1.8 μM of Nap-YIGSR was able to induce aggregation in 5 μM of Nap-FFGSO (figure 5.3 d & e). The cac results suggest that the addition of LMP reduces the cac of Nap-

FFGSO because multiple interaction points were introduced by adding LMP in the solution, which helped in nucleation and growth of the co-assembled structures. This was further extended to gelation studies to achieve macroscopic gelation which is expected to result from higher order assembly of aggregated spherical structures.

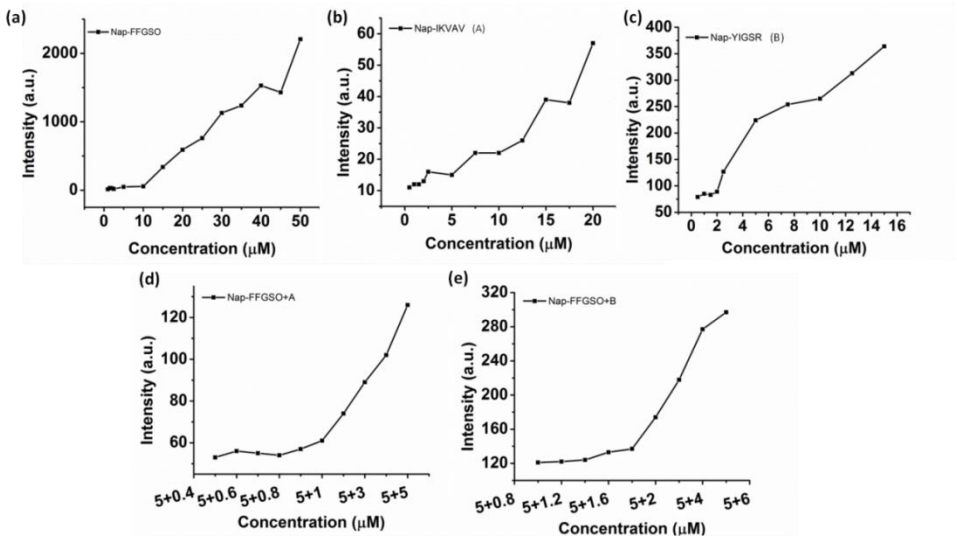

Figure 5.3 *Critical aggregation concentration determination of individual peptides(a) Nap-FFGSO, (b) Nap-IKVAV, (c) Nap-YIGSR and co-assembled peptides (d) Nap-FFGSO+A and (e) Nap-FFGSO+B using Thioflavin T dye.*

Table 5.2 *Summary of gelation studies of collagen and laminin inspired peptides individually and in different combinations.*

Nap FFGSO	Nap IKVAV (A)	Nap YIGSR (B)	Gelation status
Concentration (mM)			
30mM	--	--	Sol
--	3mM 5mM	--	Sol Gel
--	--	3mM 5mM	Sol Gel
30mM	3mM	--	Gel
30mM	--	3mM	Gel
20mM	3mM 4.5mM	-- --	Sol Gel
20mM	-- --	3mM 4.5mM	Sol Gel
30mM	1.5mM	1.5mM	Gel
20mM	1.5mM 2.25mM	1.5 2.25mM	Sol Gel

To prepare co-assembled gels, the peptides in different proportions were dissolved in DMSO/water to induce their gelation. The results for gelation studies are summarized in table 5.2. The role of DMSO fraction in the system was well explained in a report by Adams and his group. [63] The report clearly states that lower DMSO fractions result in highly turbid solutions, initially, which clears out over the course of time. The increased turbidity was caused due to the formation of dispersed spherical structures, leading to phase separation. With time, the spheres act as a nucleation sites for the growth of fibrillar network, which can be correlated with the formation of gels. On the other hand, the higher concentrations of DMSO results in higher solubility with clear transparent solutions, which sometimes may fail to form gel. Our observations were consistent with the reported phenomenon, at 2% of DMSO fraction, a lump of the solubilized peptide was formed which takes longer time to get miscible with water, with the aid of vigourous agitation. As the peptide (with DMSO) dissolution proceeds in water, the solution becomes more turbid and results into gelation after complete dissolution. The images of gels with 2% DMSO were shown in inset of figure 5.4 a. While with 10 % DMSO, the stable translucent gels were obtained (inset of figure 5.4 b). The microscopic evaluation of the gels prepared in 2% DMSO/water was consistent with the previous studies that reports the formation of turbid gels with lesser amount of DMSO and forms mixed structures with spherical aggregates and discrete fibrillar structures in both Nap-FFGSO+A and Nap-FFGSO+B (figure 5.4 a and b). In addition to this, longer vigourous agitations and lesser organised structures account for the lower mechanical strength of co-assembled CIP-LMP gels in 2% DMSO/water (figure 5.4 c and d). Therefore, we used 10% DMSO/water as a solvent for gelation of CIP peptides in further studies.

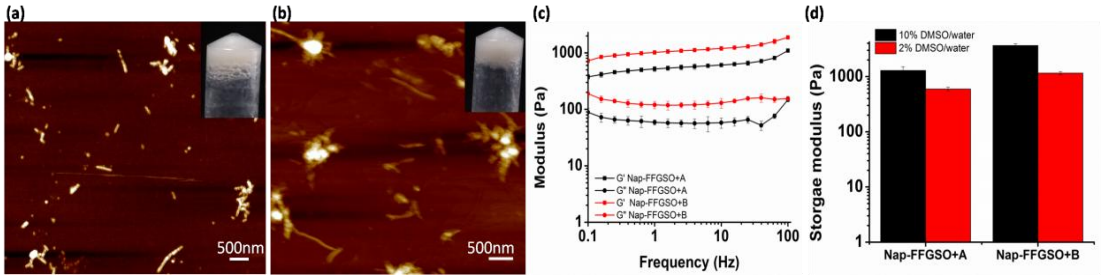

Figure 5.4 *Gelation studies of collagen and laminin inspired co-assembled gels in 2% DMSO/water with optical images and respective AFM microscopic images of gels of (a) Nap-FFGSO+A and (b) Nap-FFGSO+B; (c) Rheology studies of gels prepared in 2% DMSO/water at the concentration of 30mM of Nap-FFGSO and 3mM of either Nap-IKVAV (A) or Nap-YIGSR (B) and (d) Comparison to gel strength, when the gels were prepared in 10% DMSO/water and 2% DMSO/water.*

The self-assembly of Nap-FFGSO alone was checked over a wide range of concentrations (upto 100mM), but it failed to form gel even at higher concentrations. The probable reason for non-gelating properties of Nap-FFGSO could be the improper hydrophilic-lipophilic balance in aqueous solvent, which plays an extremely important role in determining the intermolecular interactions between the peptide molecules and thus affects the self-assembling behaviour of short amyloid like peptides. Probably, the additional hydroxyl group of serine participates in preferential H-bonding with water molecules, which disturbs the gelator-gelator interactions and thus interrupts in the formation of higher ordered structures. Interestingly, when 30mM concentration of Nap-FFGSO was mixed with 10 % of either of the LMP's (Nap IKVAV or Nap YIGSR), it resulted into the formation of self-supporting translucent to opaque gels (figure 5.5). We also observed that the combination of 5% of each LMP when mixed with 30mM of Nap-FFGSO, the peptides showed the hierarchical structure formation leading to supramolecular gels (table 5.2 and figure 5.5). In order to develop a superior surrogate of natural ECM, such co-assembled supramolecular gels with short bioactive peptide sequences will be highly beneficial, which remain unexplored, so far in the field of tissue engineering. It was also interesting to know that the concentration of the laminin peptides used in the co-assembled gels was just 10%.

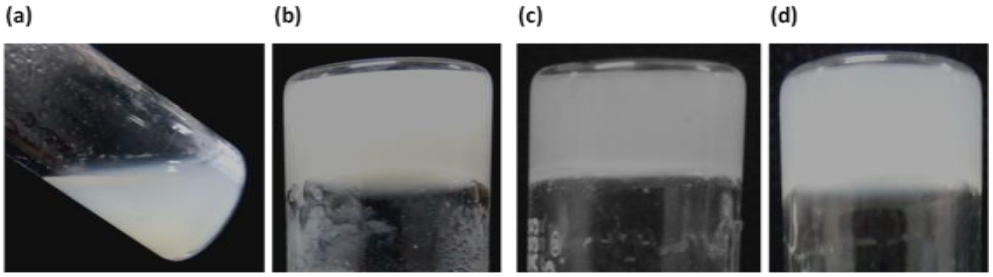

Figure 5.5 *Optical images of (a) Nap-FFGSO as a soution and (b) Nap-FFGSO+A, (c) Nap-FFGSO+B, (d) Nap-FFGSO+A+B as co-assembled gels in 10% DMSO/water.*

Surprisingly, it would be worth mentioning that at this low concentration, both Nap IKVAV and Nap YIGSR individually can induce well organized network structure, though none of these two peptides could lead to supramolecular gelation (figure 5.6). The minimum gelation concentration for Nap IKVAV and Nap YIGSR peptides separately was found to be 5mM in 10% DMSO/water system (table 5.2). The results indicated that addition of only a small quantity (~10%) of LMP, at their sub-gelation concentration, was able to induce gelation with non-gelator CIP scaffold via co-assembly.

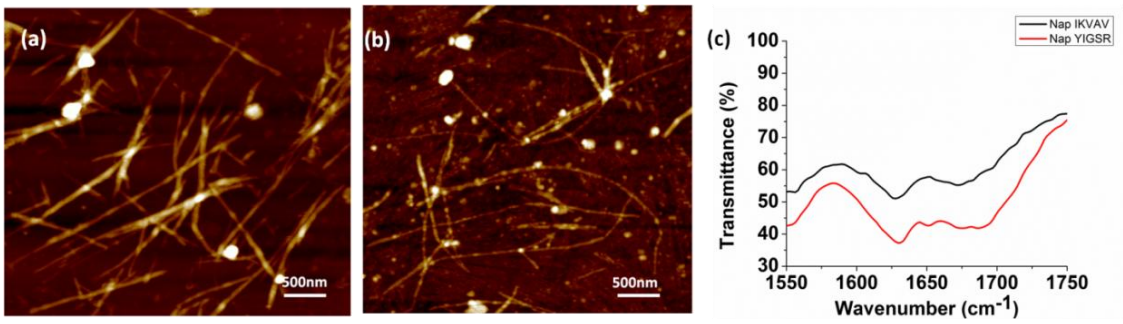

Figure 5.6 *AFM images of (a) Nap-IKVAV and (b) Nap-YIGSR at 3mM concentration. (c) FTIR spectra of LMP's.*

To check the gelation ability of CIP's in the presence of LMP's, different ratios of both the peptides were tried, as a control. On decreasing the CIP concentration upto 20mM and increasing LMP concentrations for both peptides upto 4.5mM (i.e. 15% of 30mM CIP), results into gelation (figure 5.7 a, b, e & f). The probable reason for gelation at lower concentration of CIP is that the concentration of LMP's reached near to their gelation concentration, which is 5mM. However, 20mM CIP added with 3mM of either LMP or 1.5 mM of both LMPs (i.e. 10% of 30mM), failed to form gel (figure 5.7c and g). However, the Nap-FFGSO (20mM) + A (2.25mM) + B (2.25mM) forms stable gel, showing the presence of fibrous network (figure 5.7d & h). The optical images of all the gels with 30mM of Nap-FFGSO with 3mM of LMPs are shown in figure 5.4.

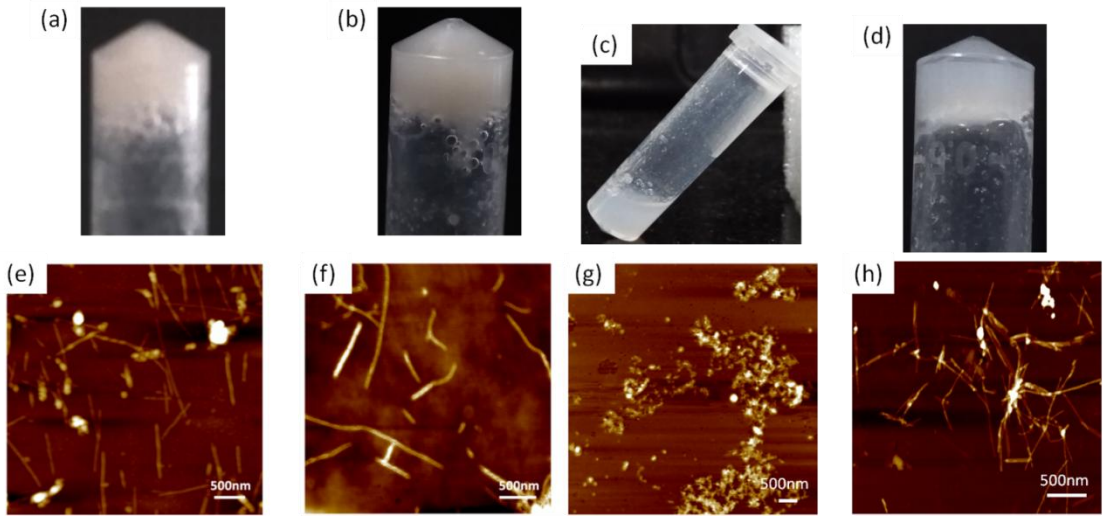

Figure 5.7 *Optical images of the control hydrogels with varied concentration of CIP and LMP peptide and their respective AFM images (a, e) Nap-FFGSO (20mM)+A (4.5mM), (b, f) Nap-FFGSO (20mM)+B (4.5mM), (c, g) Nap-FFGSO (20mM)+ A(1.5mM)+B (1.5mM) and (d, h) Nap-FFGSO (20mM)+ A(2.25mM)+B (2.25mM).*

We hypothesize that laminin peptides act as a nucleating site for self-assembly and thus trigger the growth of higher ordered structures. The nucleating centers further support the association of the peptides through extensive aromatic π- π interactions among CIP molecules. We expect that in addition to aromatic π- π interactions, the stronger hydrophobic interaction induced by IKVAV and additional intermolecular H-bonding domain in YIGSR facilitates the growth of nucleated nanostructures. Thus, addition of LMPs probably improves the hydrophilic-lipophilic balance of the system in aqueous environment by enhancing the intermolecular interactions, which could trigger supramolecular gels formation. [32]

5.3.3 Morphological characterization

It is highly crucial to know the morphology of these co-assembled gels at nanoscale, as the variable topology is expected to induce differential cell-matrix interactions. Atomic Force Microscopy (AFM) was used to investigate the morphology of the nanostructures formed due to co-assembly (figure 5.8 a-d). As anticipated, the non-gelator Nap-FFGSO at 30mM concentration showed the random aggregate like morphology. As discussed earlier, at 3mM concentration, which is the sub-gelation concentration, both the LMPs i.e. A and B were unable to form gel but showed the presence of soluble fibrous morphologies. The LMP, A showed short fibrous structures with an average fiber diameter of 40 ± 4.5 nm, while LMP B forms thin long fibers with an average diameter of 28.7 ± 4.4 nm as evident from AFM studies (figure 5.5 and table 5.3). The induction of gel formation in Nap-FFGSO upon addition of LMP at their sub gelation concentration was monitored using AFM. In the presence of A and B, the spherical aggregates formed by Nap-FFGSO completely disappeared, and the appearance of well ordered fibrous network in the co-assembled gels was observed which led to the formation of supramolecular gels. Interestingly, the dimensions of the conjugated gels were found to be quite different. The CIP with hydrophobic LMP derivative, A showed the existence of short length twisted nanofibers of diameter ~ 62 ± 4.8nm (figure 5.8 a-d and table 5.3), whereas CIP with hydrophilic LMP B formed fibers of much longer length, however, the fiber appears to be thin with a diameter of ~17 ± 2.3 nm. In the tri-component gels with both LMP, i.e. Nap-FFGSO+A+B, the presence of fibers of variable lengths were observed with uniform diameter in the range of ~26 ± 3.1 nm. The morphological investigation clearly indicated that there were no distinct subpopulations of fibrils in co-assembled gels that might indicate the self-sorted assembly of mixed LMP peptides into mutually exclusive fibrils. [64] Therefore, it was assumed that the triconjugate peptides co-assembled to form homogenous fibrils with similar diameter. However, the length of the fibers is dependent on the laminin additive, as more hydrophobic

IKVAV derivative induces shorter length and wider fibers while the hydrophilic YIGSR derivative yield thin but longer fibrous network due to involvement of H-bonding interactions in aqueous solvents. The control gels, at 20mM concentration of CIP and 4.5 mM of LMP showed the presence of uniform fibers of shorter lengths, while 20mM of CIP with 1.5mM of each LMP showed aggregates like structure and 2.25mM of each LMP (equivalent to 4.5 mM of total LMP concentration) showed the formation of entangled fibrous network. The probable reason for the failure of gelation in Nap-FFGSO (20mM) + A (1.5mM) + B (1.5mM) was the lack of sufficient interactions which could support the growth of aggregate like nanostructures into fibers.

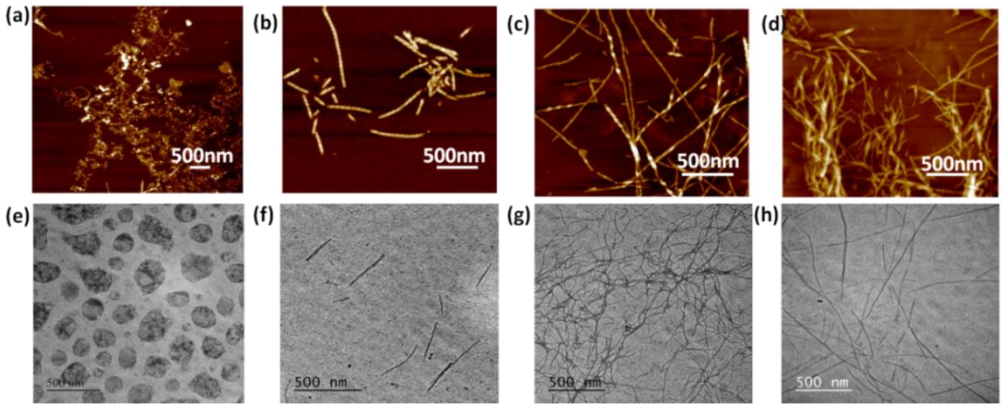

Figure 5.8 *AFM and TEM images of collagen and laminin co-assembled peptide hydrogels of (a, e) Nap-FFGSO (30mM), (b, f) Nap-FFGSO (30mM)+A (3mM), (c, g) Nap-FFGSO (30mM)+B (3mM) and (d, h) Nap-FFGSO(30mM)+A (1.5mM)+B (1.5mM).*

Table 5.3 *Comparison of morphologies of different nanostructures and the diameter of nanofibrous network of collagen-laminin co-assembled hydrogels.*

Peptide composition	**Morphology**	**Diameter (nm)**	
		AFM	**TEM**
Na-FFGSO	Aggregates	--	
Nap-IKVAV	Fibers	40 ± 4.5	35± 3.1
Nap-YIGSR	Fibers	28.7 ± 4.4	20 ± 2.3
Na-FFGSO+ A	Short fibers	62 ± 4.8	38 ± 5.6
Nap-FFGSO+ B	Long entangled fibers	17 ± 2.3	8 ± 2.7
Nap-FFGSO+ A+ B	Mixed fibers (long and short)	26 ±3.1	10.5 ± 2.3

The presence of fibrous structures further confirmed the formation of co-assembled gels (figure 5.6). To further confirm the morphology of the co-assembled peptides, transmission electron microscopy was performed (figure 5.8 e-h and table 5.3). Similar morphologies were also evident from TEM studies. As evident from AFM, the Nap-FFGSO formed spherical structures, which are incapable of entrapping water and thus cannot form gels. In corroboration, to AFM, Nap-FFGSO+ A showed short fibers of diameter in the range ~38 ± 5.6nm, and Nap-FFGSO+B forms long fibrous network with ~ 8 ± 2.7nm diameter. Also, Nap-FFGSO+A+B showed mixed length fiber population, but interestingly their diameter was in the similar range of ~10 ± 2.3nm. TEM and AFM confirmed the formation of nanofibrous structures after co-assembly which could potentially support the three dimensional gel network for further applications.

5.3.4 Mechanical strength evaluation

Matrix stiffness of the gels shows a prominent effect on cell processes such as adhesion, proliferation and differentiation. Hence, it is necessary to assess stiffness of hydrogel matrix to determine the behavior of developed biomaterials in tissue engineering applications. The mechanical strength of all the three co-assembled supramolecular gels was measured using oscillatory rheology. Higher storage modulus (G') in comparison to its corresponding loss modulus (G") for all the co-assembled systems confirmed the gelation. During amplitude sweep, the equilibrium storage moduli of all the gels remained in linear viscoelastic region upto 0.1% with minimal variation upto 10% strain and decreased significantly above 10%. This means that the gels retained elastic properties upto 10% strain and above that loses its elastic nature. Mechanical strengths of co-assembled gels were further assessed using frequency sweep mode, keeping the strain constant as 0.1% in the linear viscoelastic region. However, no considerable difference in the gel strength was noted for Nap-FFGSO + A and Nap-FFGSO + A+ B, which showed G' in the range of 1.3 ±0.2 kPa and 0.7±0.1 kPa respectively (figure 5.9 a & b). But, Nap-FFGSO + B showed relatively higher storage modulus i.e. 3.7±0.3 kPa, in comparison to other two systems. The probable reason for the relatively higher strength of Nap-FFGSO + B could be the favorable H-bonding interactions between the hydroxyl groups of Nap-FFGSO and Nap YIGSR in aqueous system. [65] Very interestingly, the higher mechanical strength of the gels can be further correlated with the thinner fiber diameters of Nap-FFGSO + B with more entanglements leading to the strongest gels of the co-assembled CIP and LMP gel family. [66] It was noted that the mechanical strength of these co-assembled gels was much higher than the short collagen inspired hydrogels reported by Z. Yang et. al., which reports storage modulus in the range of <1 Pa to <50 Pa. [37] Similarly, the storage modulus of gels

reported in our work was also comparable or greater than short collagen peptide amphiphile gels reported by Teckinay and his group. They showed the storage modulus of Col-PA/E-PA in the range of 1 kPa while we showed the storage modulus in the range of ~1kPa to ~4 kPa for the CIP-LMP co-assembled gels. [38] Thus, the co-assembled systems offer an advantage to adjust the mechanical stiffness of the nanofibrous hydrogels by modulating the nature of the dopant peptide as well as the concentration of the individual peptide components.

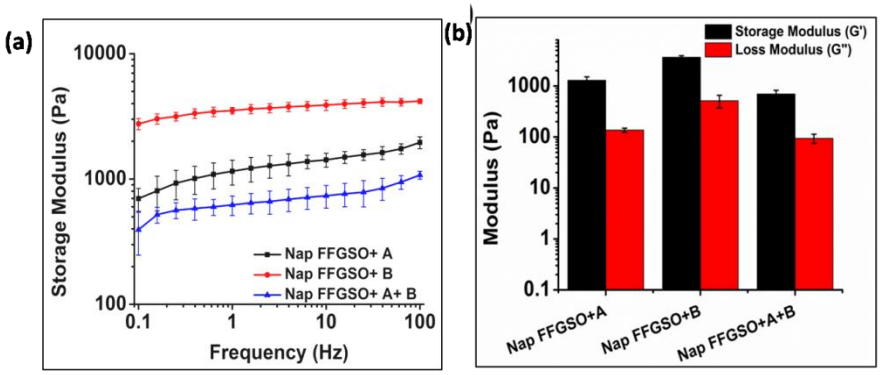

Figure 5.9 *Mechanical strength measurements of co-assembled peptide hydrogels (a) Frequency sweep graph of Nap-FFGSO with LMP A and B (b) comparison of corresponding storage and loss modulus.*

5.3.5 Mechanoresponsiveness studies

To get an insight into another important aspect, i.e. injectable behaviour of these gels, the hydrogels were subjected to different extent of mechanical stress, which is crucial for their biomedical applications. [67] The thixotropic studies were performed to study reversible gel-sol-gel transitions by applying external mechanical stress in a cyclic manner. [68] The gels were deformed by applying the strain of 50% for 100s followed by decreasing the strain upto 0.1% (LVE range) for 200s which allows the recovery of the structure of gels. [69] We observed significant difference in the percentage recovery of co-assembled gels, depending upon the type of laminin peptide added. The weak gels formed by Nap-FFGSO+A showed the highest recovery of ~50%. However, under similar experimental conditions, Nap-FFGSO+B and Nap-FFGSO+A+B showed comparatively lesser recovery ~10 % and 25 % respectively (figure 5.10). We hypothesize that the lesser recovery of Nap-FFGSO with hydrophilic laminin peptide may be attributed to compromised H-bonding interactions due to loss of water during deformation. However, in case of Nap-FFGSO+A, the hydrophobic interactions were restored faster. [70] Therefore, the thixotropic studies reveal that these co-assembled systems can be developed as potential injectable biomaterial for cell culture and drug delivery applications.

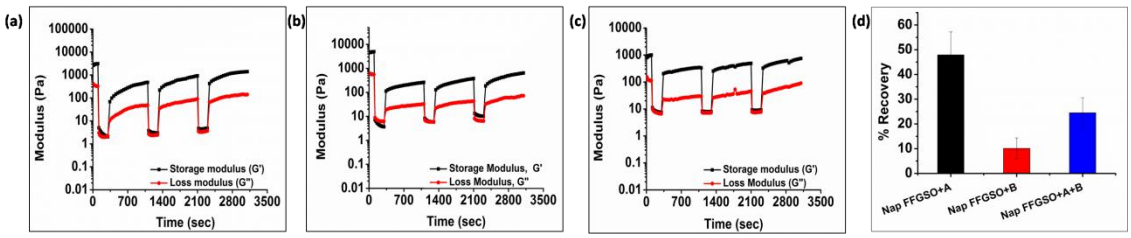

Figure 5.10 *Thixotropic behaviour of (a) Nap-FFGSO (30mM)+A (3mM), (b) Nap-FFGSO (30mM)+B (3mM) and (c) Nap-FFGSO (30mM)+A (1.5mM)+B (1.5mM) at 50% strain for 100s followed by recovery at 0.1% strain for 200s and (d) comparison of corresponding percentage recovery after 100s.*

5.3.6 Secondary structure investigation

To assess the intermolecular interactions involved in the formation of secondary structures, several spectroscopic techniques were employed. Circular dichroism (CD) is a powerful tool to elucidate the molecular arrangements of peptides and provides information regarding self-assembled supramolecular structures in the gel phase. [71] For a non-gelator, Nap-FFGSO, no characteristic CD signal was observed, which also correlates with its morphological analysis indicating the absence of any highly ordered hierarchical organization (figure 5.11a). The CD spectrum of all the three co-assembled gels showed a positive band near 195 nm, a negative peak in between 205-210nm, a broad positive band near 217nm with an additional negative peak or broad band near 230 nm (n- π* transition) indicating the existence of β-turns as the major secondary structures (figure 5.11a). [71] The negative cotton effect in co-assembled gels induces helical orientation of the naphthalene groups, as evidenced by the distinct peak maxima at 288nm. [72] The peak corresponds to the π- π* transition of naphthalene moiety. The single type of characteristic signal in Nap-FFGSO+A+B also indicates that homogenous structures were formed via co-assembly and there has been no sign of self-sorting of different peptide fibers. Such observation again correlated well the morphological analysis of the tri-component co-assembled gels which showed existence of single population of homogenous fibers throughout.

To further investigate the H-bonding interactions in the peptide secondary structures, FTIR spectroscopy was employed (figure 5.11b). [73, 74] The coupling of H-bonding between carbonyl and NH group of peptide backbone resulted in enhancement of signals in amide I region (1600-1700cm^{-1}). For all the peptide systems in our studies, a transmittance at ~1645cm^{-1} and ~1680 cm^{-1} were observed which is indicative of 'β-turns' conformation in the structures (figure 5.11b). [73, 74] The FTIR spectra of LMP's (Nap IKVAV and Nap YIGSR) alone showed the

presence of β-sheet structure, supporting the fibrous morphology (figure 5.6 c). The FTIR results support the CD analysis, as both the techniques indicated the formation of β-turns in the co-assembled gels.

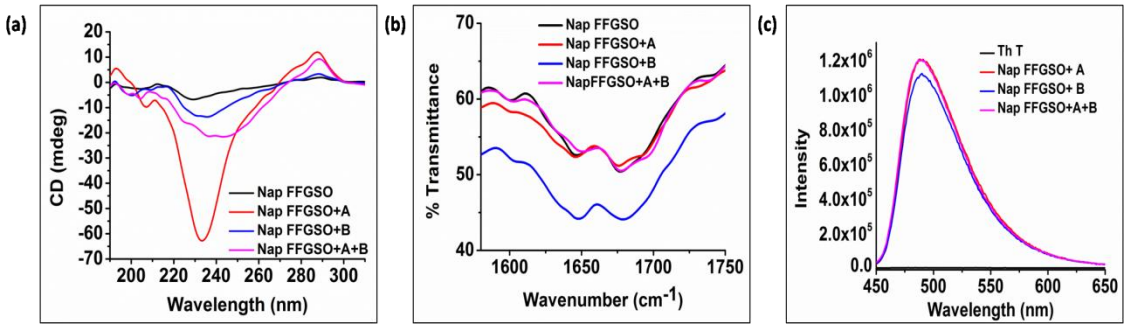

Figure 5.11 *Secondary structure investigation of co-assembled hydrogels prepared 30mM concentration of CMP and 10% LMP (3mm) using (a) CD spectroscopy and (b) FTIR spectroscopy and (c) Th T binding assay through fluorescence spectroscopy.*

Further, to authenticate the secondary structures within these gels, Thioflavin T (Th T) binding assay was carried out. Th T is a widely used tool for the detection of cross β- structures as formed by the amyloid fibrils. Interestingly, the Th T binding is mediated by contacts through aromatic residues in the hydrophobic pockets. [75] As analyzed by CD and FTIR, the β-turn secondary structures were formed by the co-assembly of CIPs and LMPs which also exhibits Th T binding (figure 5.11c). The Th T binding with the aromatic residues of these peptides is marked by the enhancement in fluorescence intensity of emission peak at ~480 nm. [75] The relative enhancement with Nap-FFGSO+A and Nap-FFGSO+A+B were found to be comparatively higher than Nap-FFGSO+B. The more hydrophobic nature of IKVAV in comparison to YIGSR might create more hydrophobic pockets and thus relatively higher increment in the Th T fluorescence intensity was observed (figure 5.11c). The Th T bound amyloid like fibrils can be examined using fluorescence microscope (figure 5.12). In all the three co-assembled, the fluorescent fibrous patches can be observed, which confirmed the amyloid like behavior of supramolecular assemblies formed from short peptide sequences derived from collagen and laminin. [76, 77]

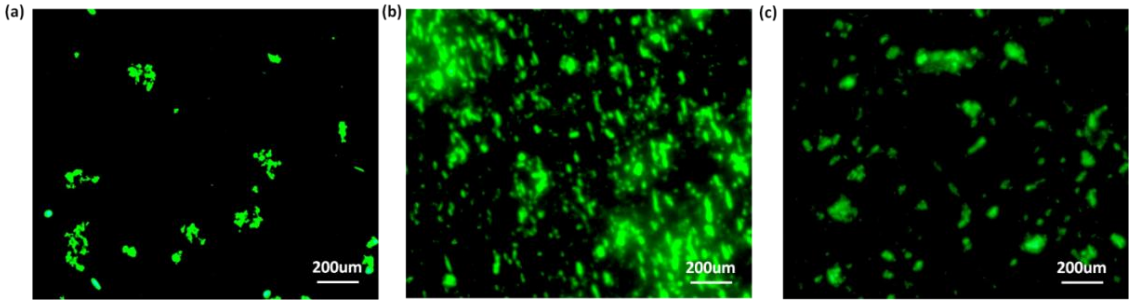

Figure 5.12 *Fluorescence microscopic images of Thioflavin T bound with co-assembled peptide hydrogels (a) Nap-FFGSO + A, (b) Nap-FFGSO+B and (c) Nap-FFGSO+A+B.*

5.3.7 Evaluation of co-assembly

To get an insight into the molecular arrangement of two different peptides during co-assembly, the fluorescent tagging approach was used. One of the two co-assembling peptide was tagged with fluorophore i.e. FITC. In the absence of free fluorophore binding site (i.e. -NH2 or -COOH group), Nap-FFGSO could not be fluorescently coupled and therefore Nap-IKVAV was selected to be coupled with FITC. Both the peptides were dissolved in 10% DMSO/water and co-assembled structures were observed under fluorescence microscope. Initially, non-fluorescent aggregate like structures were observed with embedded fluorescent peptides within it. With time, the peptides align in the form of fibers (figure 5.13). The presence of fluorescent patches throughout the length of the fibers was observed. This clearly reveals that the two peptides are supramolecularly arranged to form a single type of fibers, thus avoiding self-sorted fiber formation. [78] We hypothesize that due to less hydrophobicity of LMP peptides, their faster gelation kinetics in aqueous solvent can be observed, leading to the formation of nucleation centers (short fibrous structures) for the further self-assembly of Nap-FFGSO.

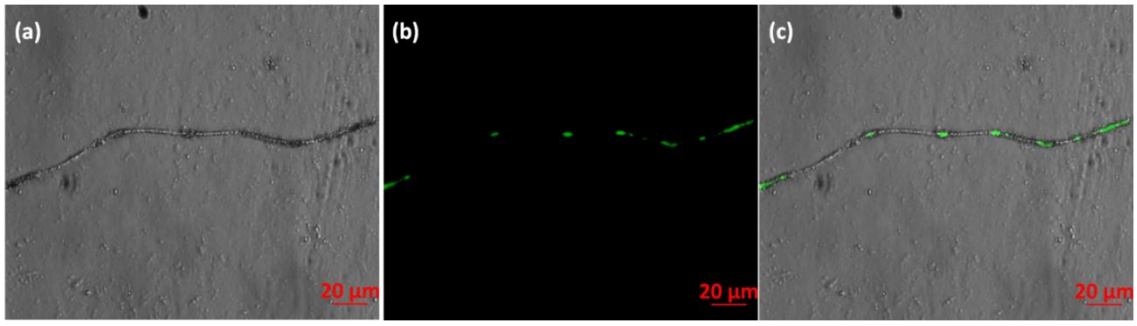

Figure 5.13 *Images of co-assembled peptides with (a) bright field, (b) fluorescence and (c) merged image of bright field and fluorescence showing localization of fluorescent Nap-IKVAV along the non-fluorescent Nap-FFGSO peptide fiber.*

5.3.8 Solvent Exchange

It is expected that 10% DMSO in gels can be detrimental to biological applications like cell culture. A report by T. Eljezi, showed the effect of different concentrations on the proliferation of cells. This report suggests that DMSO concentrations above 1% can reduce the cell proliferation significantly. [79] However, the tunabilibity achieved using solvent switch is highly appreciable. Therefore, to eliminate the deleterious effects of solvents, we considered solvent exchange method post-gelation, which was earlier shown by Dave Adams and co-workers. [80] The CIP-LMP gels (30+3mM) were initially prepared in 10% DMSO/water according to the procedure described. Post-gelation, 1ml of milli-Q water was added gently at the top of the gel and allowed to exchange with the solvent entrapped in gel network for 2 hrs. The supernatant aqueous layer was removed without disturbing the gel. Subsequently, the similar exchange was done three more times. The gels remain intact after the three cycles of solvent exchange. The removal of DMSO was confirmed by FTIR which was indicated by the diminished sulfoxide peak at 1020 cm^{-1}, in comparison to sharp peak present in 10% DMSO as control (figure 5.14 a). [80] It was important to evaluate the effect of solvent exchange on the mechanical strength of the gels, so we carried out rheology of solvent exchanged gels (figure 5.14 b). A reduction in mechanical strength was observed after solvent exchange, but gels retain their structural integrity. For Nap-FFGSO+A and Nap-FFGSO+B gels, the mechanical strength reduces to 0.8 ± 0.1 kPa from 1.3± 0.3 kPa and 2± 0.3 kPa from 3.7± 0.3 kPa, respectively. However, for Nap-FFGSO+A+B gels do not show very significant reduction in storage modulus and showed 0.5± 0.06 kPa after exchange in comparison to 0.7± 0.1 kPa without exchange. Interestingly, the mechanical strength of the gels remained higher, even after solvent exchange, in comparison to the previously reported short collagen mimetic peptide hydrogels. Similar exchange can be done with cell culture media in order to make these gels more suitable for cell culture applications.

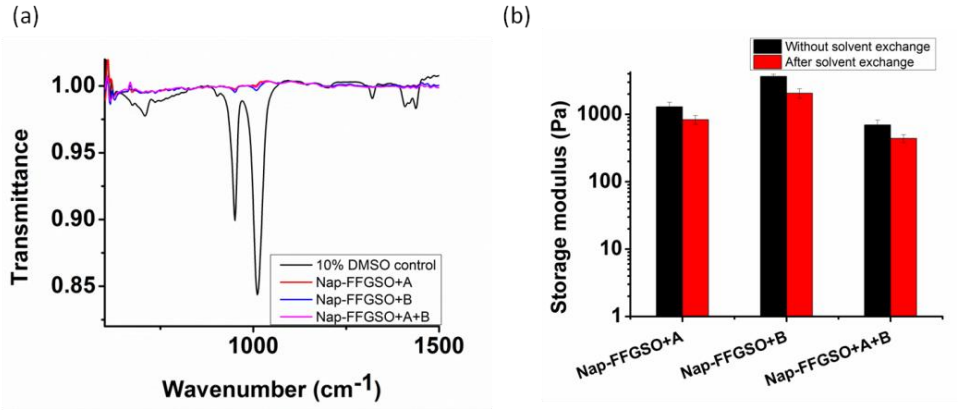

Figure 5.14 *Solvent exchange of gels prepared at concentration of 30mM Nap-FFGSO and 3mM of LMP in 10% DMSO/water (a) FTIR spectra of CIP-LMP gels after solvent exchange showing diminished sulfoxide peak at 1020 cm^{-1} and (b) Rheology measurement of gels without and after solvent exchange. The measurements were done after three consecutive cycles of solvent exchange with water.*

5.3.9 Metabolic activity assay

Cytotoxicity studies are pre-requisite criteria to assess the suitability of these CIP/LMP co-assembled peptide gels as biomaterials. [81] The short duration treatment (4hr) was performed to assess the initial contact cytotoxicity of peptides with the cells. [82] The colorimetric MTT assay was performed quantitatively to determine the number of metabolically active cells after treatment with respect to control cells (figure 5.16 and 5.18). The mouse fibroblast L929 cells and rat glioma C6 cells were seeded in 96 well plates and allowed to adhere for 24hrs. The cells were then treated with different concentrations i.e. 100µg/ml (~0.13mM) and 1000µg/ml (~1.3mM) of soluble peptides for 4 hrs to check the cytotoxicity of these peptides. [83] The reason for using sub-gelation concentrations for cytotoxicity studies was that the previous reports suggested that oligomeric lower order self-assembled structures of amyloid peptides are more toxic to cells than the higher ordered self-assembled fibrous network. [84] Moreover, the dilution of peptide stock (5mg/ml or 6.5mM) also reduces the DMSO content to 0.2% in 100µg/ml and 2% in 1000µg/ml, which further reduces the chances of toxicity due to DMSO. The presence of soluble self-assembled structures in the diluted peptide solutions at concentration of 100µg/ml (0.13mM) and 1000µg/ml (1.3mM) was confirmed by using AFM (figure 5.15).

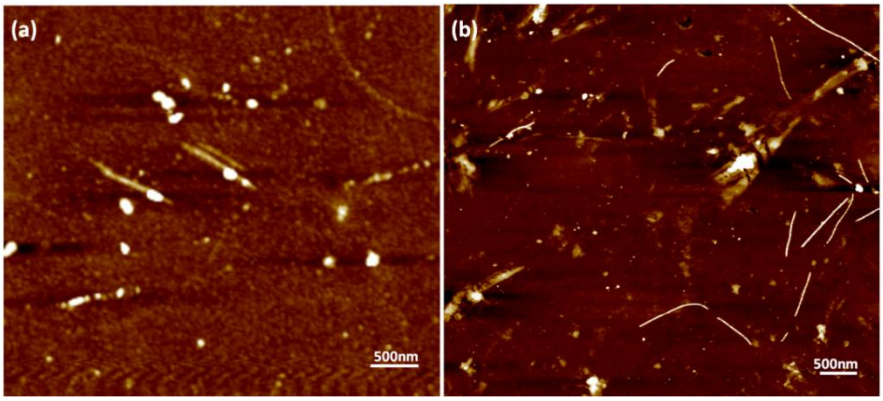

Figure 5.15 *AFM images of 5mg/ml (6.5mM) stock diluted to (a) 100 µg/ml (0.13mM) and (b) 1000µg/ml (1.3mM) peptide concentration.*

The control cells were treated with 10% DMSO containing media with similar dilution (0.2% and 2%). The results suggest that peptides does not affect the metabolic activity of the cells; however, the percentage of viable cells was relatively higher with L929 cells in comparison to C6 cells. With both the cell types, CIP alone (Nap-FFGSO) showed more than 100% cell viability, which might be due to promoted proliferation (figure 5.16). The biocompatibility of the co-assembled gels was found to be inversely proportional to the hydrophobic nature of the resulting gels. Among all the three co-assembled gel systems, the most hydrophobic sequence, Nap-FFGSO+ A resulted in a comparatively less cytocompatible matrix, which showed nearly 80% viability with L929 cells and nearly 60% for C6 cells at 1000μg/ml (1.3mm) concentration (figure 5.16 a and b). The greater hydrophobicity of IKVAV which leads to the formation of shorter length fibers may not provide uniform network structure for adherence of cells, which is likely to affect its interaction with cells and makes it comparatively less cytocompatible. In contrast, the hydrophilic Nap-FFGSO+ B induces less toxicity to the cells with ~90% viability of C6 cells and 93% viability of L929 cells, at 1000μg/ml concentration of peptide. However, doping of hydrophobic A (5%) with Nap-FFGSO+B, in a triconjugate gels, metabolic activity of cells was found to be reduced than Nap-FFGSO+B, which becomes ~70% for C6 cells and ~84% for L929 cells. We also checked the morphology of cells after the treatment of peptides and it was observed that cells retain their healthy morphology and remain unaffected by the treatment even at higher concentrations i.e. 1000μg/ml (1.3mM) (figure 5.17).

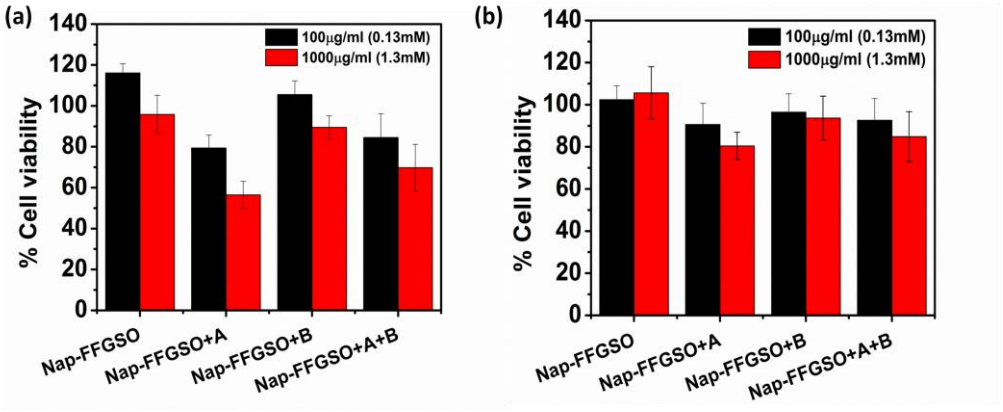

Figure 5.16 *Cytotoxicity studies of collagen inspired peptide and its co-assemblies with laminin mimetic peptides at the concentration of 100μg/ml (0.13mM) and 1000μg/ml (1.3mM) with (a) C6 cells and (b) L929 cell lines, using MTT.*

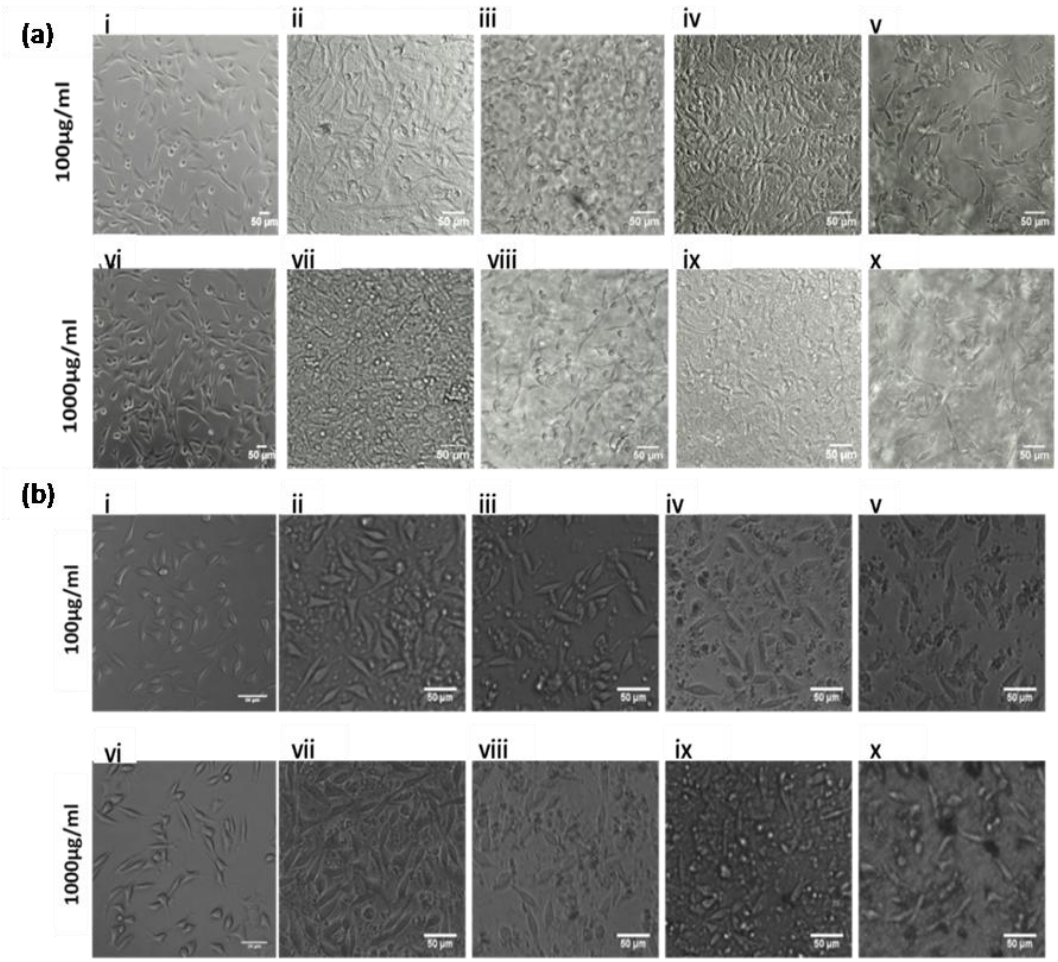

Figure 5.17 *Cytotoxicity studies: microscopic images of (a) C6 cells and (b) L929 cells as (i and vi) control (TCP) and after treatment with (ii and vii) Nap-FFGSO, (iii and viii) Nap-FFGSO+A, (iv and ix) Nap-FFGSO+B and (v and x) Nap-FFGSO+A+B at 100µg/ml (0.13mM) and 1000µg/ml (1.3mM) concentrations, after 4 hrs of treatment.*

Further, to check the long term cytotoxicity of the peptides, the metabolic activity assay after the treatment of 24hr, 48hr and 72hrs was also performed with both C6 and L929 cells (figure 5.18). The concentration used for the treatment was 1000ug/ml (1.3mM). The cell viability of more than 80% was observed even after 72hrs for all the peptides except for Nap-FFGSO+A, which showed ~70% cell viability upto 72hr. The cytotoxicity study results suggested that the peptides were relatively more compatible with L929 cells than C6 cells.

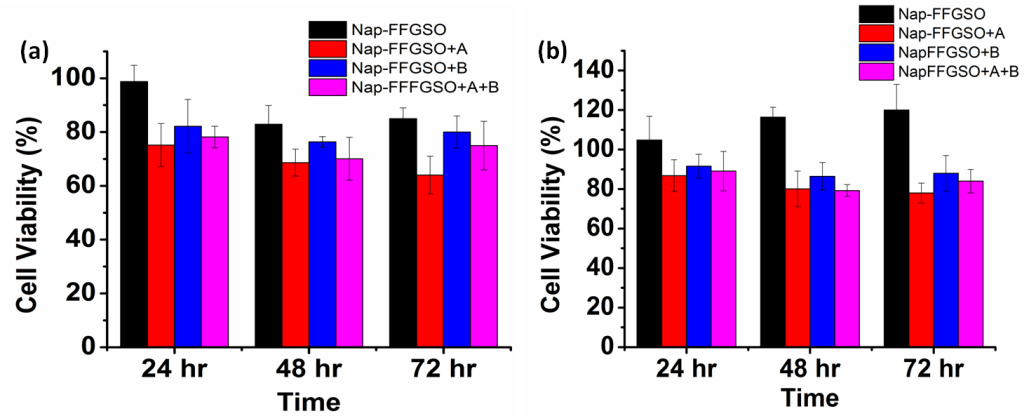

Figure 5.18 *Cytotoxicity studies of CIP-LMP peptide self-assembled structures with (a) C6 cells and (b) L929 cells when treated with peptide concentration of 1000μg/ml (1.3mM) for 24 hrs, 48 hrs and 72hrs.*

5.3.10 2D cell culture

Prior to assessment of these co-assembled gels as substrate for cell culture applications, we checked the integrity of these gels by exposing them to cell culture media. The perfusion of self-assembled gels with culture media also replaces the organic co-solvent (DMSO) used during gelation procedure. [85] The pre-formed hydrogels prepared in 10% DMSO/water were spreaded uniformly over a coverslip and allowed to set for 24 hrs. The cell culture media was added on the top of the gels and kept for perfusion for next 24 hrs, after which the media was replaced. After several washes with culture media, all the three co-assembled gels retained their integrity and remain adhered on the surface of coverslips. It was also expected that the washings with media would reduce the DMSO content of gels and results in better cytocompatability. [86] The gels showed excellent stability upto 7 days which can offer a biocompatible bioactive scaffold for cell culture applications.

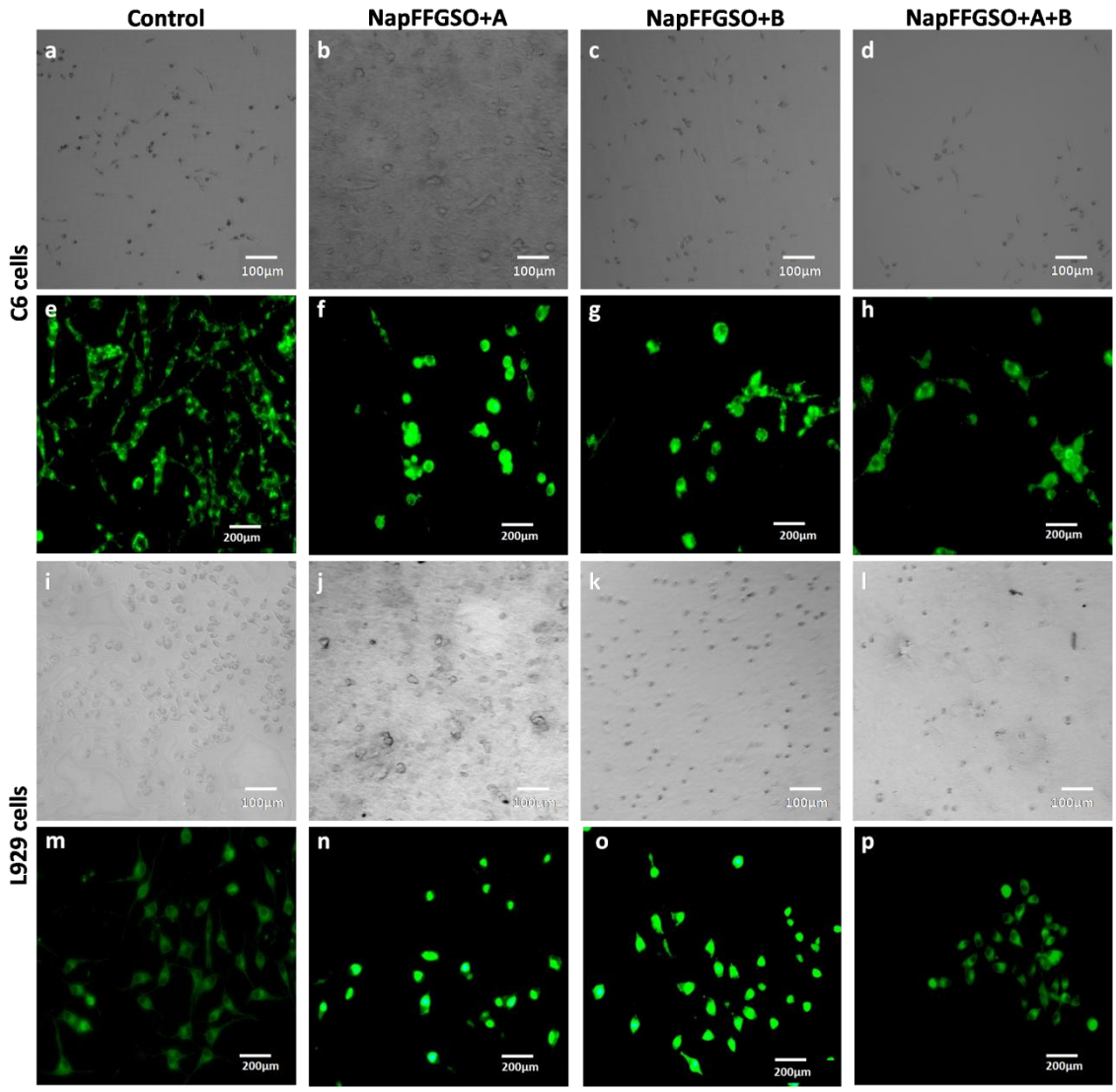

Figure 5.19 *Microscopic evaluation of 2D cultured C6 cells (a-h) and L929 (i-p) cells over collagen laminin co-assembled gels after 24hrs using phase contrast microscopy and fluorescence microscopy.*

Further, these co-assembled hydrogels containing the functionality similar to both collagen as well as laminin proteins were employed for the 2D cell culture applications. [87] Mouse fibroblast L929 and rat glioma C6 cells were seeded onto the surface of each co-assembled gels (10,000 cells/ well in a 6-well plate). For control, the cells were seeded on untreated coverslip. After 24 hrs of seeding, cell adhesion was observed with cells adapting the polyhedral or spindle shapes (figure 5.19). Live/dead staining was performed after 24, 48 and 72 hrs after seeding (figure 5.19, 5.20 & 5.21). The cell density on the co-assembled hydrogels was found to be comparatively less in comparison to control cell culture surface, but the healthy morphology

was retained, similar to that of control. The probable reason for this difference in cell density may arise due to unfamiliar microenvironment, on which they are grown. Initially, cells may take time to adapt to their microenvironment and prolonged cell survival can be observed. [85] Interestingly, after 24 hrs, no dead cells were found (figure 5.19). The cultured cells were checked for viability after 48 hrs and 72 hrs using confocal laser microscopy. All the co-assembled gels were highly biocompatible upto 72 hrs. In corroboration with MTT results, the CIP in combination with hydrophilic laminin derivative, i.e. Nap-FFGSO+ B, which showed thin-entangled long fibrous network exhibited excellent biocompatibility, with a negligible number of dead cells, for both the cell lines (C6 and L929) even after 72 hrs (figure 5.20 and 5.21), whereas Nap-FFGSO+A showed very few dead cells which might probably due to the hydrophobic nature or IKVAV and also shorter fiber lengths might not provide proper support to the growing cells. [88] For both the cell types, the Nap-FFGSO+A+B gels resulted in enhancement of cell density after 72 hrs along with the distinguished cell morphology. However, in case of Nap-FFGSO+A and Nap-FFGSO+B, the clusters of C6 cells were observed which indicates the dominant proliferation phase of the cells, after 72 hrs. [40]

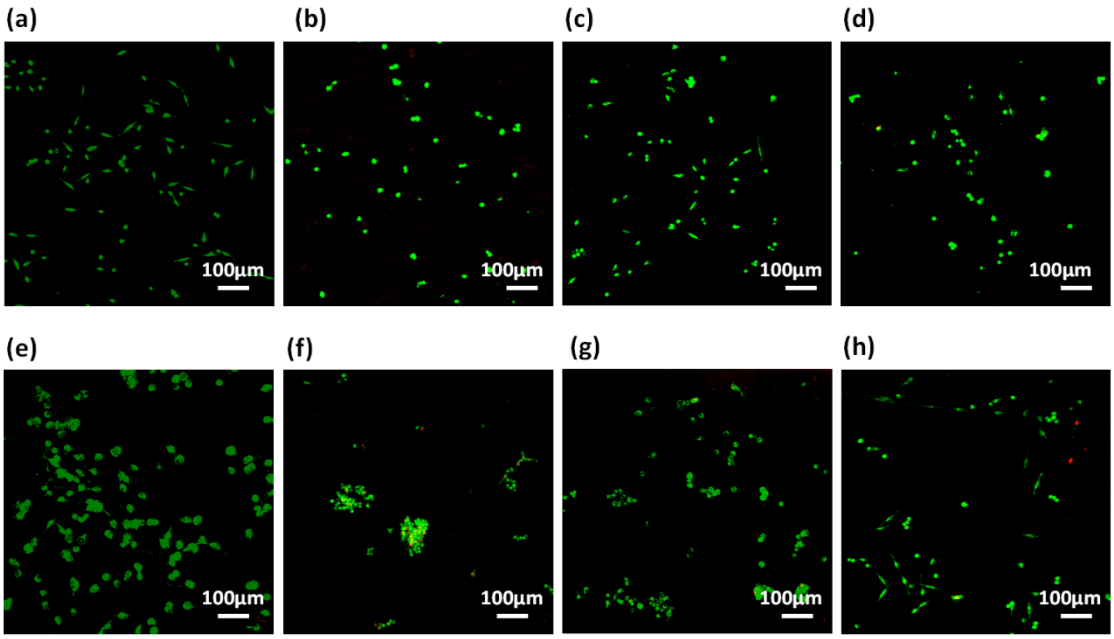

Figure 5.20 *Confocal laser scanning microscopic images using C6 cells showing live (green) and dead (red) cells cultured over (a and e) plastic (control), (band f) Nap-FFGSO+A gels (c and g) Nap-FFGSO+B gels and (d and h) Nap-FFGSO+A+B gels after 48 hrs and 72 hrs respectively.*

In contrast to this, L929 cell density has been relatively increased after 72 hrs, in comparison to 48 hrs, indicating growth phase. The above difference in cell growth and proliferation of different cell types with different peptides clearly shows the differential interaction of each co-assembled gels with the cells. The probable reason for such differential behavior is variable mechanical stiffness and morphology of the hydrogels, along with its biofunctional moieties. We believe that the positive charge of lysine and arginine residues in IKVAV and YIGSR on the co-assembled peptide gels surface is likely to interact with the negative surface of cells and provides suitable cell-matrix interactions. [89, 90] Thus the 2D culture observations clearly indicated that these collagen and laminin mimetic peptide co-assembled gels promote cell adhesion and proliferation and might result in prolonged cell viability.

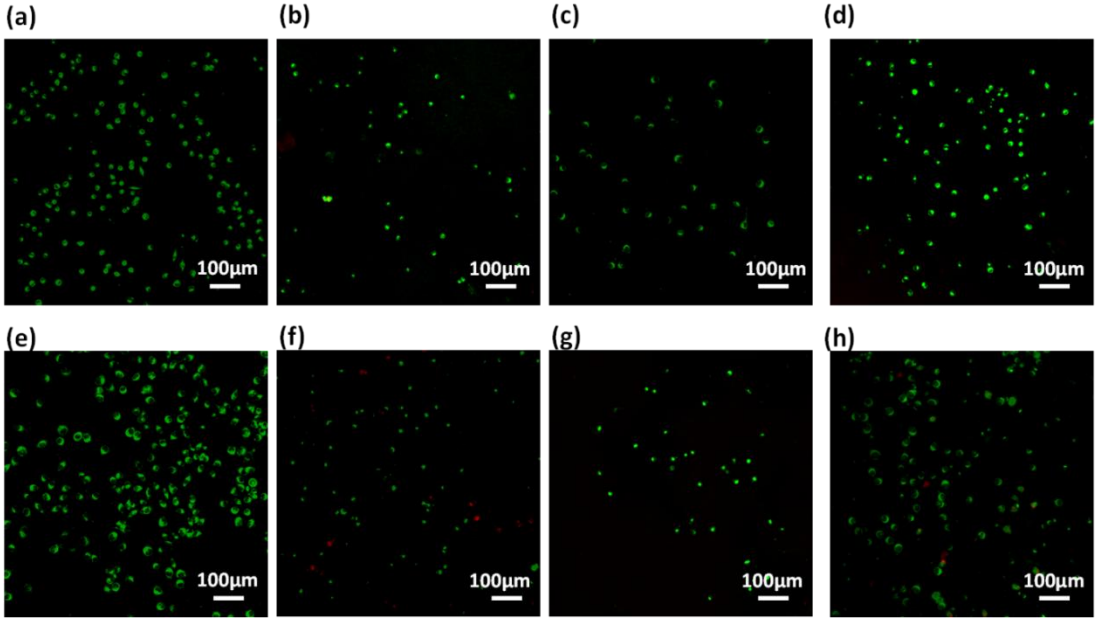

Figure 5.21 *Confocal laser scanning microscopic images using L929 cells showing live (green) and dead (red) cells cultured over (a and e) plastic (control), (band f) Nap-FFGSO+A gels (c and g) Nap-FFGSO+B gels and (d and h) Nap-FFGSO+A+B gels after 48 hrs and 72 hrs respectively.*

5.3.11 Cell Proliferation and Migration Studies

The cell proliferation behaviour of C6 cells and L929 cells in the presence of co-assembled CIP/LMP peptides was quantified by using Alamar blue reduction at different time points. [91] Alamar blue is a resazurin based colorimetric reagent, widely used for quantification of metabolically active cells, without interfering the viability of the cells, over the period of time.

[92] The matrigel was used as positive control to compare the bioactivity of our peptide hydrogels. The results suggested that there was a slight difference in the cell viability of all the three co-assembled gel systems after 24hr, 48hrs, and 72hrs as indicated by nearly similar fluorescence intensity of reduced Alamar blue (figure 5.22 a and b). On comparing the proliferation of cells treated with matrigel with the CIP treated cells, it was found that Nap-FFGSO showed higher proliferation rates than matrigel. While other CIP/LMP combined peptides showed relatively similar proliferation rates to that of matrigel, which indicates the equivalent bioactivity of our developed peptides. The results reveal that our peptide gels showed comparatively better bioactivity than commercial matrigel in promoting proliferation. In comparison to control, all the peptide treated cells showed relatively higher intensity, at all the three time points. It was also observed that the Nap-FFGSO+B showed statistically significant proliferation from 24 hr to 72 hrs, while matrigel treated cells does not show statistically significant difference in the proliferation rates of the cells. This difference was more prominent with L929 cells. This indicates that our designed peptides were non-cytotoxic and promoted proliferation of both types of cells owing to its dual functionality. The results were in agreement with live/dead assay, which indicated increased live cell density in the confocal images of treated cells (figure 5.20 and 5.21).

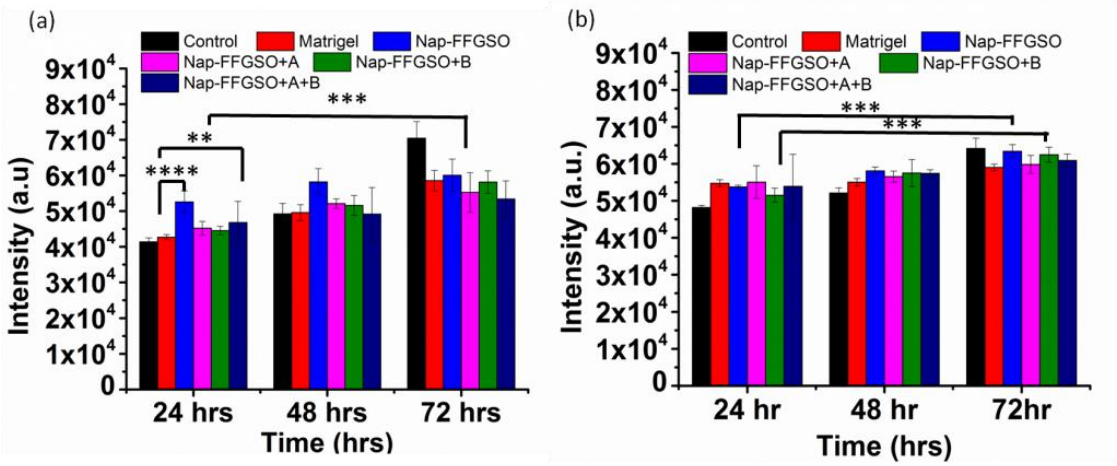

Figure 5.22 *Proliferation studies of (a) C6 cells and (b) L929 cells after treatment with positive control as matrigel and different co-assembled CIP - LMP gels diluted to concentration of 1000µg/ml (1.3mM), after 24 hrs, 48hrs and 72 hrs, using Alamar blue reagent. Data is represented as mean±SD with N=3 indicating $p \leq 0.0059$ for ** , $p \leq 0.003$ for *** and $p \leq 0.0001$ for ****.*

The proliferation was visually studied by migration studies. Proliferation followed by migration is an important phenomenon for wound healing and this wound healing capability of co-

assembled nanostructures were assessed by in vitro scratch assay. [93] This assay is based on the creation of artificial gap in the monolayer of cells which was filled by the migration of proliferating cells present at the edges of the gap. [94] The cell suspension with soluble peptide nanostructures were seeded in 48 well plates. When the 60-70% confluency was reached, a scratch was made using a sterile micropipette tip. The movement of proliferated cells towards scratched region was visualized at different time points, as indicated by the region covered by box in the images in figure 5.23 and 5.24. After 24 hrs, very few numbers of cells invaginate into the marked region. However, in comparison to control (without treatment), the treated wells showed no significant difference in migration rates (figure 5.23 and 5.24).

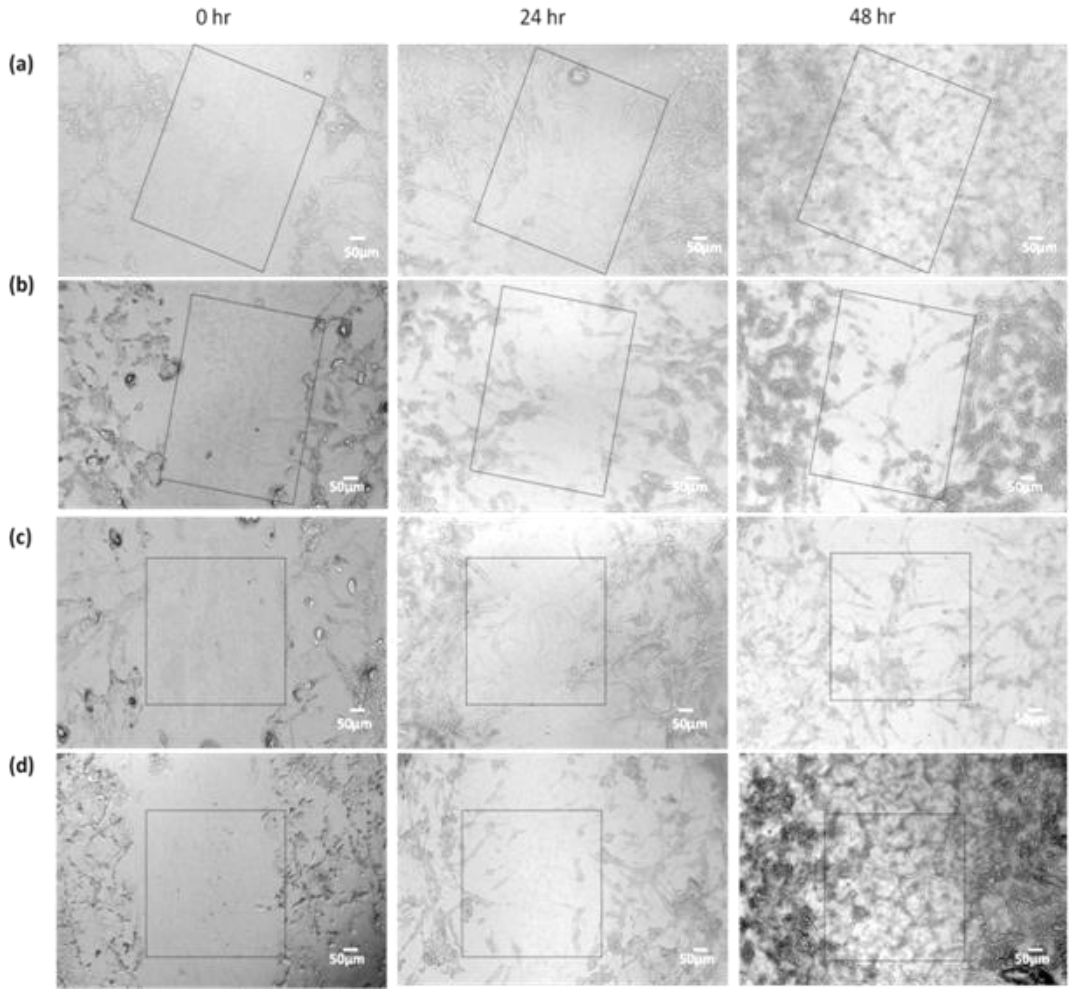

Figure 5.23 *Proliferation and migration response of C6 cells in the presence of diluted peptide gels, assessed by microscopic images of scratched region after 0 hr, 24 hrs and 48 hrs time points after treatment with (a) control (2% DMSO/water, blank), (b) Nap-FFGSO+A, (c) Nap-FFGSO+B and (d) Nap-FFGSO+A+B at concentration of 1000µg/ml (1.3mM).*

The treated cells remain adhered and retain their healthy morphology, even after 48 hrs. In corroboration with cell viability assay results and live/dead microscopic assessement, the hydrophilic Nap YIGSR along with CIP showed higher rate of proliferations, as shown by dense network of cells, after 48 hrs, for C6 cells (figure 5.23). Similarly, for L929 cells, relatively more cells migrate towards the scratched region within 24 hrs and nearly 50% confluency was reached after 48 hrs (figure 5.24). As expected from 2D culture, the hydrophilic laminin derivative in combination with CIP, i.e. Nap-FFGSO, was found to show maximum potency for development of a tissue engineering scaffold. The results demonstrated that collagen-laminin co-assembled peptides supported proliferation and migrations, which are important steps of wound healing and can be promising materials for wound healing applications.

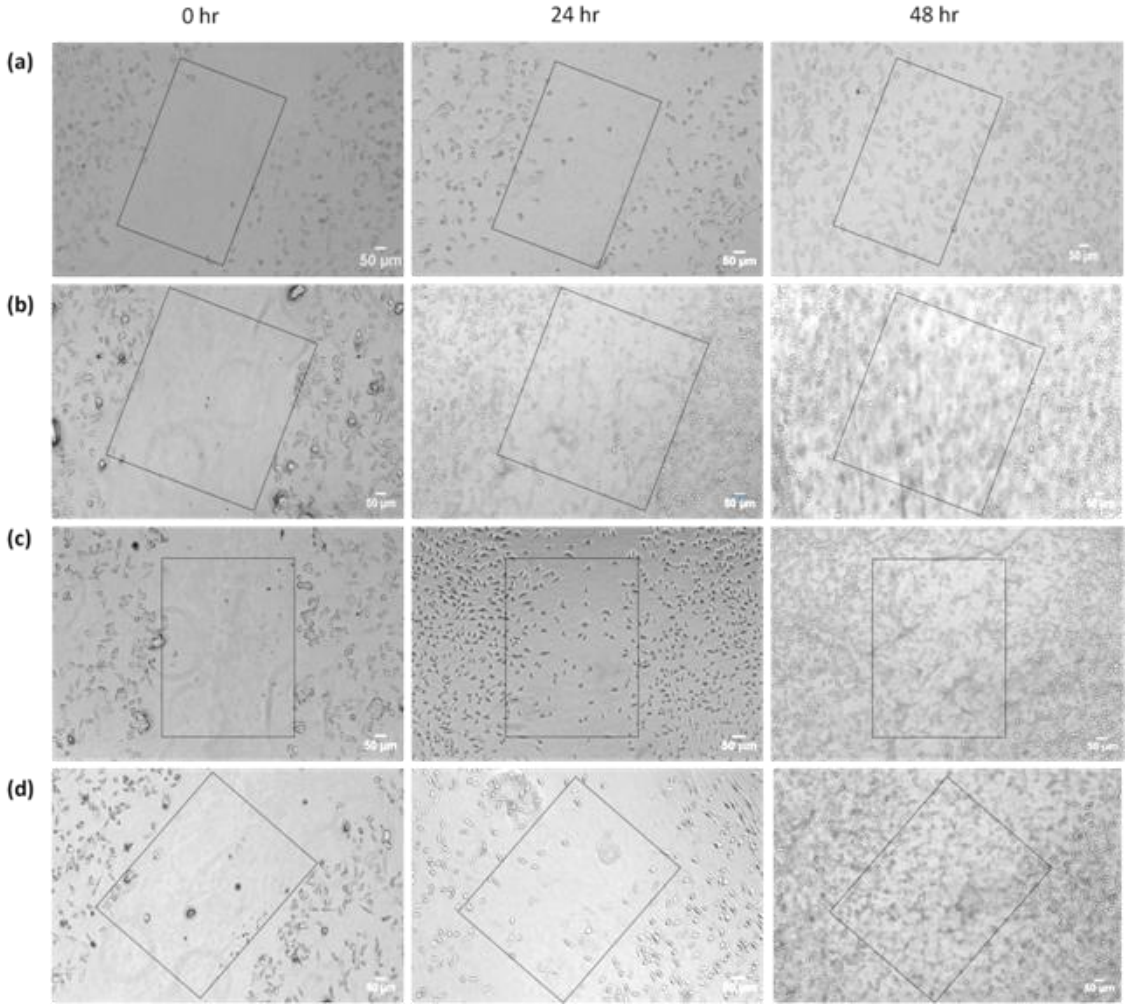

Figure 5.24 *Proliferation and migration response of L929 cells in the presence of diluted peptide gels, assessed by microscopic images of scratched region after 0 hr, 24 hrs and 48 hrs*

time points after treatment with (a) control (2 % DMSO/water, blank), (b) Nap-FFGSO+A, (c) Nap-FFGSO+B and (d) Nap-FFGSO+A+B at concentration of 1000μg/ml (1.3mM).

5.4 Conclusions

In this chapter, we showed the sophisticated design of the self-assembling peptide hydrogel scaffolds which could play dual functionality. The minimalist design approach was used to develop the shortest structural mimic of collagen. By simply exploring non-covalent interactions, we coupled short laminin derived peptides with CIP's without relying on the covalent modification of the collagen peptide monomer. We, for the first time, reported the co-assembled supramolecular hydrogels solely based on bioactive peptides, without any polymeric scaffold or long chain hydrophobic domain. Although, these self-assembled scaffolds form β-turns but they shared similarity with structure and nanofibrous morphology of the collagen, which have the potential to adapt functional attributes of the native collagen protein. The in-vitro studies demonstrated that these scaffolds are highly biocompatible and its dual functionality supports both fibroblasts as well as neuronal cells. The mechanical stiffness along with the chemical functionality determines the cellular response like adhesion, proliferation, and growth. Studies are underway to understand the differential role of both structural protein and functional protein mimics of natural ECM for controlling cell behavior for their prolonged use. In the future, these hydrogels can be explored for the encapsulation of cells for cell delivery for tissue repair applications. We envisage that these collagen-laminin derived biomimetic systems provide an excellent biocompatible platform to be explored for stem cell differentiation and tissue regeneration.

Note:

- ✓ The permission has been granted by authors and corresponding author of the published paper prior to its adoption in the present thesis. The publication associated with this work is:

  Rashmi Jain, Sangita Roy, Designing bioactive scaffold from co-assembled collagen-laminin short peptide hydrogels for controlling cell behavior, *RSC Adv.* 9 (2019) 38745-38759.

5.5 References

1. H. Geckil, F. Xu, H. Zhang, S. Moon, U. Demirci, Engineering hydrogels as extracellular matrix mimics, *Nanomedicine*, 5 (2010) 469–484.

2. Y. Loo, M. Goktas , A. B. Tekinay , M. O. Guler , C. A. E. Hauser, A. Mitraki , Self-assembled proteins and peptides as scaffolds for tissue regeneration, *Adv. Healthcare Mater*. 4 (2015) 2557–2586.
3. H. Chang, C. Li, R. Huang, R. Su, W. Qi , Z. He, Amphiphilic hydrogels for biomedical applications, *J. Mater. Chem. B*, 7 (2019) 2899-2910.
4. N. Singh, M. Kumar, J. F. Miravet, R. V. Ulijn, B. Escuder, Peptide-based molecular hydrogels as supramolecular protein mimics, *Chem. Eur. J*. 23 (2017) 981-993.
5. K. Liang, K. Hyun Bae and M. Kurisawa, Recent advances in the design of injectable hydrogels for stem cell-based therapy, *J. Mater. Chem. B*, 7 (2019) 3775-3791.
6. S. Wan, S. Borland, S. M. Richardson, C. L. R. Merry, A. Saiani, J.E. Gough, Self-assembling peptide hydrogel for intervertebral disc tissue engineering, *Acta Biomater*. 46 (2016) 29–40.
7. N. D. Evans, E. Gentleman, The role of material structure and mechanical properties in cell–matrix interactions, *J. Mater. Chem. B*, 2 (2014) 2345–2356.
8. H. Green, G. Ochbaum, A. Gitelman-Povimonsky, R.Bitton, H. Rapaport, RGD-presenting peptides in amphiphilic and anionic β-sheet hydrogels for improved interactions with cells, *RSC Adv*. 8 (2018) 10072–10080.
9. J. Luo, Y. W. Tong, Self-Assembly of collagen-mimetic peptide amphiphiles into biofunctional nanofiber, *ACS Nano*, 5 (2011) 7739–7747.
10. M. M. Islam, R. Ravichandran, D. Olsen, M. K. Ljunggren, P Fagerholm, C. J. Lee, M. Griffith, J. Phopase, Self-assembled collagen-like-peptide implants as alternatives to human donor corneal transplantation, *RSC Adv*. 6 (2016) 55745–55749.
11. O'Leary, J. A. Fallas, E. L. Bakota, M. K. Kang, J. D. Hartgerink, Multi-hierarchical self-assembly of a collagen mimetic peptide from triple helix to nanofibre and hydrogel, *Nat. Chem.* 3 (2011) 821-828.
12. V. A. Kumar, N. L.Taylor, A. A. Jalan, L. K. Hwang, B. K. Wang, J. D. Hartgerink, A Nanostructured Synthetic collagen mimic for hemostasis, *Biomacromolecules*, 15 (2014) 1484−1490.
13. S. M. Yu, Y. Li, F. Kim, Collagen Mimetic Peptides: progress towards functional applications, *Soft Matter*, 7 (2011) 7927–7938.,
14. O. D. Krishna, K. L. Kiick, Supramolecular assembly of electrostatically stabilized, hydroxyproline-lacking collagen-mimetic peptides, *Biomacromolecules*, 10 (2009) 2626–2631.

15. L. Yao, M. He, D. Li, H. Liu, J. Wua, J. Xiao, Self-assembling bolaamphiphile-like collagen mimetic peptides, *New J. Chem*. 42 (2018) 7439-7444.
16. M. Bansal, C. Ramakrishnan, G. N. Ramachandran, Stabilization of the collagen structure by hydroxyproline residues, *Proc. Indian Acad. Sci*. 82 (1975) 152-164.
17. W. Wang, G. Li, W. Zhang, J. Gao, J. Zhang, C. Li, D. Ding, D. Kong, Reduction-triggered formation of EFK8 molecular hydrogel for 3D cell culture, *RSC Adv*. 4 (2014) 30168–30171.
18. T. Luo, K. L. Kiick, Collagen-like peptide bioconjugates, *Bioconjugate Chem.* 28 (2017) 816−827.
19. B. Brodsky, G. Thiagarajan, B. Madhan, K. Kar, Triple-helical peptides: an approach to collagen conformation, stability, and self-association, *Biopolymers*, 89 (2008) 345-53
20. J. Sun, Y. Guo, R. Xing, T. Jiao, Q. Zou, X. Yan, Synergistic in vivo photodynamic and photothermal antitumor therapy based on collagen-gold hybrid hydrogels with inclusion of photosensitive drugs, *Colloids and Surfaces A: Physicochem. Eng. Aspects*, 514 (2017) 155-160.
21. R. Xing, L. Liu, T. Jiao, N. Zhang, K. Ma, R. Zhang, Q. Zou, G. Ma, X. Yan, An injectable self-assembling collagen–gold hybrid hydrogel for combinatorial antitumor photothermal/ photodynamic therapy, *Adv. Mater*. 28 (2016) 3669–3676.
22. S. Rele, Y. Song, R. P. Apkarian, Z. Qu, V. P. Conticello, E. L. Chaikof, D-Periodic Collagen-Mimetic Microfibers, *J. Am. Chem. Soc*. 129 (2007) 14780–14787.
23. T. Jiang, C. Xu, Y. Liu, Z. Liu, J. S. Wall, X. Zuo, T. Lian, K. Salaita, C. Ni, D. Pochan, V. P. Conticello, Structurally Defined Nanoscale Sheets from Self-Assembly of Collagen-Mimetic Peptides, *J. Am. Chem. Soc.* 136 (2014) 4300–4308.
24. M. A. Cejas, W. A. Kinney, C. Chen, G. C. Leo, B. A. Tounge, J. G. Vinter, P. P. Joshi, B. E Maryanoff, Collagen-Related Peptides: Self-Assembly of Short, Single Strands into a Functional Biomaterial of Micrometer Scale, *J. Am. Chem. Soc*. 129 (2007) 2202–2203.
25. M. A. Cejas, W. A. Kinney, C. Chen, J. G. Vinter, H. R. Almond, K. M. Balss, C. A. Maryanoff, U. Schmidt, M. Breslav, A. Mahan, E. Lacy, B. E. Maryanoff, Thrombogenic collagen-mimetic peptides: Self-assembly of triple helix-based fibrils driven by hydrophobic interactions, *Proc. Natl. Acad. Sci*. 105 (2008) 8513–8518.
26. C. C. Chen, W. Hsu, T. C. Kao, J. C. Horng, Self-assembly of short collagen-related peptides into fibrils via cation-π interactions, *Biochemistry*, 50 (2011) 2381–2383.

27. D. E. Przybyla, C. M. R. Perez, J. Gleaton, V. Nandwana, J. Chmielewski, Hierarchical assembly of collagen peptide triple helices into curved disks and metal ion-promoted hollow spheres, *J. Am. Chem. Soc.* 135 (2013) 3418–3422.
28. M. M. Pires, J. Chmielewski, Self-assembly of Collagen peptides into microflorettes via metal coordination, *J. Am. Chem. Soc.* 131 (2009) 2706–2712.
29. M. He, L. Wang, J. Wu, J. Xiao, Ln3+ -mediated self-assembly of a collagen peptide into luminescent banded helical nanoropes, *Chem. Eur. J.* 22 (2016) 1914–1917.
30. M. M. Pires, J. Lee, D. Ernenwein, J. Chmielewski, Controlling the morphology of metal-promoted higher ordered assemblies of collagen peptides with varied core lengths, *Langmuir*, 28 (2012) 1993–1997.
31. W. Hsu, Y. L. Chen, J. C. Horng, Promoting self-assembly of collagen-related peptides into various higher-order structures by metal−histidine coordination, *Langmuir*, , 28 (2012) 3194–3199.
32. B. Sarkar, L. E. O'Leary, J. D. Hartgerink, Self-assembly of fiber-forming collagen mimetic peptides controlled by triple-helical nucleation, *J. Am. Chem. Soc*. 136 (2014) 14417–14424.
33. K. McGuinness, I. J. Khan, V. Nanda, Morphological Diversity and Polymorphism of Self-Assembling Collagen Peptides Controlled by Length of Hydrophobic Domains, *ACS Nano*, 8 (2014) 12514-12523.
34. T. Luo, M. A. David, L.C. Dunshee, R. A. Scott, M. A. Urello, C. Price, K. L Kiick, Thermoresponsive elastin-b-collagen-like peptide bioconjugate nanovesicles for targeted drug delivery to collagen-containing matrices, *Biomacromolecules*, 18 (2017) 2539-2551.
35. C. M. Yamazaki, S. Asada, K. Kitagawa, T. Koide, Artificial collagen gels via self-assembly of de novo designed peptides, *Biopolymers*, 90 (2008) 816–823.
36. P. J. Skrzeszewska, F. A. de Wolf, M. W. T. Werten, A. P. H. A. Moers, M. A. C. Stuart, J. van der Gucht, Physical gels of telechelic triblock copolymers with precisely defined junction multiplicity, *Soft Matter*, 5 (2009) 2057–2062.
37. Y. Hu, H. Wang, J. Wang, S. Wang, W. Liao, Y. Yang, Y. Zhang, D. Kong, Z. Yang, Supramolecular hydrogels inspired by collagen for tissue engineering, *Org. Biomol. Chem*. 8, (2010) 3267–3271.
38. O. Uysal, E. Arslan, G. Gulseren, M. C. Kilinc, I. Dogan, H. Ozalp, Y. S. Caglar, M. O. Guler, A. B. Tekinay, Collagen Peptide Presenting Nanofibrous Scaffold for Intervertebral Disc Regeneration , *ACS Appl. Bio Mater*, 2 (2019) 1686-1695.

39. M. D. Shoulders, R. T. Raines, Collagen structure and stability, *Annu. Rev. Biochem.* 78 (2009) 929–958.
40. C. Deister, S. Aljabari, S. E. Schmidt, Effects of collagen 1, fibronectin, laminin and hyaluronic acid concentration in multi-component gels on neurite extension, *J. Biomater. Sci. Polym. Ed*. 18 (2007) 983-97.
41. S. P. Baldwin, C. E. Krewson, W. M. Saltzman, PC12 cell aggregation and neurite growth in gels of collagen, laminin and fibronectin, *Int. J. Deul Neuroscience*, 14 (1996) 351–3641.
42. R. J. Linnola, M. Sund, R. Ylo¨nen, T. Pihlajaniemi, Adhesion of soluble fibronectin, laminin, and collagen type IV to intraocular lens materials, *J Cataract Refract Sur.* 25 (1999) 1486-91.
43. J. P. Jung, A. K. Nagaraj, E. K. Fox, J. S. Rudra, J. M. Devgun, J. H. Collier, Co-assembling peptides as defined matrices for endothelial cells, *Biomaterials*, 30 (2009) 2400–2410.
44. K. Tashiro, G. C. Sephel, B. Weeks, M. Sasaki, G. R. Martin, H. K. Kleinman, Y. Yamada, A synthetic peptide containing the IKVAV sequence from the a chain of laminin mediates cell attachment, migration, and neurite outgrowth, *J. Biol. Chem*. 264 (1989) 16174-16182.
45. B. Mammadov, M. Sever, M. Gecer, Fatih Zor, S. Ozturk, H. Akgun, U. H. Ulas, Z. Orhan, M. O. Guler, A. B. Tekinay, Sciatic nerve regeneration induced by glycosaminoglycan and laminin mimetic peptide nanofiber gels, *RSC Adv.* 6 (2016) 110535–110547.
46. A. L. Rodriguez, T. Y. Wang, K. F. Bruggeman, C. C. Horgan, E. Li, R. J. Williams, C. L. Parish, D. R. Nisbet, In vivo assessment of grafted cortical neural progenitor cells and host response to functionalized self-assembling peptide hydrogels and the implications for tissue repair, *J. Mater. Chem. B*, 2 (2014) 7771-7778.
47. C. C. Horgan, A. L. Rodriguez, R. Li, K. F. Bruggeman, N. Stupka, J. K. Raynes, L. Day, J. W. White, R. J. Williams, D. R. Nisbet, Characterisation of minimalist co-assembled fluorenylmethyloxycarbonyl self-assembling peptide systems for presentation of multiple bioactive peptides, *Acta Biomater*. 38 (2016) 11–22.
48. R. O. Labrador, M. Butı´, X. Navarro, Influence of collagen and laminin gels concentration on nerve regeneration after resection and tube repair, *Exp. Neurol*. 149 (1998) 243–252.
49. K. D. Newman, C. R. Mclaughlin, D. Carlsson, F. Li, Y. Liu, M. Griffith, Bioactive hydrogel-filament scaffolds for nerve repair and regeneration, *Int. J. Artif. Organs*, 29 (2006) 1082-1091.

50. S. Sur, M. O. Guler, M. J. Webber, E. T. Pashuck, M. Ito, S. I. Stupp, T. Launey, Synergistic regulation of cerebellar Purkinje neuron development by laminin epitopes and collagen on an artificial hybrid matrix construct, *Biomater. Sci.* 2 (2014) 903.
51. M. Hiraoka, K. Kato, T. Nakaji-Hirabayashi, H. Iwata, Enhanced survival of neural cells embedded in hydrogels composed of collagen and laminin-derived cell adhesive peptide, *Bioconjugate Chem*. 20 (2009) 976–983.
52. J. H. Collier, J. S. Rudra, J. Z. Gasiorowski, J. P. Jung, Multicomponent extracellular matrices based on peptide self-assembly, *Chem. Soc. Rev*. 39 (2010) 3413-3424.
53. Y. Zheng, S. Ji, A. Czerwinski, F. Valenzuela, M. Pennington, S. Liu, FITC-conjugated cyclic rgd peptides as fluorescent probes for staining integrin αvβ3/αvβ5 in tumor tissues, *Bioconjugate Chem.* 25 (2014)1925−1941.
54. C. B. Berkholtz, B. E. Lai, T. K. Woodruff, L. D. Shea, Distribution of extracellular matrix proteins type I collagen, type IV collagen, fibronectin, and laminin in mouse folliculogenesis, *Histochem Cell Biol.* 126 (2006) 583–592.
55. M. J. Horacek, J. C. Thompson, M. O. Dada, L. Terracio, The extracellular matrix components laminin, fibronectin, and collagen IV are present among the epithelial cells forming Rathke's pouch, *Acta Anat (Basel).* 147 (1993) 69-74.
56. R. Jain, G. Khandelwal, S. Roy, Unraveling the design rules in ultrashort amyloid-based peptide assemblies toward shape-controlled synthesis of gold nanoparticles, *Langmuir*, 35 (2019) 5878-5889.
57. X. Du, J. Zhou, J. Shi, B. Xu, Supramolecular hydrogelators and hydrogels: from soft matter to molecular biomaterials, *Chem. Rev*. 115 (2015) 13165−13307.
58. Y. Zhang, Y. Kuang, Y. Gao, B. Xu, Molecule motifs for self-assembly in water and the formation of biofunctional supramolecular hydrogels, *Langmuir*, 27 (2011) 529–537.
59. K. Kar, S. Ibrar, V. Nanda, T. M. Getz, S. P. Kunapuli, B. Brodsky, Aromatic interactions promote self-association of collagen triple-helical peptides to higher order structures biochemistry, 48 (2009) 7959–7968.
60. C. J. Bowerman, W. Liyanage, A. J. Federation, B. L. Nilsson, Tuning β-sheet peptide self-assembly and hydrogelation behavior by modification of sequence hydrophobicity and aromaticity, *Biomacromolecules*, 12 (2011) 2735–2745.
61. C. Chen, Y. Zhang, Z. Hou, X. Cui, Y. Zhao, H. Xu, Rational design of short peptide-based hydrogels with mmp-2 responsiveness for controlled anticancer peptide delivery, *Biomacromolecules*, 18 (2017) 3563-3571.

62. A. Kroes-Nijboer, P. Venema, J. Bouman, E. van der Linden, The Critical Aggregation Concentration of β-Lactoglobulin-Based Fibril Formation, *Food Biophysics*, 4 (2009) 59–63.
63. L. Chen, J. Raeburn, S. Sutton, D. G. Spiller, J Williams, J. S. Sharp, P. C. Griffiths, R. K. Heenan, S. M. King, A. Paul, S. Furzeland, D. Atkins, D. J. Adams, Tuneable mechanical properties in low molecular weight gels, *Soft Matter*, 7 (2011) 9721–9727.
64. C. Colquhoun, E. R. Draper, E.G. B. Eden, B. N. Cattoz, K. L. Morris, L. Chen, T. O. McDonald, A. E. Terry, P. C. Griffiths, L. C. Serpell, D. J. Adams, Controlling the network type in self-assembled dipeptide hydrogels, *Nanoscale* , 6 (2014) 13719–13725.
65. C-L. Shen, R. M. Murphy, Solvent effects on self-assembly of 1b-amyloid peptide, *Biophys. J.* 69 (1995) 640-651.
66. J. B. Guilbaud, C. Rochas, A. F. Miller, A. Saiani, Effect of enzyme concentration of the morphology and properties of enzymatically triggered peptide hydrogels, *Biomacromolecules*, 14 (2013) 1403−1411.
67. N. Nandi, K. Gayen, S. Ghosh, D. Bhunia, S. Kirkham, S. K. Sen, S. Ghosh, I. W. Hamley, A. Banerjee, Amphiphilic peptide-based supramolecular, noncytotoxic, stimuli responsive hydrogels with antibacterial activity, *Biomacromolecules*, 18 (2017) 3621−3629.
68. A. Baral, S. Roy, S. Ghosh, D. Hermida-Merino, I. W. Hamley, A. Banerjee, A peptide-based mechano-sensitive, proteolytically stable hydrogel with remarkable antibacterial properties, *Langmuir*, 32 (2016) 1836-1845.
69. C. K. Thota, N. Yadav, V. S. Chauhan. A novel highly stable and injectable hydrogel based on a conformationally restricted ultrashort peptide, *Sci. Rep.* 6 (2016) 1-12.
70. C. Yan, A. Altunbas, T. Yucel, R. P. Nagarkar, J. P. Schneider, D. J. Pochan, Injectable solid hydrogel: mechanism of shear-thinning and immediate recovery of injectable β-hairpin peptide hydrogels, *Soft Matter*, 6 (2010) 5143–5156.
71. C. Shu, T. Li, W. Yang, D. Li, S. Ji, L. Ding, Amphotericin B-conjugated polypeptide hydrogels as a novel innovative strategy for fungal infections, *R. Soc. open sci*. 5 (2018) 171814.
72. Z. Yang, G. Liang, M. Ma, Y. Gaoa, B. Xu, Conjugates of naphthalene and dipeptides produce molecular hydrogelators with high efficiency of hydrogelation and superhelical nanofibers, *J. Mater. Chem.* 17 (2007) 850–854.
73. E. Vass, M. Hollo´si, F. Besson, R. Buchet, Vibrational spectroscopic detection of beta- and gamma-turns in synthetic and natural peptides and proteins, *Chem. Rev.* 103 (2003) 1917-1954.

74. J. Kong, S. Yu, Fourier Transform Infrared Spectroscopic Analysis of Protein Secondary Structures, *Acta Biochim. Biophys. Sin*. 39 (2007) 549–559.
75. M. Biancalana, S. Koide, Molecular mechanism of Thioflavin-T binding to amyloid fibrils, *Biochim. Biophys. Acta*, 1804 (2010) 1405–1412.
76. M. J. Krysmann, V. Castelletto, I. W. Hamley, Fibrillisation of hydrophobically modified amyloid peptide fragments in an organic solvent, *Soft Matter*, 3 (2007) 1401–1406.
77. P. Sharma, H. Kaur, S. Roy, Inducing differential self-assembling behaviour in ultrashort peptide hydrogelators using simple metal salts, *Biomacromolecules*, 207 (2019) 2610-2624.
78. S. Onogi, H. Shigemitsu, T. Yoshii, T. Tanida, M. Ikeda, R. Kubota, I. Hamachi, In situ real-time imaging of self-sorted supramolecular nanofibers, *Nat. Chem.* 8 (2016) 743-752.
79. T. Eljezi, P. Pinta, D. Richard, J. Pinguet, J-M. Chezal, M-C. Chagnon, V. Sautou, G. Grimandi, E. Moreau, In vitro cytotoxic effects of DEHP-alternative plasticizers and their primary metabolites on a L929 cell line, *Chemoisphere*, 173 (2017) 452-459.
80. J. Raeburn, C. Mendoza-Cuenca, B. N. Cattoz, M. A. Little, A. E. Terry, A. Z. Cardoso, P. C. Griffiths and D. J. Adams, The effect of solvent choice on the gelation and final hydrogel properties of Fmoc-diphenylalanine, *Soft Matter*, 11 (2015) 927-935.
81. A. D. Martin, A. B. Robinson, P. Thordarson, Biocompatible small peptide super-hydrogelators bearing carbazole functionalities, *J. Mater. Chem. B*, 3 (2015) 2277–2280.
82. P. Gavel, D. Dev, H. S. Parmar, S. Bhasin, A. K. Das, Investigations of peptide-based biocompatible injectable shape-memory hydrogels: differential biological effects on bacterial and human blood cells, *ACS Appl. Mater. Interfaces*, 10 (2018) 10729-10740.
83. Z. Tu, M. Volk, K. Shah, K. Clerkin, J. F. Liang, Constructing bioactive peptides with pH-dependent activities, *Peptides*, 30 (2009) 1523–1528.
84. N. Habibi, N. Kamaly, A. Memic, H Shafiee, Self-assembled peptide-based nanostructures: Smart nanomaterials toward targeted drug delivery, *Nano Today*, 11 (2016) 41–60.
85. W. Liyanage, K. Vats, A. Rajbhandary, D.S. W. Benoit, B. L. Nilsson, Multicomponent dipeptide hydrogels as extracellular matrix-mimetic scaffolds for cell culture applications, Chem. Commun. 51 (2015) 11260-11263.
86. H. Choi, M. Go, Y. Cha, Y. Choi, K-Y Kwon, J. H. Jung, A facile method to fabricate hydrogels from DMSO polymer gels via solvent exchange, *New J. Chem*. 41 (2017) 4793-4796.
87. K. M. Hainline, F. Gu, J. F. Handley, Y. F. Tian, Y. Wu, L. de Wet, D. J. Vander Griend, J. H. Collier, Self-assembling peptide gels for 3d prostate cancer spheroid culture, *Macromol. Biosci*. 19 (2019) 1800249.

88. A. T. Wood, D. Everett, S. Kumar, M. K. Mishra, V. Thomas, Fiber length and concentration: Synergistic effect on mechanical and cellular response in wet-laid poly (lactic acid) fibrous scaffolds, *J. Biomed. Mater. Res. B Appl Biomater*. 107 (2019) 332-341.
89. S. A. Makohliso, R. F. Valentini, P. Aebischer, Magnitude and polarity of a fluoroethylene propylene electret substrate charge influences neurite outgrowth *in vitro, J. Biomed. Mater. Res.* 27 (1993) 1075–1085.
90. G. B. Schneider, A. English, M. Abraham, R. Zaharias, C. Stanford, J. Keller, The effect of hydrogel charge density on cell attachment, *Biomaterials*, 25 (2004) 3023-8.
91. W. Sun, T. Incitti, C. Migliaresi, A. Quattrone, S. Casarosa, A. Motta, Viability and neuronal differentiation of neural stem cells encapsulated in silk fibroin hydrogel functionalized with an IKVAV peptide, *J Tissue Eng. Regen. Med*. 11 (2017) 1532–1541.
92. G. Damodaran, R. Collighan, M. Griffin, H. Navsaria, A. Pandit, Tailored laminin-332 α3 sequence is tethered through an enzymatic linker to a collagen scaffold to promote cellular adhesion, *Acta Biomater.* 5 (2009) 2441–2450.
93. X. Zhang, X. Kang, L. Jin, J. Bai, W. Liu, Z. Wang, Stimulation of wound healing using bioinspired hydrogels with basic fibroblast growth factor, *Int. J. Nanomedicine*, 13 (2018) 3897 -3906.
94. C-C. Liang, A. Y. Park, J-L. Guan, In vitro scratch assay: a convenient and inexpensive method for analysis of cell migration in vitro, *Nat. Protocols*, 2 (2007) 329-333.

Chapter 6

Understanding the structure-function correlation of ultra short amyloid peptides towards synthesizing organic-inorganic hybrids

6.1 Introduction

As evident from previous chapters that self-assembling peptides offer tremendous opportunities for developing functional nanomaterials, making them suitable for multifarious applications like drug delivery, cell-culture, tissue engineering, catalysis, etc. [1-10] However, in addition to diverse functionality of peptide hydrogels, a well knitted fibrous network with viscoelastic nature of the hydrogels make them indispensable material for controlling many chemical reactions, including structure directed metal nanoparticle synthesis. [11, 12] Short aromatic peptides are the interesting candidates to be explored for in situ syntheses of metal-nanoparticles. [13, 14] The non-covalent interactions during the peptide self-assembly render highly dynamic and responsive nano-structured environments, which can be tuned by varying the hydrophobicity, overall charge density and sequence pattern of the amino acids. [15] Therefore, it is highly desirable to understand the structural and mechanistic aspects of self-assembling short peptides and find its close correlation with their structural hierarchy and mechanical functions. These findings could be an ideal guiding tool for controlled synthesis of organic-inorganic hybrid nanomaterials. [16]

The formation of the fibrillar, ordered, supramolecular structures of proteins/peptides have significant pathological implications and can be related to the amyloid based assemblies. [17] The insights from previous studies on amyloid peptide self-assembly provide the basis of designing short peptide sequences capable of forming complex hierarchical nanostructures. [18, 19] Gazit and his group for the first time, demonstrated the formation of nanotubes from diphenylalanine moieties and suggested the possible role of π- stacking in the self-assembly of amyloid fibrils. [1] Significant reports indicated the use of variety of synthetic aromatic moieties such as Fmoc [20-25], naphthalene [26, 27], pyrene [28, 29], benzyloxy-carbonyl [30-32] and azobenzene [33] to turn short peptide motifs (typically di- to penta-) into efficient gelators. However limited studies were focused on finding the detailed structure-function relationship of these self-assembling peptides which offers a great challenge in predicting the emergent properties of resulting materials. For example, Adam's group investigated the influence of varying hydrophobicity on gelation using a library of Fmoc-peptides, having different constituent amino acids. [34] In a similar line, Xu's group demonstrated the role of aromatic-aromatic interactions as a powerful driving force for the formation of supramolecular hydrogels. [27] Hughes et al., elucidated the sequence/structure relationships in Fmoc-dipeptide-methyl esters which can form thermodynamically favoured structures using enzyme-assisted self-assembly. [35] A recent report by B. Nilsson's group provided an insight into role of amino acid hydrophobicity and sequence pattern on controlling

the self-assembly behavior of the octapeptide. They also showed how non-polar substitutions can be exploited to tune the properties of resulting self-assembled materials. [36] However, none of these studies explored a systematic investigation to elaborate the simultaneous participation of aromatic capping as well as altered peptide sequence pattern towards controlling their intermolecular interactions and hence their self-assembling behavior in water, which can have significant implications in the function induced in the final gel phase material. Such correlation of structural variation with the functional properties of the variable nanostructures is certainly not elaborated in the literature. Therefore, such investigation will help to identify the relative importance of the aromatic stacking interactions over the hydrogen bonding/hydrophobic interactions of the peptide backbone, which would be useful for formulating the rules for rational molecular design of short self-assembling peptides.

Furthermore, the inspiration for utilization of proteins and peptides for in situ syntheses of metal nanoparticles is derived from natural biomineralization process. [37] Gold nanoparticles have attracted considerable interest in the field of sensing, biological imaging, catalysis, therapeutics and diagnostics due to their size tunable optoelectronic properties. [12, 38, 39] Most popular methods of gold nanoparticle synthesis employ external reducing agents and long chain cationic amphiphiles to stabilize the nanoparticles, which make them unfavourable for the biological applications. [40] Although synthesis of gold nanoparticles has made great progress, controlling their shape, size and surface chemistry remains as a challenge. [41] To this end, low molecular weight peptide hydrogels offer great opportunity to be used as templates for controlling the shape and size of the nanoparticles. [13, 14, 42] In an elaborate study by Tan et al., the role of all 20 natural amino acids and several combinatorial peptide sequences in the reduction of chloroaurate ions to form gold nanoparticles was investigated. [43] This study developed the understanding of peptide sequence-crystal growth relationships at the amino acid level.

In particular, the peptide hydrogel network offers dual advantages: firstly acts as a nanoreactor to catalyze the reduction of the gold solution to nanoparticles and secondly the fibrillar entangled network prevents the nanoparticle aggregation. So far, a very few number of organogelators and hydrogelators has been reported for the synthesis of gold nanoparticles. [44, 45] For example, Banerjee and his group employed tyrosine containing oligopeptides for the synthesis of gold and silver nanoparticles. [46] The pioneering work by Das's group demonstrates the in situ preparation of gold nanoparticles of different shapes using a tryptophan based cationic hydrogelator. [47] A very recent report by Ulijn's group demonstrated a new perspective of biocatalytic self-assembly to tune the size of gold nanoparticles. [48] The study clearly

demonstrates that the controlled hydrolysis can regulate the rate of reduction of Au^{+3} to Au^{0}. All these bio-inspired gold nanoparticle synthesis relies on the use of aromatic functional amino acid residues. However, none of these reports address the role of aliphatic functional amino acid based gelators towards controlling the gold nanoparticle synthesis. Hence, we were curious to explore the effect of nature of redox-active moiety (aromatic or aliphatic) in controlling the shape and size of the in situ synthesized gold nanoparticles. This systematic study will open up new avenues for the rational design of peptides for shape and size-tunable synthesis of metal nanostructures.

Our rationally designed library of aromatic dipeptides attempts to elucidate the role of aromatic capping as well as in the specific amino acid sequence in the peptide backbone towards controlling their self-assembling behavior. To the best of our knowledge, this is the first systematic report that attempts to establish the structure-function relationship with a minimalist peptide design, through controlled variation at the N-terminal and C-terminal simultaneously in a single gelator domain. Our ultimate objective is to explore this understanding for further shape and size-controlled synthesis of metal nanoparticles. For the first time, we established a comparison between reduction properties of the aliphatic and aromatic amino acids to control the shape and size of the synthesized nanoparticles. The reports on the synthesis of the rectangular plate-like gold nanoparticles are very rare and by far, this is the first report on rectangular shaped nanoparticles synthesis using low molecular weight peptide hydrogels. We envisaged that the better understanding of sequence-structure relationship will not only provide the basis for designing the biomaterials of desired properties but also helps in tuning the functional behavior of these nanoscale organic-inorganic hybrids.

6.2 Experimental Section

6.2.1 Materials

All N- and C- terminal protected amino acids, HBTU (O-(Benzotriazol-1-yl)-N,N,N′,N′-tetramethyluronium hexa-fluoro-phosphate) and DIPEA (N,N-Diisopropylethylamine) were purchased from Sigma- Aldrich and used as recieved. All the other reagents and solvents used were obtained from Merck.

6.2.2 Synthesis

The reported dipeptides were synthesized using solution phase synthesis. The steps for the synthesis differ for all the three aromatic capping moieties. A single step synthesis was done for Fmoc-capped peptides. The Fmoc-Phe is coupled with tert-butyl ester protected amino acid in

the presence of HBTU and DIPEA. The C-terminal ester group is deprotected using 95% trifluoroacetic acid in dichloromethane. Similarly, Cbz-protected peptides were prepared by coupling Cbz -Phe with different methyl ester protected amino acids followed by deprotection of methyl ester group by using THF / NaOH, followed by acid neutralization leading to precipitation of the dipeptide product. In each coupling step, column purification was carried out using 5% MeOH/ $CHCl_3$.

However, the synthesis of Nap-protected peptides differs from the above two, as it involves two steps of coupling reaction. The first step was based on coupling of Boc-Phe with different methyl ester protected amino acid. After coupling, the acid labile Boc-group is cleaved in the presence of 95% TFA in DCM, following which, the next coupling of napthoxy acetic acid with the deprotected dipeptide was done using HBTU and DIPEA. The methyl ester deprotection at C-terminal was done in the same way as described for Cbz-capped peptides. After final deprotection of esters, all the peptides with free C-terminal end were dried and characterized using ^{1}H-NMR and ^{13}C NMR spectroscopy (Appendix I). The mass of the synthesized peptides was also confirmed using LC-MS (Appendix I). The optical rotation of the peptides was checked using polarimeter. (Appendix I)

6.2.3 Hydrogel Preparation

The required concentrations of peptides were dispersed in water. Gradually NaOH (0.5 M) was added to the above suspension until the pH reaches upto 10.5 for complete dissolution of the peptide derivatives. To ensure that high pH did not cleave the carbamate bond of Fmoc moiety, HPLC was done. After adjusting the pH 10.5, no emergence of new peak was observed indicating no cleavage of the Fmoc dipeptides during that time. Further, addition of HCl (0.5 M) helps to attain the physiological pH. The solution turned into self-supporting hydrogels when left undisturbed. The hydrogels were left overnight before performing experimental measurements.

6.2.4 Spectroscopic Characterization

6.2.4.1 Fluorescence Spectroscopy

Interactions between the aromatic groups of the dipeptide molecules were investigated by Edinburgh spectrofluorometer (FS5). Excitation and emission slit-width were set as 2 and 2 nm respectively with an average of 3 accumulations. The fluorescence emission spectra were recorded in the range between 280nm to 500 nm using excitation wavelength of 280nm (for Fmoc), 270 nm (for Napthoxy) and 265 nm (for Cbz) using FLUORACLE software.

6.2.4.2 Fourier Transform Infrared spectroscopy (FTIR)

FTIR Spectra was collected on an Agilent Cary 620 FTIR spectrophotometer with gel placed between two calcium fluoride discs and scanned between 4000cm^{-1} to 400cm^{-1}. Peptide gels were prepared in deuterated water (D_2O).

6.2.4.3 Circular Dichroism (CD) Spectroscopy

The supramolecular arrangements of dipeptides within the self assembled nanostructures were studied using CD on Jasco J-1500 CD spectrophotometer. The different concentrations of prepared gels were placed between quartz cell of 0.1mm pathlength and spectra were collected from 190 to 320 nm. Temperature of the experiments was maintained at 20^0 C by a water circulator.

6.2.4.4 Thioflavin T assay for Amyloid like β-sheet Determination

The fluorescence spectroscopy of Th T before and after binding the peptide amyloid like fibrils were performed on the Edinburgh spectrofluorometer (FS5) in a 1.0cm quartz cuvette. Th T stock solution of 250μM (8mg in 10 ml PBS buffer pH 7.4) was freshly prepared and filtered through 0.2 mm syringe filters. The working solution of 5μM was prepared by diluting stock solution (1ml to 50ml) with PBS pH 7.4. The fluorescence intensity was measured with 1ml of working solution titrated with 50μl of hydrogels/solutions, at emission maxima of 482nm by exciting the fluorophore at 440nm. The slitwidth of 1nm for each excitation and emission was set with an average of 5 accumulations. For each sample the spectra was recorded from 450 to 600nm, at room temperature and the spectral analysis was done using FLUORACLE software. The final intensity for each sample was plotted after subtracting the blank Th T spectrum.

The similar experiment was done with hydrogels to monitor the growth of amyloid fibril formation. Th T (100ul) was added to 1ml hydrogel and incubated and change in fluorescence intensity was measured at 0 hrs and 24 hrs.

6.2.5 XRD Analysis

The dipeptide gels prepared at concentration of 30 mM as described in hydrogel preparation method. The gels were lyophilized to form dry powder. The powdered sample was placed on glass holder. The spectra were recorded in the 2θ range of 5^0 to 60^0 using Bruker D8 Advance X-ray diffractometer instrument equipped with Cu Kα radiation source (λ = 1.541 Å) under the accelerating voltage of 40 kV and 25 mA.

6.2.6 Microscopic Analysis

6.2.6.1 Transmission Electron Microscopy (TEM)

The TEM samples were prepared by diluting the peptide gels and allowing the 5µl of it to adsorb for 2 min on the carbon coated copper TEM grids. Excess sample was wicked off with the filter paper. It was followed by the addition of 2% (w/v) uranyl nitrate with incubation of 3-5 minutes and wicking off the excess stain. Samples were then vacuum dried before imaging. TEM micro-graphs were recorded with a JEOL JEM 2100 instrument with a Tungsten filament at an accelerating voltage of 200 kV.

6.2.6.2 Atomic Force Microscopy (AFM)

The morphology of self-assembled hydrogels was investigated using Bruker Multimode atomic force microscope (AFM) operated in tapping mode with Nanosope controller and a J-scanner. The samples were prepared by diluting the peptide gels (at MGC) upto 10 times and allowing 10 µL of sample mounted on the silicon wafer to air dry.

6.2.7 Mechanical Properties by Rheology

Mechanical properties were determined using Anton Parr MCR302 with 50mm parallel plate geometry. The dynamic moduli of the hydrogels were measured as a function of frequency between 0.01-100 Hz. To ensure that the measurements were made in the linear regime, an amplitude sweep was performed and optimum strain value was obtained from the linear viscoelastic region. The experiments were performed at 20^0C with temperature being controlled by an integrated electrical heater. The thixotropic behavior of hydrogels was studied in the LVE range by applying the alternating strain of 100% and 0.1% for 100sec and 200sec. The hydrogels were subjected to three repeated cycles of deformation and recovery. The hydrogels used for the rheology and thixotropic measurements were of 40mM concentration.

6.2.8 In situ Gold Nanoparticle Synthesis

Two peptides were selected i.e. Fmoc FY and Fmoc FS for the in situ reduction of gold solution to synthesize gold nanoparticles. The required amount of peptide was weighed and dissolved in 1 ml of water using 0.1 N NaOH. The pH of the solutions was adjusted to ~8 and ~11 using 0.1 N HCl. To these solutions, the required amount of gold chloride which was equivalent to molar ratio of 5:1 (peptide: gold). After addition of $HAuCl_4$, the yellow color of gold solution disappeared ($Au^{+3} \rightarrow Au^{+}$) and then ruby red/violet colour started appearing owing to further

reduction ($Au^{+} \rightarrow Au^{0}$). These nanoparticles were then characterized using UV-visible spectroscopy, dynamic light scattering (DLS) and transmission electron microscopy (TEM).

6.2.8.1 UV-Vis NIR spectroscopy: The absorption spectrum was recorded on Cary UV-Vis NIR Spectrophotometer, Agilent. The samples were diluted (5 times) and the scanned in the wavelength range from 200 nm to 1300 nm.

***6.2.8.2 Size measurements using Dynamic Light Scattering*:** The size of the colloidal solution were measured using Malvern Zeta Sizer Nano (ZSP).The diluted colloidal solution (5 times) was scanned three times and the average intensity of the peak has been reported.

6.2.8.3 TEM and EDS analysis: The shape of the metal nanoparticles was observed using JEOL (JEM 2100) high-resolution transmission electron microscope at an accelerating voltage of 200kV. The 5µl of diluted (5 times) colloidal suspension was drop cast on carbon-coated copper grid and kept for 2 minutes. Then the excess sample was removed off by a capillary action of filter paper and the grid was vacuum dried and tested for shape assessment. The dried samples were analyzed by TEM, STEM and EDS mapping. AFM was carried out to visualize the gold nanoparticles adsorbed on peptide self-assembled structures.

6.2.8.5 Rheology: The Fmoc FY and Fmoc FS hydrogels at MGC were prepared by the protocol mentioned above. After adjusting the pH 8, the gold solution in 5:1 ratio (peptide: gold) was added to the peptide solutions. The samples were left undisturbed for self-assembly and visual colour change. The strength was measured for Fmoc FY hydrogels after 24 hrs and for Fmoc FS hydrogels, after 48 hrs of gold nanoparticle synthesis.

6.3 Results and Discussion

6.3.1 Molecular design of peptide gelators

To establish the rules for rational molecular design of short aromatic peptides, we chose the shortest possible peptide sequence i.e. dipeptide to design our library. The rationale behind the molecular design is to highlight the importance of sequence hydrophobicity for driving the self-assembly behavior of short peptide in water. [49-51] Our design includes the simultaneous variation of N-terminal aromatic capping (Fmoc, Nap, and Cbz) and C-terminal amino acid residues, which together contribute towards the overall hydrophobicity of the resulting peptides.

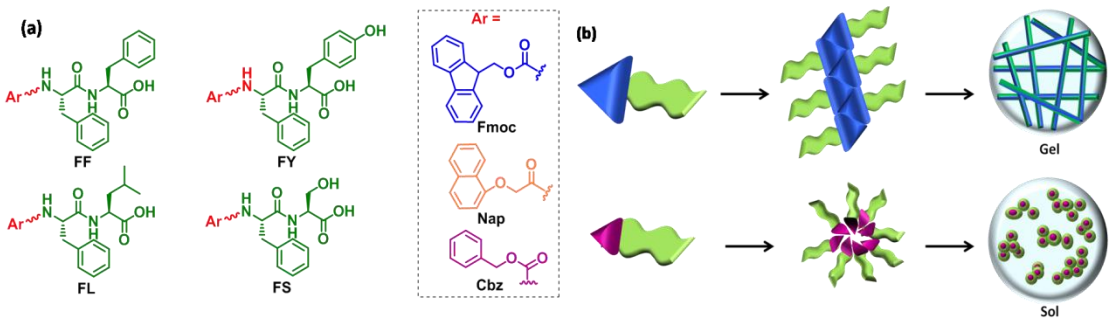

Figure 6.1 *(a) Design of the library of variable dipeptide sequences attached to different aromatic cappings (Ar) such as Fluorenyl (Fmoc), Napthoxy (Nap) and Benzyloxy-carbonyl (Cbz) at N-terminal end and different amino acids at C-terminal (b) Representative schematic diagram describing the self-assembly of aromatic dipeptides resulting in differential self-assembled nanostructures depending on the size and hydrophobicity of the aromatic capping. The green wavy ribbon indicates the dipeptide backbone, and blue and purple arrow heads are the representative large (Fmoc) and small (Cbz) aromatic groups, molecular structure of which are shown in (a) part. The larger and smaller aromatic groups result in differential self-assembly as indicated by fibers and micellar aggregates in the figure, respectively.*

Our design was focused on variable amino acids, which cover the wide range of hydrophobicity. The selected specific amino acid residues represent the different chemical functionalities, such as the classical aromatic phenylalanine, polar aromatic tyrosine, non-polar aliphatic leucine, and polar aliphatic serine, as shown in figure 6.1a. Nevertheless, phenylalanine was selected to be at the N- terminal end of our peptide design which has significant propensity for aggregation through π-π stacking interactions in water. [52] The pH switch was used to trigger the gelation of these short aromatic peptides, as the change in pH causes the deprotonation of terminal carboxylic acid. These peptides showed clear solution at higher pH ~10.5 which transformed into gels (sol-gel transition) as the pH of the medium reached near to physiological pH ~7. [53] The evidence for no Fmoc cleavage was shown just after the pH was adjusted to 10.5 was evident through HPLC analysis. Further analysis after 24 hrs revealed the same peak, which clearly indicated that the Fmoc group remained intact even after the exposure with alkaline pH. The short duration exposure to high pH showed no cleavage effect on Fmoc-capping. The retention of self-assembling capacity was confirmed by AFM, which showed similar fibrillar morphology after 24 hrs, while aggregates after 5mins (figure 6.2). [54]

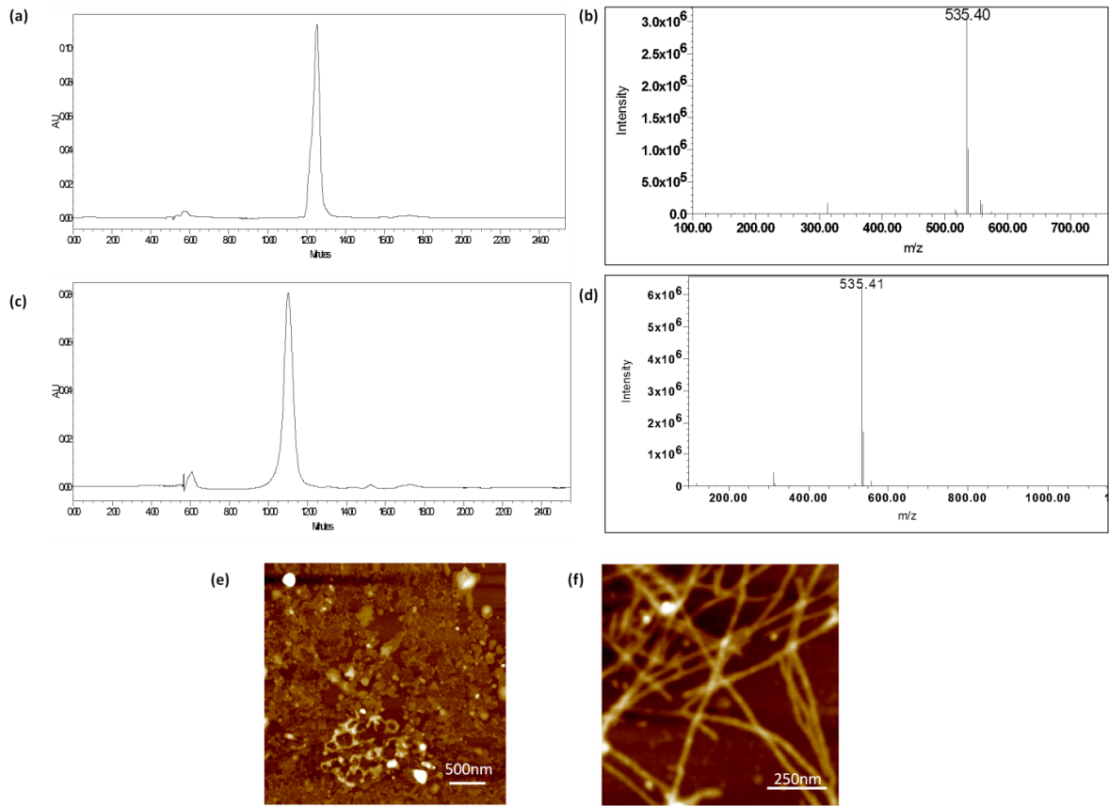

Figure 6.2 *HPLC analysis of Fmoc FY (a) immediately when pH was adjusted to 10.5 and (c) 24 hrs after pH was adjusted to pH 7. (b) and (d) represents the corresponding mass spectra collected using LC-MS (QDA). (e) and (f) shows the microscopic images at corresponding time points using AFM. The HPLC and AFM results confirmed that time for which pH 10.5 is maintained for the dissolution of peptides in pH method, does not cleave the carbamate group of Fmoc.*

Our observation demonstrated that the hydrophobicity of the peptide sequence plays a crucial role in determining the resultant gelation behavior of the peptides, which is explained by the schematic diagram in Figure 6.1b. Primarily, the self-assembling behavior of the peptides was found to be highly susceptible to the subtle change in hydrophilic lipophilic balance (HLB) of the designed molecules. The peptides with larger aromatic groups, like, Fmoc resulted in highly ordered nanofibrillar structures whereas the peptides with smaller aromatic capping, like, Cbz failed to form fibrillar network structures due to insufficient π-π interactions. [33]

6.3.2 Gelation Behaviour

An inverse relation was observed for minimum gelation concentration (MGC) of the peptides with hydrophobicity (c log P) of peptides, which has been shown in figure 6.3a and b and Table 6.1. In general, the Fmoc peptides were found to self-assemble at lower concentrations compared to their analogues capped with Nap and Cbz groups. Besides this, the MGC of Fmoc capped peptide was found to vary even with different amino acid sequences at C-terminal end from 2.5mM for Fmoc FF to 15mM for Fmoc FS. Interestingly, Fmoc FY and Fmoc FL showed identical MGC (10mM) although their hydrophobicity different as indicated by their c log P values (figure 6.3 b). The possible reason for such observation could be additional H-bonding offered by aromatic hydroxyl group of tyrosine residue of Fmoc FY.

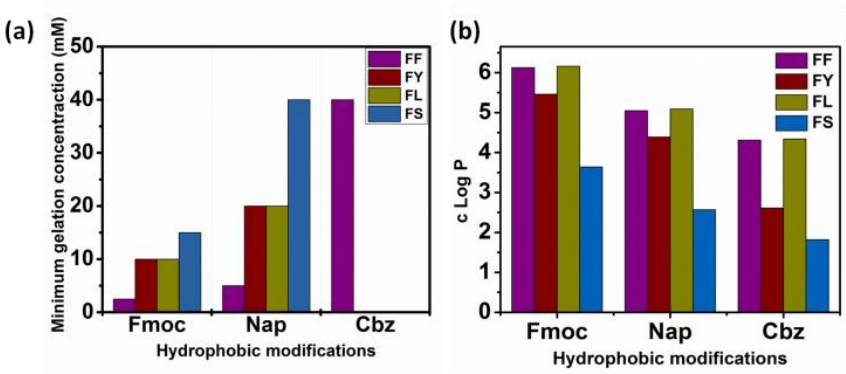

Figure 6.3 *(a) Minimum gelation concentrations of the hydrophobically modified dipeptides and (b) c Log P values of same peptides calculated through ChemDraw Ultra 12.0*

Similar trend has also been observed for Nap appended peptides, although the MGC for each peptide was found to be increased due to relatively weaker π-π interactions with Nap group compared to Fmoc substitution. A significant increase in the MGC of polar derivatives (FY and FS) was observed in comparison to their non-polar analogues (FF and FL respectively), which could be attributed to greater gelator-solvent interactions due to additional H-bonding and hence decrease in the gelator- gelator interaction. Moreover, the smallest aromatic group Cbz formed gel only with the most hydrophobic amino acid residue, phenylalanine, and the plausible reason for other sequences failing to form gel in water could be the insufficient π-π interactions between Cbz groups compared to another hydrophobic capping. The results also suggested that change in aromaticity of the peptide has more prominent effects on gelation behavior than changing the polarity of the terminal amino acid. [28]

Table 6.1: *Summary of the minimum gelation concentrations (MGC) of different aromatic dipeptides and their c log P values.*

Aromatic group / ***Dipeptide***	**Fmoc**		**Nap**		**Cbz**	
	c Log P	***MGC (mM)***	***c Log P***	***MGC (mM)***	***c Log P***	***MGC (mM)***
FF	6.127	2.5	5.054	5	4.310	40
FY	5.460	10	4.387	20	2.609	Sol
FL	6.166	10	5.093	20	4.348	Sol
FS	3.639	15	2.567	40	1.822	Sol

6.3.3 Molecular mechanism of self-assembly

6.3.3.1 Fluorescence spectroscopy: The major driving force behind the supramolecular assembly of aromatic short peptides is considered to be the π-π stacking interactions between the aromatic moieties and H-bonding between the amino acid backbones. Significant change was expected to arise in the fluorescence spectra of variable aromatic groups with change in local hydrophobic environment due to formation of aggregates of peptides. Irrespective of the sequence, the extensive reduction in intensity was observed due to self-assembly of the peptide molecules, accompanied by the red shift of characteristic emission peak (figure 6.4). The Fmoc and Nap gelators, when excited at 280nm and 270 nm showed the shift of emission peaks from 315nm to 325nm and 345nm to 365 nm, respectively, when sol transforms to gel. [22, 27] The substantial decrease in relative fluorescence intensity was found to be the function of monomeric gelator concentration and provided the information regarding intermolecular packing of aromatic groups during self-assembly. [20] The greater extent of quenching in Fmoc capped peptides can be attributed to higher extent of π-π stacking of fluorenyl groups, than napthoxyl groups. However, the smallest Cbz capping in non-gelator peptide tends to show concentration dependent increase in fluorescence intensity which is indicative of weaker aromatic interaction (Figure 6.4). The emission spectra of Fmoc FY and Nap FY (the tyrosine based peptides) showed a broad excimeric peak at ~ 450nm which indicates the formation of extended π-stacked systems, induced from additional H-bonding interaction of the peptide backbone leading to higher order in the final gel phase material. [55]

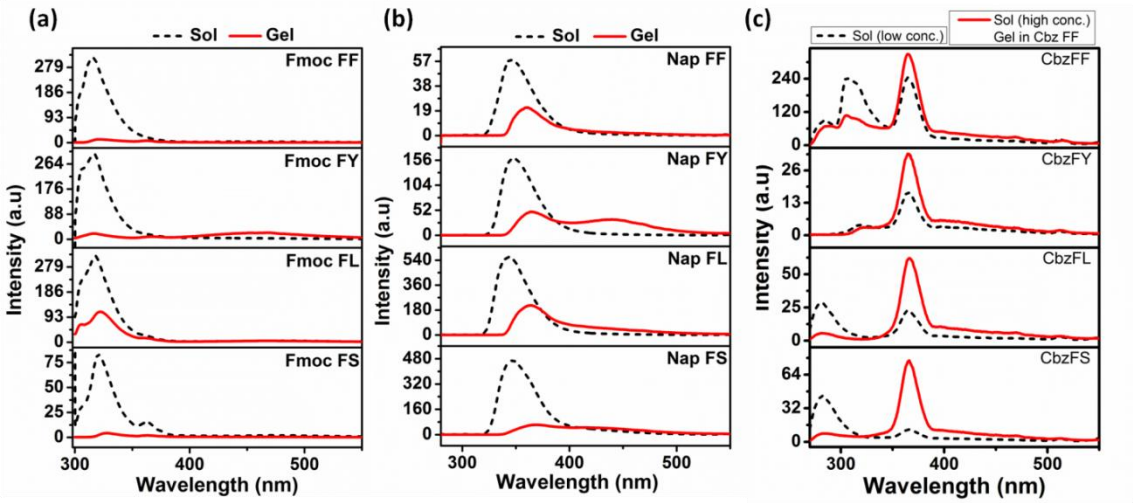

Figure 6.4 *Fluorescence spectra of aromatic dipeptides peptides (a) Fmoc, (b) Nap and (c) Cbz showing the fluorescence intensity of peptides in monomeric state (low conc.) and subsequent quenching of the corresponding emission peak at ~320nm for Fmoc and ~350nm for Nap peptides in gel state (gelation concentration) when excited at 280 and 270 nm respectively. In case of Cbz, the enhanced emission peak at ~365nm at higher concentration is observed when excited at 254 nm, as a function of concentration.*

6.3.3.2 FTIR spectroscopy: Another important driving force involved in the self-assembly of these amyloid-like peptides is H-bonding that can be monitored using FTIR spectroscopy. Hydrogen bonding between peptide chains particularly involves carbonyl stretching vibrational modes which can be observed in the amide I region (1600-1700 cm^{-1}) of the spectra in figure 6.5. For each set of peptide amphiphiles, appended with Fmoc and Nap groups and Cbz FF, a major peak at ~1630cm^{-1} was observed, suggesting the β-sheet conformation. [56] A few recent reports suggested that a minor peak at ~1685 cm^{-1} could be possibly due to presence of carbamate moiety in Fmoc and Cbz groups. [57] However, a peak at ~1670cm^{-1} in Nap peptides is indicative of carbonyl group present within the Nap- modification of molecules. [58] Peptide amphiphiles also showed a peak at around 1580cm^{-1}, which is indicating the presence of free carboxylate ions and represents the fraction of deprotonated C-termini of the peptides at physiological pH ~7. [58] The spectroscopic studies qualitatively correlate the effect of aromaticity with the secondary structure of the individual peptide gelator, suggesting more ordered structures associated with larger aromatic capping. It was also evident that the non-gelator peptides show a peak at ~1650 cm^{-1} which indicates the presence of disordered supramolecular nanostructure like random coils. [58] Also the beta sheet signatures are in

agreement with previous studies of short hydrophobic sequences derived from the amyloid like β-peptide fragments. [56-58]

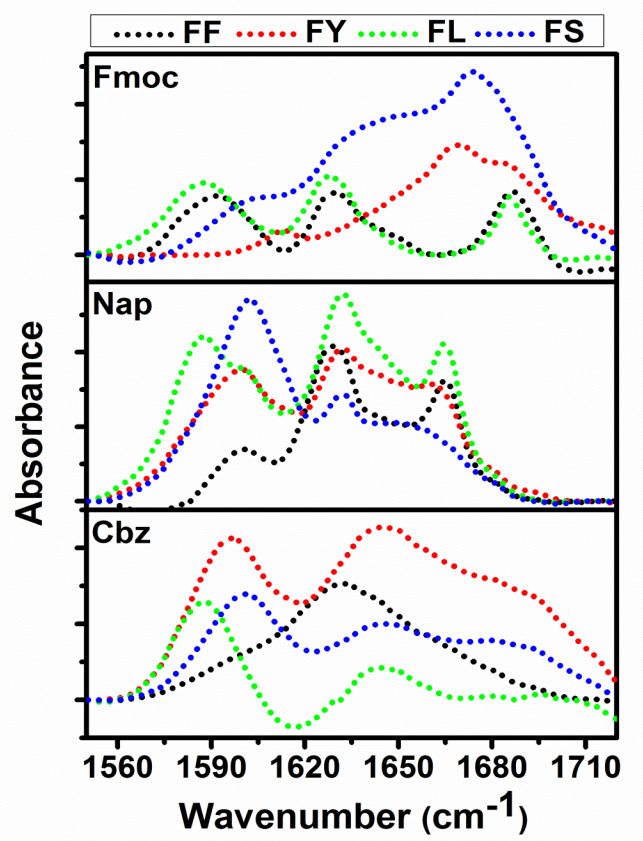

Figure 6.5 *FTIR spectra of different aromatic dipeptides having Fmoc group (in panel 1), Nap group (in panel 2) and Cbz group (in panel 3) depicting characteristic β-sheet arrangement.*

6.3.3.3 CD spectroscopy: CD was used to investigate the chiral orientations of the short aromatic peptides which were induced due to molecular self- assembly. The supramolecular arrangement induced strong chirality in the achiral aromatic groups which were evident from the corresponding signature peaks at 305 nm, 245 nm and 225 nm for Fmoc, which can be determined by the change in relative intensities of supramolecular chirality peak through CD spectra Nap and Cbz groups, respectively shown in Figure 6.6. [20, 27] As expected, the self-assembling aromatic peptide amphiphiles showed concentration dependence (shown in figure 6.6). [59] Hence, we assumed that less ordered supramolecular structures were present at the sub-gelation concentration which gives very weak CD signal. Further increasing the concentration up to MGC and above MGC, the intensity of CD signal has been increased proportionately, as evident from the spectra of Fmoc and Nap capped peptides (figure 6.6). However, Cbz capped peptides did not give sharp signals due to weaker stacking propensity of Cbz moieties, which

may also overlap with the spectral range of secondary structures. Moreover, the higher absorption in the range of 190-220 nm resulting in the overload of high tension, makes it difficult to record a CD spectrum in the wavelength range relevant to the β-sheet organization.

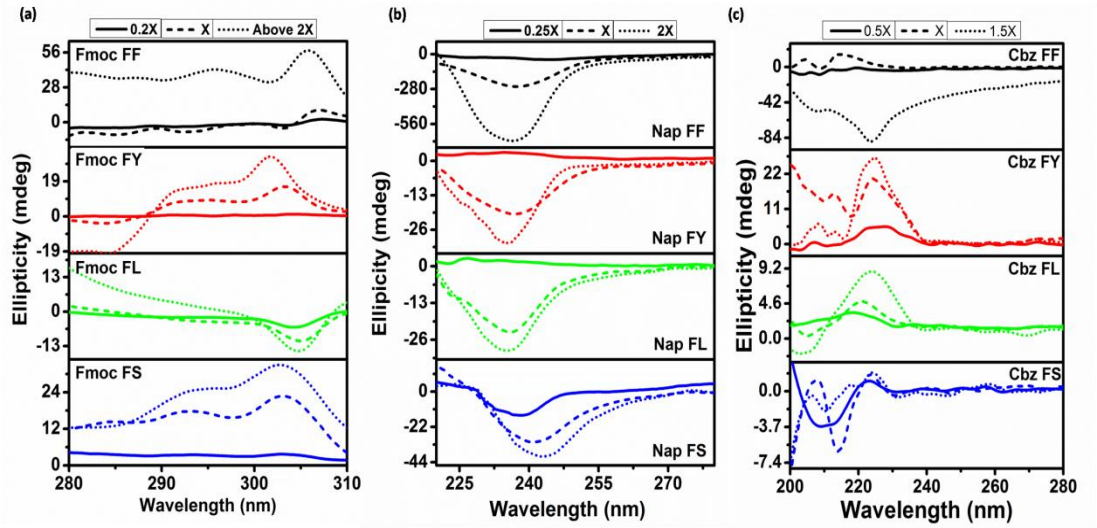

Figure 6.6 *CD spectra of (a) Fmoc appended and (b) Nap appended and (c) Cbz appended dipeptides at concentrations below MGC, at MGC (X) and above MGC, denoted by solid line (—), dashed line (- - - -) and dotted line (••••) respectively.*

6.3.3.4 Th T Fluorescence assay: To get further insight into amyloid like fibrils formed by aromatic dipeptides, classical Thioflavin T fluorimetric assay has been performed. [60] Here, we used Th T to compare the β-sheet forming propensity of two different peptides with variable aromatic capping, as a function of peptide concentration. There was enhancement in the intensity, irrespective of the size of aromatic capping. However, a remarkable increase in the relative intensity of Th T uponbinding with Fmoc capped peptides is observed which was comparatively less with Cbz capped peptides. This clearly explained the role of extensive π-stacking in fluorenyl groups, resulting in the formation of hydrophobic patches, where Th T can bind. The first panel of figure 6.7a shows the comparison of Fmoc FF and Cbz FF at two different concentrations (5mM and 20mM), which reveals that higher concentration of peptides shows greater extent of Th T binding. In addition to aromatic ligands, the peptide sequence also plays a significant role in determining the β-sheet content in the system. The results showed the relatively higher Th T fluorescene intensities with Fmoc FF than with Fmoc FL indicating the formation of greater extent of amyloid structure formation with FF due to its more hydrophobic nature than FL. However, the Cbz FL, a non gelator showed negligible change in the intensity

of Th T upon binding suggesting no β-sheet aggregation, even at higher concentration. The magnified spectra of Cbz FF and Cbz FL are shown in figure 6.7 b & c.

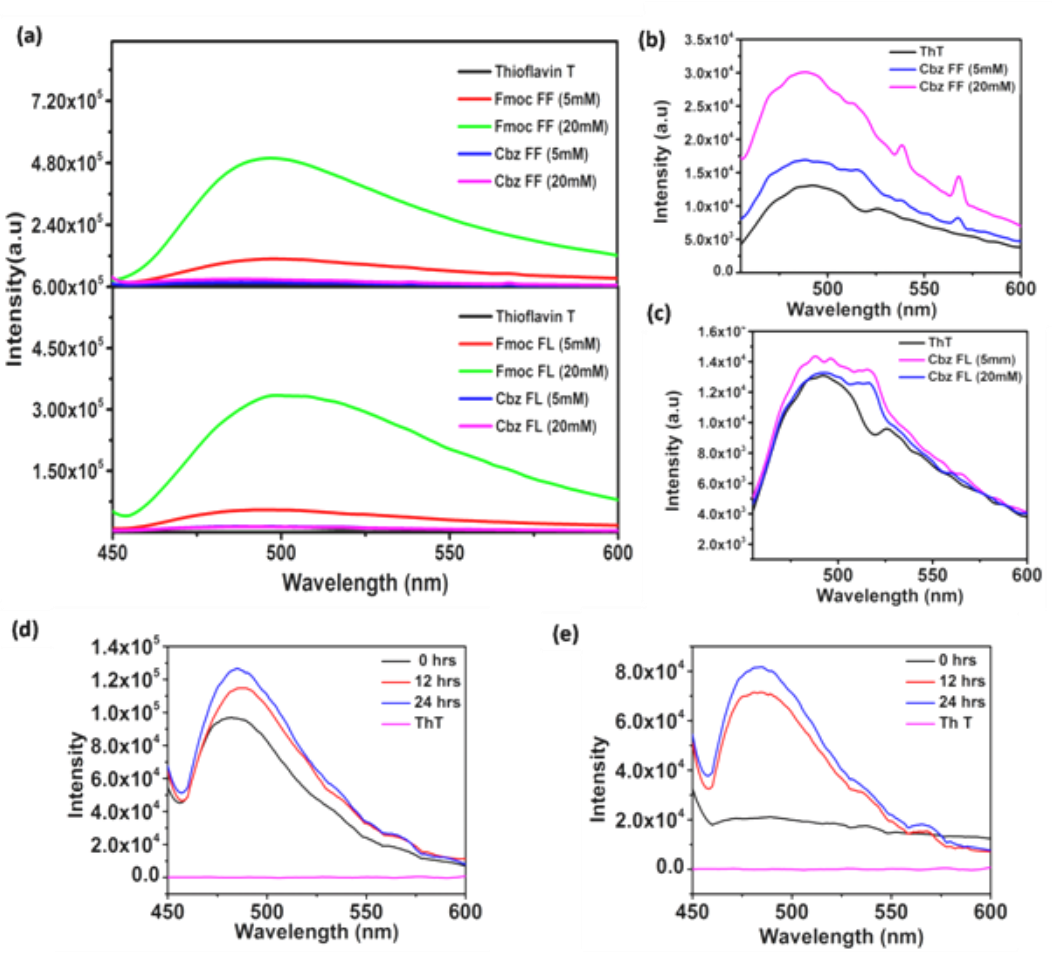

Figure 6.7 *Fluorescence emission spectra of Thioflavin T alone and (a) Fmoc FF & Cbz FF (panel a) and Fmoc FL & Cbz FL peptides (panel b) at 5mM and 20mM concentration and the magnified images of ThT binding with (b) Cbz FF and (c) Cbz FL. Th T as a fluorescent molecular rotor at 0 hrs, 12hrs and 24 hrs in comparison to control Th T with (d) Fmoc FF and (e) Cbz FF hydrogels of 40mM concentration.*

Apart from fluorescent probe for detecting β-amyloid structure, Th T can also act~~s~~ as a molecular rotor and its fluorescence intensity is dependent on local viscosity. [61] Thus to gain an insight into assembly process, the Th T binding with Fmoc FF and Cbz FF (40mM) hydrogels was observed with respect to time (figure 6.7 d & e). The increase in fluorescence intensity depicts that the rigidity of Th T local environment has been increased from initial time upto 24 hrs which can also be correlated to growth of β-sheet structures with time. The progress of self-assembly was faster in Fmoc FF gels as evident from many folds increase in Th T emission

peak at initial time point only, followed by subsequent enhancement in intensity with time. However, Cbz FF being a weak gelator takes time to self-assemble initially and showed comparatively less enhancement in Th T emission peak at zero time point. Surprisingly, in 12 hours the assembly was faster and great enhancement in the intensity was observed. After 12 hrs, the assembly process could be slowed down which was marked by relatively lesser enhancement in intensity. The results are in corroboration with FTIR, CD and fluorescence studies.

This is further supported by fluorescence microscopic investigation (Figure 6.8). The fluorescence intensity of microscopic structures showed close association with Th T fluorescence as evident from the spectroscopic analysis. The brighter fluorescent structure in Fmoc peptides signifies the formation of more hydrophobic amyloid structures in comparison to Cbz peptides which showed negligible fluorescence. These results also supported the fact that more hydrophobic modifications favored stronger π-π interactions and have greater propensity to form β-sheet structures. [62]

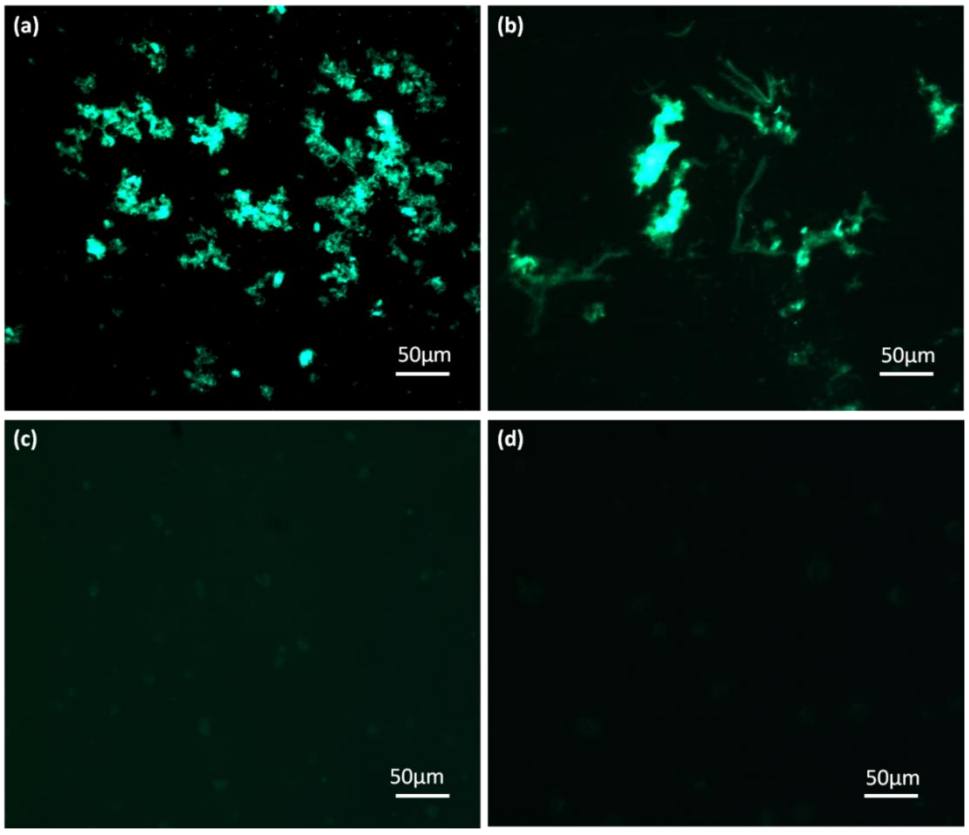

Figure 6.8 *Fluorescence microscopic analysis using Thioflavin T to compare the extended β-sheet conformation structures formed in highly hydrophobic peptides (a) Fmoc FF and (b)*

Fmoc FL and also with less hydrophobic peptides (c) Cbz FF and (d) Cbz FL at 20mM concentration.

6.3.4 XRD Analysis

In order to determine the supramolecular packing of the gelator peptides, wide angle X-ray diffraction pattern was studied. TheXRD pattern of the representative peptides from each aromatic series (Fmoc, Nap and Cbz) is shown in figure 6.9. All aromatic variants showed a peak corresponding to d-spacing 4.6 Å at 2θ angles of 19.4^0 in Fmoc, 18.5^0 in Nap and 18.7^0 in Cbz capped peptide. The periodicity of 4.6 Å is indicated as the characteristic spacing between peptide chains in β-sheet conformations. [63] This observation supports the FTIR spectroscopic studies which also indicated the presence of β-sheet (figure 6.5). Furthermore, in all the three systems, another peak at d-spacing 3.8 Å is observed, which represents the π-π stacking between the aromatic residues in the self-assembled β-sheet structures. [22] However, the intensity of 3.8 Å peak in Cbz capped peptide is very low, the possible reason for which could be lesser π-π stacking in smaller aromatic groups in comparison to Fmoc and Nap. These observations along with previous spectroscopic analysis provides the evidence that π-π stacking is one of the main driving force for the self-assembly of short aromatic peptides.

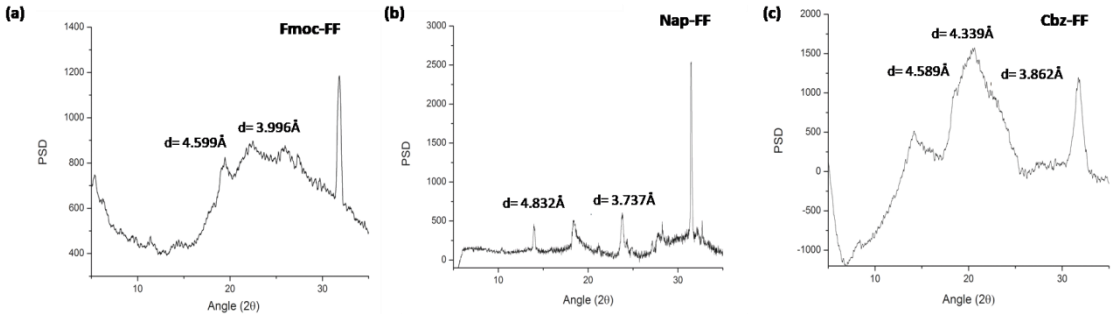

Figure 6.9 *(a) Representative XRD data of dried hydrogels having different aromatic groups (a) Fmoc FF, (b) Nap FF and (c) Cbz FF.*

6.3.5 Morphological Characterization

To gain more insight about the molecular organization of self-assembled structure from short aromatic peptides, morphological structures were investigated using transmission electron microscopy (TEM) and atomic force microscopy (AFM). As shown in figure 6.10, TEM images of Fmoc and Nap capped hydrogelators revealed the dense interwoven network, suggesting the occurrence of a three dimensional nanofibrous structure within the hydrogels.

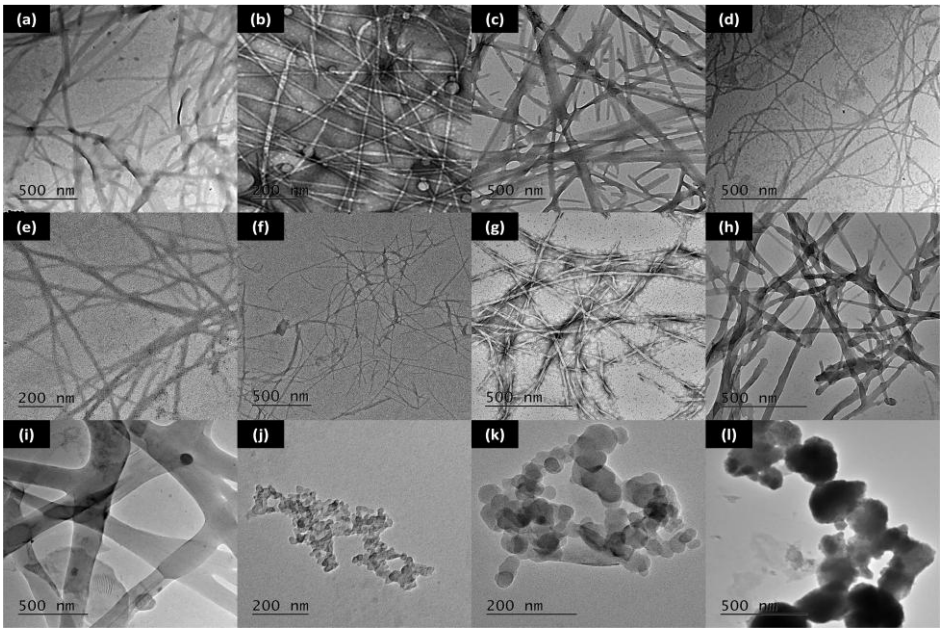

Figure 6.10 *Morphological studies of different aromatic dipeptides (a)Fmoc FF, (b)Fmoc FY, (c) Fmoc FL, (d) Fmoc FS, (e) Nap FF, (f) Nap FY, (g) Nap FL, (h)Nap FS, (i) Cbz FF, (j) Cbz FY, (k) Cbz FL and (l) Cbz FS using TEM microscopy.*

The morphology of Fmoc FF, Fmoc FL, Nap FF and Nap FS showed the existence of non-homogenous fibres indicating the presence of bundles of individual nanofibers while Fmoc FS and Nap FY showed the presence of homogenous fibrous network with the fibers of average thickness of ~15nm. The diameter of thicker fibers in non-homogenous hydrogels was found to be double to that of individual fibres which range from 19-35nm. However, the different morphology was observed in Fmoc FY hydrogel which resembles to nanotubes of ~19 ± 3.7nm thickness, while Nap FL showed the presence of nanoribbons having thickness of ~15 ± 4.3nm. [64, 65] Interestingly, Cbz FF, having weaker aromatic interactions tends to form wider fibers of diameter 172 ± 42 nm compared to its analogues with Fmoc and Nap substitutions (Fmoc FF and Nap FF). Whereas, the other members of Cbz series failed to form peptides fibrous network and displayed spherical aggregates like morphology. The fiber diameters of all the hydrogels are compared in Table 6.2. The results also supported the fact that less ordered aggregates have less water entrapment efficiency and thus, are unable to form self-supporting gels. Thus we speculate that the degree of hydrophobicity of aromatic groups and the side chain functionality of the amino acid residues in the peptides have a direct influence on the differential non-covalent interactions leading to differential molecular packing resulting in variable shape and size of self-assembled structures. [28]

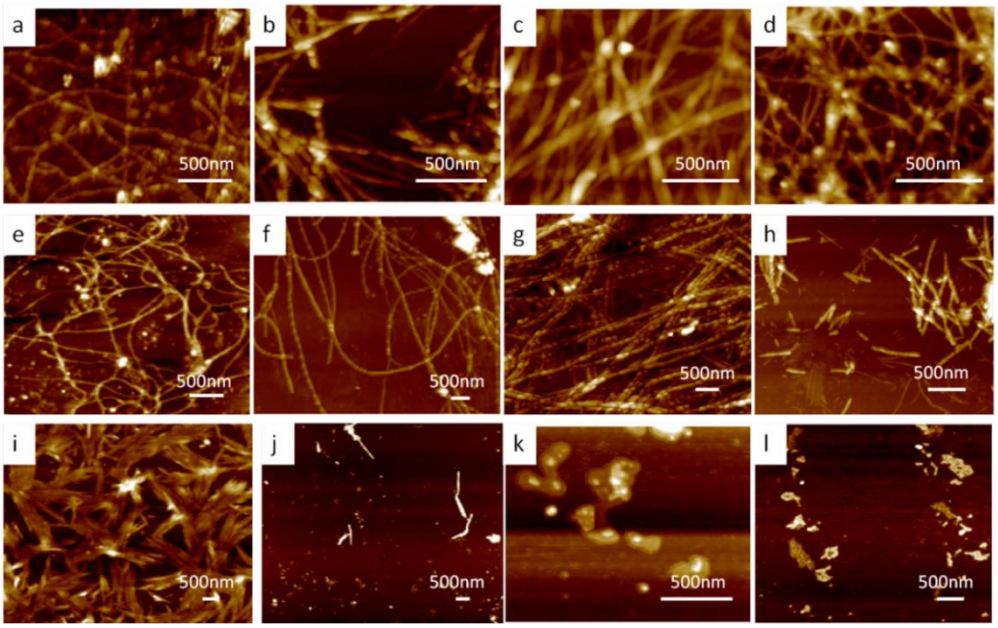

Figure 6.11 *AFM images of different aromatic peptide hydrogels (a) Fmoc FF, (b) Fmoc FY, (c) Fmoc FL, (d) Fmoc FS, (e) Nap FF, (f) Nap FY, (g) Nap FL, (h) Nap FS , (i) Cbz FF, (j) Cbz FY, (k) Cbz FL and (l) Cbz FS.*

Furthermore, AFM results also support TEM results and confirm the presence of nanofibrous assemblies, which was anticipated for such type of short peptide amphiphiles based on aromatic interactions, β-sheet reinforced fibrous networks. AFM images also showed the presence of entangled fibrous network with more hydrophobic Fmoc or Nap peptides but short bundled fibers or micellar aggregates with less hydrophobic Cbz peptides. In corroboration with TEM, AFM also showed that the fiber diameter of polar peptides (FY and FS) was comparatively lesser than the non-polar analogues (FF and FL) (figure 6.11 and Table 6.2).

Table 6.2 *Fiber dimensions of nanofibers observed in TEM and AFM microscopy of different aromatic dipeptide hydrogels.*

Aromatic / Cap / Peptides	Fmoc (nm)		Nap (nm)		Cbz (nm)	
	TEM	AFM	TEM	AFM	TEM	AFM
FF	33.5 ± 6	30.15 ± 7	18.8 ± 4.7	22.6 ± 6	172 ± 42	195± 35
FY	18.6 ± 3.7	21.4 ± 4	12 ± 4	16.8 ± 2	--	--
FL	35 ± 8	40.5 ± 6	14.8 ± 4.3	20 ± 5	--	--
FS	13 ± 2.7	18.5 ± 3.5	29.4 ± 8.5	34.2 ± 7.5	--	--

6.3.6 Mechanical Properties

6.3.6.1 Rheological Measurements: The hydrogels possess distinctive viscoelastic properties owing to the differential molecular structure of the hydrogelators. The rheological measurement for the deformation and flow property of each hydrogel was performed through strain sweep followed by frequency sweep. During strain sweep, the rheological properties of the hydrogels remain independent of strain upto the critical point of deformation and this strain dependent region is the linear viscoelastic region (LVE). Then the frequency sweep experiment was done at constant strain within the LVE range, by varying the oscillation frequency. [66] Figure 6.12 and table 6.3 compares the viscoelastic behavior of different aromatic peptide hydrogels prepared at 40mM of concentration. The strain value of these hydrogels varies from 0.1 to 1% and applied accordingly for measuring the storage modulus (G') and loss modulus (G"). For each hydrogel, the storage modulus was higher than loss modulus, which indicates the formation of strong and rigid hydrogels. It is evident from the plots that storage modulus (G') have negligible dependence on the frequency, for all the gels. The Fmoc peptides show higher values of storage (G') and loss (G") modulus than that of Nap and Cbz peptides (as shown in figure 6.12 e). For example, Fmoc FF, Nap FF and Cbz FF showed storage modulus of 1.1 ± 3.3 kPa, 0.27 ± 0.14 kPa and 0.14 ± 0.08, respectively. On the other hand, if we compare the strength of dipeptides within the same series (Fmoc or Nap), the peptides containing aromatic amino acid residues dominate the series. The reason for the excellent viscoelastic properties of more hydrophobic peptides is the stronger aromatic π-π interactions between peptide molecules during self-assembly. [49] Interestingly, the strength of Fmoc FY and Nap FY was found to be significantly higher compared to the other members in the respective series. The plausible reason for this increase in the strength is the contribution of additional H-bonding between the peptide backbones arising from polar hydroxyl groups, in addition to aromatic π-π interactions. These results can be correlated with the fluorescence emission spectra and fiber thickness. The excimeric peak in emission spectra of Fmoc FY and Nap FY at ~450nm clearly indicates the extended interactions between the aromatic moieties, which were also reflected in their morphologies, as both possess relatively lesser fiber diameter in the range of ~15-20nm in comparison to its FF derivatives having thickness of ~20-30 nm (Table 6.3). [67]

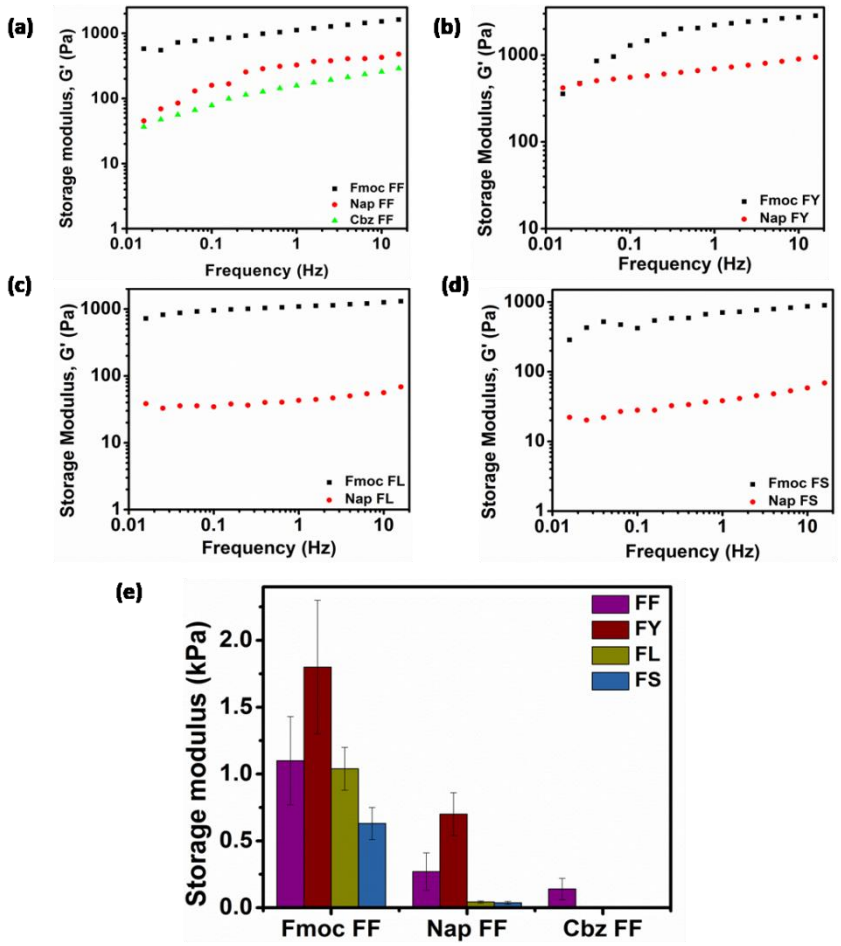

Figure 6.12 *Rheology plots showing storage moduli as a function of frequency for the different aromatic dipeptide hydrogels (a) FF, (b) FY, (c) FL and (d) FS; (e) Bar graph comparing the storage modulus of different hydrophobically modified dipeptides gels.*

Table 6.3 *Comparison of storage modulus (G') and loss modulus (G") of different aromatic dipeptide hydrogels.*

Peptides	Storage modulus, G' (kPa) [a,b]	Loss modulus, G" (kPa) [a,b]
Fmoc FF	1.1 ± 0.33	0.23 ± 0.06
Fmoc FY	1.8 ± 0.5	0.15 ± 0.05
Fmoc FL	1.04 ± 0.16	0.2 ± 0.04
Fmoc FS	0.63 ± 0.12	0.12 ±0.03
Nap FF	0.27 ± 0.14	0.051 ± 0.02
Nap FY	0.7 ± 0.16	0.1 ± 0.03
Nap FL	0.043 ± 0.009	0.06 ± 0.003
Nap FS	0.037 ± 0.01	0.01 ±0.006
Cbz FF	0.14 ± 0.08	0.05 ± 0.02

(a)Frequency range of 0.1-100 Hz at 200C temperature; (b) Strain values for each measurement were obtained from corresponding amplitude sweep experiments which varies from 0.1 to 1%.

6.3.6.2 Thixotropic Studies: Interestingly, these dipeptide gels also exhibited gel-sol transition upon application of external mechanical stress. [68] The mechano-responsive behavior of gels was studied by applying cyclic stress. The strain of 100% and 0.1% was applied alternatively for 100sec and 200sec, respectively to study the deformation and recovery of strength of the gels. We found that, under similar conditions, the peptides with different aromatic groups exhibited variable extent of recovery. As for Fmoc FF, the recovery was found to be ~77% while with Nap FF it was ~ 93% after 60 sec. However, with Cbz FF the recovery was ~95% after 60 sec (figure 6.13). The results suggested that with less hydrophobic aromatic groups, the interactions were weak; however, the self-assembled nanofiber network structure can recover faster after deformation. On the contrary, the stronger interactions led to a slower recovery after deformation.

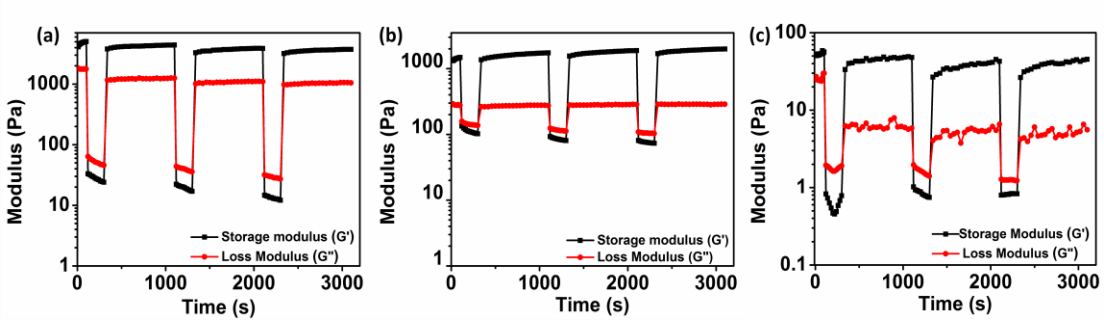

Figure 6.13 *Thixotropic studies of representative aromatic peptide gels (a) Fmoc FF, (b) Nap FF and (c) Cbz FF using a cyclic reversible strain of 100% to deform the gels and reduced to 0.1% to allow recovery of gels, for the time of 100 s and 200 s respectively.*

6.3.7 Shape controlled synthesis of gold nanoparticles

6.3.7.1 Gold nanoparticle formation: At this point, we were curious to explore our detailed understanding of the structure-function relationship of these highly tunable gels towards biomimetic synthesis of metal nanoparticles with different optical properties. These organic-inorganic hybrids can find use in biomedical applications, including biosensors, cell targeting, bioimaging, biomineralization, biocatalysts, and drug delivery. [38, 39] The specific amino acids such as tyrosine and serine are known as redox active moieties and have electron donating properties which can be utilized for the reduction of gold (Au^{3+}) ions to metallic gold. [69] To the best of our knowledge, utilization of hydrogels for gold nanoparticles is interesting area of

research as the 3D network of hydrogels acts as a structure directing template without aid of external additives. The gel phase ensures the controlled growth and stability of the synthesized nanoparticles. [13, 14] Herein, we investigated the differential property of hydrophobically modified dipeptides in controlling the shape and size of the gold nanoparticles as shown in figure 6.14a. We selected Fmoc FY and Fmoc FS, from the library of our synthesized peptides owing to their hydroxyl groups in the C-terminal amino acid residue. The mechanism of reduction of Au^{+3} to Au^{0} using hydroxyl groups on the surface of nanofibers is demonstrated in figure 6.14b.

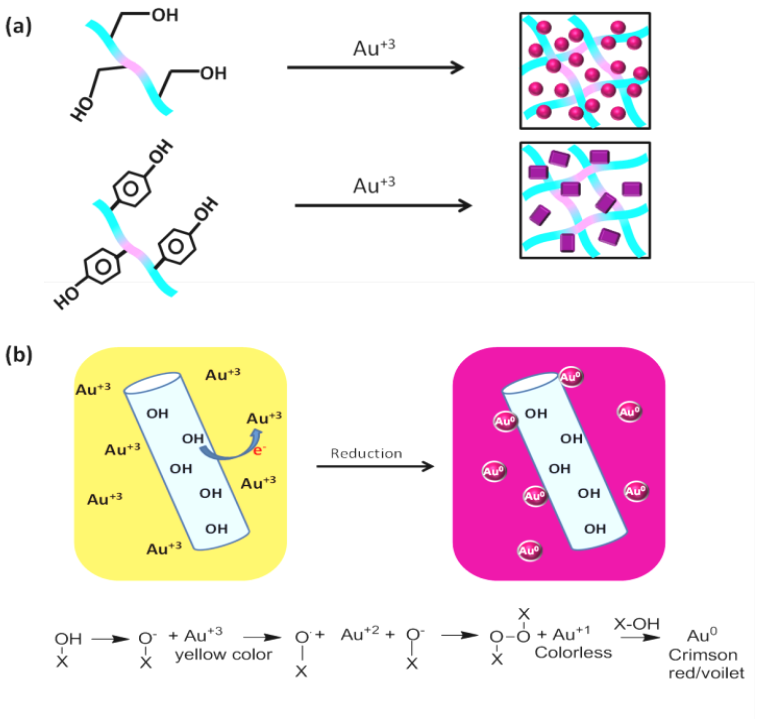

Figure 6.14 *(a) Schematic representation of in-situ reduction of gold (Au^{+3}) using serine (Fmoc FS) and tyrosine (Fmoc FY) based peptides resulting in shape controlled synthesis of gold nanoparticles (Au^{0}) and further stabilization in gel network. (b) Mechanism of gold reduction from Au^{+3} to Au^{0} by electron transfer from hydroxyl group on the surface of peptide nanofiber.*

6.3.7.2 Effect of pH on gold nanoparticle formation: We also studied the effect of pH on the reduction properties of peptides. As indicated earlier, few reports showing the use of peptide based hydrogels, majorly containing tyrosine and tryptophan, for reducing gold solution into nanoparticles. [46, 47] However, the use of aliphatic functional amino acid like serine remains unexplored. We demonstrated for the first time the reduction properties of serine containing peptide hydrogels, which can play a crucial role toward synthesis and stabilization of the gold

nanoparticles in hydrogel network. The reduction of gold was indicated by visual colour change from yellow to violet/crimson red for both the peptides (figure 6.15).

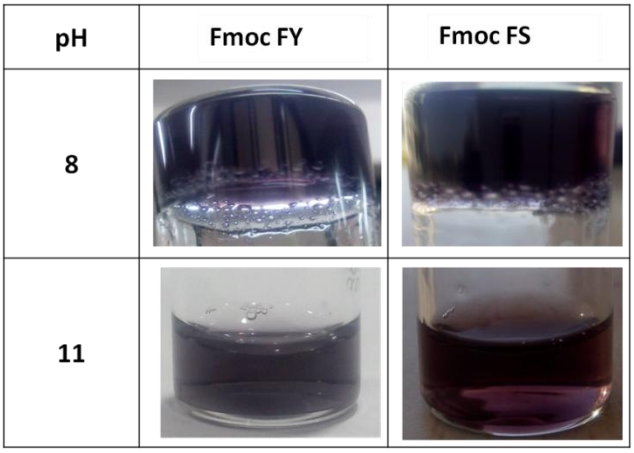

Figure 6.15 *Optical images of gold nanoparticles entrapped in hydrogels at near physiological pH (8) and peptide nanofibers solutions at higher pH (11), reduced by Fmoc FY and Fmoc FS peptides.*

The pH plays an important role in the ionization of hydroxyl groups, as higher pH (~11) offers greater ionization of hydroxyl group and thus shows faster reduction of Au^{+3} into gold nanoparticles in comparison to lower pH (~8). Also, we have demonstrated in the peptide design and gelation behavior section of this work (figure 6.2), the Fmoc group is stable at pH 10.5 and can self-assemble to form soluble fibers which stabilize the synthesized gold nanoparticles as indicated by the AFM images in (figure 6.16).

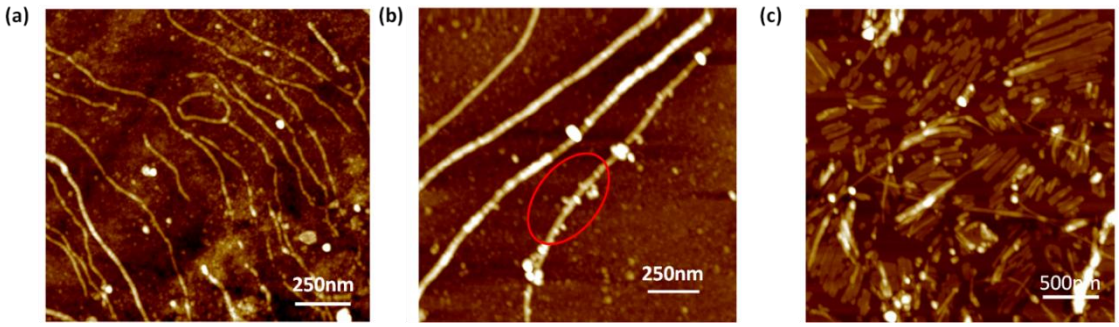

Figure 6.16 *AFM images of soluble fibers of (a) Fmoc FY at pH 11 and (b) Fmoc FY and (c) Fmoc FS nanostructures embedded gold nanoparticles at pH 11. The highlighted area in (b) and (c) shows the gold nanoparticles.*

6.3.7.3 Characterization of synthesized gold nanoparticles:

6.3.7.3a SPR Measurement using UV-visible NIR Spectroscopy: The gold nanoparticles are known to exhibit shape and size dependent surface plasmon resonance absorption. The subtle difference in SPR band indicates the formation of different sized gold nanoparticles. The optical properties of gold nanoparticles synthesized with different peptides at variable pH are depicted in figure 6.17 (a & d) measured by UV-Vis NIR spectroscopy. At higher pH (~11), the faster reduction gave rise to smaller sized gold nanoparticles, which is also reflected by the absorption maxima at lower wavelength (531 nm for Fmoc FY and 527 nm for Fmoc FS) in comparison to larger sized particles reduced by the peptides at pH 8 (546 nm for Fmoc FY and 530 nm for Fmoc FS). Interestingly, a distinct peak in the visible region at ~970 nm is observed which is characterized by the anisotropic nature of the gold nanoparticles, synthesized by Fmoc FY at pH 11. The optical properties of anisotropic gold nanoparticles are mainly governed by the longitudinal dipolar surface Plasmon resonance of the isolated nanoparticles, which is observed by the peak at higher wavelength in the UV–visible spectra. [71]

6.3.7.3b Mechanism of gold nanoparticle formation with different shapes: It is known from the literature that in the absence of pre-synthesized seeds, the formation of metal nanoparticles is controlled by synergistic effects of thermodynamic and kinetic parameters. The synthesis process may involve three major steps: (i) nucleation of metal ions in the form of small clusters called as nuclei's, (ii) development of seeds by the fusion of nuclei's and (iii) growth of seeds leads to the formation of colloidal nanoparticles of various shapes. The thermodynamically favored growth leads to the formation of spherical structures due to uniform growth of all facets leading to global minimum of Gibbs free energy landscape. [72, 73] In case of kinetically favored reaction, preferential directional growth along unstable facets takes place that results in formation of different shapes of nanoparticles corresponding to different local minima. [72, 74]

It has been observed that the shape of nanoparticles is also largely governed by the nature of the reducing agents. A report by Prado et. al. compares the reducing capabilities of sodium borohydride ($NaBH_4$) and sodium citrate ($Na_3C_6H_5O_7$) and discussed the potential differences in the mechanism of formation of resultant particles. The report also suggested the formation of small sized nanoparticles due to well known strong reducing capabilities of $NaBH_4$, whereas the $Na_3C_6H_5O_7$ as a mild reducing agent has good stabilizing ability. Thus, small sized spherical nanoparticles formed by mild reducing agents were favored by the stabilization phase of growth process. [75] The stabilization occurs by the chemisorption of peptides as capping agents which reduces the surface free energy and prevents the further growth of all stabilized facets. Further addition of gold atoms at higher energy facets results in anisotropic growth leading to different

shaped nanoparticles. [72, 73] However, in the absence of any template, both mild as well as strong reducing agents resulted in the formation of spherical nanoparticles, but of different sizes, because of the lowest surface to volume ratio of spheres. Similarly, a detailed report by J. Polte on fundamentals of growth principles of colloidal nanoparticles describes that rapid reduction of metal salts by strong reducing agents followed by growth is supposed to occur via kinetically favored mechanism, while the thermodynamically favored mechanism is well correlated with mild reducing agents. [76] The formation of anisotropic gold nanoparticles begins with the initial faster reduction of gold ions and their quick accumulation in the form of small nuclei with minimal or no re-dissolution. The nuclei formation step is the main kinetic barrier in homogenous solutions because of the less stability of the nuclei's due to their extremely smaller size and insufficient solvation. As the saturation of nuclei reaches above critical level, the unstable nuclei's grows in size to form stable seeds. Thus this mechanism suggests that even before formation of faceted nanoparticles, the spherical intermediates were formed in the solution. Indeed this faster initial stage is the kinetically controlled reaction and is later on followed by the growth stage that involves the deposition of monomers on stable seeds to form faceted anisotropic nanoparticles. The growth step occurs at much slower rate and is energetically favored. [73] It is also known that peptide hydrogels can act as a template for providing direction to growing nanoparticle along certain facets resulting in formation of anisotropic shaped nanoparticles. [47]

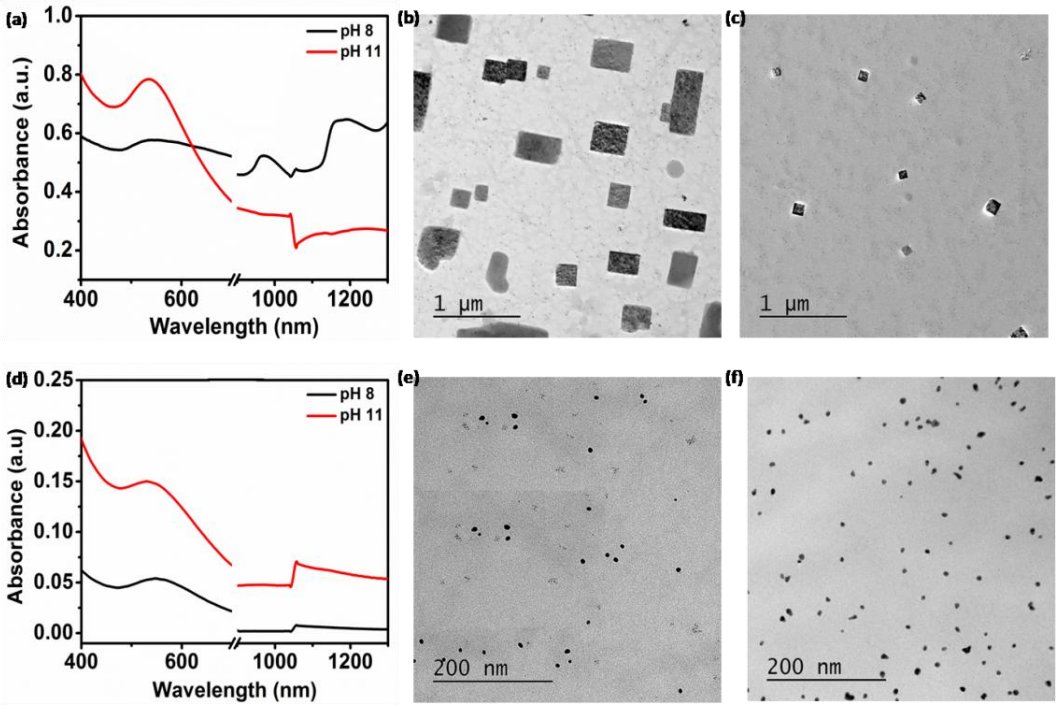

Figure 6.17 *Surface Plasmon resonance spectra of gold nanoparticles with (a) Fmoc FY and (d) Fmoc FS at different pH; TEM images of gold nanoparticles synthesized with Fmoc FY (b & c) and Fmoc FS (e & f) at pH 8 and pH 11 respectively.*

In this work, Fmoc FY, having the aromatic hydroxyl group acts as a strong reducing agent and resulted in formation of anisotropic shaped nanoparticles. The nanoparticle formation mechanism using Fmoc FY probably proceeded by kinetically favored route. We hypothesize that, at first, faster reduction of $HAuCl_4$ resulted in formation of small sized spherical particles which further coalesce to anisotropic rectangular shaped nanoparticles where our peptide hydrogel network acts as a template. The presence of two SPR peaks in the UV-Vis spectrum corresponds to the primary nanoparticles of smaller size (~530 nm) and larger coalesced anisotropic particles (~970 nm). In contrast to Fmoc FY, the aliphatic hydroxyl group containing Fmoc FS acts as a mild reducing agent. It is also reported by Cai et. al. that amino acids without aromatic groups are weak reducing agents and cannot effectively reduce the gold salt, at room temperature, according to which serine, can be considered as a mild reducing agent. [69] Therefore, at the expense of minimal energy Fmoc FS resulted into formation of spherical nanoparticles, which corresponds to the lowest energy shape and is primarily formed by reduction of metal salts. As previously known, the stabilizing ability of mild reducing agents inhibits the further growth of these spherical nanoparticles. This has been reflected in the SPR spectrum of these nanoparticles showing single peak in the range of ~530 nm. Therefore, the differential reduction behavior of aromatic and aliphatic hydroxyl groups of Fmoc FY and Fmoc FS probably resulted in the formation of nanoparticles of different shapes and sizes.

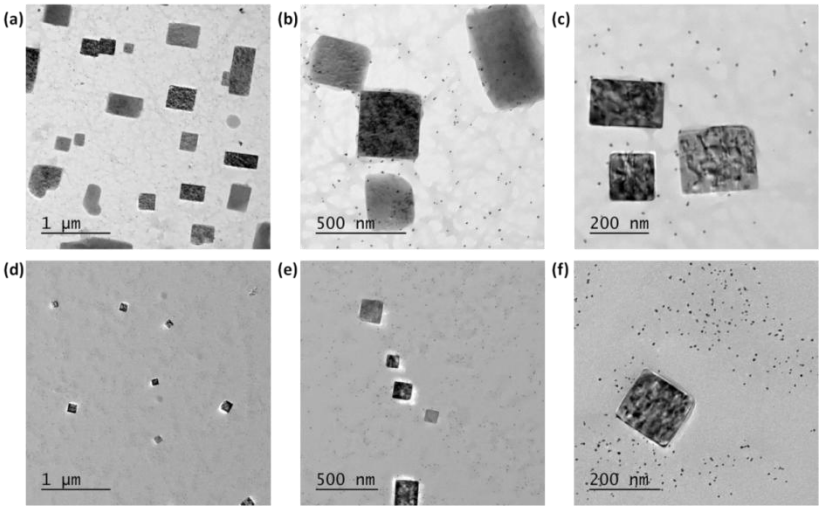

Figure 6.18 *TEM images of rectangular gold nanoparticles synthesized by Fmoc FY (a-c) at pH 8 and (d-f) at pH 11 at different magnifications.*

Further, the morphology of synthesized GNPs was analyzed using TEM shown in figure 6.17(b, c, e and f) and figure 6.18. The peptide with aliphatic hydroxyl group (Fmoc FS) showed the formation of spherical gold nanoparticles with an average size of 9.3 ± 1.7nm for pH 8 and 6.6 ± 2.1nm for pH 11, which can be corroborated with their surface plasmon resonance spectra (figure 6.22). However, the aromatic hydroxyl peptide, surprisingly, showed majorly the formation of rectangular plate shaped gold nanoparticles at both pH in addition to spherical particles. [77] The average aspect ratio of these nanoparticles at pH 8 and 11 were found to be 1.35 ± 0.38 and 1.1 ± 0.05, respectively, by measuring the length and breadth of 50 nanoparticles. The higher aspect ratio of pH 8 rectangular nanoparticles was also supported by the presence of an anisotropic peak in the absorption spectra of these nanoparticles. However nanoparticles with pH 11 have aspect ratio near to 1, which indicates more symmetric morphology in comparison to nanoparticles synthesized at pH 8, which may be the probable reason for the lack of anisotropic peak at pH 11. The selected areas of gold nanoparticles were studied using EDX for the confirmation of gold in the rectangular nanoparticles, shown in figure 6.19 a & b. The AFM confirms the presence of elongated fibers at pH 11 in which the nanoparticles are entrapped (figure 6.16 a & b). The TEM imaging was done after negative staining of the grids to visualize the entangled fibrous network entrapping nanoparticles within it at pH 11. The AFM and TEM analysis suggests that although gels were not formed at pH 11 but the self-assembly occurred and the fibrous structures were formed which were responsible for the stability of in situ synthesized gold nanoparticles.

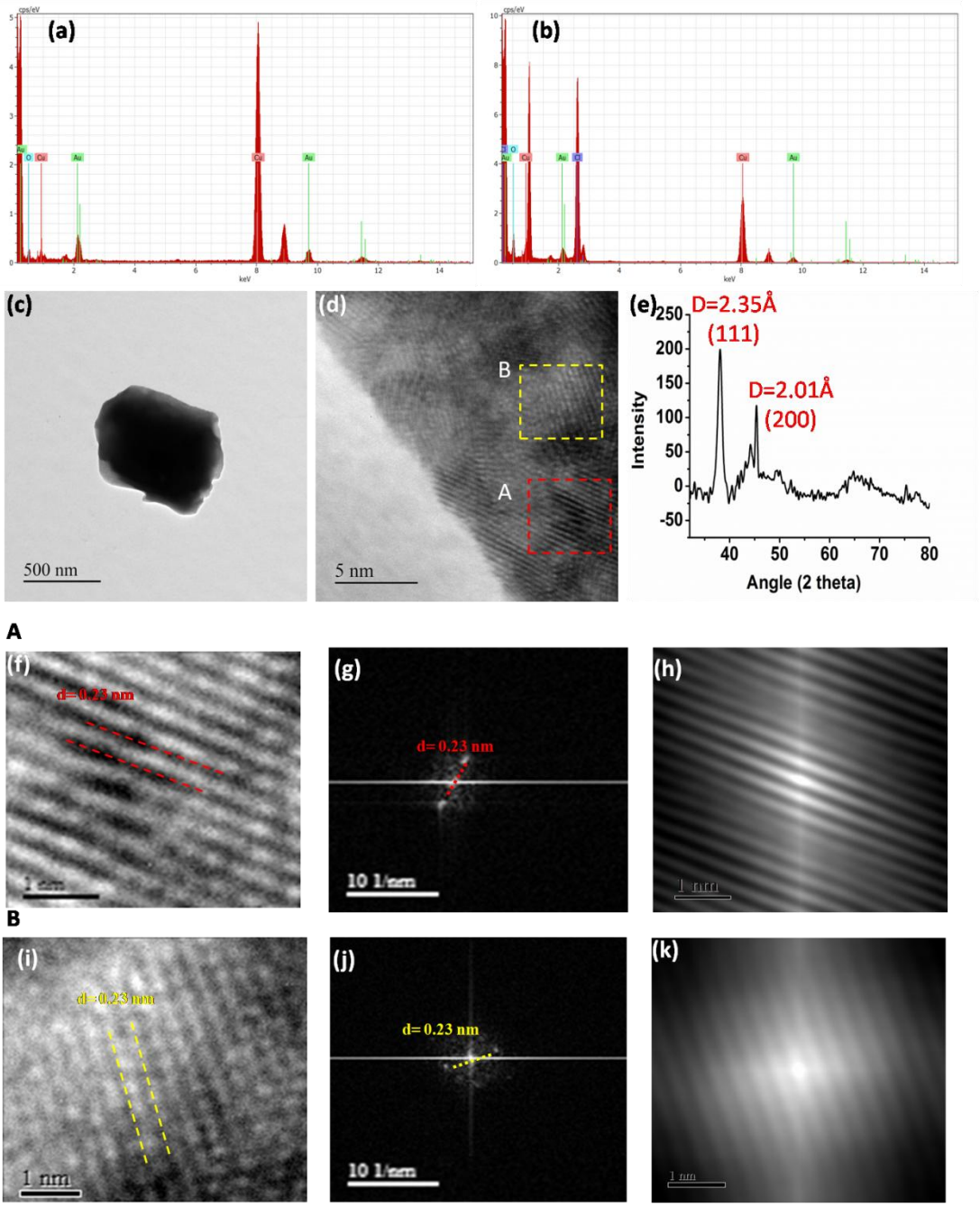

Figure 6.19 *EDX elemental analysis of gold nanoparticles synthesized by (a) Fmoc FY and (b) Fmoc FS;(c)TEM and (d) HRTEM image of single rectangular gold nanoparticle, (f and i) Magnified HRTEM in two different planes A and B (marked with red and yellow boxes) showing adjacent lattice fringe width of 0.23nm which corresponds to (111) face-centered cubic crystal structure of gold as confirmed by the major peak in (e) XRD spectra at* $2\theta = 38.1^0$*; (g and j) shows FFT and (h and k) shows auto-correlation pattern of the corresponding gold nanoparticle.*

To characterize rectangular gold nanoparticles, HRTEM and EDS mapping was performed using TEM and STEM techniques (figure 6.19 and 6.20). The HRTEM images showed the interplanar distance of adjacent lattice fringes equal to 0.235 nm, calculated by using Gatan Microscopy Suite software. This distance corresponds to the (111) planes of face centered cubic (fcc) crystal structure of gold (figure 6.19 d, f and i). The XRD diffraction pattern exhibited the strongest peak at 2θ=38.10 which corresponds to the d-spacing of 0.235nm that also confirms the presence of typical fcc gold structure (figure 6.19e). [47, 76] The FFT and auto-correlation pattern further verified the crystalline structure of the rectangular gold nanoparticles (figure 6.19 g, h, j and k). To obtain a deeper insight of elemental composition of these anisotropic nanoparticles, EDS elemental mapping was performed. The images in figure 6.20 b-f clearly revealed the uniform distribution of gold signal throughout the rectangular nanostructure. Apart from gold, carbon, nitrogen and oxygen were the other elements present within the nanostructure which were also found in EDX line scan done along the length of the rectangular nanoparticle (figure 6.21a). The atomic percentage of corresponding elements from the line scan signals were obtained as gold=22.67%, nitrogen= 40.86%, oxygen= 27.24 and carbon=9.23% (figure 6.21b). The elemental mapping results suggested that peptide template supports the anisotropic rectangular gold structures.

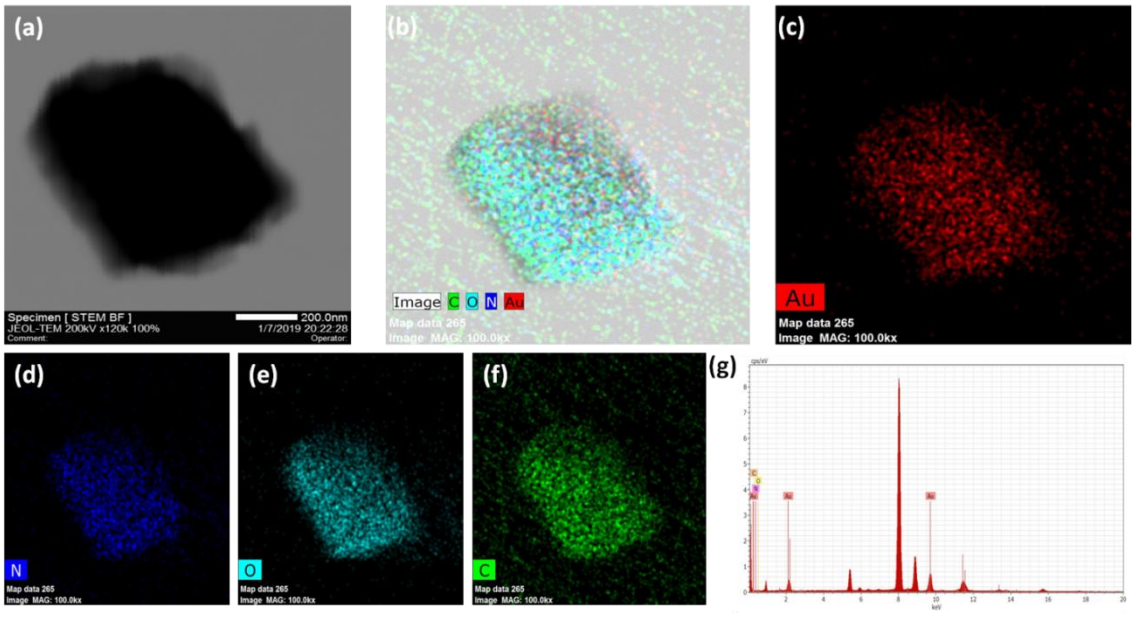

Figure 6.20 *(a) Bright field STEM image of rectangular gold nanoparticle, (b-f) corresponds to its elemental mapping with (b) showing the presence of carbon (green dots), oxygen (cyan dots), nitrogen (blue dots) and gold (red dots), followed by individual images of each element(c-f); (g)*

shows EDX elemental spectra of same rectangular gold nanoparticle, confirming the presence of gold.

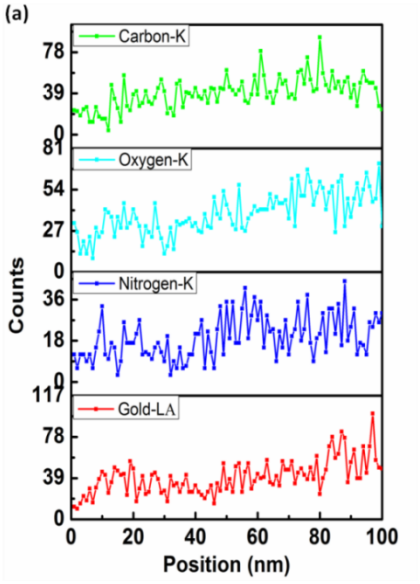

(c)

Elements	Weight %	Atomic %	Error Weight %
Gold	79.96	22.67	1.77
Nitrogen	10.25	40.86	2.27
Oxygen	7.80	27.24	1.57
Carbon	1.99	9.23	0.68

Figure 6.21 *(a) EDX line scans of Carbon-K, Nitrogen- K, Oxygen- K and Gold-LA signals, (b) STEM image of rectangular gold nanoparticle analysed for line EDX analysis (yellow line) and (c) Quantification of different elements from EDX line spectra.*

The DLS measurements were done to confirm the size of the nanoparticles as measured by TEM (shown in figure 6.22 a and b). The results showed close agreement with the TEM values however the values obtained through DLS were higher in comparison to TEM results, as it measures the hydrodynamic radii of the particles. The gold nanoparticles reduced by Fmoc FS exhibits average size of 22.9 ± 3nm and 16.1 ± 6nm at pH 8 and 12 respectively. Whereas, the gold nanoparticles with Fmoc FY showed the average size of 141 ± 33 nm and 144 ± 13 nm at pH 8 and 11 respectively.

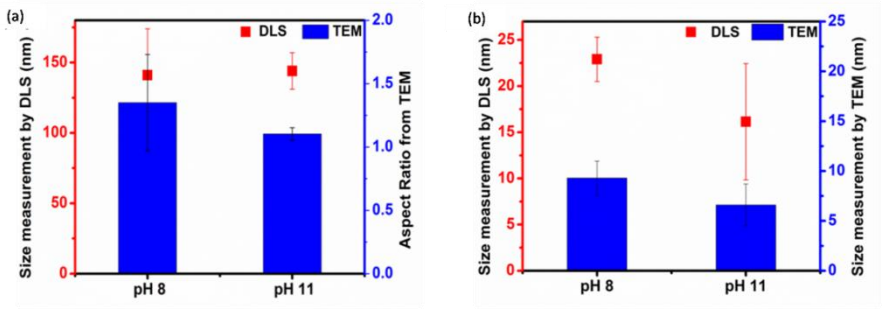

Figure 6.22 *Size distribution analysis of nanopartices with (d) Fmoc FY and (h) Fmoc FS using TEM and DLS*

Now it would be interesting to know the mechanical strength of the organic-inorganic hybrid materials i.e the gel embedded gold nanoparticles. The storage (G') and loss modulus of Fmoc FY and Fmoc FS hydrogels was compared in the presence and absence of gold nanoparticles at MGC (figure 6.23). It was also noted that visible colour change indicating Au^{+3} to Au^{0} was observed in less than 24 hrs for Fmoc FY, whereas it took more than 24 hrs with Fmoc FS and the rheology measurements were done after 24 and 48 hrs respectively. Such differential reduction time again confirmed the strong reducing capability of Fmoc FY over Fmoc FS. We observed the reinforcement of mechanical strength of hydrogels upon incorporation of gold nanoparticles in case of both the hydrogels. In Fmoc FY gels, the mechanical strength was found to be an order of magnitude higher with gold nanoparticles (figure6.23), while for Fmoc FS, the strength was found to be nearly twice than that of hydrogels without gold nanoparticles(figure 6.23b). The enhancement in the mechanical strength was also observed in previous reports. [79-81] The probable reason for this enhancement could be that the nanoparticles might act as physical crosslinking centers and joins multiple peptide strands, resulting in denser network. [79, 80] Another report by Adibnia et. al. stated that the reinforcement of mechanical properties also depends upon the distribution of nanoparticles in gel network. [81] The porous hydrogel network provides the space for uniform distribution of nanoparticles which is also responsible for the long term stability of the synthesized nanoparticles, avoiding aggregation. Thus, preparation of such metal-organic hybrids elucidates a successful route for altering the physical properties of the peptide hydrogels, without any chemical modifications.

Thus, we successfully demonstrated the utility of low molecular peptides in preparation of GNP of varying shapes and sizes by in situ reduction of $HAuCl_4$, without involvement of any external reducing/capping agent. Hence, the tyrosine and serine-based hydrogelators are elegant hosts as structure-directing templates for in situ shape-controlled preparation and stabilization of GNPs.

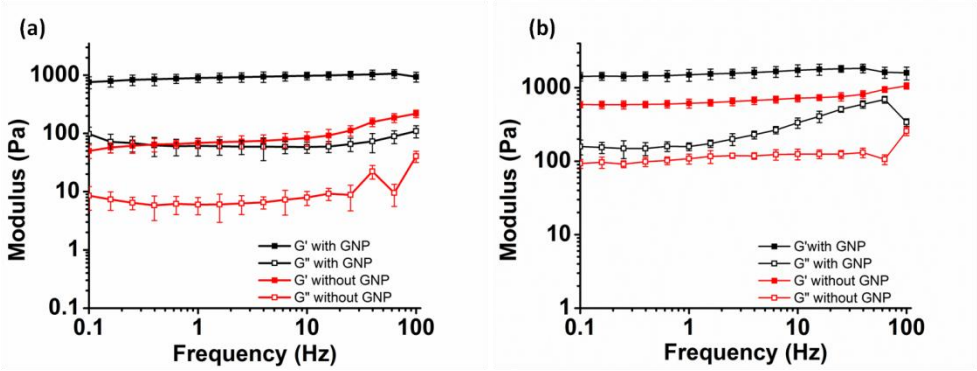

Figure 6.23 *Comparison of mechanical stiffness of (a) Fmoc FY and (b) Fmoc FS hydrogels in the presence and absence of gold nanoparticles formed after 24 hrs and 48 hrs respectively, at pH 8.*

6.4 Conclusions

In summary, we elucidate the fundamental role of molecular structure in determining the physiochemical properties of the self-assembled peptides that can promote the rational design of amyloid based short peptides as functional nanomaterial. Our observations and structural data not only provide an insight into the role of amino acid hydrophobicity in self-assembly but also demonstrate the profound effect of aromatic capping on the self-assembly propensity and morphology of the resulting materials. For the first time, we clearly demonstrated the difference in participation of aliphatic and aromatic hydroxyl functionality towards controlling the shape of synthesized gold nanoparticles. To the best of our knowledge, it is the first report of synthesis of rectangular plate like GNP, using such short peptide sequence. The nanofibrous structure of the peptides results in remarkable stability of GNP's in aqueous solutions. The bioinpired approach makes them suitable for biomedical applications. We hope that our study will provide strong evidences for understanding the relationship between peptide sequence and nanoparticle growth. Thus we anticipate that the continuous efforts and a detailed understanding towards rational design of multifunctional peptides will open up new avenues for nanomaterial synthesis with controlled geometric parameters, depending upon their utilities.

Note:

- ✓ The permission has been granted by authors and corresponding author of the published paper prior to its adoption in the present thesis. The publication associated with this work is:

  Rashmi Jain, Gaurav Khandelwal, Sangita Roy, Unraveling the Design Rules in Ultrashort Amyloid-Based Peptide Assemblies toward Shape-Controlled Synthesis of Gold Nanoparticles, *Langmuir*, 35 (2019) 5878-5889

6.5 References

1. M. Reches, E. Gazit, Casting Metal Nanowires within Discrete Self-assembled Peptide Nanotubes, *Science* 300 (2003) 625-627.
2. D. K. Smith, Self-assembling Fibrillar Networks-Supramolecular Gels in Supramolecular Chemistry: From *Molecules to Nanomaterials*, ed. J W. Steed and P. A. Gale, Wiley (2012) DOI: 10.1002/9780470661345.smc142.

3. N. Singh, M. Kumar, J. F. Miravet, R. V. Ulijn, B. Escuder, Peptide-Based Molecular Hydrogels as Supramolecular Protein Mimics. *Chem. Eur. J.* 2017, 23, 981 – 993.
4. J. Zhou, J. Li, X. Du, B. Xu, Supramolecular biofunctional materials, *Biomaterials* 129 (2017) 1-27.
5. D. Zheng, Z. Gao, T. Xu, C. Liang, Y. Shi, L. Wang Z. Yang, Responsive peptide-based supramolecular hydrogels constructed by self-immolative chemistry, *Nanoscale*, 10 (2018) 21459-21465.
6. Y. Wang, Y. Zhang, X. Li, C. Li, Z. Yang, L. Wang, A Peptide-Based Supramolecular Hydrogel for Controlled Delivery of Amine Drugs, *Chem. Asian J*. 13 (2018) 3460-3463.
7. H. Wang, Z. Yang, Short-peptide-based molecular hydrogels: novel gelation strategies andapplications for tissue engineering and drug delivery, *Nanoscale*, 4 (2012) 5259-5267.
8. K. Ma, R. Xing, T. Jiao, G. Shen, C. Chen, J. Li, X. Yan, Injectable Self-Assembled Dipeptide-Based Nanocarriers for Tumor Delivery and Effective In Vivo Photodynamic Therapy, *ACS Appl. Mater. Interfaces* 8 (2016) 30759−30767.
9. S. Li, R. Xing, R. Chang, Q. Zou, X. Yan, Nanodrugs based on peptide-modulated self-assembly: Design, delivery and tumor therapy, *Curr. Opin. Colloid Interface Sci*., 35 (2018) 17-25.
10. R. Draper, D. J. Adams, Low-Molecular-Weight Gels: The State of the Art, *Chem*, 3 (2017) 390–410.
11. T. Kar, P. K. Das, Molecular Gels as Templates for Nanostructured Materials, *Functional Molecular Gels*, Royal Society of Chemistry 1 (2013) 255- 303.
12. N. Sahiner, Soft and flexible hydrogel templates of different sizes and various functionalities for metal nanoparticle preparation and their use in catalysis. *Prog. Polym. Sci*, 38 (2013) 1329- 1356.
13. B. Adhikari, A. Banerjee, Short-Peptide-Based Hydrogel: A Template for the In Situ Synthesis of Fluorescent Silver Nanoclusters by Using Sunlight. *Chem. Eur. J*. 16 (2010) 13698- 13705.
14. S. Si, R. R. Bhattacharjee, A. Banerjee, T. K. Mandal, A Mechanistic and Kinetic Study of the Formation of Metal Nanoparticles by Using Synthetic Tyrosine-Based Oligopeptides. *Chem. Eur. J*. 12 (2006) 1256- 1265.
15. C. J. Bowerman, D. M. Ryan, D. A. Nissan, B. L. Nilsson, The effect of increasing hydrophobicity on the self-assembly of amphipathic b-sheet peptides. *Mol. BioSyst*. 5 (2009) 1058- 1069.

16. A. Lampel, R. V. Ulijn, T. Tuttle, Guiding principles for peptide nanotechnology through directed discovery, *Chem. Soc. Rev*. 47 (2018) 3737-3758.
17. M. J. Krysmann, V. Castelletto, A. Kelarakis, I. W. Hamley, R. A. Hule, D. J. Pochan, Self-Assembly and Hydrogelation of an Amyloid Peptide Fragment. *Biochemistry* 47(2008) 4597- 4605.
18. M. Tena-Solsona, J. F. Miravet, B. Escuder, Tetrapeptidic Molecular Hydrogels: Self-assembly and Co-aggregation with Amyloid Fragment Aβ1-40.*Chem. Eur. J*. 20 (2014) 1023-1031.
19. D. Marti, E. Mayans, A. M. Gil, A.Diaz, I. Jimenez, A. I. Yousef, I. Keridou, C. Cativiela, J. Puiggali, C. Aleman, Amyloid-Like Fibrils from a Diphenylalanine Capped with an Aromatic Fluorenyl. *Langmuir* 34 (2018), 15551-15559.
20. G. Cheng, V. Castelletto,C. M. Moulton, G. E. Newby I. W. Hamley, Hydrogelation and Self-Assembly of Fmoc-Tripeptides: Unexpected Influence of Sequence on Self-Assembled Fibril Structure, and Hydrogel Modulus and Anisotropy. *Langmuir,* 26 (2010) 4990- 4998.
21. S. Fleming, S. Debnath, P. W. J. M. Frederix, T.Tuttle, R. V. Ulijn, Aromatic peptide amphiphiles: significance of the Fmoc moiety. Chem. Commun. 49 (2013) 10587- 10589.
22. E. R. Draper, K. L. Morris, M. A. Little, J. Raeburn, C. Colquhoun, E. R Cross, T. O. McDonald, L. C. Serpell. D. J. Adams, Hydrogels formed from Fmoc amino acids. CrystEngComm 2015, 17, 8047- 8057.
23. S. Roy, N. Javid, J. Sefcik, P. J. Halling, R. V. Ulijn, Salt-Induced Control of Supramolecular Order in Biocatalytic Hydrogelation. *Langmuir* 28 (2012) 16664−16670.
24. K. Tao, A. Levin, L. Adler-Abramovich, E. Gazit, Fmoc-modified amino acids and short peptides: simple bio-inspired building blocks for the fabrication of functional materials. *Chem. Soc. Rev* 45 (2016) 3935-3953.
25. L. Chen, K. Morris, A. Laybourn, D. Elias, A. Hicks, M. R. Rodger, L. Serpell, D. J. Adams, Self-Assembly Mechanism for a Naphthalene-Dipeptide Leading to Hydrogelation. *Langmuir*, 26 (2010) 5232- 5242.
26. X. Yan, P. Zhu, J. Li, Self-assembly and application of diphenylalanine-based nanostructures, *Chem. Soc. Rev.* 39 (2010) 1877–1890.
27. Z. Yang, G. Liang, M. Ma, Y. Gao, B. Xu, Conjugates of naphthalene and dipeptides produce molecular Hydrogelators with high efficiency of hydrogelation and superhelical nanofibers, *J. Mater. Chem.* 17 (2007) 850- 854.

28. M. Ma, Y. Kuang, Y. Gao, Y. Zhang, P. Gao, B. Xu, Aromatic-Aromatic Interactions Induce the Self-Assembly of Pentapeptidic Derivatives in Water To Form Nanofibers and Supramolecular Hydrogels. *J. Am. Chem. Soc.* 132 (2010) 2719- 2728.
29. J. Li, X. Du, S. Hashim, A. Shy, B. Xu, Aromatic−Aromatic Interactions Enable α Helix to β Sheet Transition of Peptides to Form Supramolecular Hydrogels, *J. Am. Chem. Soc.* 139 (2017) 71−74.
30. N. Brown, J. Lei, C. Zhan, L. J. W.Shimon, L. Adler-Abramovich, G.Wei, E. Gazit, Structural Polymorphism in a Self-Assembled Tri-Aromatic Peptide System. *ACS Nano*, 12 (2018) 3253−3262.
31. C. Ou, J. Zhang, X. Zhang, Z. Yang M. Chen, Phenothiazine as an aromatic capping group to construct a short peptide-based 'super gelator', *Chem. Commun*. 49 (2013) 1853-1855.
32. D. M. Ryan, S. B. Anderson, F. T. Senguen, R. E. Youngman, B. L. Nilsson, Self-assembly and hydrogelation promoted by F5-phenylalanine, *Soft Matter* 6 (2010) 475-479.
33. T. M. Doran, E. A. Anderson, S. E. Latchney, L. A. Opanashuk, B. L. Nilsson, An Azobenzene Photoswitch Sheds Light on Turn Nucleation in Amyloid-β Self-Assembly, *ACS Chem. Neurosci*. 3 (2012) 211−220.
34. D. J. Adams, L. M. Mullen, M. Berta, L. Chen, W. J. Frith, Relationship between molecular structure, gelation behaviour and gel properties of Fmoc-dipeptides, *Soft Matter* 6 (2010) 1971- 1980.
35. M. Hughes, P. W. J. M . Frederix, J. Raeburn, L. S. Birchall, J. Sadownik, F. C. Coomer, I-H. Lin, E. J. Cussen, N. T. Hunt, T. Tuttle, S. J. Webb, D. J. Adams, R. V. Ulijn, Sequence/structure relationships in aromatic dipeptide hydrogels formed under thermodynamic control by enzyme-assisted self-assembly, *Soft Matter* 8 (2012) 5595-5602.
36. R. J. Betush, J. M. Urban. B. L. Nilsson, Balancing hydrophobicity and sequence pattern to influence self-assembly of amphipathic peptides, *Biopolymers* 110 (2018)1-13 DOI: 10.1002/bip.23099.
37. M. B. Dickerson, K. H. Sandhage, R. R. Naik, Protein- and Peptide-Directed Syntheses of Inorganic Materials, *Chem. Rev.* 108 (2008) 4935-4978.
38. K. Saha, S. S. Agasti, C. Kim, X. Li, V. M. Rotello, Gold Nanoparticles in Chemical and Biological Sensing, *Chem. Rev.* 112 (2012) 2739- 2780.

39. M. C. Daniel, D. Astruc, Gold Nanoparticles: Assembly, Supramolecular Chemistry, Quantum- Size-Related Properties, and Applications toward Biology, Catalysis, and Nanotechnology, Chem. Rev. 104 (2004), 293- 346.
40. A. Jimenez-Ruiz, P. Perez-Tejeda, E. Grueso, P. M. Castillo, R. Prado-Gotor, Nonfunctionalized Gold Nanoparticles: Synthetic Routes and Synthesis Condition Dependence, *Chem. Eur. J.* 21 (2015) 9596 – 9609.
41. M. Grzelczak, J. Perez-Juste, P. Mulvaney, L. M. Liz-Marzan, Shape control in gold nanoparticle synthesis, *Chem. Soc. Rev.* 37 (2008) 1783-1791.
42. X. Yan, Blacklock, J. Li, H. Mohwald, One-Pot Synthesis of Polypeptide Gold Nanoconjugates for in Vitro Gene Transfection, *ACS Nano*, 6 (2012), 111-117.
43. Y. N. Tan, J. Y. Lee, D. I. C. Wang, Uncovering the Design Rules for Peptide Synthesis of Metal Nanoparticles, *J. Am. Chem. Soc*. 132 (2010) 5677- 5686.
44. Y. Li, Z. Tang, P. N. Prasad, M. R. Knecht, M. T. Swihart, Peptide-mediated synthesis of gold nanoparticles: effects of peptide sequence and nature of binding on physicochemical properties, *Nanoscale* 6 (2014) 3165- 3172.
45. P. K. Vemula, G. John, Smart amphiphiles: hydro/organogelators for in situ reduction of gold, *Chem. Commun*. 21 (2006) 2218-2220.
46. S. Ray, A. K. Das, A. Banerjee, Smart oligopeptide gels: in situ formation and stabilization of gold and silver nanoparticles within supramolecular organogel networks, *Chem. Commun*. 26 (2006) 2816- 2818.
47. R. N. Mitra, P. K. Das, In situ Preparation of Gold Nanoparticles of Varying Shape in Molecular Hydrogel of Peptide Amphiphiles, J. Phys. Chem. C 112 (2008) 8159- 8166.
48. J. K. Sahoo, S. Roy, N. Javid, K. Duncana, L. Aitken, R. V. Ulijn, Pathway-dependent gold nanoparticle formation by biocatalytic self-assembly, *Nanoscale* 9 (2017) 12330-12334.
49. M. A. Elsawy, A. M. Smith, N. Hodson, A. Squires, A. F. Miller, A. Saiani, Modification of β-Sheet Forming Peptide Hydrophobic Face: Effect on Self-Assembly and Gelation. *Langmuir* 32 (2016) 4917− 4923.
50. Y. Zhao, W. Yang, C. Chen, J. Wang, L. Zhang, H. Xu, Rational design and self-assembly of short amphiphilic peptides and applications, *Curr Opin Colloid In*. 35 (2018) 112-123.
51. A.M. Smith, R.J. Williams, C. Tang, P. Coppo, R. F. Collins, M. L.Turner, A. Saiani, R.V. Ulijn, Fmoc-Diphenylalanine Self Assembles to a Hydrogel via a Novel Architecture Based on π–π Interlocked β-Sheets, *Adv. Mater*. 20 (2008) 37- 41.

52. S. Awhida, E. R. Draper, T. O. McDonald, D. J. Adams, Probing Gelation Ability for a Library of Dipeptide Gelators, *Colloids and Surfaces A* 535 (2017) 242–250.
53. R. Li, C. C. Horgan, B. Long, A. L. Rodriguez, L. Mather, C. J. Barrow, D. R. Nisbet, R. J. Williams, Tuning the mechanical and morphological properties of self-assembled peptide hydrogels via control over the gelation mechanism through regulation of ionic strength and the rate of pH change, *RSC Adv*. 5 (2015) 301–307.
54. C. A. Tang, M. Smith, R. F. Collins, R. V. Ulijn, A. Saiani, Fmoc-Diphenylalanine Self-Assembly Mechanism Induces Apparent pKa Shifts, *Langmuir*, 25 (2009) 9447- 9453.
55. A. K. Das, R. Collins , R. V. Ulijin, Exploiting Enzymatic (Reversed) Hydrolysis in Directed Self-Assembly of Peptide Nanostructures, *Small* 4 (2008) 279- 287.
56. E. T. Pashuck, H. Cui, S. I. Stupp, Tuning Supramolecular Rigidity of Peptide Fibers through Molecular Structure. J. Am. Chem. Soc. 132 (2010) 6041- 6046.
57. S. Fleming, P. W. J. M. Frederix, I. R. Sasselli, N. T. Hunt, R. V. Ulijn, T. Tuttle, Assessing the Utility of Infrared Spectroscopy as a Structural Diagnostic Tool for β-Sheets in Self-Assembling Aromatic Peptide Amphiphiles, *Langmuir* 29 (2013) 9510−9515.
58. S. Fleming, R. V. Ulijn, Design of nanostructures based on aromatic peptide amphiphiles, *Chem. Soc. Rev.* 43 (2014) 8150- 8177.
59. B. Adhikari, J. Nanda, A. Banerjee, Multicomponent hydrogels from enantiomeric amino acid derivatives: helical nanofibers, handedness and self-sorting, *Soft Matter* 7 (2011) 8913- 8922.
60. M. J. Krysmann, V. Castelletto, I. W. Hamley, Fibrillisation of hydrophobically modified amyloid peptide fragments in anorganic solvent, *Soft Matter* 3 (2007) 1401- 1406.
61. J. Raeburn, L. Chen, S. Awhida, R. C. Deller, M. Vatish, M. I. Gibson, D. J. Adams, Using molecular rotors to probe Gelation, *Soft Matter* 11 (2015) 3706-3713.
62. S. Marchesan, K. E. Styan, C. D. Easton, L. Waddington, A. V. Vargiu, Higher and lower supramolecular orders for the design of self-assembled heterochiral tripeptide hydrogel biomaterials, *J. Mater. Chem. B* 3 (2015) 8123- 8133.
63. J. Naskar, G. Palui, A. Banerjee, Tetrapeptide-Based Hydrogels: for Encapsulation and Slow Release of an Anticancer Drug at Physiological pH, *J. Phys. Chem. B* 113 (2009) 11787- 11792.
64. A. Rajbhandary, D. M. Raymond, B. L. Nilsson, Self-Assembly, Hydrogelation, and Nanotube Formation by Cation-Modified Phenylalanine Derivatives, *Langmuir* 33 (2017) 5803−5813.

65. J. Adamcik, J. M. Jung, J. Flakowski, P. D. L. Rios, G. Dietler, R. Mezzenga, Understanding amyloid aggregation by statisticalanalysis of atomic force microscopy images. Nat. Nanotech. 5 (2010) 423- 428.
66. R. Orbach, I. M. Harpaz, L. A. Abramovich, E. Mossou, E. P. Mitchell, V. T. Forsyth, E. Gazit, D. Seliktar, The Rheological and Structural Properties of Fmoc-Peptide-Based Hydrogels: The Effect of Aromatic Molecular Architecture on Self-Assembly and Physical Characteristics, *Langmuir* 28(2012) 2015- 2022.
67. S. M. Hashemnejad, S. Kundu, Probing Gelation and Rheological Behavior of a Self-Assembled Molecular Gel, *Langmuir* 33 (2017) 7769−7779.
68. A. Baral, S. Roy, S. Ghosh, D. Hermida-Merino, I. W. Hamley, A. Banerjee, A Peptide-Based Mechano-sensitive, Proteolytically Stable Hydrogel with Remarkable Antibacterial Properties. *Langmuir* 32 (2016) 1836−1845.
69. H. Cai, P. Yao, Gold nanoparticles with different amino acid surfaces: Serum albumin adsorption, intracellular uptake and cytotoxicity. *Colloids and Surfaces B: Biointerfaces* 123 (2014) 900- 906.
70. A. Tofanello, E. G. A. Miranda, I. W. R. Dias, A. J. C. Lanfredi, J. T. Arantes, M. A. Juliano, I. L. Nantes, pH-Dependent Synthesis of Anisotropic Gold Nanostructures by Bioinspired Cysteine-Containing Peptides, *ACS Omega* 1(2016) 424- 434.
71. J. Biswal, S. P. Ramnani, S. Shirolikar, S. Sabharwal, Synthesis of rectangular plate like gold nanoparticles by in situ generation of seeds by combining both radiation and chemical methods. Radiat. Phys. Chem. 80 (2011) 44- 49.
72. Y. Xia, X. Xia, H. Peng, Shape-Controlled Synthesis of Colloidal Metal Nanocrystals: Thermodynamic versus Kinetic Products, *J. Am. Chem. Soc*. 137 (2015) 7947−7966.
73. Y. Wang, J. He, C. Liu, W. H. Chong, H. Chen, Thermodynamics versus Kinetics in Nanosynthesis, *Angew. Chem. Int. Ed.* 54 (2015) 2022 – 2051.
74. P. R. Sajanlal, T. S. Sreeprasad, A. K. Samal, T. Pradeep, Anisotropic nanomaterials: structure, growth, assembly, and functions, *Nano Reviews*, 2 (2011) 5883-5945.
75. A. Prado, J. P. Oliveira, W. J. Keijok, B. A. Milaneze, B. V. Nogueira, M.C.C. Guimaraes, M. J. Pontes, Ribeiro, M. R. N. Comparison between the synthesis of gold nanoparticles with sodium citrate and sodium tetraboreto, *BMC Proceedings* 84 (2014) 252-254.
76. J. Polte, Fundamental growth principles of colloidal metal nanoparticles – a new perspective, *CrystEngComm.* 17 (2015) 6809-6830.

77. K. Park, H. Koerner, R. A. Vaia, Depletion-Induced Shape and Size Selection of Gold Nanoparticles, *Nano Lett.* 10 (2010) 1433- 1439.
78. N. Li, P. Zhao, D. Astruc, Anisotropic Gold Nanoparticles: Synthesis, Properties, Applications, and Toxicity, *Angew. Chem. Int. Ed.* 53 (2014) 1756 – 1789.
79. M. K. Jaiswal, J. R. Xavier, J. K. Carrow, P. Desai, D. Alge, A. K. Gaharwar, Mechanically Stiff Nanocomposite Hydrogels at Ultralow Nanoparticle Content, *ACS Nano* 10(2016) 246-56.
80. M. R. Reithofer, A. Lakshmanan, A. T. K. Ping, J. M. Chin, C. A. E. Hauser, In situ synthesis of size-controlled, stable silver nanoparticles within ultrashort peptide hydrogels and their anti-bacterial properties, *Biomaterials* 35 (2014) 7535-7542.
81. V. Adibnia, S. M. Taghavi, R. J. Hill, Roles of chemical and physical crosslinking on the rheological properties of silica-doped polyacrylamide hydrogels, *Rheol Acta*, 56 (2017) 123–134.

Chapter 7

Highly tuneable gels formed by the co-assembly of peptide and protein

7.1 Introduction

Protein-peptide interactions play crucial role in many cellular processes and are related with several human diseases. [1] Significant studies have been reported in the literature that explored protein-peptide interactions to understand the fundamentals of cellular functions and regulate them. Improving the efficacy of peptide therapeutics is also based on the principle of protein-peptide interactions. [2] The design of effective peptide based drugs to inhibit malfunctioning proteins require detailed understanding of protein-peptide interactions that can avoid certain ambiguities regarding selectivity and specificity of peptide drugs. The binding mechanism of synthetic peptides with cellular proteins is similar to binding of short fragment of polypeptide chain with proteins, for example, MHC complex proteins, peptide transporters, peptide harmones-receptor complexes, etc. [3] The peptides can interact with proteins in several ways including additional β-sheet, binding to clefts in extended β-sheet or proline type II helical conformations. [3] Despite high significance and estimated abundance there is a lacking of information on detailed characterizations of protein-peptide interactions.

Protein-peptide interactions are more transient and have significantly weak interaction affinity, in comparison to protein protein interactions. The high conformational flexibility of peptides along with these factors results in more complex structural characterization of protein-peptide interactions. [4] Furthermore, supramolecular assemblies are yet another interesting aspect of protein-peptide interactions. However, not many reports are available on the self-assembling protein-peptide systems. Most of the examples of synthetic binary systems include peptide-peptide or sugar-peptide composites. For example, Stupp's group showed the co-assembly of lipids and peptide amphiphiles that involves non-covalent anion-π interactions. [5] The self-assembled combined systems have great potential to be developed as functional systems. The literature suggests plenty of examples of functional composites based on covalent binding. [6] However, literature remains scarce with respect to exploration of non-covalent interactions for developing binary systems. The molecular self-assembly process becomes more difficult to understand when one of the components in composite is macromolecular. The self-assembly of small molecules under the influence of macromolecules such as proteins, DNA, polysaccharides, etc is a complex phenomenon and rarely studied. [7-9]

It is obvious that mixing of macromolecules with small molecules such as short peptides can dramatically affect the self-assembly behavior. To this direction, Stupp et al. have demonstrated the formation of interfacial mixing membrane by combining peptide amphiphiles with high molecular weight polysaccharide hyaluronic acid. [10] Other reports demonstrated the use of

different materials such as polysaccharide dextran [11] or clay particles [12] to modulate the mechanical properties of the small molecule hydrogels. In the similar line, a report by Xu and coworkers demonstrated the interaction of peptide amphiphile with cytosolic protein that significantly influenced their nanoscale structure. [13] Another report by Ulijn's group demonstrated the drastic effects on the supramolecular nanostructure properties through co-operative self-assembly of amphiphilic short peptides and proteins. They proposed the concept of mesoscale protein clusters at very low protein concentration, at room temperature, and under physiological conditions. [14] The co-operative self-assembly results in confinement by cluster of chiral macromolecules which have significant effects on morphological and mechanical properties of peptide derived hydrogels. In all the above described examples, the peptide amphiphiles have inherent self-assembling capabilities and addition of macromolecules was intended to modulate the properties of the self-assembled systems.

However, some peptide amphiphiles may lack the inherent self-assembling ability. These molecules might lack the appropriate strength of intermolecular interactions that could support the formation of 3D matrix. [15-17] The weak interactions favoured the Brownian motion and thus result in peptide solutions instead of gels, which narrow down the scope of their potential applications. The self-assembly in these peptide solutions or dispersions can be triggered by adding certain additive stimuli which are expected to enhance the intermolecular interactions between the soluble self-assembled structures. To this direction, metal ions have been widely explored by the several groups to induce gelation in self-assembled fibers via cross-linking. [18-20] There are very few reports showing examples of polymeric hydrogels that are formed by the involvement of specific protein-peptide interactions. [21-23] A report by Z. Yang and co-workers demonstrated the rational design of fusion protein with four binding sites and explored protein-peptide binding interactions to induce gelation in weakly interacting self-assembled peptide fibers. [24]

Enzyme assisted self-assembly is regarded as a powerful route of self-assembly and has been widely studied. But, we believe that, in addition to catalytic functions of enzyme proteins, they can also assist in the self-assembly of low molecular weight gelators. So far, in most of the studies based on enzyme triggered gelation, specific catalytic activity of enzymes has been explored. In this context, Jierry and co-workers demonstrated the enzyme assisted strategy to achieve spatiotemporal control over peptide self-assembly. [25] Their Fmoc based precursor is designed with a reversible disulfide bond, which itself is unable to self assemble due to highly negatively charged C-terminal. Glutathione reductase is used to cleave disulphide bonds of the

precursor and induce gelation, however, the formation and cleavage of disulphide bonds are in equilibrium and acts as a self-fuelled self-assembly cycle. To the best of our knowledge, no enzyme has been reported to induce gelation in a non-gelating molecular domain by simple physical interaction, without any catalytic activity. However, a report by Z. Yang's group showed the formation of molecular gels of a hydrophobic peptide through BSA protein stabilization. [26] Similar to other adducts like metal ions, salts, etc. the enzymatic proteins can also help in physical cross linking of peptide gelators, which otherwise may have weak interactions. The enzyme surface is rich in diverse functionality and can provide several sites for variable interactions such as hydrophobic interactions, aromatic interactions or H-bonding interactions.

In this work, we have explored the unusual property of enzymes in inducing gelation in the non gelator peptides, without utilizing their catalytic action. The gelation is expected to be based on non-covalent interactions, which takes place between proteins and non-gelator peptides after simple mixing. To the best of our knowledge, this is the first report which demonstrates the formation of hydrogels from the non-gelator dipeptides through non-covalent protein-peptide interactions. The previously reported works showed hydrogelation in long peptides (~13-mer sequence) through interaction with specially designed fusion proteins that have multiple binding sites. The effect was found to be quite universal since different varieties of commercially available proteins were used to trigger gelation. It depends on the hydropathy index of the protein employed to induce hydrogelation. Interestingly, the studies suggested that the protein-peptide interaction is non-specific and can occur with variety of dipeptide derivatives as well as different proteins. By using this approach, diverse morphological and mechanical properties can be accessed within a single peptide domain by either changing the type or the concentration of protein. The docking studies revealed that the proteins provide several sites for peptide interaction, which could act as a template for nucleation of peptide self-assembly and enhances interactions between peptide-peptide molecules, which results in fibrillar nanostructures. Excellent mechanoresponsive behavior of such gels can be explored for injectable carriers for biomedical applications. The present study extends the scope of supramolecular assembly beyond the use of single type of component to create functional biomaterials. The work also paves the way to generate nanofibrous hydrogel scaffold from non-gelator peptides also, which could overcome the limitations of conventional synthetic approach that involves the design of several chemical molecules. Additionally, the entrapment of enzymes within the hydrogel scaffold shows enzyme immobilization without losing their bioactivity and can be further used for biocatalytic applications.

7.2 Experimental

Material and Methods: Cbz-protected phenylalanine, C-terminal protected amino acids, HBTU (O-(benzotriazol-1-yl)-N,N,N′,N′-tetramethyluronium hexa-fluorophosphate) and DIPEA (N,N-diisopropylethylamine), were purchased from Sigma-Aldrich and used as received. The proteins lipases, thermolysin and chymotrypsin were purchased from Sigma-Aldrich and stored as per the prescribed conditions.

7.2.1 Peptide synthesis: The Cbz protected dipeptides were synthesized using solution phase peptide synthesis as discussed in chapter 6. The synthesized peptide was purified and analysis of purity was confirmed using mass spectroscopy. [27]

7.2.2 Gelation method: pH triggered gelation method was employed for dissolution of dipeptides. The weighed amount of peptide was added to 500µl water. Gradually 0.1 N NaOH was added until the complete peptide is dissolved resulting in clear basic solution (pH~11-12). Then, the pH was reduced to physiological pH by adding 0.1 N HCl. The protein stock solution (10mg/ml i.e. 1%) was prepared separately and 500µl and 250 µl of stock were added to the above prepared peptide solution to make protein concentration upto 0.5% and 0.25% respectively. The mixture was allowed to rest and set as a gel. The gels after 24 hrs were used for further characterization.

Dipeptide Cbz FL interaction with different types of proteins: The peptide solution (50mM) prepared by pH switch method was mixed with stock solutions of different types of proteins such as lipase, thermolysin, and chymotrypsin. For gelation, two different types of lipases were used obtained from same source, Candida rugosa. One lipase having more number of enzymatic units (type VII, ≥700U/mg of solid) is termed as L1 and the other having a lesser number of activity units (>2U/mg of solid) is termed as L2, in our work. The thermolysin used was obtained from Geobacillus stearothermophilus (Type X, 30-175 units/mg protein) while chymotrypsin used was from bovine pancreatic origin (type II, protein composition ≥85%).

Similarly, different dipeptide analogue (Cbz FY, Cbz FV & Cbz FI) solutions were prepared at 50mM-100mM concentration using pH gelation method, as described above. To this solution, different types of protein solutions were added to trigger gelation.

7.2.3 HPLC of composite gels: To check any cleavage of dipeptide in the presence of lipase enzyme, the composite gels after 24 hrs were diluted and injected into HPLC column. The Waters HPLC system with C18 reverse phase analytical column (Waters Spherisorb 5µm ODS1, with 4.6 X 250mm dimensions) was used with mobile phase having gradients of 5%

ACN/water to 90% ACN/water. Peptide solution without added lipase was used as control to compare the retention time in composite gels.

7.2.4 Morphology assessment

Atomic force microscopy (AFM) was used to study the morphology of protein-peptide composite hydrogels. For AFM sample preparation, 20µl of each gel was diluted in 200 µl of water. The diluted solution was drop-casted on clean silicon wafer. After 3 minutes, the excess sample was wicked off by the capillary action of filter paper. The sample was allowed to air dry and kept under vacuum overnight, before imaging. The imaging was done using Bruker MultiMode atomic force microscope operated in a tapping mode with a NanoScope controller and a J-scanner.

7.2.5 Mechanical strength measurement

Mechanical properties were determined using Anton Parr MCR302 rheometer with 50 mm parallel plate geometry and 0.2mm gap. The dynamic moduli of the hydrogels were measured as a function of frequency between 0.1 and 100 Hz. Amplitude sweep measurements were performed to ensure that the frequency sweep measurements were made in the linear regime and to obtain the optimum strain values from the linear viscoelastic region (LVE). The temperature of the instrument was controlled with integrated electrical heater and maintained at 20^0C throughout the experiments.

The thixotropic behavior of hydrogels was studied in the LVE range by applying the alternating strain of 100% and 0.1% for 100 and 200 s. The hydrogels were subjected to three repeated cycles of deformation and recovery. The hydrogels used for the rheology and thixotropic measurements were of 50 mM concentration of peptide.

7.2.6 Denaturation of proteins and gelation with denatured proteins

The proteins are sensitive to high temperatures and are liable to lose their structures upon heating at high temperatures. The lipase and chymotrypsin were subjected to heat in hot air oven maintained at 100^0C. While, for thermolysin, which is the most stable enzyme at temperature upto 90^0C was heated upto 120^0C to denature. The confirmation of denaturation was monitored by recording the CD spectra. The characteristic CD signals of denatured proteins were compared with native proteins before denauration, in aqueous solution.

Further, the denatured proteins were used for gelation with Cbz FL dipeptide (50mM), using above discussed gelation protocol. These gels were allowed to set for 24 hrs, after which the

rheological measurements were done using frequency sweep in the frequency range of 0.1 to 100Hz.

7.2.7 Biolayer Interferometry (BLI) for protein-peptide interaction

The interaction between protein and peptides was determined using an Octet K2 biolayer interferometer instrument by ForteBio (Pall Life Sciences). APS (aminopropylsilane) dip and read sensors supplied by ForteBio were used to immobilize the ligand protein through non-covalent interactions. In a 96 well plate, the first pair of wells were filled with baseline buffer, followed with protein solution (100μg/ml concentration) for loading of sensor. Next well contains another baseline buffer, in which the peptide solution was prepared to equilibrate the sensor surface, prior to its interaction with peptide solution. The further wells contained the sequential dilutions of peptide solutions ranging from 100μM to 1000 μM. After each peptide solution well, the dissociation buffer is placed to study the dissociation behavior of the two interacting components. The last wells contained the regeneration buffer to regenerate the sensor after the completion of study. The water was used as equilibration buffer before protein loading and regeneration buffer, while pH neutralized water (with similar amount of NaOH and HCl that was used in peptide solution preparation) was used. The protein loading was done was 600s while association and dissociation of peptides was studied for 100s each. The data was recorded by the Forte Bio Octet data acquisition software and analysed using global fitting with hetrogenous heterogenous ligand model (2:1).

7.2.8 Docking studies

SwissDock server, a online available tool based on the EADock DSS engine was employed for docking protein-peptide interactions. The algorithm of this software involves following steps: 1) many binding modes are generated, 2) CHARMM energies of each mode is estimated on the grid, 3) the clusters are created on the basis of most favorable energies, which are evaluated with FACTS, and 4) online visualization of most favorable clusters. The structure files of target and ligand can be directly uploaded for docking through the server. Target structures for proteins were selected from PDB records, or user-defined structures files can be uploaded (in various supported formats). A range of docking parameters could be set, including docking type (accurate, fast, very fast), which enables the user to select the desired docking time and exhaustiveness, and it also provides an option to define the region of interest. In this work, the docking was applied to the whole protein structure. We have used the aacurate accurate type of docking analysis. After obtaining the online result, it could be analyzed using Swissdock inbuilt software Jmol and offline with UCSF-Chimera.

7.2.9 Lipase catalytic activity

Lipase activity was tested using the hydrolysis of p-Nitrophenyl Butyrate (PNPB) into p-nitrophenol. For this assay, the p-nitrophenyl butyrate stock was prepared in ACN at 50mM concentration. The gels prepared at 50mM concentration were diluted upto 1mM concentration in water. 20µl of PNPB stock (i.e. 1mM) was added to 1 ml of diluted gel. The kinetics was recorded immediately after addition of PNPB, at 400nm for 300s, using a UV-visible spectrophotometer.

7.3 Results and discussion

7.3.1 Gelation of a non-gelator dipeptide

Our molecular design includes simple dipeptide sequence based on amyloid derived protein. We have selected Cbz FL dipeptide from our previous study described in chapter 6, which was reported to be a non gelator peptide under ambient conditions. This peptide was further employed for its binding to different enzymatic proteins in an attempt to induce its gelation. Cbz FL was synthesized using liquid phase synthesis and analysed for its purity using HPLC, mass spectroscopy and NMR spectroscopy, as described in chapter 6. [27] The C log P value of Cbz FL was found to be 4.34, as calculated through Chem Draw 12.0. The pH method was used to trigger gelation in Cbz-FL, but it failed to gelate even at higher concentration of ~100mM. Further, a protein lipase (L1) obtained from Candida rugosa having activity of ≥700 U/mg solid was added to Cbz FL solution at different concentrations (0.1%, 0.25 %, 0.5% and 1% w/v) in physiological conditions. Interestingly, gelation was observed at all concentrations of lipase with 50mM of Cbz FL, however, 0.1% lipase produced weak gel.

To check any hydrolytic reaction over Cbz FL by L1, HPLC was performed by diluting the gel. The chromatogram showed no change in the retention time of dipeptide, Cbz FL, which confirmed no enzymatic activity of lipase over Cbz FL (figure 7.2). Further, the protein induced peptide self-assembled gels were characterized for other physiochemical properties.

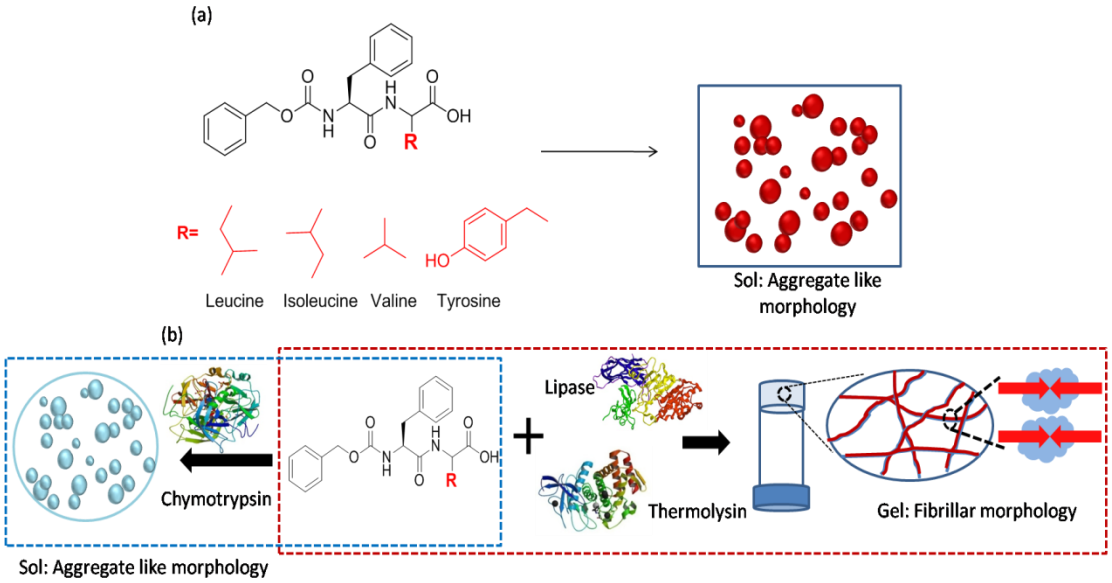

Figure 7.1 *(a) Molecular structure of Cbz-dipeptide having variable C-terminal amino acids, which are non gelator and shows aggregate like morphology. (b) Schematic representation of gelation of non-gelator dipeptide analogues in the presence of different proteins, which triggered formation of fibrillar network resulting in gelation except with chymotypsin, which forms aggregate like morphology.*

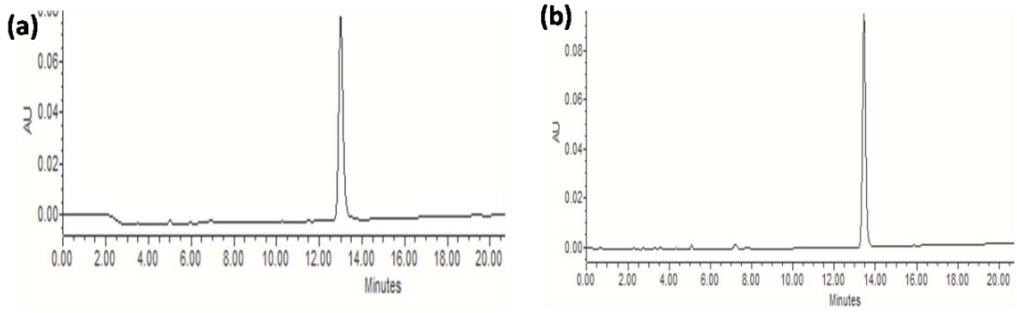

Figure 7.2 *HPLC chromatogram of Cbz FL (a) without lipase (b) after 24 hrs of lipase addition.*

7.3.2 Determination of specificity of the peptide to the proteins with different hydropathy index :

After the successful induction of self-assembly in a non-gelator by lipase protein, it was crucial to check the specificity of the interaction. In this direction, we used other hydrolytic enzyme proteins such as thermolysin and chymotrypsin. In addition to this, another grade of lipase i.e. L2 obtained from same origin (Candida rugosa) was also used, which have lower amount of enzymatic units (>2 units/mg). This enzyme was used to check the effect of enzyme activity on

gelation properties. Interestingly, L2 and thermolysin also induced gelation in Cbz FL, which indicated that the enzyme acts as a template for binding, which either promotes peptide-peptide interaction or it provides additional anchoring sites for the peptides to bind through non-covalent interactions leading to co-operative assembly. However, chymotrypsin failed to form gel, at any concentration (table 7.1). The probable reason for differential behavior of chymotrypsin is the hydropathy index. The hydropathy index of chymotrypsin was found to be -0.0131 in comparison to lipase and thermolysin having values in the range of -0.0556 and -0.409 respectively, as calculated from GRAVY calculator (table 7.1). [28] The higher values of hydropathy index indicate the more hydrophilic nature and vice versa. The lower value of hydropathy index of chymotrypsin signifies its hydrophobic nature that results in its poor water solubility, which corroborates to its reported solubility. (29) Poorly soluble proteins likely have lesser chances to interact with peptides and thus cannot induce gelation. The results also emphasized the role of appropriate hydrophilic lipophilic balance in controlling the self-assembly and gelation. The gelation of Cbz FL with multiple proteins suggested that the interaction between the two is non-specific and also demonstrated a non-conventional route for inducing gelation in a non-gelator ultra-short peptide domain, without any synthetic modulation.

Table 7.1 *Gelation studies of Cbz FL with lipases from same source but different activity, thermolysin and chymotrypsin at different concentration and their hydropathy index.*

Enzyme	Gelation status at enzyme concentration (w/v %)		Hydropathy Index
	0.25%	0.5%	
Lipase (L1) (Candida rugosa, ≥700 U/mg solid)	Gel	Gel	-0.0556
Lipase (L2) (Candida rugosa, (>2 U/mg)	Gel	Gel	
Thermolysin	Weak Gel	Gel	-0.409
Chymotrypsin	Sol	Sol	-0.0131

7.3.3 Morphology of protein-peptide hydrogels

As indicated by the AFM studies, the non-gelator, Cbz FL showed the presence of aggregated morphology indicating the weaker intermolecular interactions, as shown in our previous work. However, it would be extremely interesting to study the morphology of protein induced peptide

gels. The Cbz FL with both lipase (L1 and L2) and thermolysin showed the presence of fibrous morphology. [30] While, the non-gelating peptide-chymotrypsin co-assembly resulted in aggregate like morphology, as anticipated. The results showed that both lipases yielded longer length fibers in comparison to shorter fibrillar structures with thermolysin having fiber diameter of ~39±7.2 nm, suggesting relatively weaker interactions of Cbz FL and thermolysin. The fiber diameters of Cbz FL gels with L1 and L2 were found to be in the similar range of 55±9.2 nm and 56.5±7.8 nm. It is expected that addition of proteins triggers the nucleation for self-assembly of Cbz-FL, which otherwise could be lacking due to insufficient intermolecular interactions between Cbz-FL molecules.

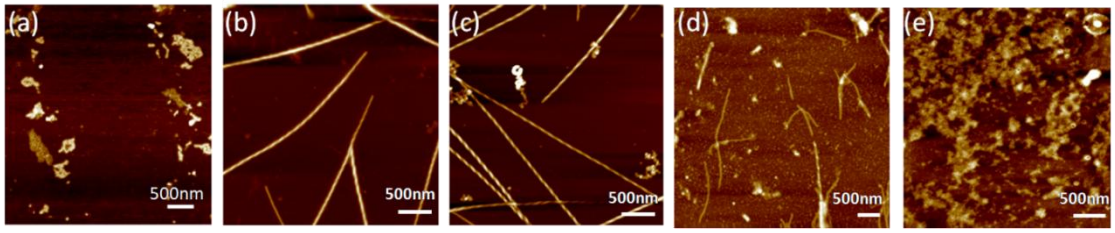

Figure 7.3 *AFM images of (a) Cbz FL, (b) Cbz FL with L1, (c) Cbz FL with L2, (d) Cbz FL with thermolysin and (e) Cbz FL with chymotrypsin with concentration of Cbz FL as 50mM and proteins with 0.5% w/v concentration.*

7.3.4 Mechanical strength evaluation of protein-peptide hydrogels

It is highly desirable to tune the mechanical properties in a single molecular gelator domain, as it can probably reduce the synthetic challenges associated with new molecular design. The mechanical properties of the gels were assessed using oscillatory rheology. The amplitude sweep was performed to determine the LVE range, which was found to be ~0.5% for all the gels. Further, using this LVE strain values, frequency sweep measurements were done in the range of 0.1 to 100Hz. The higher values of storage modulus (G') than loss modulus (G") for all the gels, indicated the viscoelastic nature of the hydrogels. The Cbz FL in the presence of L1 showed concentration dependence. It was extremely interesting to note that with the fixed concentration of Cbz FL, the mechanical stiffness of the gels can be modulated by varying the concentration of protein. With increasing concentration, the gel strength tends to increase from 0.4 kPa at 0.1% L1 to 20 kPa at 1% L1 concentration (figure 7.4a). [31]

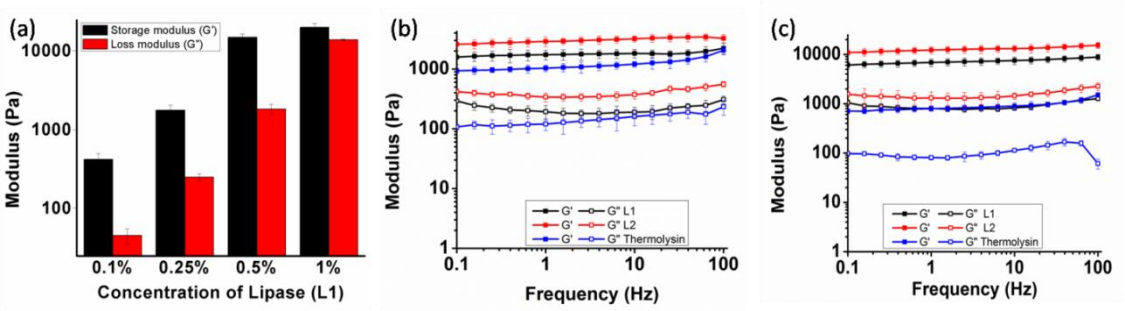

Figure 7.4 *Rheological measurements of (a) Cbz FL with different concentrations of L1, (b) Cbz FL with different proteins at 0.25% concentration and (c) Cbz FL with different proteins at 0.5% concentration.*

Further, we checked the effect of different proteins on gel strength. For this, we used 0.25% and 0.5% concentration of L1, L2 and thermolysin with 50mM Cbz FL. Interestingly, L2 showed relatively higher mechanical strength than L1 and thermolysin. The average storage modulus for L1 was found to be ~1.8±0.2 kPa and 7.3±1.3 kPa, while L2 showed the storage modulus of 3±0.4 kPa and 12.8±2 kPa at 0.25% and 0.5% concentration, respectively. However, the storage modulus of thermolysin was relatively lower than both lipases i.e.in the range of 0.9±0.1 kPa and 1.2±0.2 kPa at 0.25 and 0.5% of thermolysin concentration. The lower gel strength of thermolysin based gels can be correlated with the shorter fiber lengths, while the entanglement of longer fibers results in higher gel strength of L1 and L2 gels. The results showed a facile way to tune the mechanical properties of the gels at identical concentration of the single peptide gelator.

7.3.5 Mechanoresponsiveness of protein-peptide hydrogels

To further explore the potential of these protein-peptide gels in biological applications, injectability is an important parameter. [(34)] The thixotropic nature of gels was studied to assess the mechano-responsiveness of the gels i.e. gel- sol transformation in response to external stress. Initially, the by vial inversion method was used to see the thixotropic behavior, in which the preformed gels were vortexed to transform into sol and upon resting it again regains the gel state. It was observed that all protein peptide gels regained their gel state after deformation. Further, the recovery behaviour of these gels was measured using step-strain rheology. The gels were observed for the loss of mechanical properties upto three consecutive cycles of strain. During thixotropic measurements, a strain much higher than LVE range (i.e. 100%) was applied to deform the gels, followed by reduction of strain near to LVE region i.e. 0.5% to allow the recovery of gel structure. Interestingly, all the three protein-peptide gels showed nearly 100%

recovery of gel strength within initial 60s (figure 7.5). This indicates that these protein-peptide gels are highly mechanoresponsive and can be explored as injectable gels for biomedical applications.

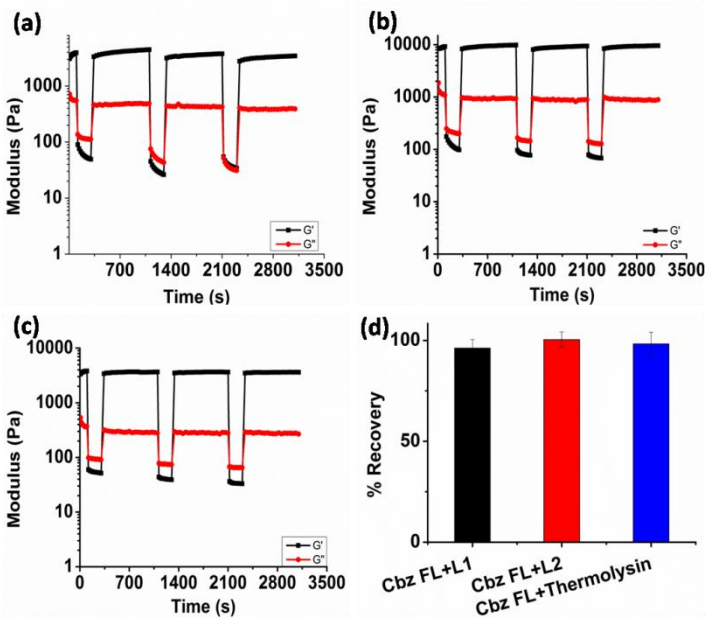

Figure 7.5 *Thixotropic measurements of protein-peptide gels composed of Cbz FL peptide (50mM) with (a) Lipase, L1; (b) Lipase, L2, (c) Thermolysin at 0.5% w/v concentration and (d) percentage recovery of corresponding gels within initial 60sec.*

7.3.6 Investigation of role of protein structure in gelation

To understand the mechanism of interaction between proteins and short peptide, it was important to determine the role of protein structural conformations in dictating the self-assembly and gelation. In this context, we first denatured the proteins by heating. [32] To confirm their denaturation, CD spectroscopy was performed and loss of characteristic protein structure signals was observed after denaturation (figure 7.6a). Surprisingly, the denatured proteins were also able to trigger gelation in non-gelator peptide, Cbz FL. This confirms that the protein-peptide interactions were not conformation specific and might involve non-covalent interactions such as π-π interactions, hydrophobic interactions, or H-bonding interactions. Further, the mechanical properties of gels formed with denatured proteins were assessed (figure 7.6b). Interestingly, the mechanical strengths of gels with denatured proteins were found to be higher than non-denatured protein gels (figure 7.6c). [33] The probable reason for such enhancement in mechanical strengths might be due to the availability of more sites exposed to non-covalent

interactions with peptide, after denaturation, which resulted in more ordered structures with higher gel strength.

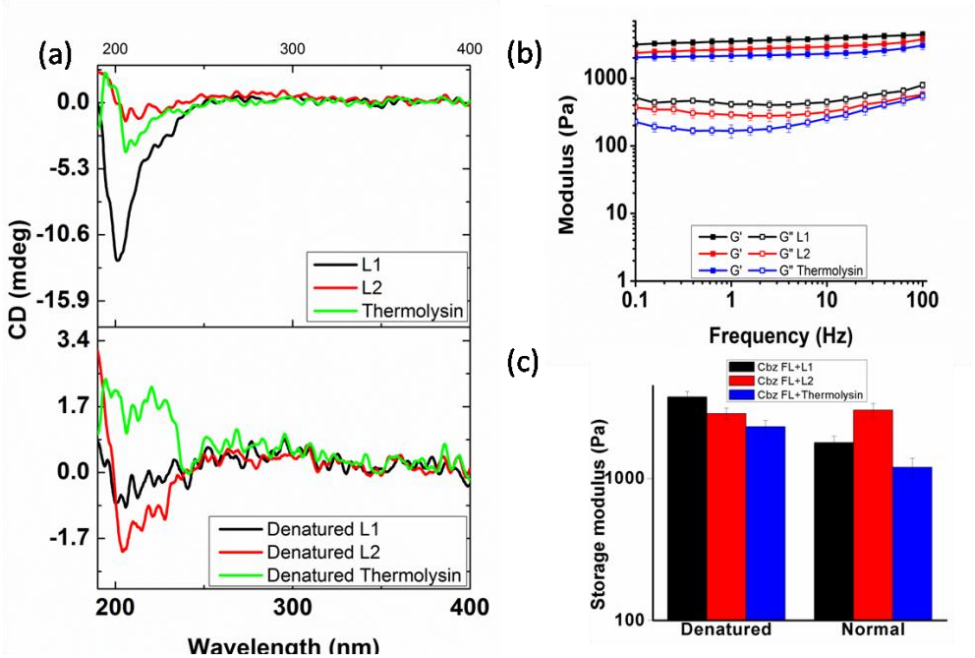

Figure 7.6 *(a) CD analysis of denatured proteins to confirm the disruption of their conformational structure, (b) mechanical strength measurement of gels prepared by 0.25% concentration of denatured proteins (L1, L2, and thermolysin) with Cbz FL and (c) comparison of storage modulus of gels normal (without denaturation) and denatured protein.*

7.3.7 Determination of versatility of the protein-peptide interactions

To get a deeper insight into such protein-peptide interaction induced self-assembly, it was crucial to investigate the selectivity of proteins towards other dipeptide analogues. [35] It was extremely interesting to find out whether such proteins can induce gelation to other non-gelator peptide analogues. In this direction, we designed three other similar dipeptide derivatives having varied C-terminal amino acids ranging from aromatic tyrosine to aliphatic valine and isoleucine. The C log P values of these analogues were 3.642 for Cbz FY, 3.82 for Cbz FV and 4.35 for Cbz FI. All three analogues were non-gelator and when mixed with proteins (L1, L2, and thermolysin), all formed gels except Cbz FI with thermolysin but surprisingly at higher peptide concentration. The gelation concentration of different protein-peptide composites is summarized in table 7.2. The dipeptides Cbz FY and Cbz FV forms gel at 80mM concentration with L1 and L2 while Cbz FY requires 100mM concentration. However, thermolysin having more hydrophilic nature forms gel at 80 mM Cbz FY and 100mM of Cbz FV and does not form

gel with Cbz FI upto 100mM concentration. The gelation results suggested that such protein-peptide induced gelation is highly versatile and can be explored for inducing gelation in other non-gelator peptides.

Table 7.2 *Gelation studies of different proteins at 0.5% w/v with variable dipeptide analogues of Cbz FL and their gelation concentration.*

Protein (0.5w/v)	**Cbz FY** 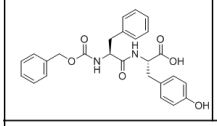	**Cbz FV** 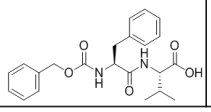	**Cbz FI** 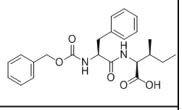
	Concentration (mM)		
Lipase (L1) (Candida rugosa, ≥700 U/mg solid)	**Gel (80mM)**	**Gel (80mM)**	**Gel (100mM)**
Lipase (L2) (Candida rugosa, >2 U/mg)	**Gel (80mM)**	**Gel (80mm)**	**Gel (100mM)**
Thermolysin	**Gel (80mM)**	**Gel (100mM)**	**Sol (100mM)**

Further, a set of gels prepared from different dipeptide analogues with lipase L1 were assessed for their mechanical and morphological properties. The rheological measurements revealed that Cbz FY formed the gel with higher mechanical stiffness having G' value ~1.1±0.1 kPa in comparison to Cbz FV and Cbz FI having storage modulus of 0.76±0.08 kPa and 0.3±0.02 kPa, respectively. However, the mechanical stiffness of all three analogues was lesser in comparison to Cbz FL, inspite of higher minimum gelation concentration of these analogues. Moreover, Cbz FI, which is the structural isoform of Cbz FL showed the least gel strength with L1 and does not form gel with thermolysin. This suggested that it might be possible that leucine structure is more favorable to participate in hydrophobic interactions with lipase and other proteins in comparison to isoleucine, resulting in stronger hydrogels at much lower concentration (nearly half) of Cbz FL than Cbz FI.

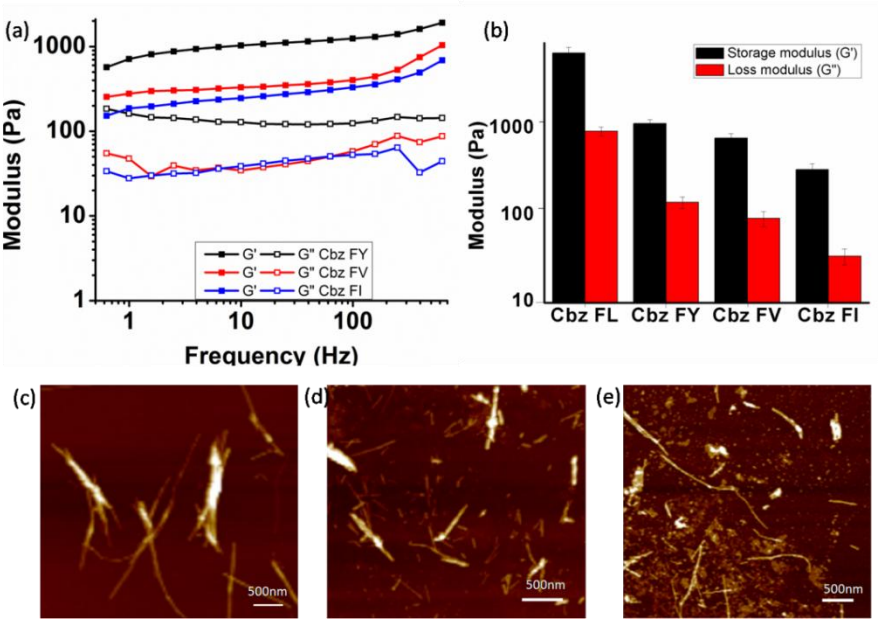

Figure 7.7 *(a) Rheological measurements of dipeptide analogue gels with lipase L1, (b) comparison of gel strengths of all four dipeptide analogues and (c, d & e) morphological assessment of hydrogels prepared from Cbz FY, Cbz FV and Cbz FI with L1, respectively.*

The morphological studies using AFM revealed the presence of fibrous morphology in gels formed from dipeptide analogues with L1. However, the length of fibers was shorter than that of Cbz FL with L1. Cbz FI with L1 showed the presence of aggregates along with the fibrillar structures, which accounts for the weaker gel strength, as observed through mechanical strength measurements.

7.3.8 Measurement of protein-peptide interactions

The studies so far suggested that certain proteins have binding affinities towards short peptide derivatives and this binding might facilitate their self-assembly. The binding affinities can be quantified to establish the correlation between protein-peptide interactions and their resultant properties. Prediction of binding energies can provide the evidences for variable properties of the resulting gels. Biolayer interferometry provides a biophysical method based on immobilization of one of the interacting component on the biosensor platform and using other components as an analyte in a micro-well plate. [36, 37] It is a highly sensitive method to qualify and quantify biomolecular interactions. To determine the binding energies of protein –peptide interactions, APS sensors were used to immobilize proteins via non-covalent interactions. The peptide at different concentrations was used as an analyte. A BLI analysis involves four

essential steps: equilibration, immobilization (loading) of ligand, analyte association and dissociation of weakly bound analyte. [38]

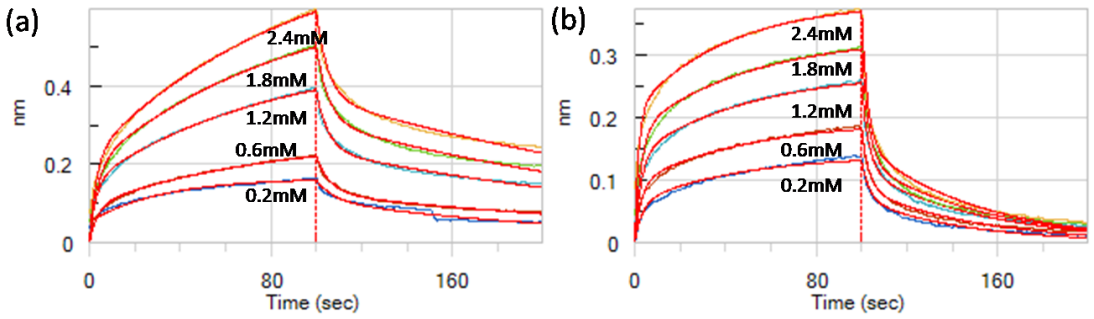

Figure 7.8 *Association and dissociation curves of different concentrations of Cbz FL with (a) Lipase (L1) and (b) thermolysin.*

The binding behavior of immobilized protein ligands such as lipase and thermolysin with different peptide analytes (Cbz FL, Cbz FY, Cbz FV & Cbz FI) is shown by the individual association and dissociation curve. In the preliminary experiments, different concentrations of each analyte were tested with each protein. Each peptide analogue interacted in concentration dependent manner as shown in figure 7.8 by the Cbz FL with lipase and thermolysin. The minimal optimum concentration of 0.6mM was selected to compare the responses of different dipeptide analogues with proteins because concentrations below it showed very less response, in case of some interacting pairs (figure 7.9). The binding constants of each dipeptide analogue with lipase and thermolysin are summarized in table 7.3. The K_D values of dipeptides interacting with lipase were relatively higher in the range of 10^{-3} to 10^{-4} than with thermolysin that is in the range of 10^{-1} to 10^{-3}, which can be accounted as reason for lower gel strength of Cbz FL with thermolysin in comparison with lipase. The overall binding constants in range below 10^{-4} indicate the weak binding, which is also clearly visible from the steep dissociation curves in figures 7.8 and 7.9. For both the proteins, Cbz FL showed highest binding constants in comparison to other dipeptide analogues, indicating relatively stronger binding and that can be correlated with lower minimum gelation concentration (50mM) and its higher gel strengths. The weaker binding affinity confirms that the interactions involve non-covalent interactions. [39]

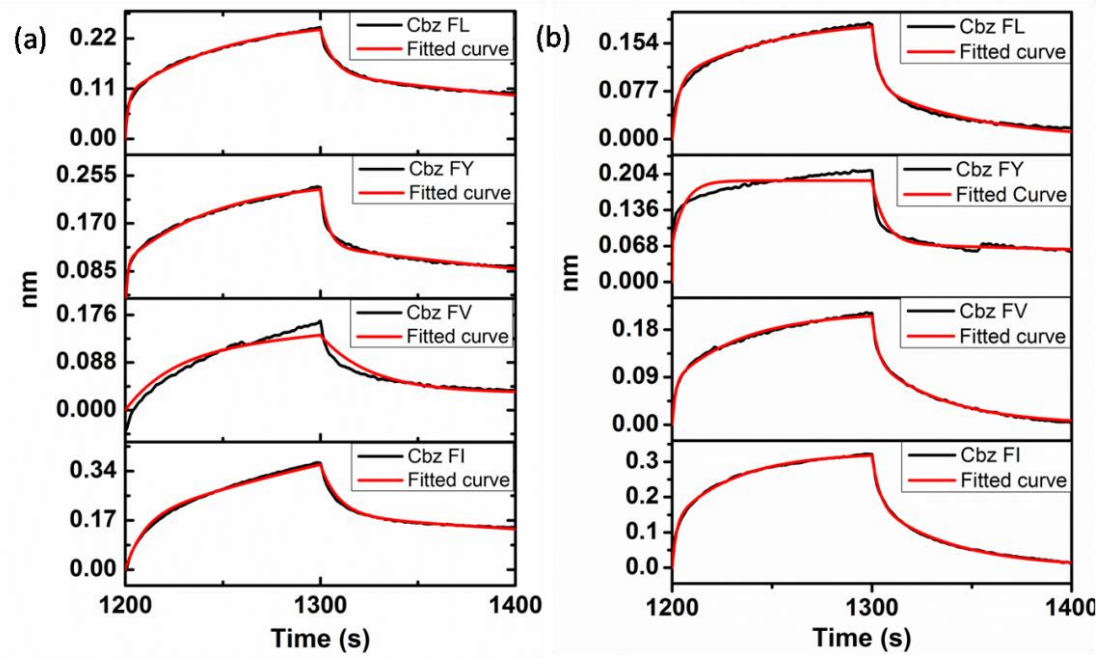

Figure 7.9 *Association and dissociation curve of different peptide analogues with (a) lipase L1and (b) thermolysin.*

Table 7.3 *Kinetic rate constants and affinities were determined for the interactions between lipase (L1) and thermolysin with different dipeptide analogues.*

Peptide	Protein	K_D (M)	K_{on}(1/Ms)	K_{dis} (1/s)
Cbz FL	Lipase (L1)	$4.26E^{-4}$	$1.28E^{+1}$	$5.46E^{-3}$
Cbz FI		$2.54E^{-3}$	$1.05E^{+1}$	$2.57E^{-2}$
Cbz FV		$6.08E^{-3}$	$6.17E^{-3}$	$2.19E^{-2}$
Cbz FY		$1.28E^{-4}$	$2.88E^{+1}$	$3.68E^{-3}$
Cbz FL	Thermolysin	$1.49E^{-3}$	$1.33E^{0}$	$1.98E^{-2}$
Cbz FI		$1.97E^{-1}$	$5.34E^{-1}$	$1.05E^{-1}$
Cbz FV		$3.33E^{-2}$	$8.29E^{-1}$	$2.76E^{-2}$
Cbz FY		$2.54E^{-2}$	$6.13E^{0}$	$1.55E^{-1}$

7.3.9 Prediction of binding energies of protein-peptide interactions

To understand the mechanism of self-assembly of such proteins and peptides, it is crucial to understand the interactions at molecular level. [40, 41] The docking studies of 3D protein models with the interacting peptides would help to understand the underlying mechanism of protein induced peptide self-assembly. Swissdock is a docking web server that automatically performs

the docking analysis for a given set of ligand and target. [42, 43] It searches the whole target protein structure from PDB and performs the binding analysis of different small molecules at different binding pockets using the default parameters. The visualization and interpretation of docking results are facilitated by UCSF Chimera molecular viewer. The results were obtained in the form of energy full fitness (ΔG, Kcal/mol). From all the obtained energy predictions, the best ΔG for lipase interaction with Cbz FL was found to be -7.54 Kcal/mol. While for other dipeptide analogues best ΔG with lipase was found to be -8.38 for Cbz FY, -7.57 for Cbz FV and -7.28 for Cbz FI. The highest ΔG for Cbz FY probably can be due to the additional aromatic interaction with tyrosine moiety. The docking studies also give an idea of number of H-bonds participating in these interactions like Cbz FL and Cbz FV showed presence f 1 H-bonding with lipase, while Cbz FY and Cbz FI showed 2 H-bonds.

Table 7.4 *Binding energies of protein peptide interactions estimated using SwissDock.*

Peptide	Protein	Estimated ΔG (kcal/mol)
Cbz FL	Lipase	-7.54
Cbz FI		-7.28
Cbz FV		-7.57
Cbz FY		-8.38

The docking studies clearly revealed that all peptides interact with different binding pockets of lipase. At the best ΔG conformations, the Cbz FL forms H-bond with Gln 187 and Cbz FV formed H-bond with Arg 518. However, Cbz FY and Cbz FI forms one H-bond with Gly 460 and Lys 229 respectively, and other H-bond with Asp 191. The values of ΔG for all the protein-dipeptide analogues range below 10 Kcal/mol, which is associated with non-covalent interactions. The docking studies confirmed that the binding between protein and peptide are weak non-covalent interactions, which acts as the nucleation sites for self-assembly. Further, growth leads to the fibrillar structures.

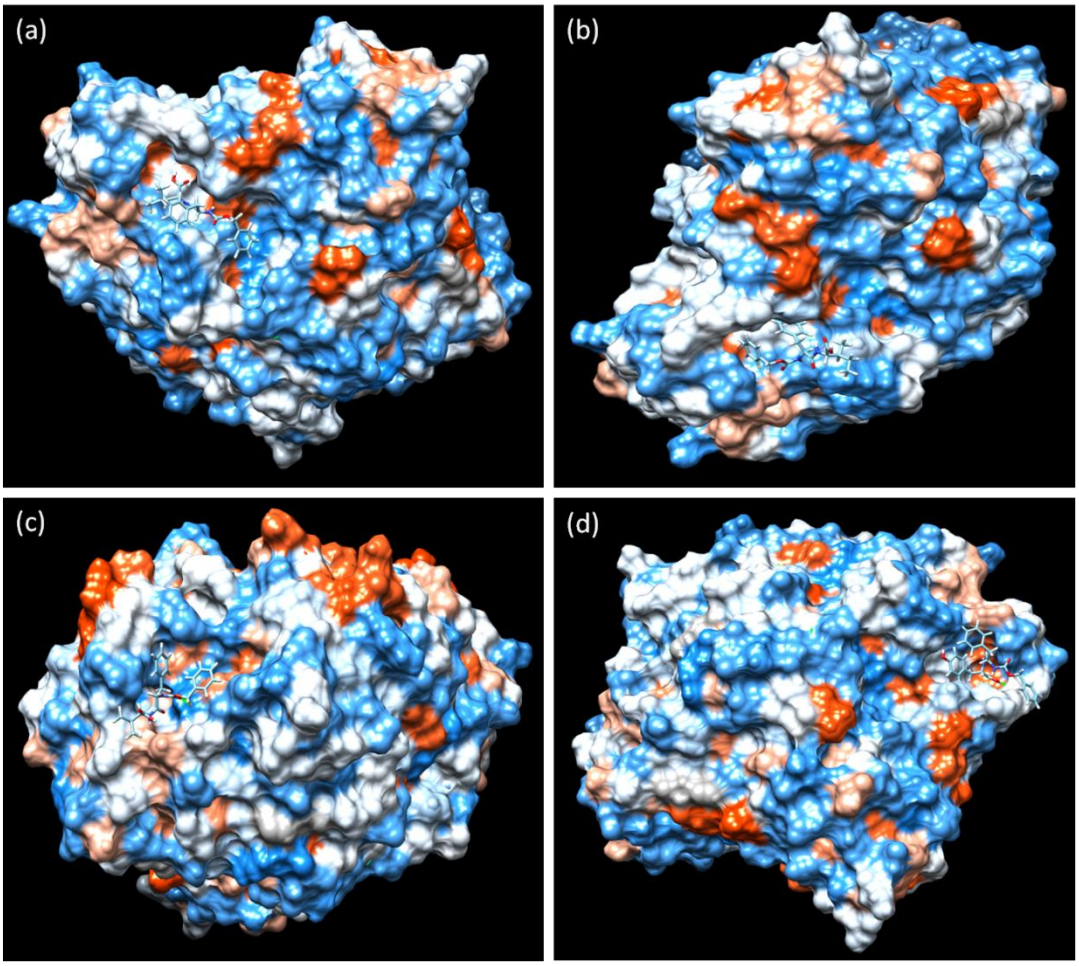

Figure 7.10 *Binding positions of Lipase with (a) Cbz FL, (b) Cbz FI, (c) Cbz FV and (d) Cbz FY having minimum estimated free energy (ΔG) calculated through SwissDock. The visual representation obtained through UCSF Chimera.*

7.3.10 Effect of peptide interactions on Lipase activity

To explore the applicability of these hydrogels in catalysis, it was important to know the effect of peptide binding on the enzymatic activity of proteins such as lipase, thermolysin. In this direction, the lipase activity assay was carried out, in which the conversion of p-nitrophenyl butyrate (PNPB) to p-nitrophenol (PNP) was measured that is indicative of the hydrolytic esterase activity of lipase as shown in figure 7.11a. [44, 45] This conversion was accompanied by the appearance of yellow colour in the solution. For this assay, the lipases (L1 and L2) were added with Cbz dipeptide analogues to check their effect on the catalytic activity of lipase. After 24 hrs of protein-peptide interaction, the gel was diluted and p-nitrophenyl butyrate solution (1mM) was added and immediately the kinetics spectra were recorded at 400nm using UV spectrophotometer (figure 7.11b-d). Interestingly, the peptides itself showed PNPB to PNP

conversion and therefore, the conversion in the presence of lipase along with peptides was observed to be higher than lipase alone. In correlation to higher catalytic of lipase L1, the saturation state of PNPB conversion reaction is obtained faster at ~150s (in figure 7.11b) in comparison to lower catalytic activity of lipase L2, which showed saturation point at ~270s, for all dipeptide analogues (figure 7.11c). The saturation level indicates the completion of reaction by consuming nearly all PNPB amount. The results indicated that binding of peptide does not inhibit protein enzymatic activity. This work suggests that enzyme embedded in hydrogel scaffolds can be used for catalytic purposes, without losing their enzymatic activity.

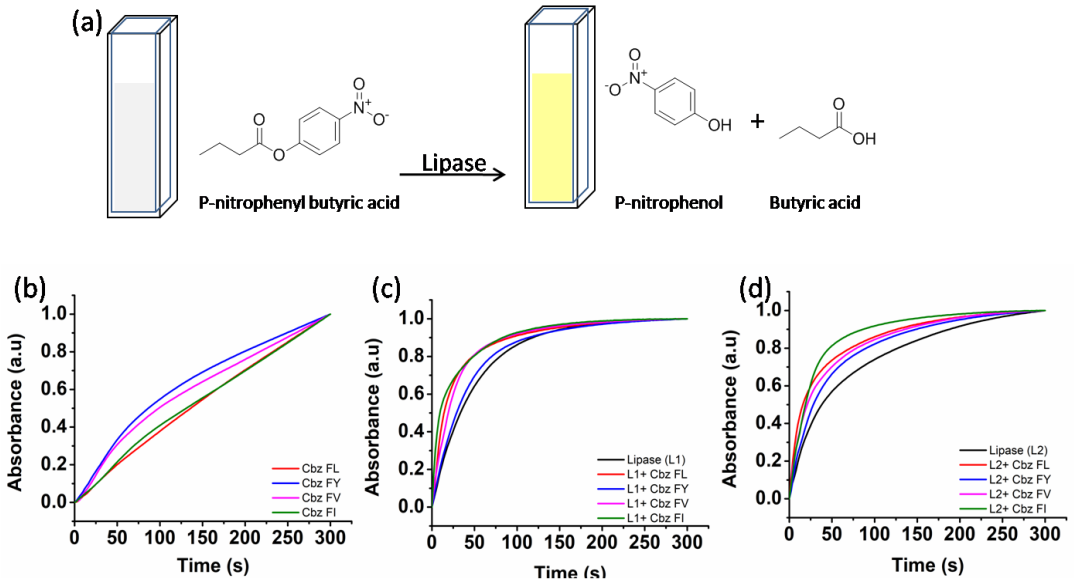

Figure 7.11 *Assessment of lipase activity showing (a) reaction scheme of p-nitrophenyl butyrate conversion to p-nitrophenol using lipase, accompanied by colour change and the quantitative estimation of conversion product with time (upto 300s) in the presence of different peptide analogues (b) with dipeptide analogues only, (c) lipase L1 with dipeptide analogues and (d) lipase L2 with dipeptide analogues, measured at 400nm.*

7.4 Conclusions

In summary, this work was directed towards developing non-conventional approach for the modulation of physical parameter of the self-assembly without changing chemistry of the gelator. We believe that it is the first report on protein co-assembly with ultra-short peptide derivatives such as dipeptides to induce supramolecular gelation. Most interestingly, the potential of protein-peptide interactions have been explored to transform non-gelator into a gelator. Diverse gels can be achieved with variable morphological and mechanical properties within a single molecular domain by just varying the concentration of proteins. The binding

constant observed in the range of 10^{-4} to 10^{-1}M indicates that these protein peptide interactions are purely based on weak non-covalent interactions between them. In the field of supramolecular assembly, this work opens up the new scope for enzymatic proteins other than catalytic self-assembly. Interestingly, retention of functional activity of proteins even after binding interaction makes them suitable candidates for catalytic applications. We believe that such protein-peptide interactions can be a powerful strategy to make highly tunable supramolecular gels leading to a development of novel hybrid hydrogel systems that can be explored in controlled drug release and tissue engineering, etc.

7.5 References

1. Johansson-Åkhe, C. Mirabello, B. Wallner, Predicting protein-peptide interaction sites using distant protein complexes as structural templates, *Sci. Rep.* 9 (2019) 4267.
2. E. O. Olmez, B. S. Akbulut, Protein-Peptide Interactions Revolutionize Drug Development, in *Binding Protein*, (2012) Kotb Abdelmohsen, IntechOpen.
3. R. L Stanfield, I. A. Wilson, Protein-peptide interactions, *Curr. Op. Struc. Biol.* 5 (1995) 103-113.
4. M. Blaszczyk, M. Kurcinski, M. Kouza, L. Wieteska, A. Debinski, A. Kolinski, S. Kmiecik, Modeling of protein-peptide interactions using the CABS-dock web server for binding site search and flexible docking, *Methods* 93 (2015), 72-83.
5. Z. Yu, A. Erbas, F. Tantakitti, L. C. Palmer, J. A. Jackman, M. Olvera de la Cruz, N-J Cho, S. I. Stupp, Co-assembly of Peptide Amphiphiles and Lipids into Supramolecular Nanostructures Driven by Anion−π Interactions, *J. Am. Chem. Soc.* 139 (2017) 7823−7830.
6. O. D. Krishna, K. L. Kiick, Protein- and Peptide-Modified Synthetic Polymeric Biomaterials, Biopolymers. 94 (2010) 32–48.
7. E. Michel, A. Plückthun, O. Zerbe, Peptide-Guided Assembly of Repeat Protein Fragments, *Angew. Chem.* 130 (2018) 4666-4669.
8. C. Lou, J. T. Boesen, N. J. Christensen, K. K. Sørensen, P. W. Thulstrup, Ma. N. Pedersen, E.Giralt, K. J. Jensen, J. Wengel, Self-assembly of DNA-peptide supermolecules: Coiled-coil peptide structures templated by D-DNA and L-DNA triplexes exhibit chirality-independent but orientation-dependent stabilizing cooperativity, *Chem. Eur. J.* (2020) https://doi.org/10.1002/chem.201905636.

9. Y. M. Abul-Haija, R. V. Ulijn, Sequence Adaptive Peptide–Polysaccharide Nanostructures by Biocatalytic Self-Assembly, *Biomacromolecules* 16 (2015) 3473-3479.

10. R. M. Capito, H. S Azevedo, Y. S. Velichko, A. Mata, S. I. Stupp, Self-assembly of large and small molecules into hierarchically ordered sacs and membranes, *Science* 139 (2008) 1812−16.

11. L. Chen, S. Revel, K.Morris, D. G. Spiller, L. C. Serpell, D. J. Adams, Low molecular weight gelator–dextran composites, *Chem. Commun*. 46 (2010) 6738−40.

12. Q. Wang, J. L. Mynar, M. Yoshida, E. Lee, M. Lee, K. Okuro, K. Kinbara, T. Aida, High-water-content mouldable hydrogels by mixing clay and a dendritic molecular binder, *Nature*, 463 (2010) 339−343.

13. Y. Kuang, D. Yuan, Y. Zhang, A. Kao, X. Du, B. Xu,. Interactions between cellular proteins and morphologically different nanoscale aggregates of small molecules, *RSC. Adv*. 3 (2013) 7704−7707.

14. N. Javid, S. Roy, M. Zelzer, Z. Yang, J. Sefcik, R. V. Ulijn, Cooperative Self-Assembly of Peptide Gelators and Proteins, *Biomacromolecules*, 14 (2013) 4368−4376.

15. K. Liu, C.Wang, Z. B. Li, X. Zhang, Superamphiphiles Based on Directional Charge-Transfer Interactions: From Supramolecular Engineering to Well-Defined Nanostructures, Angew. *Chem. Int. Ed*. 50 (2011) 4952 – 4956;

16. X. Zhang, C. Wang, Supramolecular amphiphiles, Chem. Soc. Rev. 40 (2011) 94–101.

17. J. K. Gupta, D. J. Adams, N. G. Berry, Will it gel? Successful computational prediction of peptide gelators using physicochemical properties and molecular fingerprints, *Chem Sci.* 7(2016) 4713–4719.

18. E. D. Spoerke, S. G. Anthony, S. I. Stupp, Enzyme Directed Templating of Artificial Bone Mineral, *Adv. Mater.* 21 (2009) 425 – 430.

19. C. M. Micklitsch, P. J. Knerr, M. C. Branco, R. Nagarkar, D. J. Pochan, J. P. Schneider, Zinc-triggered hydrogelation of a self-assembling β-hairpin peptide, *Angew. Chem. Int. Ed.* 50 (2011) 1577 – 1579;

20. L. Chen, G. Pont, K. Morris, G. Lotze, A. Squires, L. C. Serpell, D. J. Adams, Salt-induced hydrogelation of functionalised-dipeptides at high pH, *Chem. Commun*. 47 (2011) 12071 – 12073.

21. T. Z. Grove, C. O. Osuji, J. D. Forster, E. R. Dufresne, L. Regan, Stimuli-Responsive Smart Gels Realized via Modular Protein Design, *J. Am. Chem. Soc*. 132 (2010) 14024 – 14026.

22. F. Ito, K. Usui, D. Kawahara, A. Suenaga, T. Maki, S. Kidoaki, H. Suzuki, M. Taiji, M. Itoh, Y. Hayashizaki, T. Matsuda, Reversible hydrogel formation driven by protein-peptide-specific interaction and chondrocyte entrapment, *Biomaterials* 31 (2010) 58 – 66.

23. N. Yamaguchi, L. Zhang, B. S. Chae, C. S. Palla, E. M. Furst, K. L. Kiick, Growth factor mediated assembly of cell receptor-responsive hydrogels, *J. Am. Chem. Soc*. 129 (2007) 3040 –3041.

24. X. Zhang, X. Chu, L. Wang, H. Wang, G. Liang, J. Zhang, J. Long, Z. Yang, Rational Design of a Tetrameric Protein to Enhance Interactions between Self-Assembled Fibers Gives Molecular Hydrogels, *Angew. Chem. Int. Ed.* 51 (2012) 4388 –4392.

25. J. R. Fores, M. Criado-Gonzalez, M. Schmutz, C. Blanck, P. Schaaf, F. Boulmedais, L. Jierry, Protein-induced low molecular weight hydrogelator self-assembly through a self-sustaining process, *Chem. Sci*. 10 (2019) 4761-4766.

26. D. Li, H. Wang, D. Kong, Z. Yang, BSA-stabilized molecular hydrogels of a hydrophobic compound, *Nanoscale*, 4 (2012) 3047–3049.

27. R. Jain, G. Khandelwal, S. Roy, Unraveling the Design Rules in Ultrashort Amyloid-Based Peptide Assemblies toward Shape-Controlled Synthesis of Gold Nanoparticles, *Langmuir*, 35 (2019) 5878-5889.

28. http://www.gravy-calculator.de/ *Accessed on December 2019*.

29. M. M. Burrell, *Enzymes of Molecular Biology*, ed., Humana Press 16 (1993), 277-281.

30. W. Zhang, Changyou Gao, Morphology transformation of self-assembled organic nanomaterials in aqueous solution induced by stimuli-triggered chemical structure changes, *J. Mater. Chem. A*, 5 (2017) 16059-16104.

31. A. Scelsi, B. Bochicchio, A. Smith, V. L. Workman, L. A. Castillo Diaz, A. Saiani, A. Pepe, Tuning of hydrogel stiffness using a two-component peptide system for mammalian cell culture, *J. Biomed. Mater. Res. A*, 107 (2018), 535-544.

32. V. G. Eijsink, O. R.Veltman, W. Aukema, G. Vriend, G. Venema, Structural determinants of the stability of thermolysin-like proteinases, *Nat. Struct. Biol*. 2 (1995) 374–379.

33. J. Ahmed , H. S. Ramaswamy , I. Alli & V.G.S. Raghavan, Protein Denaturation, Rheology, and Gelation Characteristics of Radio-Frequency Heated Egg White Dispersions, *Int. J. Food Prop*. 10 (2007) 145-161.

34. C. Yan, D. J. Pochan, Rheological properties of peptide-based hydrogels for biomedical and other applications, *Chem Soc Rev.* 39(2010): 3528–3540.

35. A. McFedries, A. Schwaid, A. Saghatelian, Methods for the Elucidation of Protein-Small Molecule Interactions, *Chem.Biol*. 20 (2013), 667-673.

36. M. Desai, R. Di, H. Fan, Application of Biolayer Interferometry (BLI) for Studying Protein-Protein Interactions in Transcription, *J. Vis. Exp.* 149 (2019), e59687.

37. J. Wallner, G. Lhota, D. Jeschek, A. Mader, K. Vorauer-Uhl, Application of Bio-Layer Interferometry for the analysis of protein/liposome interactions, *J. Pharmaceut Biomed. Anal*.72 (2013) 150– 154.

38. D. Seeliger, S. Soeroes, R. Klingberg, D. Schwarzer, H. Grubmüller, W. Fischle, Quantitative Assessment of Protein Interaction with Methyl-Lysine Analogues by Hybrid Computational and Experimental Approaches, *ACS Chem. Biol*. 7 (2012) 150−154.

39. Eugénie Laigre, David Goyard, Claire Tiertant, Jérôme Dejeu * and Olivier Renaudet, The study of multivalent carbohydrate–protein interactions by bio-layer interferometry, *Org. Biomol. Chem*, 16 (2018) 8899-8903.

40. Ghazaleh Taherzadeh1, Yaoqi Zhou1,2, Alan Wee-Chung Liew1 and Yuedong Yang, Structure-based prediction of protein–peptide binding regions using Random Forest, Bioinformatics, 34 (2018), 477–484.

41. P. L. Kastritis, A. M. J. J. Bonvin, On the binding affinity of macromolecular interactions: daring to ask why proteins interact, *J R Soc Interface* 10 (2013) 20120835.

42. A. Grosdidier, V. Zoete, O. Michielin, SwissDock, a protein-small molecule docking web service based on EADock DSS, *Nucleic Acids Res.* 39 (2011) 270-277.

43. K. A Ramsbottom, D. Carr, A. R Jones, D. J Rigden, Critical assessment of approaches for molecular 1 docking to elucidate associations of HLA alleles with Adverse Drug Reactions, *Mol Immunol.* 101 (2018) 488-499.

44. N. Gomes, C. Goncalves, M. Garcıa-Roman, J. A. Teixeira, I. Belo, Optimization of a colorimetric assay for yeast lipase activity in complex systems, Anal. Methods, 2011, 3, 1008-1013.

45. K. Shirai, R. L. Jackson, Lipoprotein Lipase-catalyzed Hydrolysis f p-Nitrophenyl Butyrate, *J. Biol. Chem*. 257 (1982) 1253-1258.

Chapter 8

Thesis Conclusions and Future Perspectives

8.1 Summary

This thesis presents a set of contributions towards the development of biofunctional scaffolds for tissue regeneration applications. An ideal tissue engineering scaffold would satisfy two important aspects: firstly they should be biocompatible and secondly they should have tuneable properties. Ideally, the scaffold should be designed in such a way that it can rationally incorporate single or multiple bioactive motifs, which can provide necessary biophysical as well as biochemical cues. We took inspiration from the design principles of native extracellular matrix so as to adopt its similar hierarchical structure and multiple functions. Our work applies the similar principles of nature that includes molecular self-assembly to control the properties of bioactive peptide hydrogel scaffolds. The peptide design adopts a minimalist approach to create gelators derived from ECM proteins i.e. Laminin and Collagen. Our work mainly focuses to achieve the structural and functional complexity of natural ECM through controlled synthetic parameters to direct cell growth and cellular other functions. This thesis consists of 8 chapters including this chapter.

The introductory chapter covers the overview of natural extracellular matrix (ECM), its composition, structure and functions, which motivates the design of synthetic extracellular mimics. The importance of different functional proteins and peptides of ECM are also discussed which were the basis of molecular design of peptide libraries in our work. Further, the role of hydrogels as a synthetic scaffold is discussed, especially in context with peptide hydrogels. The fundamentals of molecular self-assembly were employed to develop hydrogels with tunable properties. The β-amyloid assemblies were briefly discussed to explain the mechanistic and structural aspects of short self-assembling peptides. In brief, this chapter introduces the applicability of bioactive short peptide hydrogels for diverse biomedical and tissue engineering applications. The second chapter described the materials and principles of methodology applied for the synthesis, physical characterizations, and assessment of biological activity of the designer peptide hydrogels. The following chapters demonstrated the development of bioactive peptide based hydrogels by achieving the structural and functional complexity in a stepwise manner starting from single peptide molecular assembly to multi-component co-assembly. The research work conducted in this thesis can be summarized as in figure 8.1.

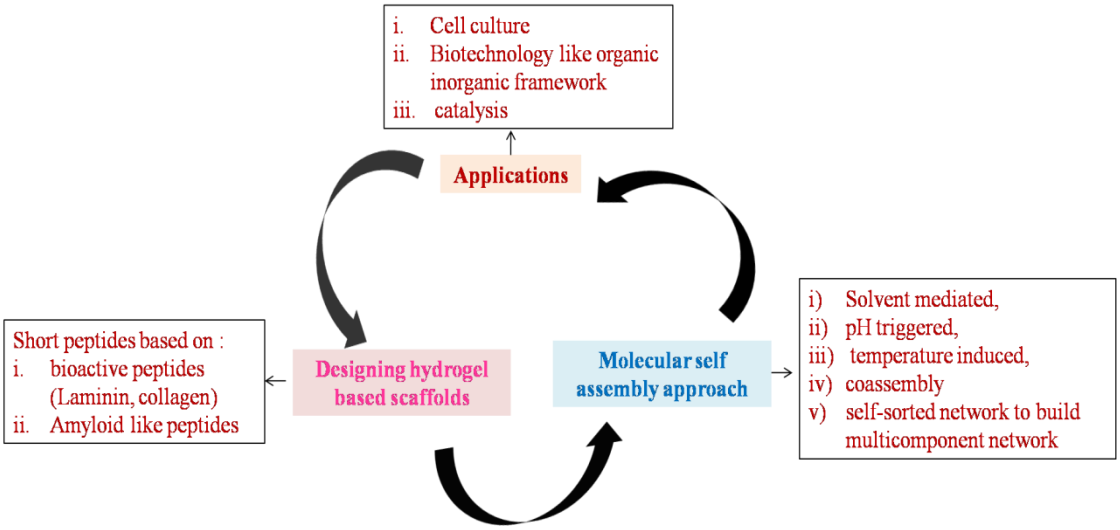

Figure 8.1 Summary of research work

The important achievements of the work can be as summarized below:

- ✓ The design of self-assembling short peptides i.e. IKVAV and YIGSR derived from native laminin protein have been proposed to develop the bioactive hydrogel scaffold, which otherwise was non-gelators. The non-conventional solvent-mediated approach was shown to tailor the properties of resulting hydrogels. The results showed that solvent environment greatly affects the intermolecular interactions of gelator molecules and thus leading to the formation of various non-equilibrium nanostructures corresponding to local minima in the free energy landscape. The variable intermolecular interaction in different solvent environments is reflected in their morphological as well as mechanical properties. The work successfully demonstrates the access to diverse nanostructures within a single gelator domain, through solvent switch. To the best of our knowledge, it is the first attempt to access differential energy levels of the free energy landscape via solvent mediated approach.

- ✓ The functional roles of laminin derived short peptides in controlling neuronal cell growth and proliferation were demonstrated. For the first time, combination of IKVAV and YIGSR self-assembling peptides, without any polymeric scaffold has been explored. The simple mixing of two components resulted in of self-sorted network in composite hydrogels, which elucidates the presentation of both functionality in a single scaffold for cell interactions. The synthetic laminin derived scaffolds were found to be highly biocompatible and promoted cell adhesion, proliferation and neurite extension.

These scaffolds supported normal cellular functions as evidenced by cell cycle analysis and neuronal marker (β-III tubulin) expression. The study also emphasizes the role of hydrophobicity and morphology of nanostructures in dictating cell behavior.

- ✓ The next step demonstrated the fabrication of complex multi-functional scaffolds by simply mixing the two functional peptides derived from ECM proteins, collagen and laminin to mimic the hierarchical composition and structure of native ECM. The incorporation of laminin peptides induced nucleation and growth in designer non-gelator collagen mimetic peptide. The nanofibrous morphology generated through co-assembly can essentially mimic the structure and function of natural ECM, which enable the scaffold to communicate with the cells through biochemical signals and promote cell growth, adhesion, proliferation and migration of fibroblast as well as neuronal cell types. This work demonstrated an effective route for the development of multifunctional biomaterials via simple non-covalent mixing approach.

- ✓ This work provides a detailed understanding on the rationale behind the gelator design. The study demonstrated the sequence-structure relationship with respect to systematic variations in hydrophobic-hydrophilic balance within designer peptides developed from the β-amyloid sequence. Extensive studies on differential aromatic modifications as well as sequence modulation of these aromatic dipeptide amphiphiles established the fact that aromatic capping has profound effect on the self-assembly propensity and morphology of the resulting materials, in comparison to variation in amino acid sequence. The detailed molecular understanding obtained was explored toward the controlled synthesis of bioinspired organic−inorganic hybrids. For the first time, this work demonstrated the differential role of aliphatic and aromatic hydroxyl moieties towards the in situ shape-controlled synthesis of gold nanoparticles in three-dimensional nanostructures of hydrogels. We were able to access rectangular platonic gold nanoparticles using simple dipeptide hydrogels, which were never reported previously. These organic-inorganic hybrid scaffolds can be developed as next generation biomaterials for different biomedical applications.
- ✓ Peptide-protein interactions can be highly beneficial to create diverse nanostructure with differential material properties. The supramolecular non-covalent interactions between protein and peptides can induce gelation in non-gelator peptides. Such interactions are non specific and can be applied to a variety of peptides. Wide variety of

mechanical and morphological properties can be accessed within a single gelator domain by simply varying the protein concentration or type.

8.2 Future perspectives

The biological existence of peptides and their excellent self-assembling properties will continue to be intrigued by the researchers in coming years. The continuous advances in the peptide synthesis strategies and better understanding of the naturally existing biological structures will encourage scientists to develop new self-assembling systems for a variety of applications.

The present work in this thesis highlights the importance of classical molecular self-assembly approach in building complex functional materials. The work underpins the development of tuneable functional materials, mainly inspired from biological origin which could essentially create the ideal microenvironment to provide essential biochemical and biophysical cues to the relevant cell types. These biomimetic materials hold great potential to be developed as next-generation biomaterials for biomedical applications. We anticipate that the work in this thesis showed promising potential in cell culture applications, which can be extended further in the field of tissue engineering and stem cell culture. The proposed work can be further explored in relevance to:

- ✓ *3 dimensional cell cultures:* The work in this thesis was mainly focused on 2D cell culture applications. The high biocompatibility and bioactivity of the designed scaffolds towards controlling cell behavior hold a great potential to be explored as 3D scaffolds with highly tuneable properties. The hydrogels as 3D scaffolds can be a closer mimic of *in vivo* conditions for cell culture.

- ✓ *Stem cell culture*: The exploration of unique regenerative and differentiating capabilities of stem cells has been rapidly explored in the present times. The tuneable physical and biochemical cues with these gels provide flexibility for culturing stem cells, which also helps in directing stem cells towards particular cell lineage.

- ✓ *Other biomedical applications*: The porous structure of hydrogels provides favourable site for drug loading and its delivery. In this direction, several functional motifs can be incorporated in our gelator design, which could facilitate the specific ligand-receptor interaction for facile transportation of the cargo and its targeted delivery. The functionalities of peptide sequences can be explored for other catalytic functions such as metal nanoparticle formation, as demonstrated for synthesis of gold nanoparticles in

chapter 6 of this thesis, which can be explored in ceullar delivery and other optical imaging applications.

- ✓ Future attempts can be made towards the functionalization of peptide hydrogel scaffolds with essential polysaccharides, which can enhance the compositional similarity with native ECM.

Appendix I

A1.1 Analytical characterization of Peptides using ^{1}H NMR, ^{13}C NMR and specific rotation:

Fmoc FF $[\alpha]^{20}_{D}$ = 27.5 (c=0.4 gm/ml in 10% MeOH in $CHCl_3$)

^{1}H NMR (400 MHz, DMSO): δ/ppm= 8.41-8.08 (d, 2H), 7.83-7.33 (m, 10H), 7.27-7.08 (m, 8H), 4.77-4.64 (m, 2H), 4.53-4.48 (m, 3H), 3.13-3.03 (t, 2H), 2.97-2.84 (t, 2H).

δ_c (DMSO, 100MHz): 171.90 (Phenylalanine C=O), 171.76 (Phenylalanine C=O), 155.76 (Fmoc C=O), 143.74 (Fluorenyl aromatic -C), 143.67 (Fluorenyl aromatic -C), 138.21 (Phenylalanine aromatic -C), 129.04 (Phenylalanine aromatic –CH), 128.14 (Phenylalanine aromatic–CH), 127.97 (Phenylalanine aromatic –CH), 127.59 (Phenylalanine aromatic –CH), 127.03 (Fluorenyl aromatic –CH), 126.16 (Fluorenyl aromatic –CH), 125.33 (Phenylalanine aromatic –CH), 125.25 (Fluorenyl aromatic –CH), 120.04 (Fluorenyl aromatic –CH), 65.62 (Fmoc aliphatic -CH_2), 55.94 (Phenylalanine α-CH), 54.68 (Phenylalanine α-CH), 46.49 (Fluorenyl –CH), 39.64 (Phenylalanine side chain –CH_2), 38.8 (Phenylalanine side chain –CH_2).

Fmoc FY $[\alpha]^{20}_{D}$ = 14.7 (c=0.3 gm/ml in 10% MeOH in $CHCl_3$)

^{1}H NMR (400 MHz, DMSO): δ/ppm= 8.13-8.08 (d, 2H), 7.83-7.76 (m, 6H), 7.46-7.32 (m, 4H), 7.24-7.18 (m, 7H), 5.61-5.58 (s, 1H), 4.79-4.3 (m, 5H), 3.49-3.20 (m, 2H), 3.08-2.51 (m, 2H).

δ_c (DMSO, 100MHz): 172.81 (Tyrosine C=O), 170.2 (Phenylalanine C=O), 155.32 (Fmoc C=O),155.1 (Tyrosine aromatic -C-OH), 143.44 (Fluorenyl aromatic -C), 142.71 (Fluorenyl aromatic -C), 136.30 (Phenylalanine aromatic -C), 129.41 (Tyrosine aromatic –CH), 128.42 (Tyrosine aromatic –CH), 127.87 (Phenylalanine aromatic –CH), 127.12 (Phenylalanine aromatic –CH), 126.13 (Fluorenyl aromatic –CH), 125.98 (Fluorenyl aromatic –CH), 125.53 (Phenylalanine aromatic –CH), 125.05 (Fluorenyl aromatic –CH), 120.14 (Fluorenyl aromatic –CH), 115.65 (Tyrosine aromatic –CH), 67.62 (Fmoc aliphatic -CH_2), 58.78 (Tyrosine α-CH) 58.21 (Phenylalanine α-CH), 46.87 (Fmoc -CH), 36.74 (Phenylalanine side chain –CH_2), 36.13 (Tyrosine side chain –CH_2).

Fmoc FL $[\alpha]^{20}_{D}$ = 7.3 (c=0.3 gm/ml in 10% MeOH in $CHCl_3$)

^{1}H NMR (400 MHz, DMSO): δ/ppm= 8.20-7.90 (d, 2 H), 7.73-7.62 (m, 4H), 7.39-7.05 (m, 9H), 4.71- 4.65 (m, 3H), 4.29-4.23 (m, 2H), 3.29-3.03 (t, 2H), 1.73-1.47 (m, 3H), 0.87-0.78 (m, 6H).

*δ_c (DMSO, 100MHz):*173.1 (Leucine C=O), 171.1 (Phenylalanine C=O), 155.21 (Fmoc C=O), 143.6 (Fluorenyl aromatic - C), 142.3 (Fluorenyl aromatic -C), 135.9 (Phenyl –C), 128.28 (Phenyl – CH), 127.9 (Phenyl –CH), 126.6 (Fluorenyl aromatic –CH), 125.7 (Phenyl –CH), 119.8 (Fluorenyl aromatic –CH), 66.67 (Aliphatic Fmoc -CH_2), 58.12 (Phenylalanine α-CH), 55.34 (Leucine α-CH), 46.76 (Fluorenyl –CH), 39.54 (Leucine side chain –CH2), 36.98 (Phenylalanine side chain –CH_2), 23.76(Leucine side chain –CH), 21.43 (Leucine side chain –CH_3)

Fmoc FS $[\alpha]^{20}_{D}$ = 49.3 (c=0.15 gm/ml in 10% MeOH in $CHCl_3$)

^{1}H NMR (400 MHz, DMSO): δ/ppm= 7.80-7.78 (d, 2H), 7.76-7.75 (d, 2H), 7.44-7.42 (2H, d), 7.35-7.30 (t, 4H), 7.24-7.12 (m, 5H), 4.75-4.54 (m, 4H), 3.53-3.51 (m, 1H), 2.52-2.50 (m, 2H), 1.33-1.11 (m, 3H).

δ_c (DMSO, 100MHz): 170.91(Serine C=O), 170.02 (Serine C=O), 154.87 (Fmoc C=O), 143.19 (Fluorenyl aromatic –C), 142.2 (Fluorenyl aromatic –C), 135.65 (Phenyl –C), 128.32 (Phenyl –CH), 127.12 (Phenyl –CH), 126.05 (Fluorenyl aromatic –CH), 125.65 (Fluorenyl aromatic –CH), 124.48 (Phenyl –CH), 123.87 (Fluorenyl aromatic –CH), 119.50 (Fluorenyl aromatic –CH), 66.49 (Aliphatic Fmoc -CH_2), 61.79 (Serine side chain –CH_2), 61.4 (Serine α-CH), 58.31 (Phenylalanine α-CH), 46.8 (Fluorenyl –CH), 36.40 (Phenylalanine side chain -CH_2).

Nap FF $[\alpha]^{20}_D$ = 43 (c=0.3 gm/ml in 10% MeOH in $CHCl_3$)

^{1}H NMR (400 MHz, DMSO): δ/ppm= 8.23-8.17 (d, 2H), 7.83-7.81 (d, 3H), 7.61-7.36 (m, 7H), 7.30-7.13 (m, 7H), 4.54 - 3.99 (m, 4H), 3.13-3.98 (t, 2H), 2.97-2.73 (t, 2H).

δ_c (DMSO, 100MHz): 172.72 (Phenylalanine -C=O), 170.81 (Phenylalanine -C=O), 167.18 (Aliphatic –C=O), 155.43 (Napthyl aromatic –C), 137.49 (Phenyl aromatic –C), 133.98 (Napthyl aromatic –C), 129.32 (Phenyl aromatic –CH), 129.10 (Phenyl aromatic –CH), 128.14 (Napthyl aromatic –CH), 127.94 (Napthyl aromatic –CH),127.47 (Napthyl aromatic –CH),126.75 (Phenyl aromatic –CH),126.4 (Napthyl aromatic –CH), 123.82 (Napthyl aromatic –CH), 118.43 (Napthyl aromatic –CH), 107.3 (Napthyl aromatic –CH),66.38 (Aliphatic –CH_2), 53.51 (Aliphatic –Cα), 53.21 (Aliphatic –Cα),39.65 (aliphatic side chain – CH_2), 37.36 (aliphatic side chain – CH_2).

Nap FY $[\alpha]^{20}_D$ = 24 (c=0.3 gm/ml in 10% MeOH in $CHCl_3$)

^{1}H NMR (400 MHz, DMSO): δ/ppm= 8.22-8.20 (d, 2H), 7.88-7.86 (d, 1H), 7.73- 7.64 (d, 2H), 7.50-7.33 (m, 5H), 7.14-6.81 (m, 6H), 6.70-6.55 (d, 2H), 4.45-4.02 (m, 2H), 3.92-3.74 (m, 2H), 3.19- 3.00(m, 2H), 2.96-2.56 (m, 2H).

δ_c (DMSO, 100MHz): 172.65 (Tyrosine -C=O), 170.94 (Phenylalanine -C=O), 168.10 (Napthoxy acetic acid –C=O), 155.78 (Napthyl aromatic –C), 154.89 (Tyrosine aromatic –C), 135.9 (Phenylalanine aromatic –C), 134.21 (Napthyl aromatic –C), 133.79 (Napthyl aromatic –C), 129.54 (Tyrosine aromatic –CH), 129.0 (Tyrosine aromatic –CH), 128.1 (Phenylalanine aromatic –CH), 127.23 (Phenylalanine aromatic –CH), 127.18 (Napthyl aromatic –CH), 125.9 (Napthyl aromatic –CH), 125.5 (Napthyl aromatic –CH),124.76 (Phenylalanine aromatic –CH), 124.21 (Napthyl aromatic –CH), 122.67 (Napthyl aromatic –CH), 120.0 (Napthyl aromatic –CH), 115.13 (Tyrosine aromatic –CH), 106.34 (Napthyl aromatic –CH), 66.4 (Napthoxy aliphatic –CH_2), 58.23 (Tyrosine α-CH), 57.76 (Phenylalanine α-CH), 36.50 (Phenylalanine side chain – CH_2), 35.87(Tyrosine side chain –CH_2).

Nap FL $[\alpha]^{20}_D$ = 14.3 (c=0.4 gm/ml in 10% MeOH in $CHCl_3$)

^{1}H NMR (400 MHz, DMSO): δ/ppm= 8.19-8.17 (d, 2H), 7.85-7.82 (d, 3H), 7.63-7.39 (m, 4H), 7.39-7.15 (m, 5H), 4.31-4.10 (m, 4H), 3.05-3.01 (m, 1H), 2.81-2.75 (m, 1H), 1.69-1.53 (m, 3H), 0.91-0.82 (d, 6H).

δ_c (DMSO, 100MHz): 173.05 (Leucine -C=O), 171.14 (Phenylalanine -C=O), 167.89 (Napthoxy acetic acid –C=O), 156.34 (Napthyl aromatic –C), 135.5 (Phenylalanine aromatic –C), 133.98 (Napthyl aromatic –C), 133.34 (Napthyl aromatic –C), 127.76 (Phenylalanine aromatic –CH), 126.53 (Phenylalanine aromatic –CH), 126.30 (Napthyl aromatic –CH), 126.04 (Napthyl aromatic –CH), 125.23 (Napthyl aromatic –CH),124.46 (Phenylalanine aromatic –CH), 124.10 (Napthyl aromatic –CH), 122.90 (Napthyl aromatic –CH), 119.60 (Napthyl aromatic –CH),107.0 (Napthyl aromatic –CH), 66.32 (Napthoxy aliphatic –CH_2), 57.76 (Phenylalanine α-CH), 55.21 (Leucine α-CH), 39.39 (Leucine side chain –CH_2), 36.76 (Phenylalanine side chain – CH_2), 24.12(Leucine side chain –CH), 22.10 (Leucine side chain –CH_3).

Nap FS $[\alpha]^{20}_D$ = 16(c=0.3 gm/ml in 10% MeOH in $CHCl_3$)

^{1}H NMR of Nap FS (400 MHz, DMSO): δ/ppm= 8.25-8.21 (d, 2H), 7.84-7.82 (d, 3H), 7.63-7.39 (m, 4H), 7.39-7.14 (m, 5H), 4.41-4.32 (m, 3H), 4.21-4.09 (m, 2H), 3.82-3.65 (m, 2H), 3.48-3.06 (t, 2H).

δ_c (DMSO, 100MHz): 170.78 (Phenylalanine -C=O), 169.84 (Serine -C=O), 167.65 (Napthoxy acetic acid –C=O), 157.00 (Napthyl aromatic –C), 135.25 (Phenylalanine aromatic –C), 133.48 (Napthyl aromatic –C), 133.14 (Napthyl aromatic –C), 128.36 (Phenylalanine aromatic –CH), 127.23 (Phenylalanine aromatic –CH), 127.00 (Napthyl aromatic –CH), 126.24 (Napthyl aromatic –CH), 125.53 (Napthyl aromatic –CH),124.86 (Phenylalanine aromatic –CH), 124.65 (Napthyl aromatic –CH), 122.69 (Napthyl aromatic –CH), 119.45 (Napthyl aromatic –CH),106.78 (Napthyl aromatic –CH), 66.67 (Napthoxy aliphatic –CH_2), 62.31 (Serine side chain – CH_2), 61.15 (Serine α-CH), 58.35 (Phenylalanine α-CH), 36.76 (Phenylalanine side chain –CH_2).

Cbz FF $[\alpha]^{20}_D$ = 39 (c=0.3 gm/ml in 10% MeOH in $CHCl_3$)

^{1}H NMR (400 MHz, DMSO): δ/ppm= 8.19-8.17 (d, 2H), 7.39-7.26 (m, 9H), 7.24-7.09 (m, 6H), 4.93 (s, 2H), 4.52-4.26 (m, 2H), 3.20-2.96 (t, 2H), 2.95-2.67 (t, 2H).

δ_c (DMSO, 100MHz): 172.76 (Phenylalanine C=O), 171.56 (Phenylalanine C=O), 155.69 (Benzyloxy carbonyl C=O), 138.05 (Phenylalanine aromatic –C), 136.96 (Benzyloxy carbonyl aromatic –C), 129.27 (Benzyloxy carbonyl Aromatic –CH), 128.25 (Phenylalanine aromatic –CH), 127.98 (Phenylalanine aromatic –CH), 127.63 (Benzyloxy carbonyl aromatic –CH), 127.36 (Benzyloxy carbonyl aromatic –CH), 126.19 (Phenyl aromatic –CH), 65.11 (Benzyloxy carbonyl aliphatic –CH_2), 55.94 (phenylalanine aliphatic α-C), 53.49 (phenylalanine aliphatic α–C), 39.43 (Phenylalanine side chain -CH_2), 37.5 (Phenylalanine side chain -CH_2).

Cbz FY $[\alpha]^{20}_D$ = 52.7 (c=0.3 gm/ml in 10% MeOH in $CHCl_3$)

^{1}H NMR (400 MHz, DMSO): δ/ppm= 8.11-8.09 (d, 2H), 7.42-7.29 (m, 4H), 7.27-7.20 (m, 5H), 7.19-6.65 (m, 5H), 4.97- 4.93 (s, 3H), 4.44-4.25 (m, 2H), 3.01-2.95 (m, 2H), 2.87-2.68 (m, 2H).

δ_c (DMSO, 100MHz): 173.16 (Tyrosine C=O), 170.56 (Phenylalanine C=O), 155.21 (Benzyloxy carbonyl -C=O), 154.98 (Tyrosine –C-OH), 136.25 (Phenylalanine aromatic –C), 135.67 (Benzyloxy carbonyl aromatic –C), 129.57 (Tyrosine aromatic –C), 128.55 (Tyrosine aromatic –CH), 128.23 (Benzyloxy carbonyl aromatic –CH), 127.93 (Phenylalanine aromatic –CH),

127.10 (Phenylalanine aromatic –CH), 126.69 (Benzyloxy carbonyl aromatic –CH), 126.43 (Benzyloxy carbonyl aromatic –CH),115.1 (Tyrosine aromatic –CH), 66.10 (Benzyloxy carbonyl aliphatic $–CH_2$), 58.76 (Tyrosine aliphatic α-C), 58.09 (phenylalanine aliphatic α–C), 36.47 (Phenylalanine side chain $-CH_2$), 35.89 (tyrosine side chain aliphatic $-CH_2$).

Cbz FL $[\alpha]^{20}_D$ = 13.7 (c=0.3gm/ml in 10% MeOH in $CHCl_3$)

^1H NMR (400 MHz, DMSO): δ/ppm= 8.18-8.16 (d, 2H), 7.40-7.31 (m, 4H), 7.30-7.17 (m, 6H), 4.93 (s, 2H), 4.34-4.24 (m, 2H), 3.04-2.70 (t, 2H), 1.70-1.53 (m, 3H), 0.93-0.80 (d, 6H).

δ_c (DMSO, 100MHz): 172.56 (Leucine C=O), 170.21(Phenylalanine C=O), 155.0 (Benzyloxy carbonyl -C=O), 136.02 (Phenylalanine aromatic –C), 135.87 (Benzyloxy carbonyl aromatic –C), 128.32 (Benzyloxy carbonyl aromatic –CH), 128.12 (Phenylalanine aromatic –CH), 127.69 (Phenylalanine aromatic –CH), 127.43 (Benzyloxy carbonyl aromatic –CH), 127.12 (Benzyloxy carbonyl aromatic –CH), 126.12 (Phenylalanine aromatic –CH), 67.10 (Benzyloxy carbonyl aliphatic $–CH_2$), , 58.90 (phenylalanine aliphatic α–C), 55.45 (Leucine aliphatic α–C), 40.78 (Leucine side chain $-CH_2$), 37.20 (Phenylalanine side chain $-CH_2$), 24.6 (Leucine side chain -CH), 23.10 (Leucine side chain $–CH_3$).

Cbz FS $[\alpha]^{20}_D$ = 24.3 (c=0.4 gm/ml in 10% MeOH in $CHCl_3$)

^1H NMR (400 MHz, DMSO): δ/ppm= 8.20-8.18(d, 2H), 7.43-7.41 (d, 2H), 7.30-7.16 (m, 9H), 4.93 (s, 2H), 4.40-4.29 (m, 2H), 3.80-3.76 (m, 2H), 3.69-3.64 (t, 1H), 3.10-2.70 (t, 1H).

δ_c (DMSO, 100MHz): 171.96 (Phenylalanine -C=O), 170.45(Serine -C=O), 156.0 (Benzyloxy carbonyl -C=O), 136.15 (Phenylalanine aromatic –C), 135.32 (Benzyloxy carbonyl aromatic –C), 129.02 (Benzyloxy carbonyl aromatic –CH), 128.72 (Phenylalanine aromatic –CH), 127.90 (Phenylalanine aromatic –CH), 126.93 (Benzyloxy carbonyl aromatic –CH), 126.32 (Benzyloxy carbonyl aromatic –CH), 126.5 (Phenylalanine aromatic –CH), 66.16 (Benzyloxy carbonyl aliphatic $–CH_2$), , 61.90 (Serine aliphatic α–C), 55.45 (Serine side chain $–CH_2$), 59.6 (Phenylalanine aliphatic α–C), 37.89 (Serine side chain $-CH_2$).

A1.2 Mass analysis of synthesized peptides using LC-MS (QD

Peptides	Predicted Mass (Chem Draw Ultra 12.0) M+1	Calculated Mass M+1
Fmoc FF	535.22	535.42
Fmoc FY	551.21	551.43
Fmoc FL	501.23	501.45
Fmoc FS	475.18	475.43
Nap FF	497.20	497.45
Nap FY	513.20	513.43
Nap FL	462.54	462.65
Nap FS	437.17	437.41
Cbz FF	447.18	447.42
Cbz FY	463.19	463.45
Cbz FL	413.20	413.42
Cbz FS	387.15	387.43

Appendix II

List of Publications

1. Rashmi Jain, Gaurav Khandelwal, Sangita Roy, Unraveling the Design Rules in Ultrashort Amyloid-Based Peptide Assemblies toward Shape-Controlled Synthesis of Gold Nanoparticles, *Langmuir*, 35 **(2019)** 5878-5889.

2. Rashmi Jain, Sangita Roy, Designing bioactive scaffold from co-assembled collagen-laminin short peptide hydrogels for controlling cell behavior, *RSC Adv.* 9 **(2019)** 38745-38759.

3. Rashmi Jain, Sangita Roy, Tuning the gelation behavior of short laminin derived peptides via solvent mediated self-assembly, *Mater. Sci. Eng. C*, 108 **(2020)** 110483.

4. Rashmi Jain, Sangita Roy, Controlling neuronal cell growth through composite laminin supramolecular hydrogels, *ACS Biomater. Sci. Eng. 6* **(2020)**, *2832–2846.*

Manuscript under preparation

5. Rashmi Jain, Vijay K. Pal, Sangita Roy, Protein induced gelation of non-gelator dipeptides, 2020.

Not included in thesis

6. Vijay Kumar Pal, Rashmi Jain, Sangita Roy, Tuning supramolecular structure and function of collagen mimetic ionic complementary peptides via electrostatic interactions, *Langmuir*, 36 **(2020),** 1003-1013.

Conference Presentations

1. Srinagar, India (April 2019), International Conference on Nanotechnology for Better Living-2019 by NIT Srinagar and IIT Kharagpur
   Rashmi Jain, Sangita Roy
   Oral presentation: Development of Bioactive Peptide based Functional Scaffolds for Tissue Regeneration.

2. Mohali, India (November 2018), 3rd Inhouse- Symposium organized by INST
   Rashmi Jain, Sangita Roy
   Oral presentation: Development of Bio-inspired hydrogels for Tissue Regeneration.

3. Mohali, India (October 2018), Indo-German Meeting-2018 organized by INST
   Rashmi Jain, Sangita Roy
   Poster: Development of Bioinspired Hydrogels for Tissue Engineering.

4. New Delhi, India (October 2018), Nanobioteck- 2018 organized by Indian Society of Nanomedicine at AIIMS
   Rashmi Jain, Sangita Roy
   Poster: Development of Bioinspired Hydrogels for Tissue Regeneration.

5. Mohali, India (December 2017), 2nd In-house Symposium organized by INST
   Rashmi Jain, Sangita Roy

Poster: Development of Bioinspired Hydrogels for Tissue Regeneration.
Received best poster award

6. Mohali, India (December 2017), Har Gobind Khorana Memorial Symposium on Genes, Genomes & Membrane Biology organized by NABI
   Rashmi Jain, Sangita Roy
   Poster: Development of Bio-inspired hydrogels for Tissue Regeneration.

7. Mohali, India (August 2017), 3rd CRIKC Nanoscience Day organized by CRSI-CSIO
   Rashmi Jain, Sangita Roy
   Poster: Differential gelation behavior of hydrophobically modified short laminin peptides via non-conventional approach.

8. Varanasi, India (February 2017), International Conference on Advances in Biological system and Materials Science in Nanoworld organized by IIT-BHU
   Rashmi Jain, Sangita Roy
   Oral presentation: Development of Bio-inspired hydrogels for Tissue Regeneration.

9. Mohali, India (August 2016), 2nd CRIKC Nanoscience Day organized by INST
   Rashmi Jain, Ashok Kumar Ganguli and Sangita Roy
   Poster: Development of Bio-inspired hydrogels for Tissue Regeneration.

10. Delhi, India (April 2016), International conference on BiTERM organized by IIT-Delhi
    Rashmi Jain, Ashok Kumar Ganguli and Sangita Roy
    Poster: Development of Bio-inspired hydrogels for Tissue Regeneration.
11. Chandigarh, India (February 2016), 10th CRSI-RSC organized by INST- Punjab University
    Rashmi Jain, Ashok Kumar Ganguli and Sangita Roy
    Poster: Highly Tuneable Gels Using Non-equilibrium Self-assembly.

12. Mohali, India (November 2015), 6th MRS Trilateral Symposium organized by INST
    Rashmi Jain, Ashok Kumar Ganguli and Sangita Roy
    Poster: Development of Bio-inspired hydrogels for Tissue Regeneration.

13. Goa, India (August 2015), Chemical Frontiers, 6th Edition organized by IIT-Bombay and JNCASR
    Rashmi Jain, Gaurav Khandelwal, Ashok Kumar Ganguli and Sangita Roy
    Poster: Development of Bio-inspired hydrogels for Tissue Engineering.

14. Mohali, India (July 2015), 1st CRIKC Nanoscience Day organized by INST
    Rashmi Jain, Gaurav Khandelwal, Ashok Kumar Ganguli and Sangita Roy
    Poster: Unraveling Molecular Design Rules in Self-assembly of Aromatic Short Peptide Hydrogelators: for Tissue Engineering Application.

15. Mohali, India (December 2014), One Day Conclave on Nano-biotechnology organized by INST
    Rashmi Jain, Gaurav Khandelwal, Ashok Kumar Ganguli and Sangita Roy
    Poster: Development of bio-inspired hydrogels for liver tissue regeneration.
    Received best poster award.

Vita

Rashmi Jain

Ph.D. Research Scholar

Institute of Nano Science and Technology

&

Indian Institute of Science Education and Research Mohali

Rashmi has completed her bachelor's from degree in Pharmacy from V. N. S. Institute of Pharmacy, affiliated to RGPV University, Bhopal in 2012. Then he completed her Master's degree from National Institue of Pharmaceutical Education and Research, Ahmedabad with specialization in Pharmaceutics in 2014. In August 2014, she joined Ph.D at Institute of Nano Science and Tcehnology, Mohali under the guidance of Dr. Sangita Roy. She authored her work in esteemed journals and presented her work n several National and International conferences. Her research interest involves designing supramolecular hydrogels primarily based on peptides for biomedical applications.